~~SECRET~~ SPECIAL HANDLING

Logged

AC-04306
VOLUME II
31 March 1965
Copy No. 3

Quill

RADAR

PROGRAM [redacted]

VEHICLE 2355 SYSTEM REPORT (U)

VOLUME II – ENGINEERING

Quill

◇ RT DATA ENTERED
DATE
◇ MICROFICHED
DATE

HANDLE VIA BYEMAN
CONTROL SYSTEM ONLY

BYE 364-54/65
SAFSS ~~SH~~

Vol II
A-12498
cy 3

~~SECRET~~ SPECIAL HANDLING

LOCKHEED MISSILES & SPACE COMPANY

AC-04306
Volume II
31 March 1965

Copy No. 3
_____ Sheets

S

BYE-36454/65 3VOL2M

PROGRAM [redacted]
VEHICLE 2355 SYSTEM REPORT (U)
Volume II - Summary

Contract [redacted]
Supplemental Agreement Number 13

Quill

Prepared:

[redacted]
Chief Operations
Program [redacted]

Approved:

[redacted]
Manager
Program [redacted]

Approved:

David D. Bradburn

David D. Bradburn
Lt. Colonel, USAF
SAFSP

BYE 36454/65

FOREWORD

This report covers the span of time from the inception of the first satellite borne radar system through the final evaluation of the on orbit performance of the first flight. An objective review is attempted, of the complete scope of activities associated with bringing a new system into being and of the system performance during an essentially nominal and troublefree mission.

From this review, it is hoped that the systems management and program control parameters which were found to be effective may be properly recognized and thereby enhance the organization and conduct of similar future activities.

The system definition and resulting configuration is reviewed in retrospect, together with the problems associated with this Program development and testing.

The engineering management concept and the test philosophy which were applied are outlined and restated, with the objectives of first recording these, and then attempting to objectively analyze them for areas susceptible to improvement. The Air Force - LMSC - Associate Contractor team is defined, as it existed during the development, testing and operation of Vehicle 2355.

The system performance from launch through recovery and thence to battery depletion is evaluated from the primary aspect of payload operation.

System performance is compared against predictions, and the performance accomplishments and achievements are enumerated.

The report is therefore, in addition to a flight report, a total summary of the composite effort associated with the preparation and operation of this system. From the system evaluation certain conclusions and recommendations are formulated which are intended to be useful for later work on similar systems.

Through the medium of the detailed information contained in this report, it is intended to properly acknowledge the efforts of all those who were instrumental in managing and conducting a program which produced a completely successful mission with the first flight of a new payload vehicle system.

AC04306

PART II

TABLE OF CONTENTS

PART II (Cont.)

TABLE OF CONTENTS

Report Numbering and Organization

The complete 2355 System Report is contained in three volumes.

Volume I - (PART I) - Summary

Volume II - (PART II) - Engineering

Volume III - (PART III) - Flight Performance

The report paragraph numbering is in accordance with the following convention:

First number indicates volume number

Second number indicates main paragraph number

Third number indicates a subparagraph

Fourth number indicates a further subdivision of a subparagraph

Figures are numbered consecutively within main paragraphs.

Reports By Participating Contractors

The complete system description and performance evaluation is contained in reports issued by the three contractors. These are listed here for reference by the reader:

Lockheed Missiles and Space Company:

Title: 2355 System Report, dated 31 March 1965.

Volume I - Summary

Volume II - Engineering

Volume III - Flight Performance

Goodyear Aerospace Corporation:

Title: Program Report, KP-II Orbital Doppler Radar, Thor/Agena Satellite Program, dated 1 March 1965.

[redacted]

Title: [redacted]

2.1 Satellite System Engineering

The subsystems of the satellite vehicle which required engineering development, study or program peculiar applications are discussed in this section. Included also are sections on radar antenna development, thermodynamics and a thorough review of the work which was directed toward control of high voltage breakdown in a vacuum. A brief discussion of vacuum measurements is included due to the early considerations of the possibilities of high voltage breakdowns on orbit and a requirement to measure pressures in the payload vehicle.

The thermodynamic work which was done on this payload vehicle; accommodating the energy dissipated by the payload and during a time period when battery temperatures were under critical review; yielded a new level of quality in on-orbit thermal control. All engineering efforts which are reviewed in this section resulted in the complete and correct operation of the total satellite vehicle through the prescribed mission, setting an enviable standard of excellence in the first flight of a new payload system. This mission was conducted to a duration which exceeded predictions without a failure of any type aboard the satellite vehicle.

2.1.1 Structural Subsystem

2.1.1.1 Requirements and Design Concepts

The first definition of the philosophy to be followed in engineering of the spaceframe indicated certain major areas where the design approach would be nearly unique for Vehicle 2355. The primary task was to install in a space vehicle, equipment normally associated with conventional aircraft, and to achieve orbit of this vehicle in such a manner that the equipment could operate normally in the acquisition and storage of data. Additionally, Subsystem "A" was to provide the mounting and ejection mechanisms for the capsule which would eventually return the stored data to the ground.

The initial approach envisioned hard-mounting of payload items in structure which was to be as light as possible consistent with the requirements dictated by predicted ascent loads and heating. This resulted in the design and/or installation of seven items tailored to the payloads and to the mission: (See Figure 2.1.1.1)

- Recovery Capsule
- Conical Payload Rack
- Cylindrical Payload Rack
- Ejectable Fairing for the C&C Antenna
- Guidance Auxiliary Rack
- Ejectable Fairing for the Radar Antenna
- Lifeboat Equipment

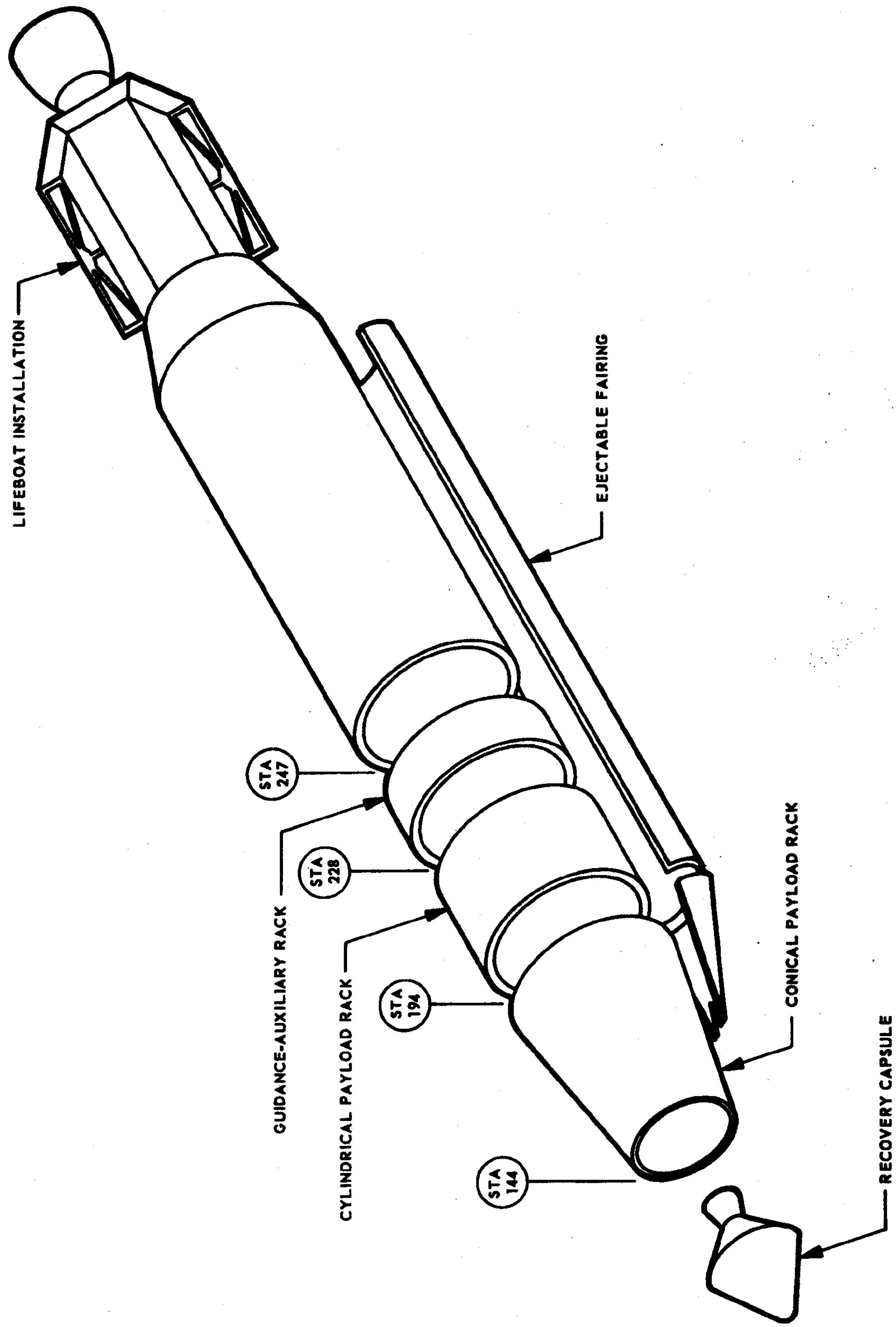

Figure 2.1.1.1 - Major SS/A Components

2.1.1.2 Configuration - Basic Concepts

Recovery Capsule. This capsule in its entirety was available as GFE. It housed the storage container for the raw data film and served as the nose cone during ascent. Since this recovery capsule had been used in other applications, its characteristics were known quantities requiring only incorporation into the 2355 System. A program peculiar installation had been made to accommodate the film takeup mechanism.

Conical Payload Rack. This structure was located just aft of the recoverable capsule and included mounting provisions for the capsule. The structure was a straightforward design comprising seven rings and a magnesium skin riveted together in the form of a truncated cone. The space inside this rack was allocated to Payload Box #7. Radiation protection for the raw data film feeding from Box #7 to the recoverable capsule was provided in the form of a thermal-tape-covered shield standing off from the inside of the forward portion of the rack. (See Figure 2.1.1.2).

Cylindrical Payload Rack. The third structure item was designed to mount to the forward face of the Guidance Auxiliary Rack, to provide mounting for the Conical Payload Rack, and to accommodate Payload Boxes 1, 2, 3, 4, 5, and 6. The structure comprised three rings, eight longerons, two torque boxes, eight doors, and eight access holes.

The floors of the two torque boxes, on which the payload boxes

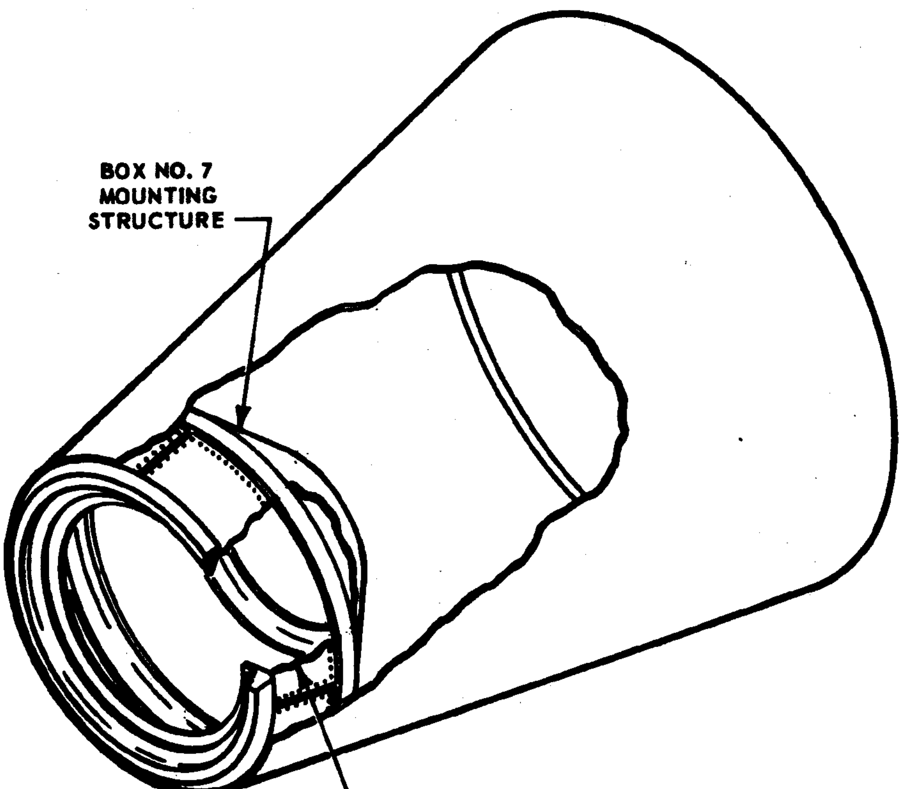

Figure 2.1.1.2-Cone and Thermal Shield

mounted, were located longitudinally between two longerons and over a third, with a web running from this middle longeron to the middle of the floor base. The magnesium skin connecting the three longerons completed each torque box. To offer access to the payload mounting devices, four access holes were located in suitable positions in the magnesium skin.

The remaining space was enclosed by four doors on each side of the rack providing access to all payloads mounted in the rack. (See Figure 2.1.1.3)

Ejectable Fairing for the C&C Antenna. The original design concept called for the Type 7 C&C Antenna to be mounted on the surface of the skin covering the Cylindrical Payload Rack. Protection for the antenna in this location would have been provided by a fairing mounted over it, secured to the outside of the vehicle by tension bolts and pinpuller assemblies. At a suitable time this fairing would have been ejected, permitting proper operation of the antenna.

The launch configuration of Vehicle 2355 did not carry the ejectable fairing. Reasons for this decision are covered in the Design Development section of this report.

Guidance Auxiliary Rack. The Guidance Auxiliary Rack structure comprised two rings, eight longerons, two floors for mounting guidance components, a web joining these floors, and a skin in

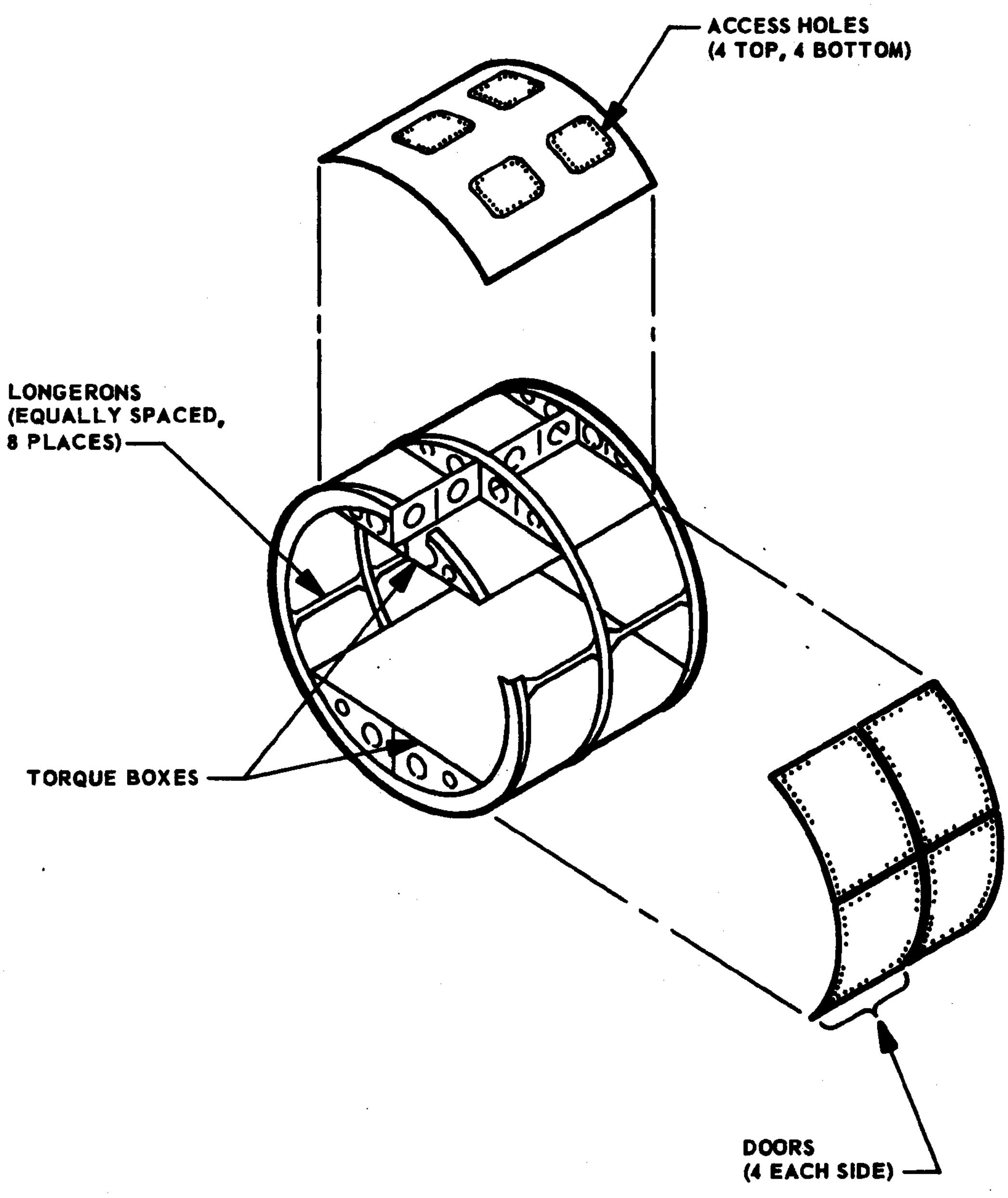

Figure 2.1.1.3 Cylindrical Payload Rack

the form of removable doors which permitted access to all equipment located in the rack. As in the equipment rack, the floors joined two longerons located ninety degrees apart with an additional web running from the center of the floor to the central longeron.

The floors extended from station 247 forward to approximately station 231, leaving a three-inch space aft of the ring at station 228 for the wave guide installation in the forward portion of the rack. (See Figure 2.1.1.4)

Ejectable Fairing for the Radar Antenna. This fairing comprised a 27-inch wide channel, six inches deep, approximately 226 inches long. It was mounted longitudinally on the skin of the vehicle in the +Y+Z quadrant, and provided aerodynamic and thermodynamic protection for the radar antenna during ascent.

The ejectable portion of the fairing, 187 inches long extending from the forward edge of the cylindrical rack aft to station 381, was secured to the vehicle by longitudinal forward-facing retainer pins (five on each side of the fairing). These pins fitted into matching sockets secured to the vehicle, thereby providing radial and transverse stability for the fairing. Longitudinal stability was provided by a tongue extending forward from the face of the ejectable portion of the fairing into the fixed portion where it was secured by a pinpuller assembly.

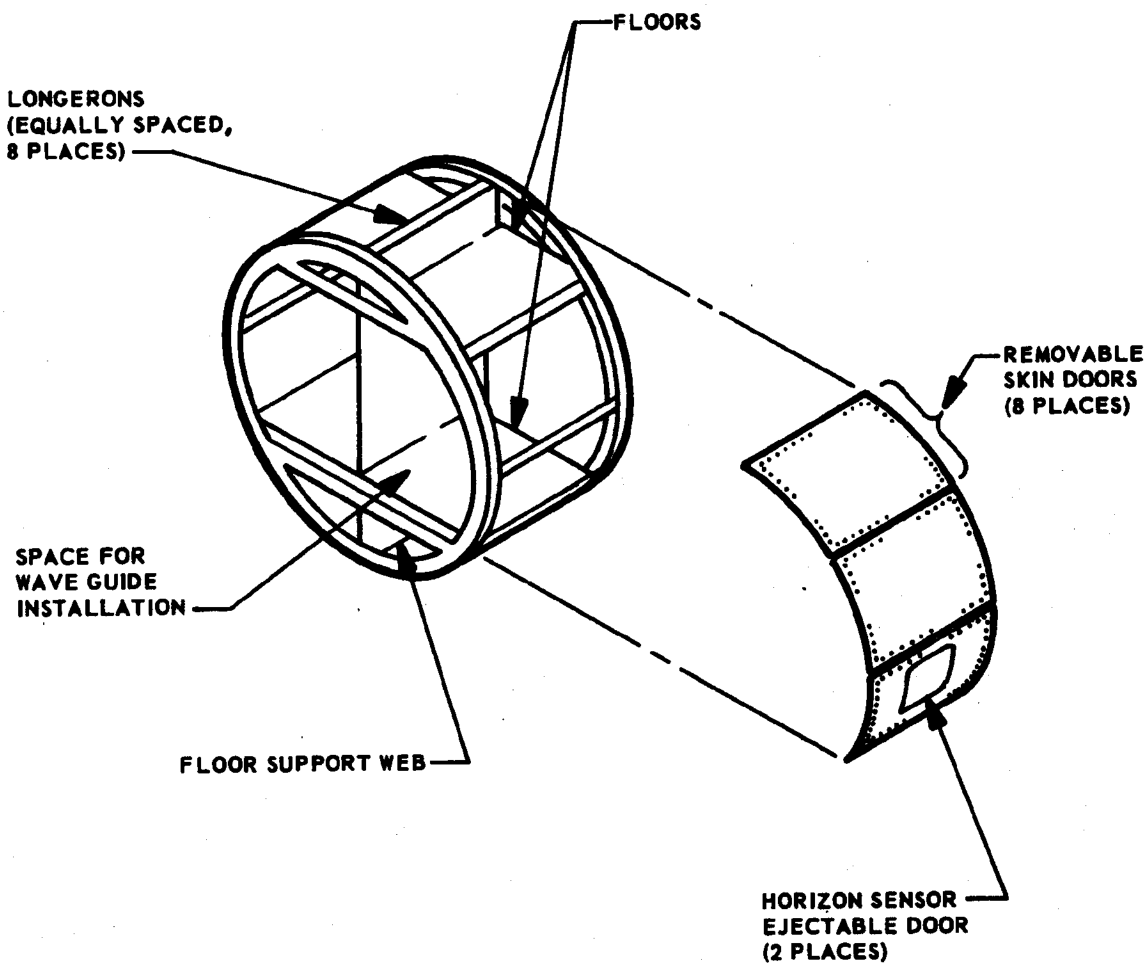

Figure 2.1.1.4 Guidance Auxiliary Rack

Lifeboat Equipment. This equipment was installed on the aft structure of the SS-01A. Since installation and functioning of the equipment had been developed and proven by other programs, a nearly identical installation was utilized for the 2355 vehicle.

2.1.1.3 Equipment Installations — Basic Concepts

Recovery Capsule. As with the Lifeboat equipment, the capsule itself, together with its attachment and separation mechanisms, had been utilized and proven by other programs. Rather than embark on a development program, the already-proven design was utilized for 2355.

Payload Units - Excepting the Recorder. These payload units were contained in the cylindrical rack. All equipment was secured to the floors of the torque boxes through hard mounting points. Traditional hardware (clips, angles, brackets, etc.) was utilized to take advantage of the structural stiffness of the rack and to carry the predicted loads back through the secondary structure into the primary structure.

Film Recorder. This unit had to be mounted in the conical rack in a manner which would permit feeding of the raw data film forward into the storage container housed in the recovery capsule. The unit was L-shaped with its base pointing forward. The mounting structure employed for the front end of this box was a truncated cone with the small diameter facing aft. The large diameter was secured to the conical rack ring at station 152.

The base of the L-shaped recorder was secured to the mounting structure with three uniball bearing assemblies.

The original concept for the mounting of this unit called for the aft end of the payload to be secured by a device which would restrain it during ascent. After the vehicle had attained orbit, this device was to release the aft end of the box from all restraint.

The design specified four legs extending inboard from the ring at station 194 toward the aft end of the payload. These legs terminated in a plate directly behind the payload. This plate was then secured to the payload with a pin which could be withdrawn upon receipt of the proper signal. In this way the payload was to be rigidly supported during launch and ascent, and free of restraint at the aft end during orbital operations. (See Figure 2.1.1.5.)

<u>C&C Antenna Fairing Ejection Mechanism</u>. The fairing covering the C&C antenna was to be secured to the outer skin of the vehicle by two tension bolts in pinpuller assemblies, one located at the aft end of the fairing, and one located at the forward end. To provide for longitudinal and transverse shear, pins mounted to the rack protruded through holes in the fairing.

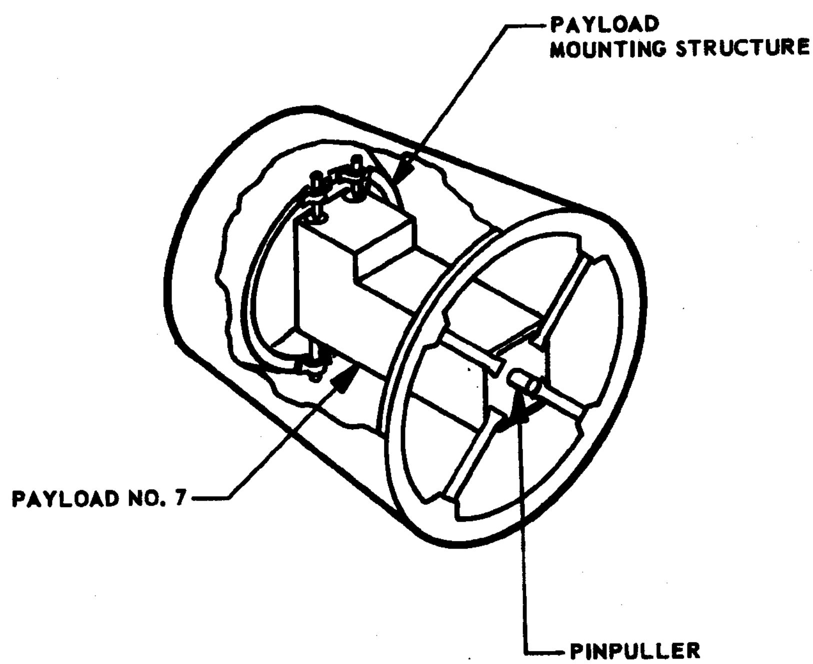

Figure 2.1.1.5 Box #7 Installation

Motive force for ejection of the fairing was provided by two compression spring assemblies between the vehicle skin and the fairing. One spring was located approximately ten inches aft of the leading edge of the fairing, and the other incorporated the aft pinpuller bolt.

Upon receipt of the proper signal the pinpullers would have retracted and the fairing would have been jettisoned, exposing the C&C antenna.

Vehicle Fairing Ejection Mechanism. Upon receipt of the command to eject this fairing, the pinpuller retracted. This permitted four compression spring assemblies mounted between the ejectable and fixed portions of the fairing to thrust the ejectable portion aft. As soon as the retaining pin cleared their sockets a radial thrust vector was imparted to the fairing by six ramps (three on each side of the fairing) riding on six needle-bearing rollers attached to the vehicle. The resultant separation was in a +X-Y direction with the fairing remaining essentially parallel to the vehicle (See Figure 2.1.1.6)

2.1.1.4 Design Development

Following the original concepts discussed above, design proceeded in a normal manner. Despite the fact that some of these concepts were relatively new, structures and equipment installation engineering was normal in relation to state-of-the-art techniques. Problems with

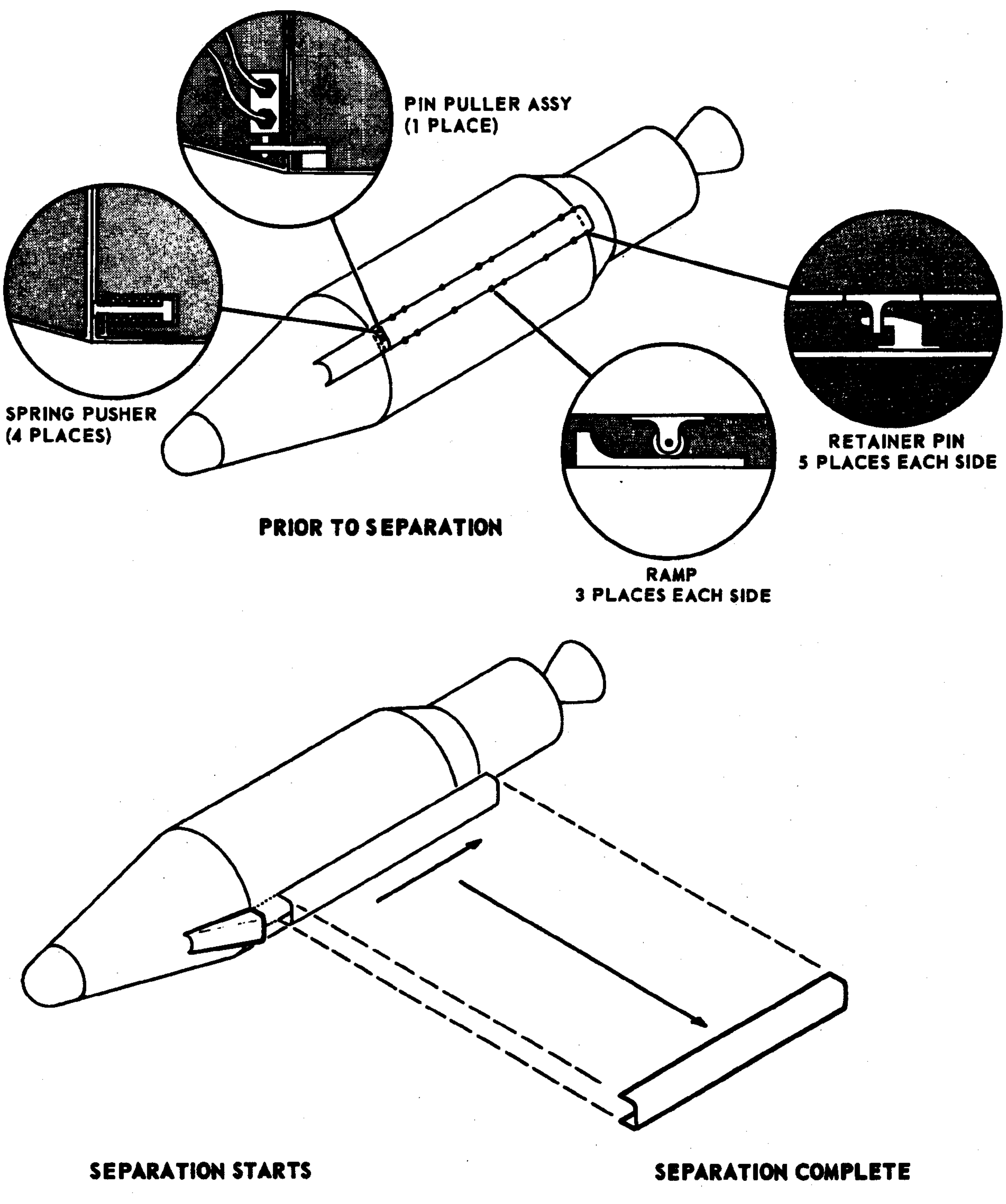

Figure 2.1.1.6 Vehicle Fairing Separation

components or changes to original design occurred in the following areas:

- Payload Mounting Vibration Difficulties
- Corona in the Transmitter/Modulator
- Wave Guide Heating (Ground Conditioning)
- Thermodynamic Requirements Changes
- Film Recorder Mounting
- Installation of Pressure Transducers
- C&C Antenna Change--Ejectable Fairing Deletion

Payload Mounting Vibration Difficulties. In accordance with the initial design approach the cylindrical rack was tailored to mount the payload boxes and to provide access to them in such a manner that the structure would be the lightest possible consistent with stress requirements. Upon completion, this design was passed to Manufacturing for fabrication and a copy of the engineering documentation was furnished to Goodyear Aerospace Corporation.

Goodyear, however, in conducting confidence tests on payload components discovered that the hard mountings originally planned could result in degradation of payload performance, particularly in light of the stringent vibration requirements called out in LMSC Spec 6117, Revision "D". Goodyear, in order to increase the confidence level in payload survival, dictated that shock mounts be utilized to isolate the critical items from vibration. The vibration isolation mounts were installed on the payloads by

Goodyear and these payloads furnished to LMSC for proper mounting in the rack.

The precision tailoring of the original design precluded the use of these mounts on a simple substitution basis. As a consequence, the cylindrical rack went through a redesign which saw a complete redistribution of equipment in the rack, and suitable modifications made to the secondary structure to provide the required structural stiffness.

Subsequent testing of the redesigned rack with the payloads restrained in the new shock mounts showed that the required confidence level had been attained.

<u>Corona in the Transmitter/Modulator</u>. Concurrent with the vibration difficulties outlined above, an unrelated problem was discovered in the transmitter. During testing by Goodyear a corona effect was observed inside the unit. Various possibilities for correction were considered; and, Goodyear's proposed solution of encapsulating the transmitter in a pressure vessel was started as an alternative to potting. This pressure vessel in turn was to be mounted in the cylindrical rack.

The eventual solution to the corona problem proved to lie in the potting techniques for components in the transmitter rather than in pressurization of the complete unit. This entailed only removal of the pressure vessel in the final installation since the mounting provisions remained the same.

Wave Guide Heating (Ground Conditioning). A modification to the original design arose in connection with the wave guide installation. A Program Office directive was received which required the addition of a device for heating the wave guide during the pre-launch phase of operation.

This requirement was fulfilled by laying heater strips on the wave guide, wrapping these strips to the guide with insulation, and providing power to the heater strips from the electrical umbilical which was disconnected at launch. The wave guide heating facilitated the outgassing of the wave guide during ascent, since the wave guide was warmed at liftoff.

Thermodynamic Requirements Changes. As the design progressed and the thermodynamic characteristics of the vehicle could be more accurately predicted, changes were initiated to assure the correct thermal environment for all components.

In response to these developing requirements Subsystem "A" revised the mounting of Payload Unit #1 (battery) by changing the insulating strips which were located between the mounting pads and the battery itself. Additionally, a radiation shield was installed over the battery; however, as thermodynamic analysis continued, it was determined that this shield should be deleted from Vehicle 2355.

Film Recorder Mounting. As outlined above, it was planned that this unit would be hard-mounted at the forward end and secured by a pinpuller to spider-legs at the aft end, the plan being to release this pinpuller after orbit injection to permit the aft end of the recorder to be unrestricted. Subsequent analysis, however, indicated that the firing of the pinpuller with its attendant shock was more likely to result in recorder malfunction than would the slight torsion effect resulting from expansion of the unequal spider-legs. As a consequence, the final design called for hard-mounting both forward and aft ends of the recorder.

Installation of Pressure Transducers. At the direction of the Program Office, vacuum measuring instruments were installed in the cylindrical and conical racks. A total of five were installed, one transducer located on the recorder, one on the transmitter, one between the transmitter and the RF-IF, in the high power wave guide, one on a structural ring at the -Y axis, and one on the same ring at the +Y axis.

Installation of the transducers was in accordance with current state-of-the-art techniques, and was problem free.

C&C Antenna Change--Ejectable Fairing Deletion. The ejectable fairing to cover the C&C Antenna was designed as outlined above. However, difficulties were arising in connection with the pattern of the Type 7 Antenna which had been planned for installation on Vehicle 2355. These difficulties were such that a substitution of antennas was required. The Type 4 C&C Antenna was selected and was installed.

Since the Type 4 Antenna is flush-mounted with the skin of the vehicle, the requirement for ejection of a fairing was obviated.

2.1.1.5 Structural Qualification

General

The size, weight and mounting provisions of the Goodyear payload components required the qualification of the payload vehicle structure for this application. In addition, the large structure which housed the radar antenna involved qualification of that item inasmuch as it was a new design. Table I lists the tests which were performed on SS/A hardware to demonstrate qualification for flight on Vehicle 2355. All testing was performed by Lockheed Satellite System Test Services with the exception of the Guidance Auxiliary Rack Vibration Test, Test Assignment No. 19-363, which was performed by Polaris Test Services (Lockheed Missiles Systems Division).

Two sets of test hardware were fabricated to accommodate the short test span, and also to provide hardware for testing in the Temperature-Altitude Simulation Chamber (TASC). Hardware was fabricated to non-released sketch type drawings due to the compressed schedule. Sketch numbers (SK) are referred to in the detailed test reports.

The following is a list which correlates SK numbers with the part numbers of the flight hardware:

Part	Released Number	Sketch Number
Struct. Assy., Conical Aux. Rack	1359864-501	DN 618631-501
Struct. Assy., Cylindrical Aux. Rack	1359839-501	SK 715631-501
Struct. Assy., Aux. Rack, Guidance	1359821-501	SK 1001050-501

TABLE 1

Test Condition	Job Request No.	Test Assignment Number	Test Hardware	Part Number	Structure Specimen Del.	Structure Test Comp.	Total Cost M/H
Static load test to simulate ascent loads on primary structure. Separation test of horizon sensor door.	A631226	5938	Struct Assy Conical Rk. Struct Assy Cylindrical Rk. Struct Assy Guidance Rk.	1359864-501 1359839-501 1359821-501	2/14/64	4/10	[redacted]
Vibration test to simulate dynamic loads on equipment mounting structure.	A631210-01	5930	Struct Assy Conical Rk. with a dynamic model of the payload recorder installed. Struct Assy Cylindrical Rk. with dynamic models of all equipment installed.	1359864-501	1/17/64	2/3/64	[redacted]
Vibration test to simulate dynamic loads on equipment mounting structure.	A630816-04	19363	Structure Assy guidance Rk., with dynamic models of payload packages installed.	1359821-501	1/8/65	2/10/64	[redacted]

TABLE I (Cont.)

Test Condition	Job Request No.	Test Assignment Number	Test Hardware	Part Number	Structure Specimen Del.	Structure Test Comp.	Total Cost M/H
Static load test on payload packages to simulate combined acceleration/vibration loads on equipment mounting structure.	A640521	1082	Struct Assy Cylindrical Rk. with dynamic models of payload packages installed.	1354839-501	7/21/64	8/7/64	[redacted]
Static load test on payload Box #7 to simulate combined acceleration/vibration loads on equipment mounting structure.	A640428-3	1048	Struct Assy Conical Aux Rk. with a dynamic model of payload recorder intalled.	1359839-501	8/3/64	8/6/64	[redacted]
Pressure test to simulate ascent burst & collapse pressures on the payload fairing.	A631219-01	5937	Struct Assy fairing mounted on a simulated vehicle.		1/6/65	2/14/64	[redacted]

TABLE I (Cont.)

Test Condition	Job Request No.	Test Assignment Number	Test Hardware	Part Number	Structure Specimen Del.	Structure Test Comp.	Total Cost M/H
Thermal/ separation test to simulate ascent heating and demonstrate separation of payload fairing.	A631118	5906	Struct Assy fairing mounted on a simulated vehicle.		1/28/64	2/5/64	[redacted]

All Test Hardware was structurally identical to the Flight Hardware.

Test Descriptions and Results

Static Load Test on Conical, Cylindrical, and Guidance Racks (TA 5938).

The test was divided into four parts as follows:

PART I: The Cylindrical Payload Rack was subjected to a collapse pressure test. This was accomplished by sealing and evaluating the entire rack to an ultimate differential pressure of 1.44 PSI. No failure was observed.

PART II: The Conical Rack, Cylindrical Rack, Guidance Rack, and an Agena D Fwd. Rack were assembled in flight configuration as shown in Fig. 2.1.1.7 (I). Hydraulic jacks exerted load P1 through P6, Fig. 2.1.1.7 (I). All loads were applied simultaneously in 20% increments to 100% design limit load (DLL), and then in 5% increments to 125% DLL. Load values are listed under Test IIA in Fig. 2.1.1.7 (II). No failure was observed.

PART III: The specimen setup was identical to that in Part II except the specimen was rotated 112.5 degrees counter clockwise (CCW)--looking aft--with respect to the bending loads P1-P3. Loads were applied in the same manner as in Part II. Load values are listed in Fig. 2.1.1.7 (II) under Test IIB. No failure was observed. After completion of this test, one Horizon Sensor Door was successfully jettisoned.

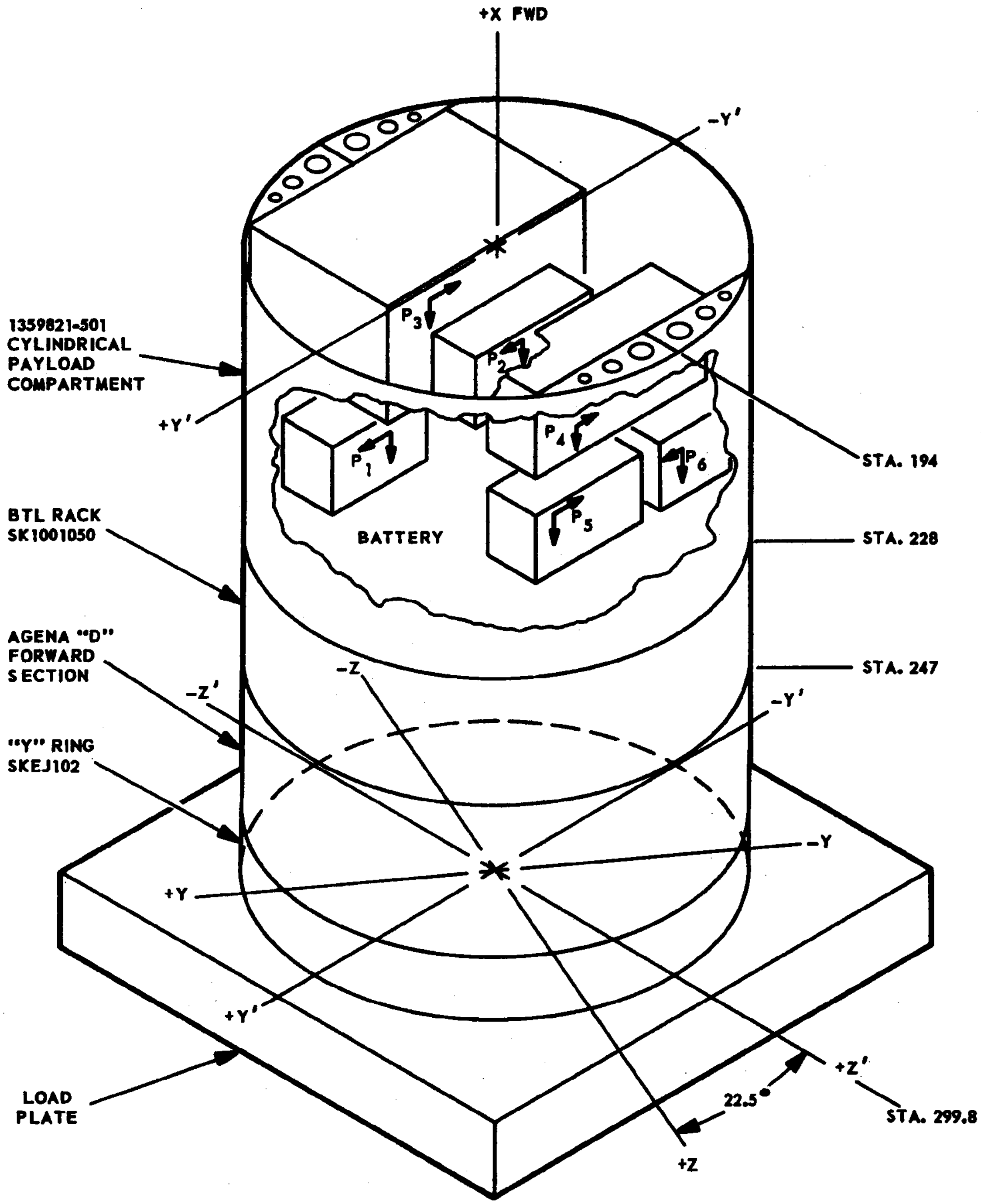

NOTES:

1. P_1V, P_2V, P_3V, P_4V, P_5V, AND P_6V LOADS ARE IN Y^r DIRECTION.
2. P_1X, P_2X, P_3X, P_4X, P_5X, AND P_6X LOADS ARE IN AXIAL DIRECTION.

Figure 2.1.1.7(I) - Equipment Mounting

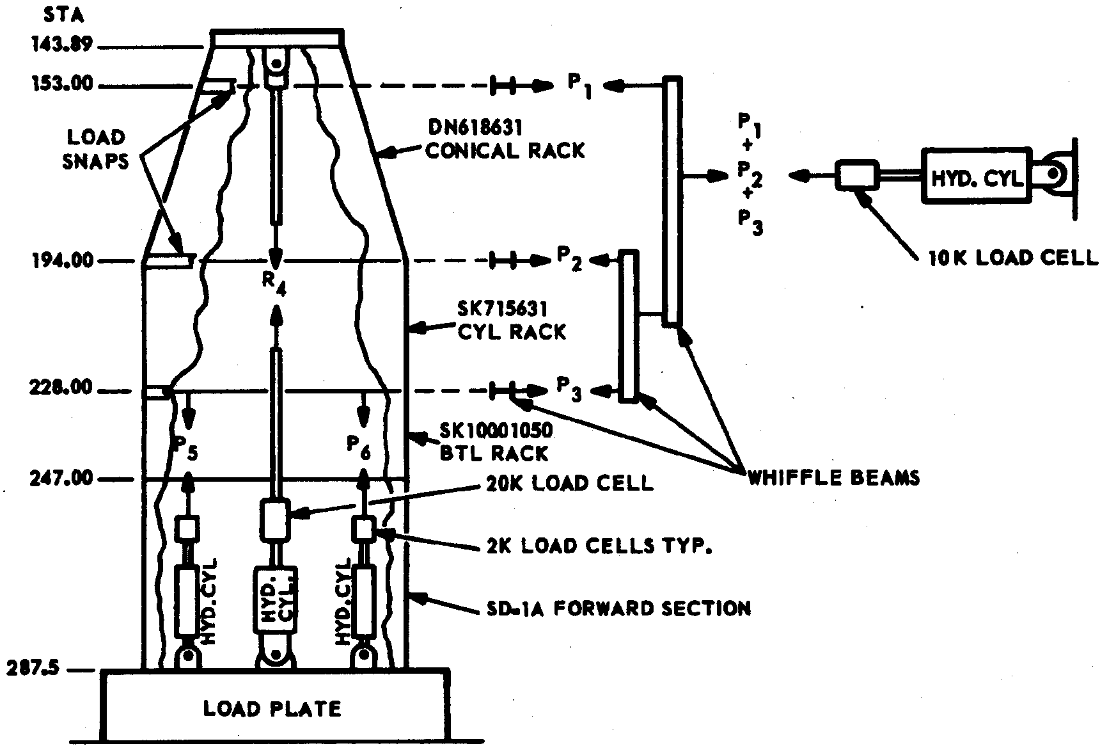

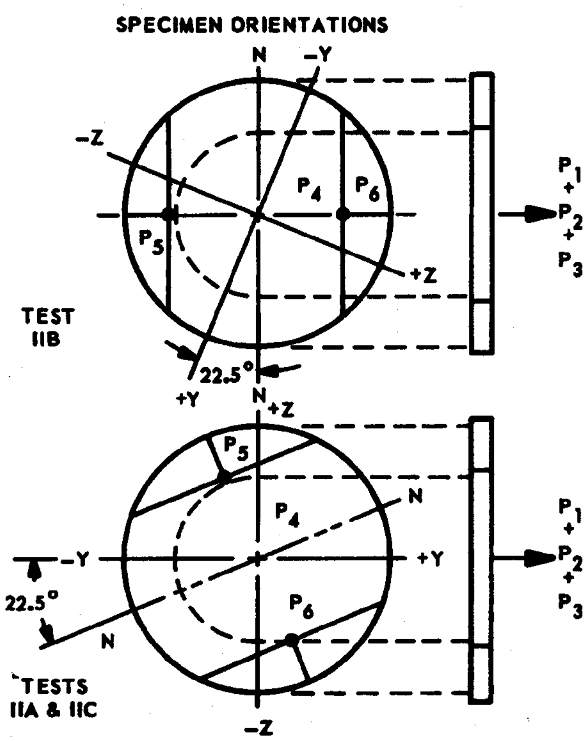

LOADS

TESTS IIA & IIC		
LOAD	100% DLL	125% DLL
P_1	5900 LB	7370 LB
P_2	1700	2120
P_3	1315	1640
P_4	10,400	13,000
P_5	650	810
P_6	650	810
TEST IIB		
LOAD	100% FLL	125% DLL
P_1	5900 LB	7370 LB
P_2	1700	2120
P_3	1315	1640
P_4	6950	8700
P_5	650	810
P_6	650	810

Figure 2.1.1.7(II) - Test Setups

PART IV: The setup and loads were identical to those in Part II. Loads were applied simultaneously at a uniform rate to 125% DLL and further in 5% increments with the intention of failing the specimen. However, 200% DLL was reached without failure. Since this was the maximum capacity of the loading system, testing was discontinued. (See Figure 2.1.1.8)

Notes: 1. The test conditions for Parts I through IV above were in accordance with Reference 1.

2. A burst-pressure test on one Horizon Sensor Door was scheduled to be performed. However, the test requirement was eliminated by redesign of the door mounting.

3. After completion of testing per Parts I through IV above, the Horizon Sensor Door separation test was rerun with instrumentation for recording pinpuller shock on the Horizon Sensor Head. Several attempts were made to reduce shock levels with only limited success. A flight item Horizon Sensor Head was then mounted in the specimen. The door was jettisoned three times with the sensor head operating. There were no adverse effects.

Vibration Test - Conical and Cylindrical Auxiliary Racks (TA 5930). The Conical and Cylindrical Auxiliary Racks were mated in flight configuration and the entire assembly mounted vertically on a vibration table. Dynamic models for all equipment weighing two pounds

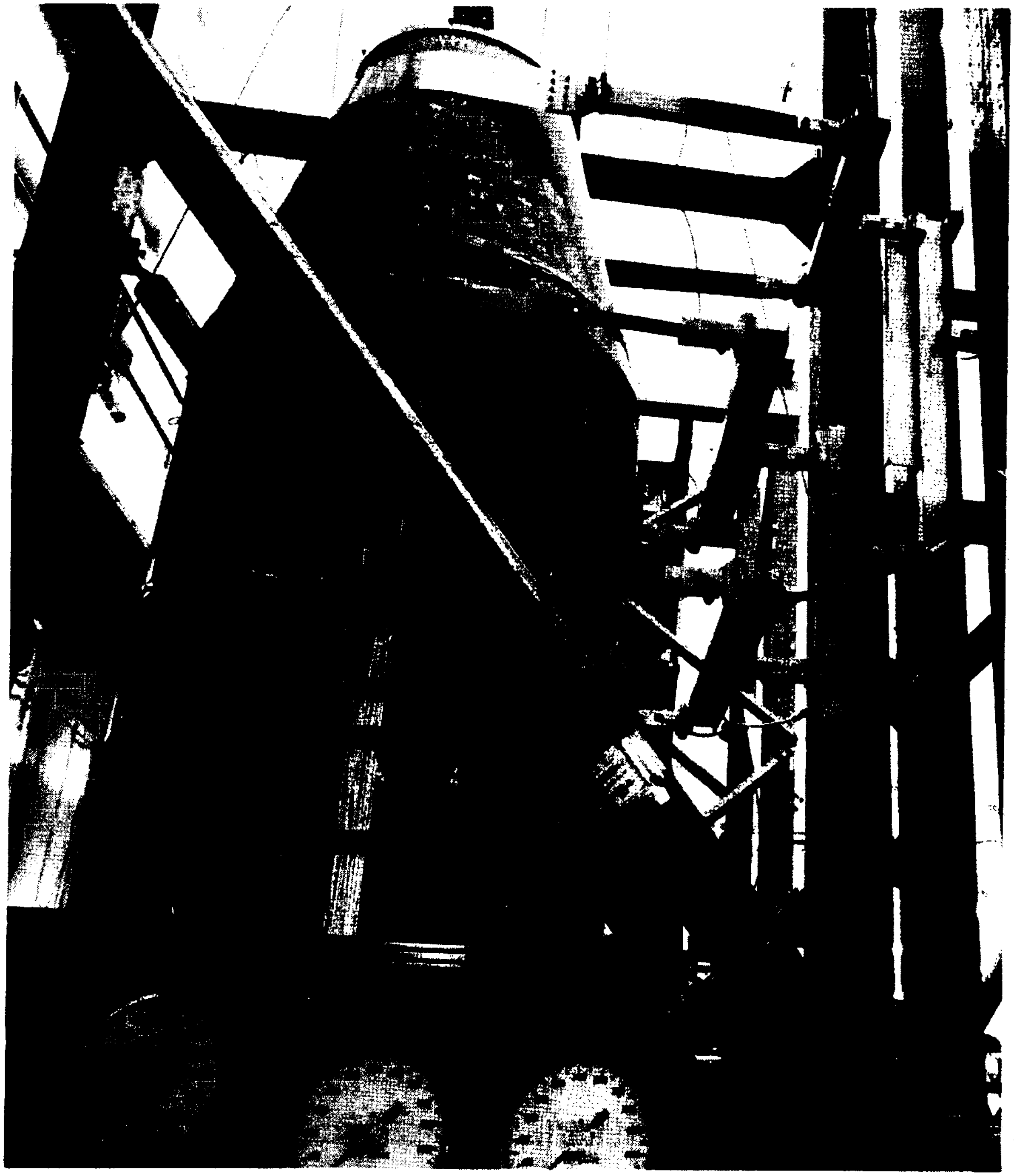

Figure 2.1.1.8 STATIC LOAD TEST

or more were installed. All wave guides were installed. Dynamic models of all payload units were provided by Goodyear Aircraft Corp.

The entire assembly was subjected to vibration levels in three mutually perpendicular axes as follows:

- Resonant Search - X axis - 2 min./octave sweep 5-150 cps @ ½G.
- Sinusoidal Qual. Test - X axis - 3 min./octave sweep
  - 9-16 cps @ 2G
  - 16-22 cps @ 4G
  - 22-30 cps @ 1.5G
  - 30-40 cps @ .5G
  - 40-63 cps @ 1G
  - 63-90 cps @ .5G
  - 90-100 cps @ 1.5G
  - 100-200 cps @ 4G
  - 200-600 cps @ 6G
- Random Qual. Test - X axis - 5 minute duration
  - .01 G^2/cps 20-200 cps
  - .03 G^2/cps 200-400 cps   11.6G RMS
  - .08 G^2/cps 400-2000 cps
- Resonant Search - Z axis - 2 min./octave sweep - 5-150 cps ½G
- Sinusoidal Qual. Test - Z axis - 3 min./octave sweep
  - 6-10 cps @ 1G
  - 10-20 cps @ .5G
  - 20-70 cps @ 1G

- 70-90 cps @ .5G
- 90-100 cps @ 1G
- 100-200 cps @ 2G
- 200-600 cps @ 5G

o Random Qual. Test - Z axis - 5 minute duration

Levels same as Test 3 above.

o Resonant Search - Y axis - 2 minute/octave sweep

- 5-150 cps @ ½G

o Sinusoidal Qual. Test - Z axis - 3 minute/octave sweep

- 6-35 cps @ 1G
- 35-50 cps @ .5G
- 50-60 cps @ 1G
- 60-80 cps @ .5G
- 80-100 cps @ 1G
- 100-200 cps @ 2G
- 200-600 cps @ 5G

o Random Qual. Test - Z axis - 5 minute duration

Levels same as test 3 above.

Notes: 1. After completion of vibration testing the pinpuller used to restrain the aft end of the recorder was actuated once, and shock levels recorded. This pinpuller was not used on the flight item and a fixed pin was substituted. No failures were observed during vibration or pinpuller release.

2. A total of 36 accelerometers were used to monitor response of payload units during vibration. Figures 2.1.1.9 thru 2.1.1.12 show some of the accelerometer locations.

Vibration Test Guidance Auxiliary Rack (TA 19,363)

The Guidance Auxiliary Rack, with Dynamic Models of all equipment weighing two pounds or more, was subjected to the following vibration levels:

RESONANCE SEARCH

Axis	Duration	Frequency, CPS	Amplitude
X)	1.5 min. per octave	6-400	.5 g vector
Y)			
Z)			

SINUSOIDAL VIBRATION TEST

Y	3 min. per octave	6-22	1 g
		22-35	.5 g
		35-60	1 g
		60-70	.5 g
		70-100	1 g
		100-200	2 g
		200-400	5 g
Z	3 min. per octave	6-27	1 g
		27-31	.5 g
		31-55	1 g

SINUSOIDAL VIBRATION TEST

Axis	Duration	Frequency, CPS	Amplitude
Z		55-65	.5 g
		65-100	1 g
		100-200	2 g
		200-400	5 g
X	3 min. per octave	5-9	.5 in. D.A.
		9-16	2 g
		16-22	4 g
		22-45	1.5 g
		45-55	.5 g
		55-75	1 g
		75-80	.5 g
		80-100	1.5 g
		100-200	4 g
		200-400	5 g

RANDOM VIBRATION TEST

Axis	Frequency, CPS	Spectral Density, g /cps	Duration
X, Y, Z	20-200	.01	5 min. per
	200-400	.03	axis
	400-2000	.08	

A total of 24 accelerometers were used to monitor equipment response.

No failure was observed after completion of vibration testing.

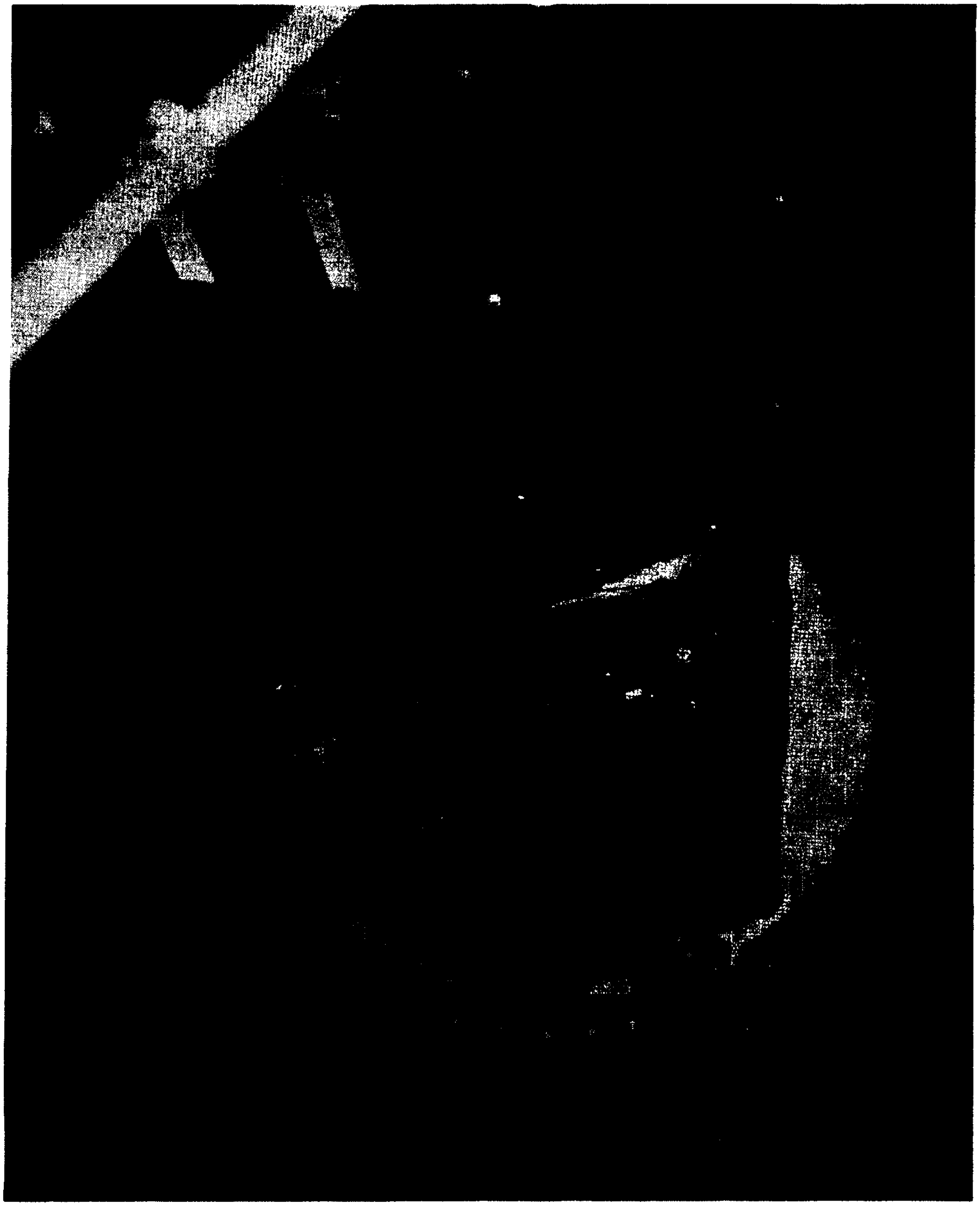

Figure 2.1.1.9 ACCELEROMETERS ON RECORDER DYNAMIC MODEL

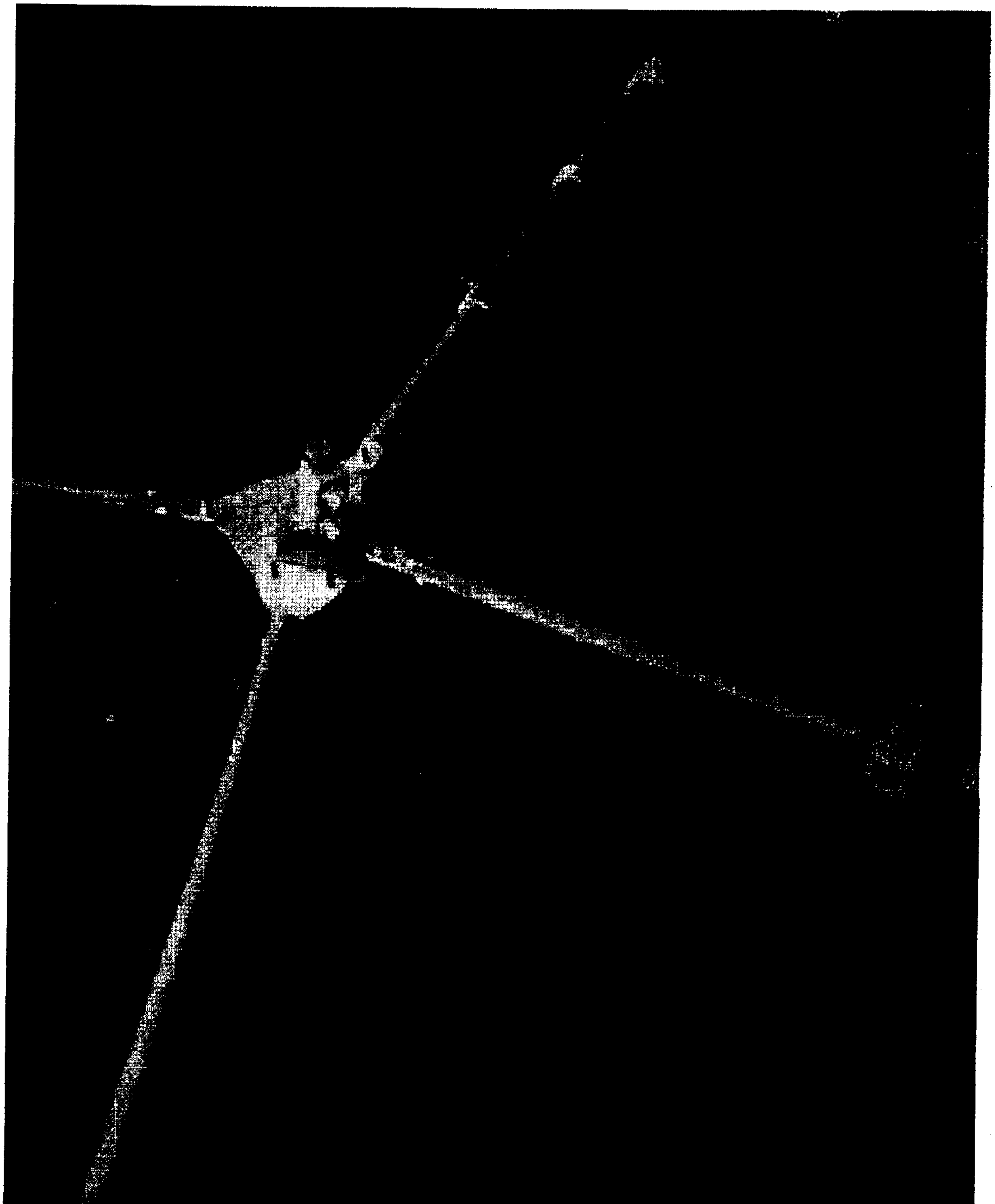

Figure 2.1.1.10 ACCELEROMETERS ON RECORDER DYNAMIC MODEL

2.1.1.11 ACCELEROMETERS-TRANSMITTER AND RF-IF DYNAMIC MODELS

Figure 2.1.1.12 ACCELEROMETERS ON DYNAMIC MODELS IN CYLINDRICAL SECTION

Static Load Test - Payload Packages - Cylindrical Rack (TA 1082)

The cylindrical auxiliary rack was mounted to the guidance rack and an Agena D Forward Rack as shown in Fig. 2.1.1.7(I). Dynamic models of the following equipment were installed:

Description	Part Number	Load Applied
Type 1-D Battery	1461793-1	P_1
High Voltage Power Supply	1464240-1	P_2
Transmitter-Modulator	1464247-1	P_3
RF-IF	1464248-1	P_4
Reference Computer	1464249-1	P_5
Control Unit	1464250-1	P_6

Hydraulic jacks were used to apply loads on each of the dynamic models (see Figures 2.1.1.7(I), .13, .14). All loads were applied in 10 percent increments up to 100 percent design limit load (DDL) and 5 percent was maintained after each increment. The test was divided into three parts.

PART I: The loads shown in Table I were applied to each package individually (two loading conditions per package).

PART II: The loads shown in Table II were applied simultaneously in the -X direction.

PART III: The battery was simultaneously subjected to loads in the -X and +Z' directions shown in Figure 2.1.1.7(I). Limit loads were 1800 pounds in the -X direction and 1920 pounds in the +Z' direction. Ultimate loads 2250 pounds in the -X direction and 2400 pounds in the +Z' direction.

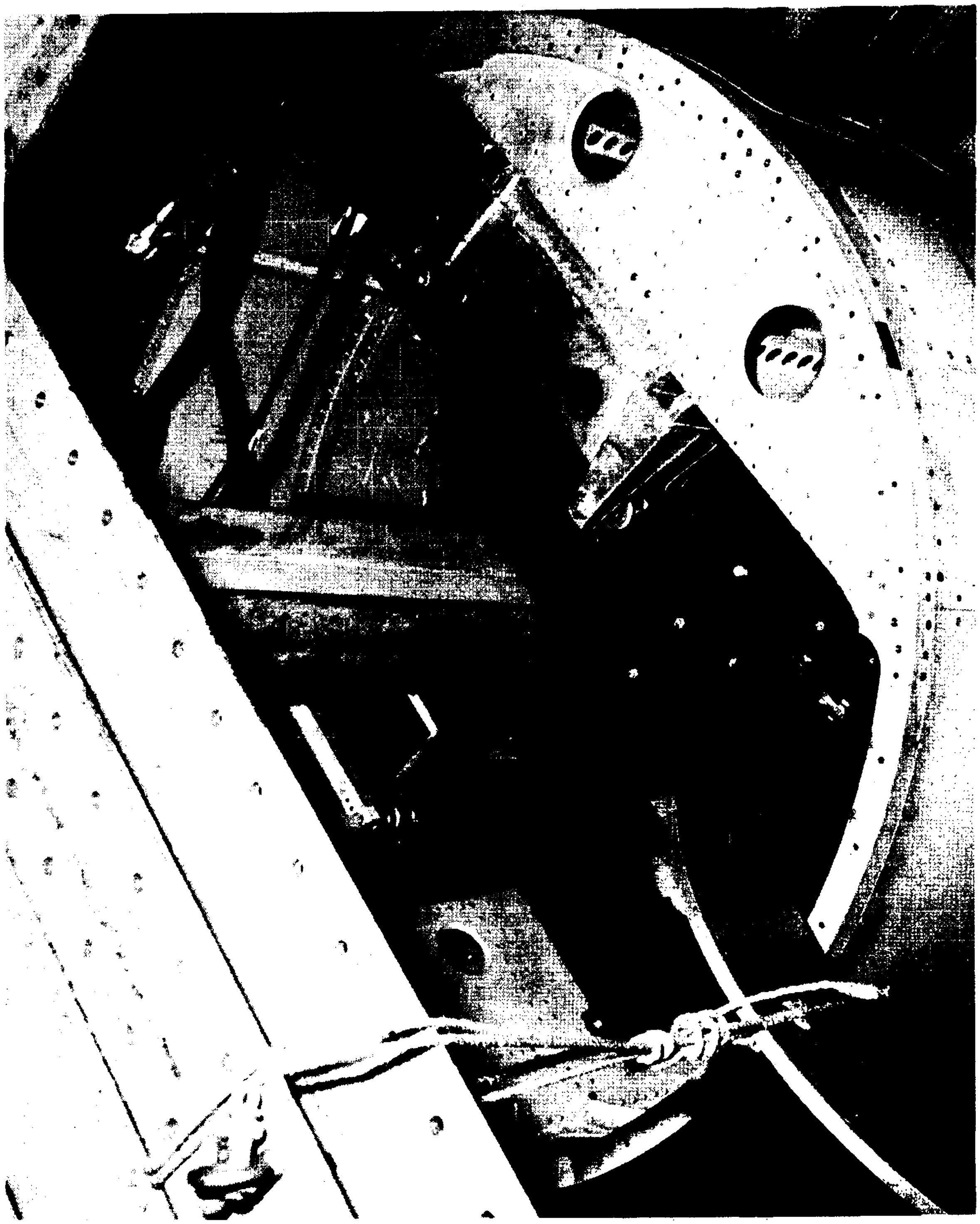

Figure 2.1.1.13 STATIC LOAD TESTING-TRANSMITTER DYNAMIC MODEL

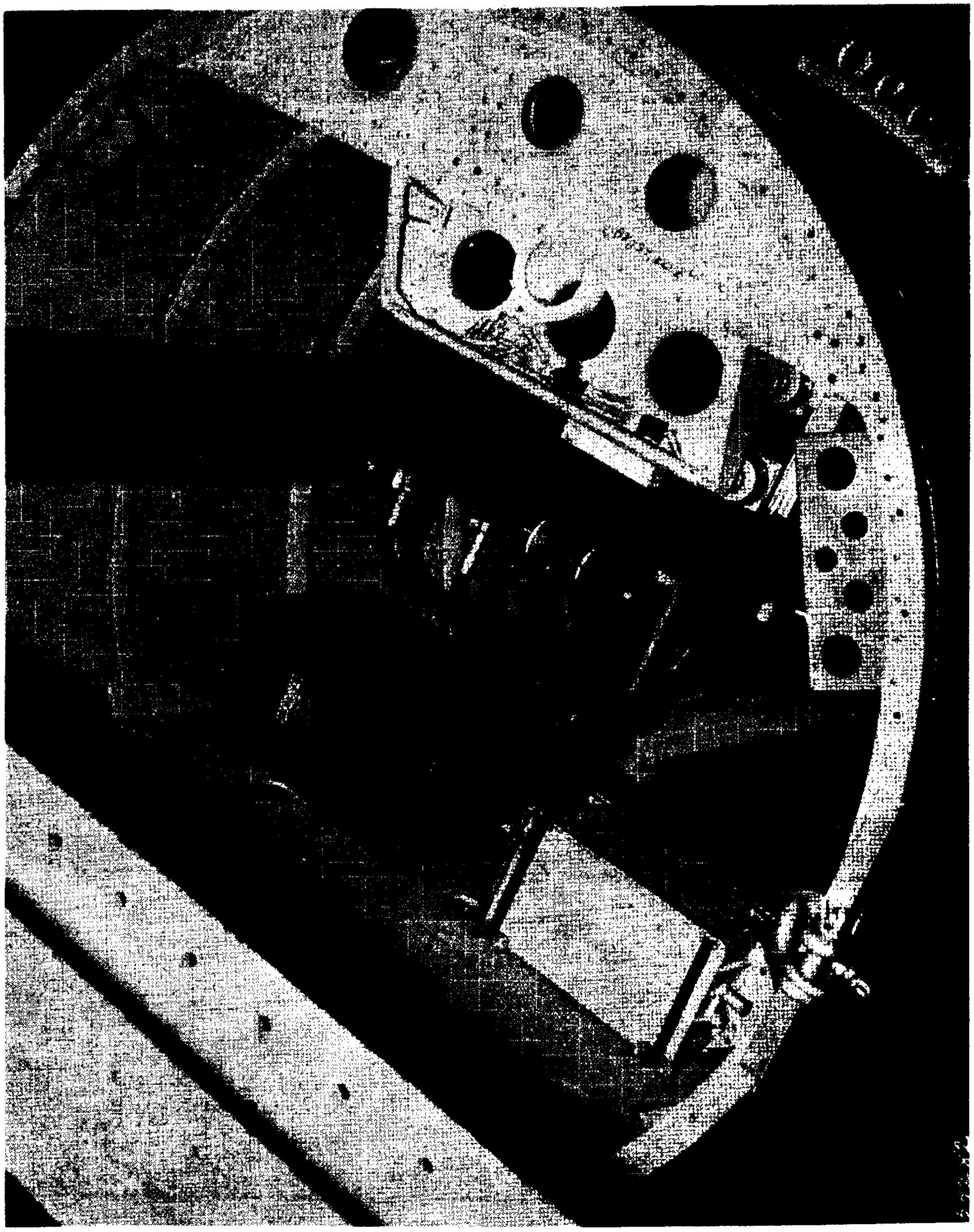

Figure 2.1.1.14 STATIC LOAD TEST - CYLINDRICAL SECTION

TABLE 1

Load	Direction	Limit (LB)	Ultimate (LB)
P_1	-X	1920	2400
	Y'	480	600
P_2	-X	700	875
	Y'	500	625
P_3	-X	3270	4090
	Y'	1635	2042
P_4	-X	1104	1382
	Y'	553	692
P_5	-X	888	1110
	Y'	444	555
P_6	-X	612	765
	Y'	306	383

TABLE 2

Load	Direction	Limit	Ultimate
P_1	-X	1240	1550
P_2	-X	563	705
P_3	-X	2420	3230
P_4	-X	691	865
P_5	-X	555	695
P_6	-X	382	478

No failures were observed after completion of testing per Part I through III. No instrumentation was used on this test except that required to record loads. It was noted that the deflection of the transmitter under load was in excess of the predicted deflection.
A test was performed on two of the HT2-100 vibration isolators used to mount the component. Load deflection curves were generated. These were compared to curves from an unused isolator. It was concluded that the spring constant of the isolators tends to deteriorate under continued usage. It was recommended that fresh isolators be used on the flight item.

Static Load Test - Payload Package - Conical Rack (TA 1048)

The conical and cylindrical auxiliary racks were mated and the entire assembly bolted to a load plate (see Figure 2.1.1.15). A dynamic model of the recorder was mounted in the conical rack. One hydraulic jack was attached to this unit and load applied as shown in Figure 2.1.1.16. No failures were observed as a result of the two loading conditions.

Payload Fairing Pressure Test (TA 5937)

The payload fairing and transition (ramp) section were mounted to a simulated vehicle (two booster adapters and a nose cone bolted together) as shown in Figure 2.1.1.17. Pressure loads were applied to both sections by evacuating or pressurizing the fairing. Pressure bags were also used to apply collapsing pressures. The test was divided into four parts.

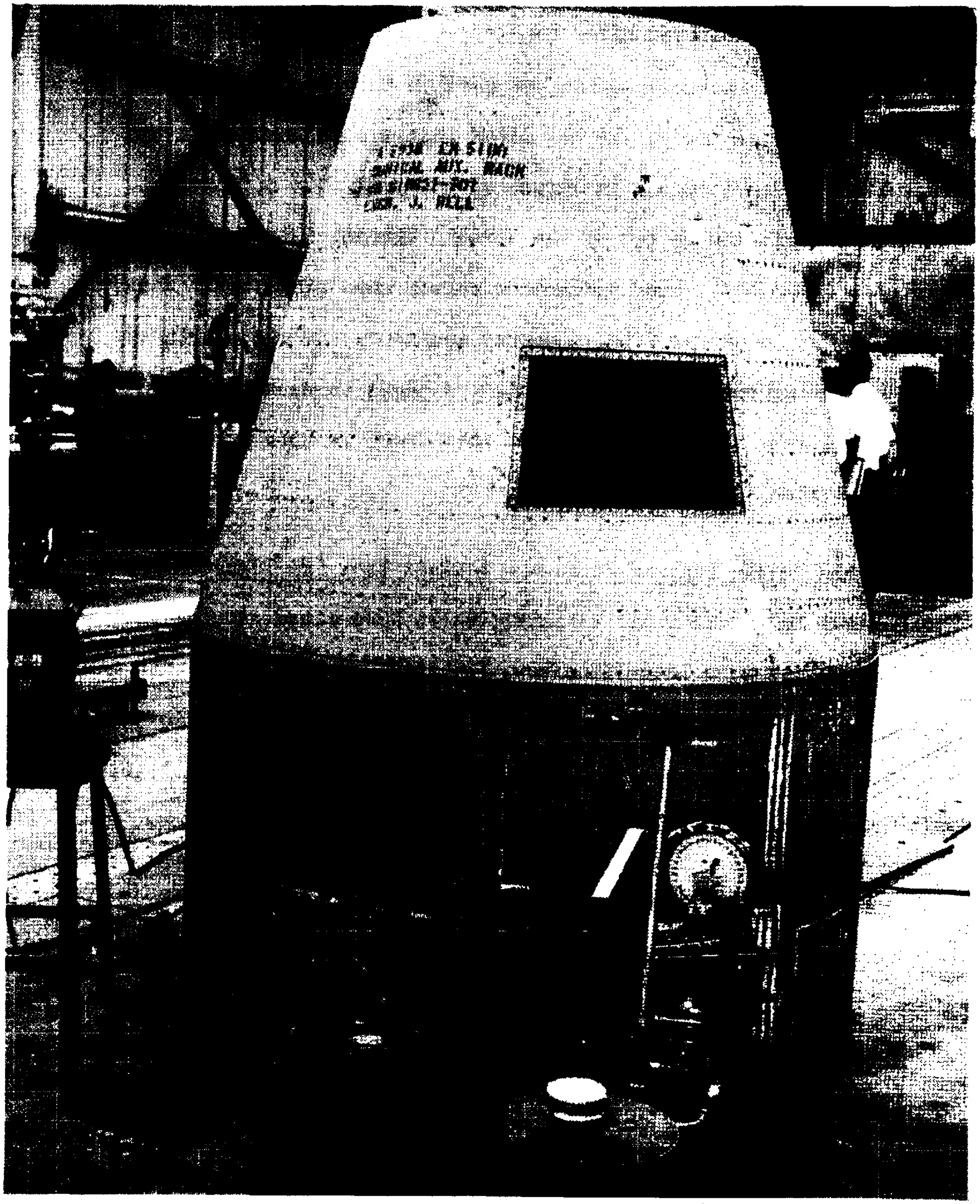

Figure 2.1.1.15 STATIC LOAD TEST - RECORDER DYNAMIC MODEL

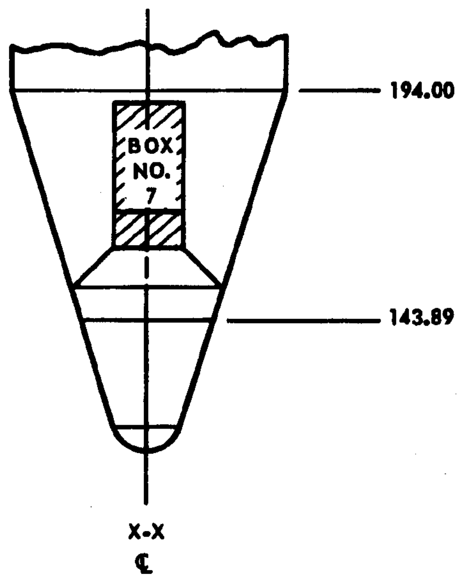

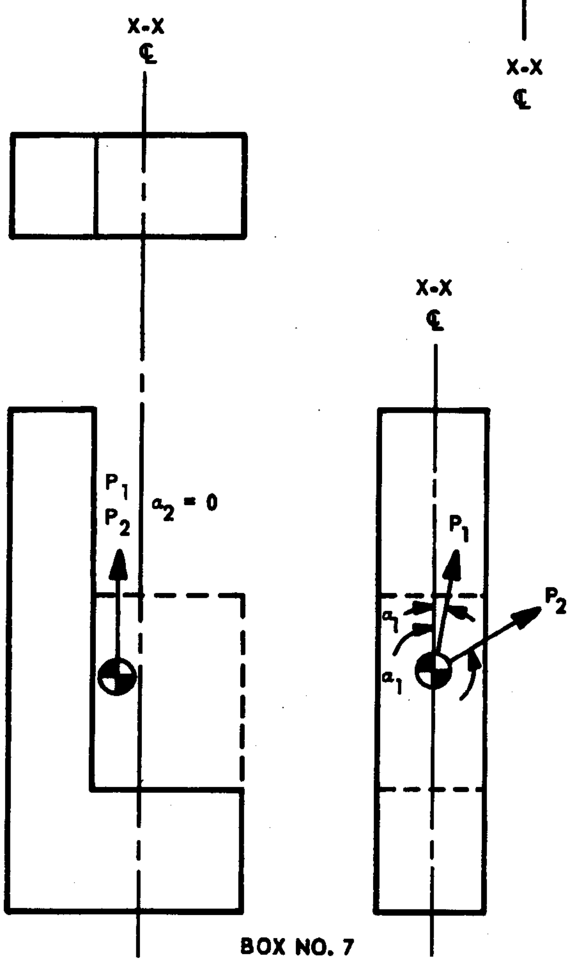

LOAD	LOADING CONDITION NO. 1			
	α_1	α_2	LIMIT	ULTIMATE
P_1	7.6	0	1670#	2090#

LOAD	LOADING CONDITION NO. 2			
	α_1	α_2	LIMIT	ULTIMATE
P_2	545	0	946#	1185#

Figure 2.1.1.16 Inertia Loads Box No. 7

Figure 2.1.1.17 RADAR ANTENNA FAIRING - PRESSURE TEST

Part I

The internal pressure of the entire fairing was reduced to obtain a differential pressure of 1.0 psi and 1.25 psi (100 percent and 125 percent design limit load).

Although canning of the skin was observed, at approximately 100 percent design limit load between stations 194 and 252, visual inspection after testing showed no indication of damage.

Part II

The ramp fairing (SKWBK 10-7) was pressure tested to 125 percent design limit load. The test consisted of reducing the internal pressure of the entire ramp to obtain a differential pressure of 5.6 psi to the sides of the ramp and 12.1 psi to the top surface.

Part III

The entire fairing as shown in Fig. 2.1.1.18 was simultaneously subjected to the following differential pressures.

(a) The internal pressure of the fairing between stations 179 and 230 was increased to obtain a differential of 6.0 psi (100 percent design limit load) and 7.5 psi (125 percent design limit load).

(b) The internal pressure of the fairing between stations 230 and 384 was increased to a differential pressure of 2.0 psi (100 percent design limit load) and 2.5 psi (125 percent design limit load).

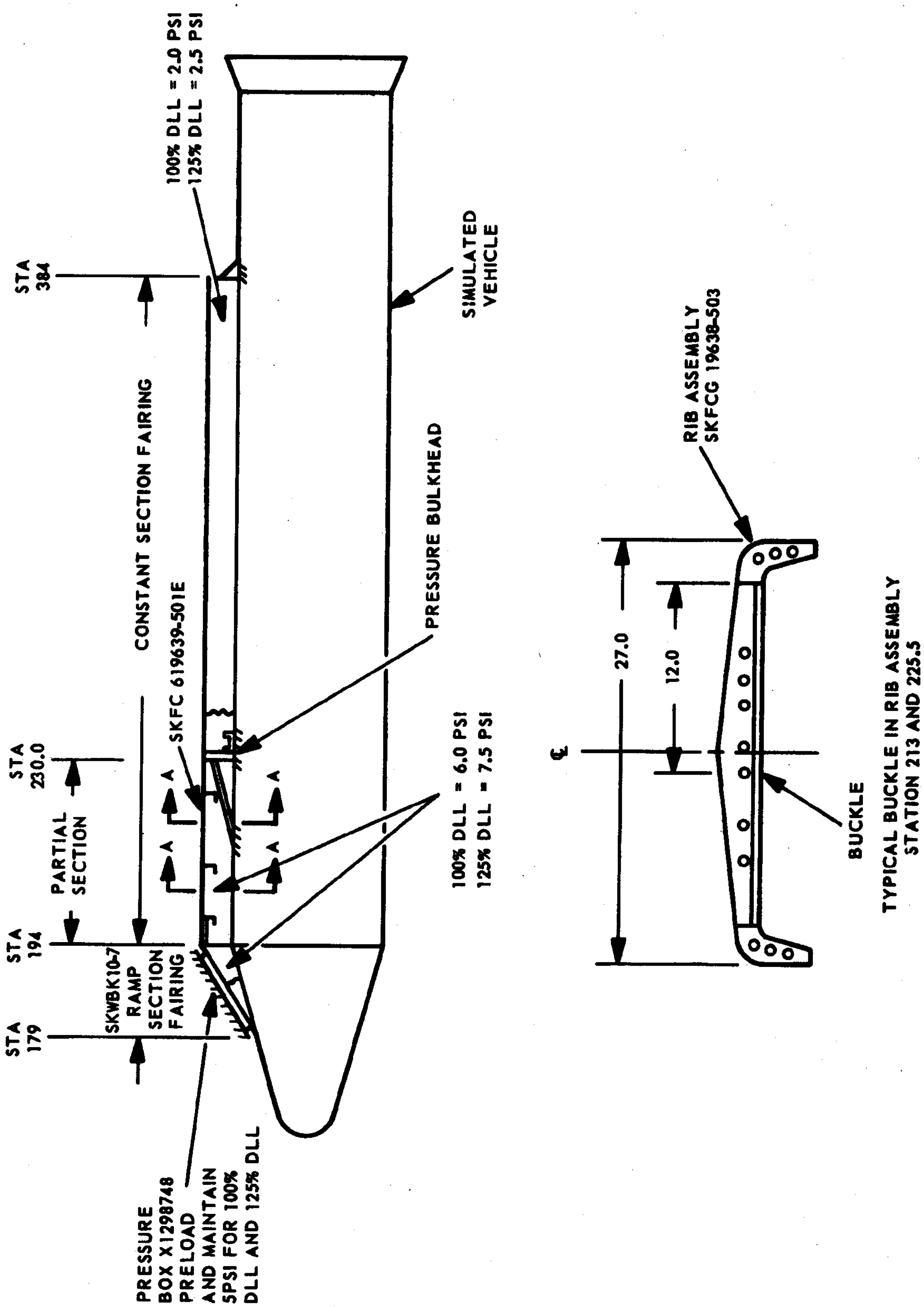

Figure 2.1.1.18 Test Setup - Phase 3 Test 1 and 2

Above 112% of design limit load two rib assemblies buckled (see Figure 2.1.1.18 - .19). After review of the design loads it was concluded that the pressure load at 112% actually exceeded the predicted ultimate load in the area of the ribs. This condition is due to the fact that it is almost impossible to apply the exact predicted load profile with a pressure test of this type.

Part IV

The fairing (SKFCG 19639-501E) was subjected to an axial load of 1275 lb. (100% design limit) and 1595 lb. (125% design limit) in the aft direction. Inspection after testing showed no indication of damage to the specimen.

Payload Fairing - Thermal Separation Test (TA 5906)

The payload fairing and transition section were mounted to a simulated vehicle (two booster adapters and a nose cone bolted together) as shown in Figure 2.1.1.20. A 70 foot long cable attached to the fairing at the center of gravity. The fairing was then subjected to the following test sequence:

(a) The fairing was heated with a bank of quarts lamps (see Figure 2.1.1.21). The power to the lamps was programmed to simulate the maximum predicted ascent heating pulse.

(b) The lamp bank was removed. The pin puller holding the fairing was actuated and the fairing separated under the force of the spring actuators.

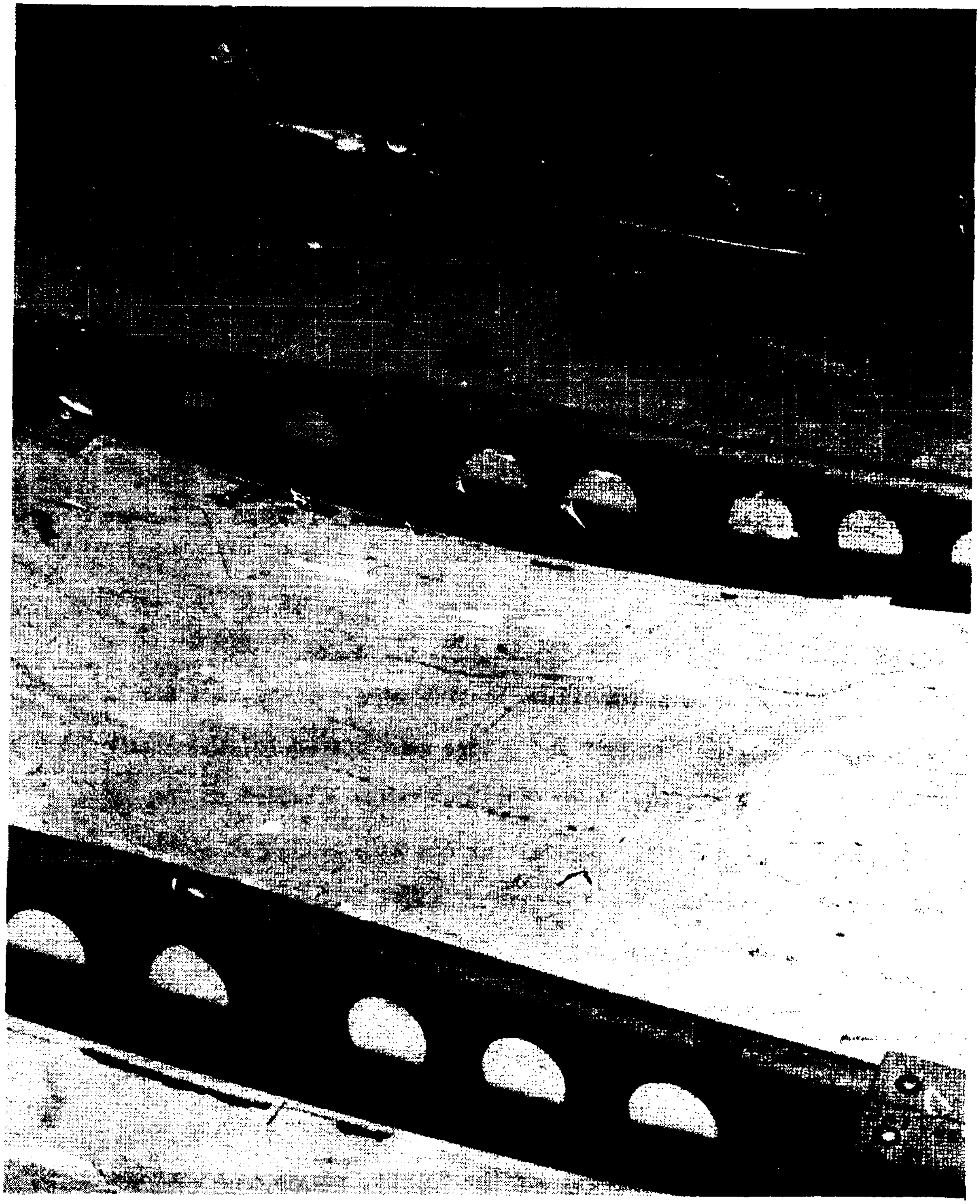

Figure 2.1.1.19 ANTENNA FAIRING - BUCKLED RIBS

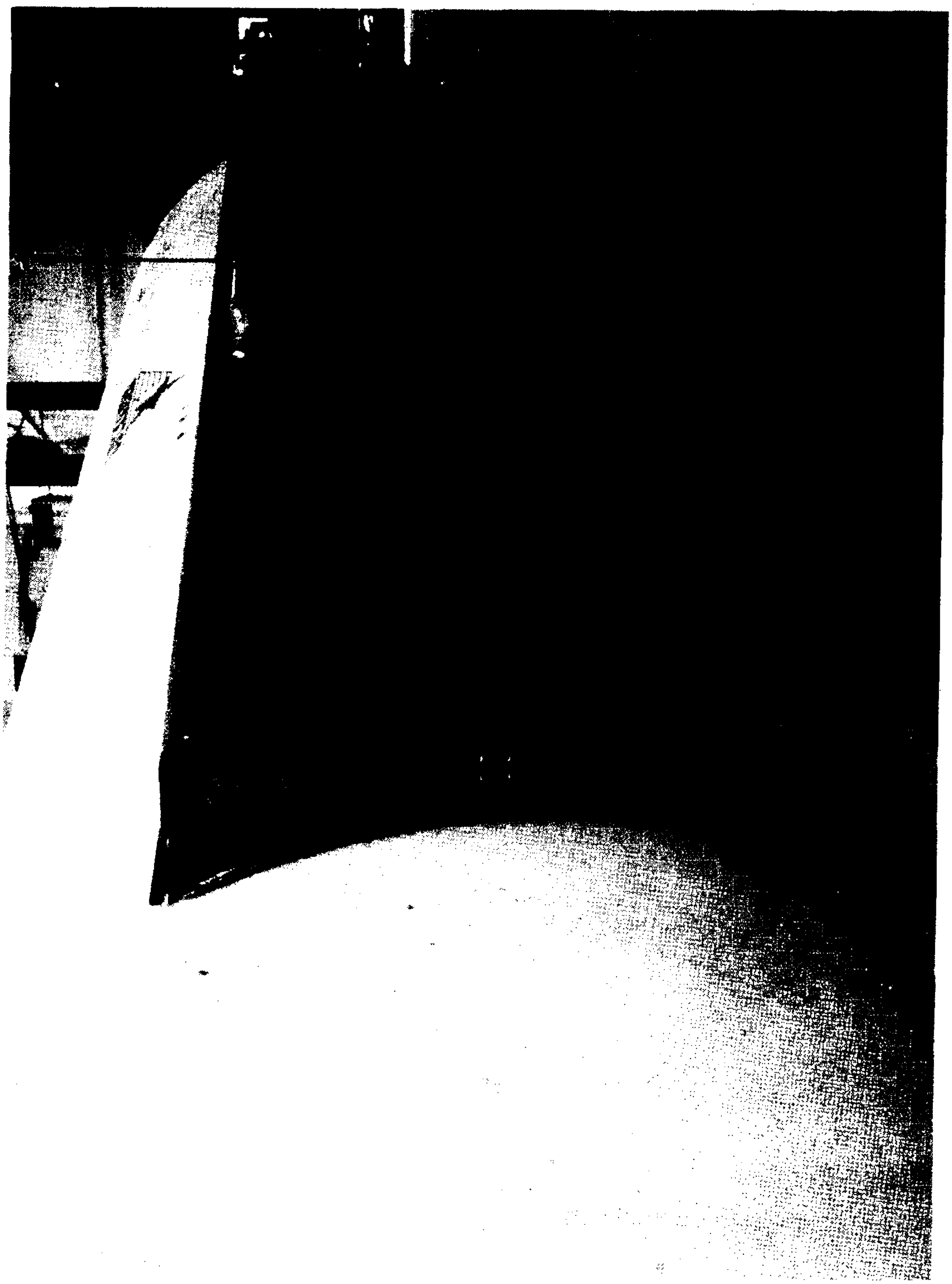

Figure 2.1.1.20 FAIRING THERMAL - SEPARATION TEST

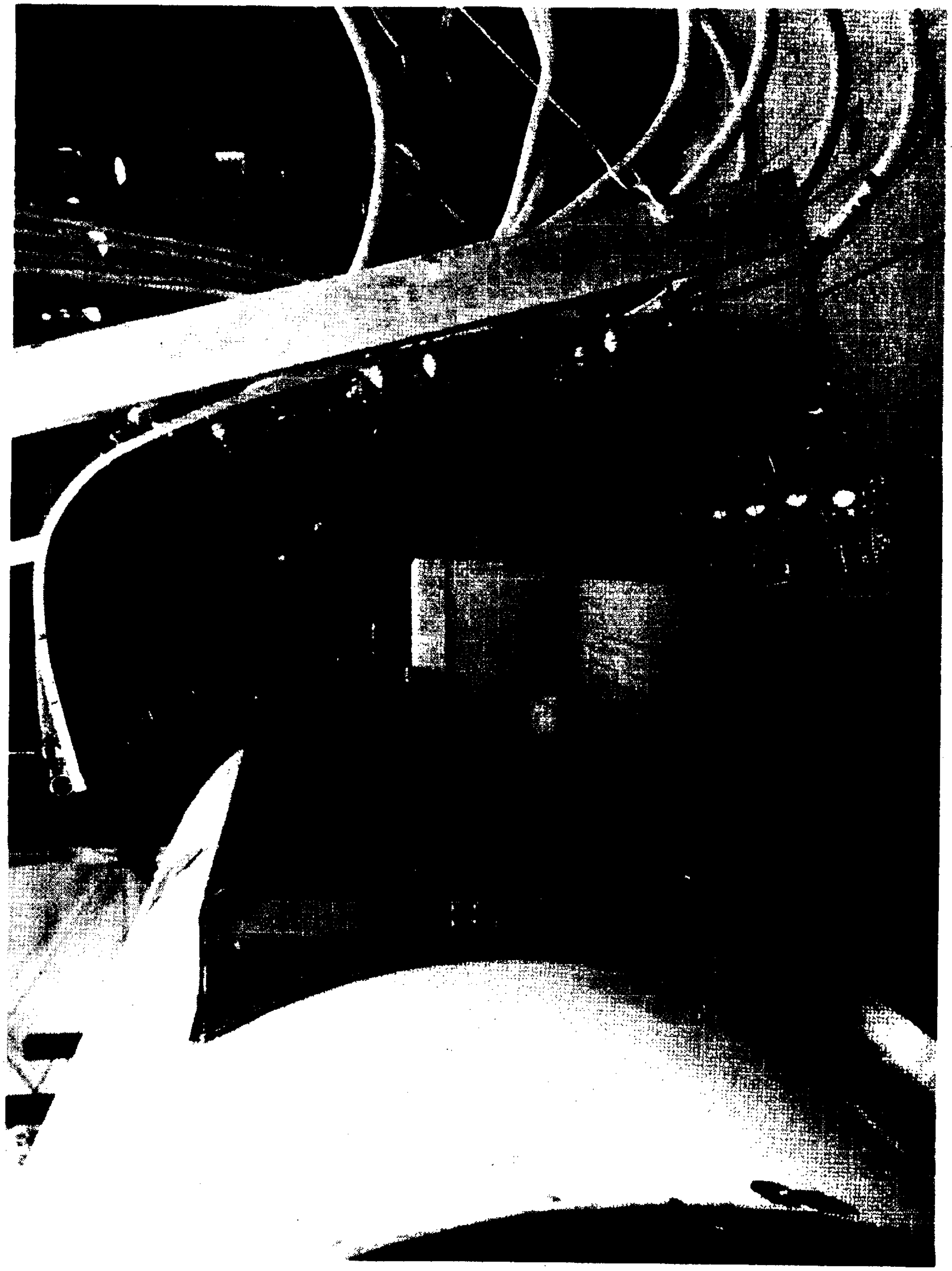

Figure 2.1.1.21 FAIRING THERMAL TEST - HEAT LAMPS

The sequence of testing was the same as the flight sequence. Three successful test runs were made. Three 200 frame/second 16 MM cameras recorded the separation characteristics of the fairing. The film data was reduced and the terminal velocity was found to be 27.5 in/sec. in the X direction and 22.0 in/sec. in the Y direction. These test results indicated that the fairing would not strike the vehicle after separation.

Ref. 1 - IDC SW/40.429, to [redacted] from [redacted], dated 8 November 1963, "Static Qualification Test Requirements for Program [redacted] Vehicle 45205-2355".

Ref. 2 - IDC SSD/227, to [redacted] from [redacted], dated 17 January 1964, "Revised Dynamic Test Requirements - Vehicle 2355".

Ref. 3 - Structures report SS/825/5522, dated 24 August 1964, "Results of Dynamic Qualification Tests Conducted on the Vehicle 2355 Forward Auxiliary Rack Structures".

Ref. 4 - IDC SW 40.520, to [redacted] from [redacted] dated 26 March 1964, "Revision to Static Qualification Test Requirements for Program [redacted] Vehicle 45205-2355".

Ref. 5 - IDC TSS 343-17, to [redacted] from [redacted], dated 23 January 1964, "Temperature inputs to Vehicle 2355 Separation and Heating Test".

2.1.2 Electrical Power Subsystem

2.1.2.1 Subsystem Description

Simplified Schematic - A simplified schematic of the 2355 Electrical Power System is shown in Fig.2.1.2.1. Three Type 1-D primary batteries are provided as a power source during ascent and orbital operation. A fourth battery, Type VI-A, is provided for recovery pyrotechnic events and the Lifeboat backup recovery system. Two of the Type 1-D batteries are located in the Agena vehicle and the third 1-D battery is located in the payload section. The payload battery is also utilized as a pyrotechnic power source for ascent functions, being diode-isolated from the vehicle batteries at that time. In orbit, the three batteries are connected in parallel as a single source for Agena and payload operation.

Telemetry instrumentation of battery parameters includes voltage, current, amper-hours, and temperature. The payload battery performance is monitored by Ampere-Hour Meter #2 and the C179 shunt. The two vehicle batteries are monitored by AHM #1 and the C4 shunt. Assuming normal current division between the batteries, AHM #1 will step at a rate twice as fast as AHM #2. Total power consumption is the sum of the two Ampere-Hour Meters.

Vehicle Power Conversion Equipment consists of a 400-cycle three-phase inverter Type XII, and two DC/DC converters,

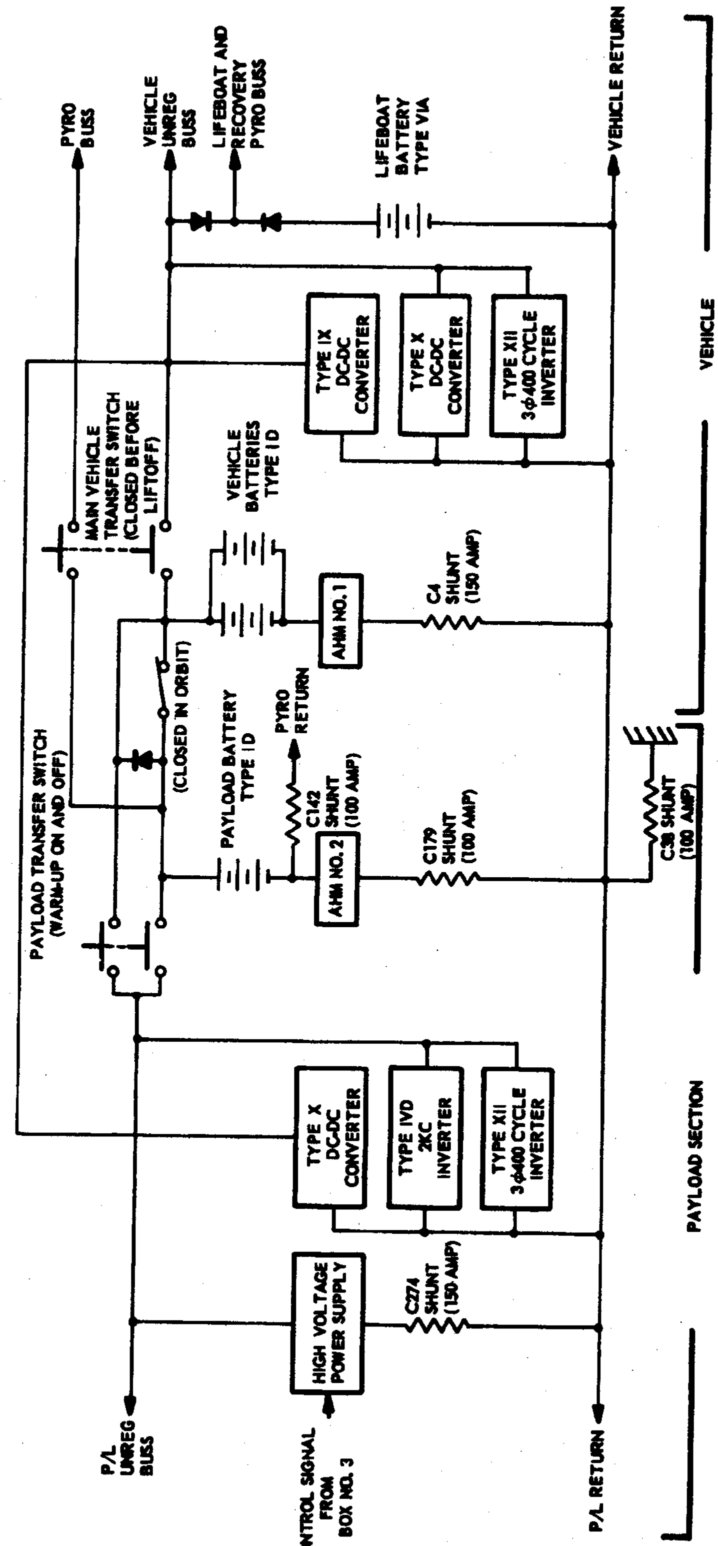

Figure 2.1.2.1 Simplified Schematic 2355 Power System

Types IX and X. The Type IX converter is the basic Agena regulated power source for guidance components. The Type X converter is utilized for certain Communications and Control components and as a telemetry excitation source for all subsystems.

Payload Power Conversion Equipment consists of a 400-cycle three-phase inverter Type XII, a 2000 cps inverter Type IV-D, a DC/DC converter Type X, and a high voltage power supply. These units are located in the payload cylindrical rack and provide the total regulated power to payload components. The Goodyear payload units require no unregulated power. The high voltage power supply is provided with an input power shunt (C274, 150 amp) for current monitoring on telemetry.

Subsystem Operation and Control - Prior to lift-off the Main Vehicle Transfer Switch is closed, connecting the vehicle and payload batteries to the vehicle and pyro busses, respectively. When the transfer switch is closed, both Ampere-Hour Meters are automatically reset to zero. All Vehicle Power Conversion equipment at this point is operating from battery power and will operate continuously until the end of the mission. The Payload Type X DC/DC Converter is also connected to the vehicle buss and operates continuously. Near the end of the ascent sequence, the isolation diode between the vehicle and payload batteries is bypassed, connecting the three batteries in parallel for orbital operation.

On orbit the Payload Power Conversion equipment is activated (with the exception of the Type X DC/DC Converter which is on continuously) by closing the Payload Transfer Switch. This is effected by an Orbital Programmer Brush 7 or 8, Payload Warmup. Additional switching of regulated power is executed by payload relays in the Power Control Unit and the Recorder. The High Voltage Power Supply "ON" signal originates in the transmitter and is the result of an "Operate ON" command. After receipt of this "ON" signal, a nominal 5-second delay precedes the high voltage output.

In the event a high voltage overload should occur, a protective circuit will turn off the supply output for a nominal 5-second interval; then the high voltage will be reapplied to the load and, if the overload condition has been removed, normal output will be restored. If the overload is sustained, the supply will continue to cycle at 5-second intervals until the overload is removed.

At the end of a payload "active period" the Payload Transfer Switch is opened, switching off all Payload Power Conversion equipment with the exception of the Type X DC/DC Converter. The switch is opened by an Orbital Programmer Brush 4 or 2, Payload Warmup Off.

2.1.2.2 High Voltage Power Supply Development

Development - Early work on design concept and approach to develop a High Voltage Power Supply to meet special Program requirements was underway in June 1963.

In July 1963, technical proposals were evaluated by Engineering to select a vendor to design and package the supply in accordance with the design specifications and drawings. Proposals were received from three Vendors from which Lear-Siegler and Engineered Magnetics were selected to submit a working breadboard of their design. These breadboards were delivered during the month of October 1963 and were tested and evaluated with a prototype payload system. Both units showed satisfactory results and were acceptable for electrical parameters. In the final evaluation, Lear-Siegler Corporation was selected over Engineered Magnetics Corporation to package their design for further compatibility and qualification tests.

The deciding factor in selecting the Lear-Siegler Corporation was the ability to support schedule requirements. One of the major differences between the two designs was in the choice of output circuitry. Engineered Magnetics' approach was for a single output transformer with multiple windings; Lear-Siegler used multiple "C" core transformers connected in series on the output.

The first package from Lear-Siegler was an engineering model delivered in December 1963. After compatibility tests were satisfactorily completed, the follow-on units were started. The first two of the production units were scheduled for qualification testing.

The power supply (Part Number 1464240-1) is designed to deliver a regulated output of 4400 VDC at 0.460 amps from a 22-29 VDC unregulated source. It has the special features of output short circuit protection, input overvoltage protection, output current monitoring and limited redundant operation. The external dimensions of the power supply are 18" long, 12" wide, and 9" high with an overall weight of approximately 58 pounds.

Printed circuit boards and modular construction are used in the internal design. All transformers and critical high voltage areas are potted in epoxy compound. All exposed terminals and connections are conformal coated. The overall construction is so arranged that the majority of components are readily accessible for easy repair.

Qualification Testing - Construction for the follow-on units began late in December 1963. The first two of seven units total were to be used for qualification testing. Qualification testing started in February 1964. The power supply was subjected to the qualification tests as outlined in the qualification test procedure. The data in the qualification test report showed that this unit passed all tests without failure or deviations from the specified performance limits.

Prior to the completion of this Qualification Test period, the second unit which was to be used for additional qualification testing was needed for electrical payload test at LMSC. It was shipped in March 1964.

Qualification testing on the second unit was delayed until June 1964. This delay was caused by a program change which affected the general construction of the supply. The new or changed configuration qualification test power supply was subjected to the same qualification test levels as the first supply. There were no failures or deviations on the new configuration. This completed the requirements for environmental conditioning.

Design Changes - At the end of February, requirements were issued to eliminate all incidence of corona within the power supply when the unit was operating from sea level to flight altitude. Special tests were run on the design approaches for the corona elimination.

The first approach was to use a metallic covering which was painted on the corona emitting surface. Several compounds were used in this test. One was a graphite type of material and the other was a metallic epoxy. Both types proved to be unsuccessful. The graphite material sublimed under altitude pressure covering all surfaces. The epoxy paint flaked and chipped when leads were moved or dressed for soldering leaving voids on the surface.

The second approach was to can individual output transformers and rectifier assemblies and completely encapsulate with epoxy compound. This proved to be successful. The final redesign effort included canning of individual output transformers, rectifier assemblies and output AC filtering components. Shielding of leads and potting of all high potential leads and terminations was accomplished at this time. The electrical design was not changed during the above modifications. However, minor changes were made during the manufacturing of the follow-on units.

These changes were necessary due to subsequent failures which will be mentioned in the individual case history discussion.

Test Programs - Each power supply received acceptance testing at the Vendor's. These normal tests consist of electrical performance, low level vibration and a programmed 68-cycle altitude test.

Due to a series of failures of high voltage breakdowns during checkout procedures, it was necessary to conduct a series of special altitude tests at LMSC. The purpose of these tests was first to determine the cause of failure and secondly to obtain a level of confidence before flight. These tests were performed on supply number three and repeated on supply number five and six.

Each unit was subjected to 68 duty cycles at a pressure of 100 microns. The supply was operated under two load conditions, full load and half load, for a period of ten minutes ON and twenty minutes OFF for each duty cycle.

The results of these tests caused a change in potting compound around all high voltage terminations. (Refer to individual case histories for Units #3 and #5 for detail test results.) These tests proved the reliability of the unit under adverse conditions.

A special qualification test was performed on the High Voltage Capacitor used in the output of the converter. This capacitor was classified as a critical item due to a failure early in the test period. In August 1964, four high voltage capacitors of two configurations were subjected to vibration shock, temperature, altitude, overvoltage and stress tests. The level of magnitude was in accordance with 6117B, an LMSC qualification test document and the Design Specification of the Power Supply.

All capacitors successfully survived all tests except for one unit which was damaged during low temperature tests. The type of failure was a decrease in capacitance and an increase in leakage current.

Individual Case History - Additional changes were made during manufacturing of the follow-on units. These changes were necessary due to subsequent failures on different units. The units will be classified in two configurations, Configuration "B" and Configuration "C". These concur with the latest design specification change.

Unit #1 Serial #11593 - Configuration "B"

1. Number one qualification test unit.
2. Sustained all environmental qualification levels.
3. Shipped to LMSC on 1 April 1964.
4. Failed Capacitor C141 during payload testing (preliminary run).
5. Returned to Vendor for repair, 10 April 1964.
6. Replaced Capacitor with an improved design.
7. Returned unit to LMSC.
8. To be used as a test model.

Unit #1 is the old design. Transformers and high potential leads are not potted. Altitude testing lower than 10 microns is not recommended.

Unit #2 Serial #111632 - Configuration "B"

1. Shipped on 9 March 1964.
2. Tested with payload and verified operation was successful.

3. Failed a regulator module.
4. Used for follow-on testing with restricted input.

The unit operated successfully with the payload and subsequently failed. One regulator module failed power transistors and the associated high voltage rectifier block. The failed section was disabled and the unit put back in service with restricted input voltage levels. Possible cause of failure was due to parasitic oscillations due to improper wiring. No repair is scheduled for this unit.

<u>Unit #3</u> Serial #113985 - Configuration "C"

1. Formal vendor ATP includes altitude tested for 68 cycles at 10 microns.
2. Unit shipped in June of 1964.
3. Altitude tested with payload LMSC.
4. High voltage breakdown, C141 area.
5. Unit returned for repair.
6. Altitude tested at Vendor - 68 cycles, 10 microns.
7. Returned to LMSC.
8. Altitude tested at LMSC - 68 cycles at 100 microns.
9. Total number of test cycles = 204.

Unit #3 was the first unit manufactured to the "C" revision, which required elimination of all corona. During altitude load testing at IMSC, the unit developed intermittent high voltage dropouts.

Arrangements were made to altitude test the unit with externally connected dynamic load. During the first hour of testing the unit demonstrated the same failing conditions. Investigation showed that the failure was due to an insulation breakdown around the insulator on the high voltage output capacitor. The failure was attributed to insufficient bonding of potting material. Corrective action was to:

1. Abrade the insulator on the high voltage capacitor for better insulation adhesion.
2. Change the type of potting material from epocast to scotch case, the latter having a longer pot life.
3. Encase all high voltage connecting wires and terminations.

Unit #4 Serial #114626 - Configuration "C"

1. Unit shipped on 24 July 1964.

Unit #4 was used as the second qualification test unit. The unit passed all environmental levels of testing without failure. It will be used for ground and altitude load testing. Unit #4 contains all modifications.

Unit #5 Serial #114538 - Configuration "C"

1. Formal vendor ATP includes altitude testing at 10 microns for 68 cycles.

2. Unit shipped 15 July 1964.
3. Altitude tested at LMSC at 100 microns.
4. Potting failure at 11 cycles during above test.
5. Returned to vendor and repaired. (The potting compound in the high voltage channel was changed to scotch cast.)
6. Altitude tested at vendor's plant, 10 microns for 68 cycles.
7. Unit returned to LMSC.
8. Retested unit at altitude 100 microns for 68 cycles.
9. Completed system and compatibility test.
10. Intermittent line capacitor C-1, dc input line.
11. Unit returned to vendor for repair.
12. Unit altitude tested at vendor's plant, 10 microns for 68 cycles.
13. Unit returned to LMSC.

This unit has been tested for a total of 215 cycles. During the cycling period high voltage was ON for a 10-minute period each cycle.

Unit #5 has had two repairs:

1. During the first altitude test performed at LMSC at 100 micron level, the epocast material in the high

voltage channel punctured. It was repaired by repotting with scotch cast.

2. The second repair was to replace an intermittent capacitor C-1. At normal input voltage the power supply operated satisfactorily, but when input resistance measurements were made, the results did not agree with the previous measurements. Investigation showed that one capacitor was low in resistance. In addition, a zener diode CR115 was replaced with one of higher wattage capacity. Units, numbers 6 and 7, have the above change.

Unit #6 Serial #115326 - Configuration "C"

1. Unit shipped on 18 September 1964.
2. Unit altitude tested at vendor, 10 microns for 68 cycles.
3. Unit altitude tested at LMSC 100 microns for 68 cycles.
4. Replaced CR115.
5. Used on 2355 flight successfully.

Unit #7 Serial #115326 - Configuration "C"

1. ATP at vendor - altitude tested at 10 microns for 68 cycles.
2. Unit shipped to LMSC on 22 October 1964.
3. Replaced CR115.

2.1.2.3 Battery Testing and Development

Battery History - The early configuration of the 2355 Power System required the development of a high current battery to supply the payload. This battery, located in the payload section, in conjunction with two 1-D Batteries located in the vehicle were to provide the total mission requirements. Two significant events during the development phase affected this early configuration. The first item was a reduction of power required by the payload. This factor opened discussion of alternate configurations and most significantly, the possibility of using existing batteries to supply payload requirements.

Initial Battery Testing - A series of battery surge tests was initiated in early June 1963 to determine voltage, current and temperature characteriestic of 1-A and 1-D batteries. The results of these tests are summarized below:

Five primary Silver-Zinc batteries, 2 Type 1-D and 3 Type 1-A, containing Eagle-Picher Type 2598 cells were discharged at rates up to 100 amperes over a temperature range of 30° to $125^{\circ}F$. Voltage and activated stand characteristics limit effective operation to the 45° to $100^{\circ}F$ range.

These primary batteries were tested to obtain data on their surge capability at various temperatures. The 1-D units had been in dry storage for approximately one year and the 1-A units for approximately three years prior to activation. The batteries which were tested and the corresponding ambient temperatures are as follows:

Battery Type	Serial Number	Temperature °F
1D	38	30
1A	298	45
1A	291	70
1A	297	100
1D	41	125

Each battery was discharged according to the following sequences with minor deviations as dictated by test conditions:

- 25 amperes for 15 minutes
- 1/2 ampere for 75 minutes
- 50 amperes for 15 minutes
- 1/2 ampere for 75 minutes
- 75 amperes for 15 minutes
- 1/2 ampere for 75 minutes
- 100 amperes for 15 minutes

The sequence was repeated four times per battery during the day. The overnight discharge rate was 1/2 ampere.

The temperature was monitored by nine thermocouples located externally on the battery case, and internally between cells and on a connector strap. Battery voltage was recorded continuously and cell voltages were recorded at regular intervals during each discharge.

The five batteries were activated, allowed to stabilize at the preset temperature and discharged according to the sequence outlined above. Minimum voltages and maximum temperature rises obtained during discharge at various rates and ambient temperatures during these tests provided the data shown in Fig. 2.1.2.2

The tests showed that batteries containing Eagle-Picher's Type 2598 cell are capable of repeatedly delivering 15 minute discharge of up to 100 amperes. Temperature range was 45° to 125°F. At higher temperatures cells could develop internal shorting, and at lower temperatures the voltage under load could drop below 20 volts.

It was recommended that flight operation be limited to 70° to 100°F, to minimize possibility of shorting cells and to assure operation above 22.0 volts.

This series of Battery Tests resulted in a decision to use three 1-D type primary batteries to supply the payload requirements.

Anechoic Test (2356) - Vehicle 2356 was operated in the Anechoic Chamber for a full mission life. Three new 1-D batteries were installed in flight position to power the system. Operation of the vehicle up to approximately Pass 47 was normal, with balanced current from the three batteries.

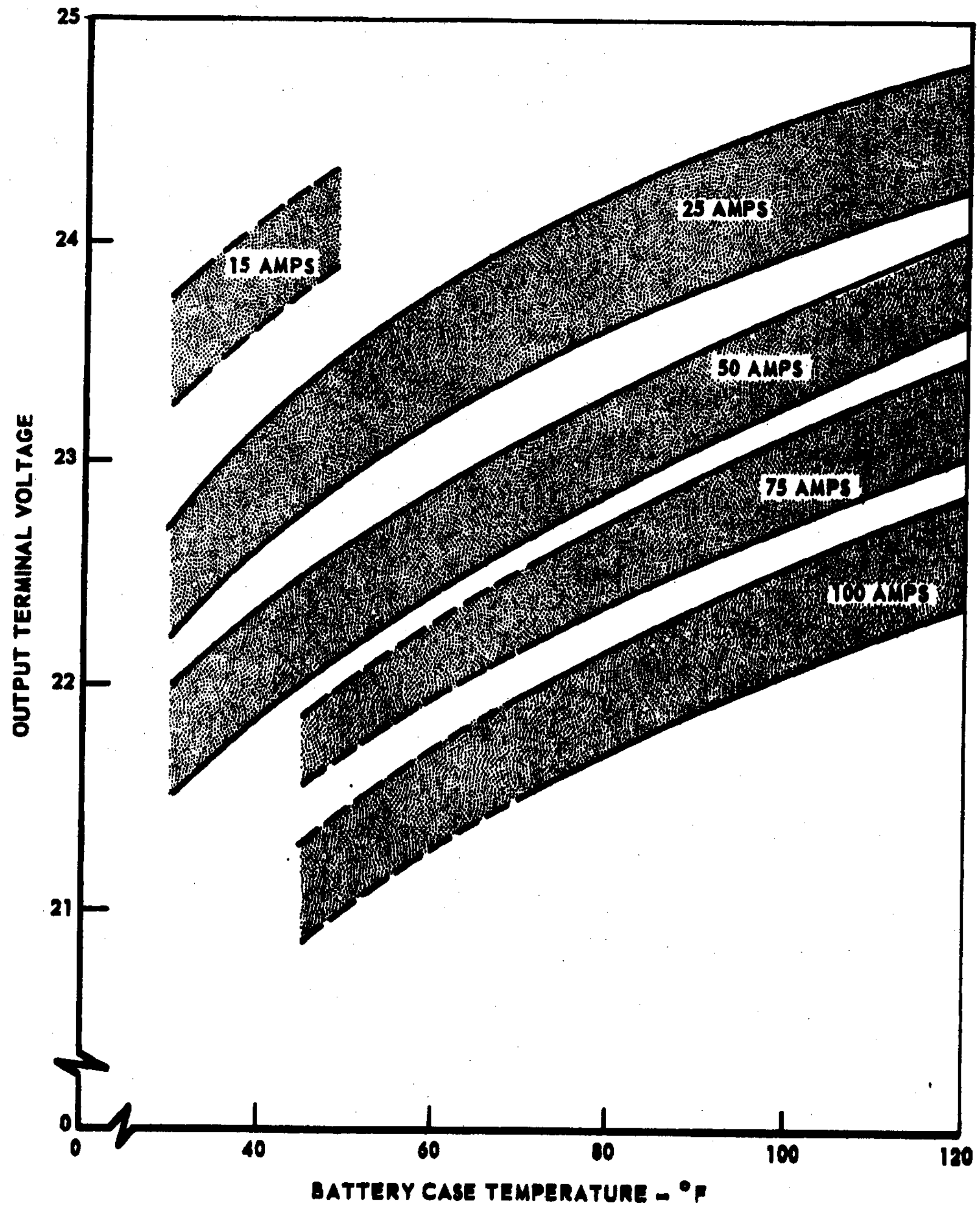

Figure 2.1.2.2 Current Loading Curve "ID" Type Primary Battery

Beginning with Pass 47 and continuing until Pass 71, the current became unbalanced with the forward battery carrying approximately 40 to 50% of the load. The shift in load is attributed to a shorted cell in a battery at Pass 47. Analysis of the batteries after the test revealed one battery had a shorted cell with approximately 100 amp-hours capacity remaining. The other two batteries were depleted. The reason for the short has never been proven conclusively, however, excess electrolyte accumulating on cell separators is the most probable cause. This test showed the effect of operating payload with batteries in the peroxide region, in that the first operate command lowered the bus to 22.7 volts while subsequent operates were above 23.5 volts.

Cell Evaluation at Elevated Temperature - Additional 1-D battery parameters were established in tests which were concluded in December 1964. Purpose of these tests was to determine the terminal voltage of the Type 1-D battery cells as a function of discharge current, temperature, and A/H capacity expended. Three Type 1-D battery cells were series-connected and maintained at $60^{\circ}F$, $80^{\circ}F$, and $100^{\circ}F$ respectively. The cells were subjected, cyclically, to current drains of 1, 2, 4 and 8 amperes for a period of 15 minutes at each current level.

The significant conclusions and development in this series of tests were the following:

- o The peroxide plateau will last longer at higher temperatures.
- o Curves were generated to predict battery voltage at various temperatures and degree of discharge. (See Fig. 2.1.2.3.
- o Internal impedance of 1-D batteries varies inversely with temperature.

Pre-flight Battery Conditioning - Special procedures were used during the activation, selection, and conditioning of the batteries used for the 2355 Flight. During activation, tests were made to limit cell voltage variance and to verify electrolyte absorption.

Three flight batteries were selected after studying the characteristics of the eight batteries activated for 2355.

To eliminate the possibility of low voltage during the first operate period, 50 amp-hours were removed from each battery during activation. This was done to bring the batteries down to the monoxide plateau where effects of battery temperature differences would have less effect on terminal voltage under load.

During the R-3 day RF tests and the countdown, the flight batteries were used to supply power to the vehicle. The

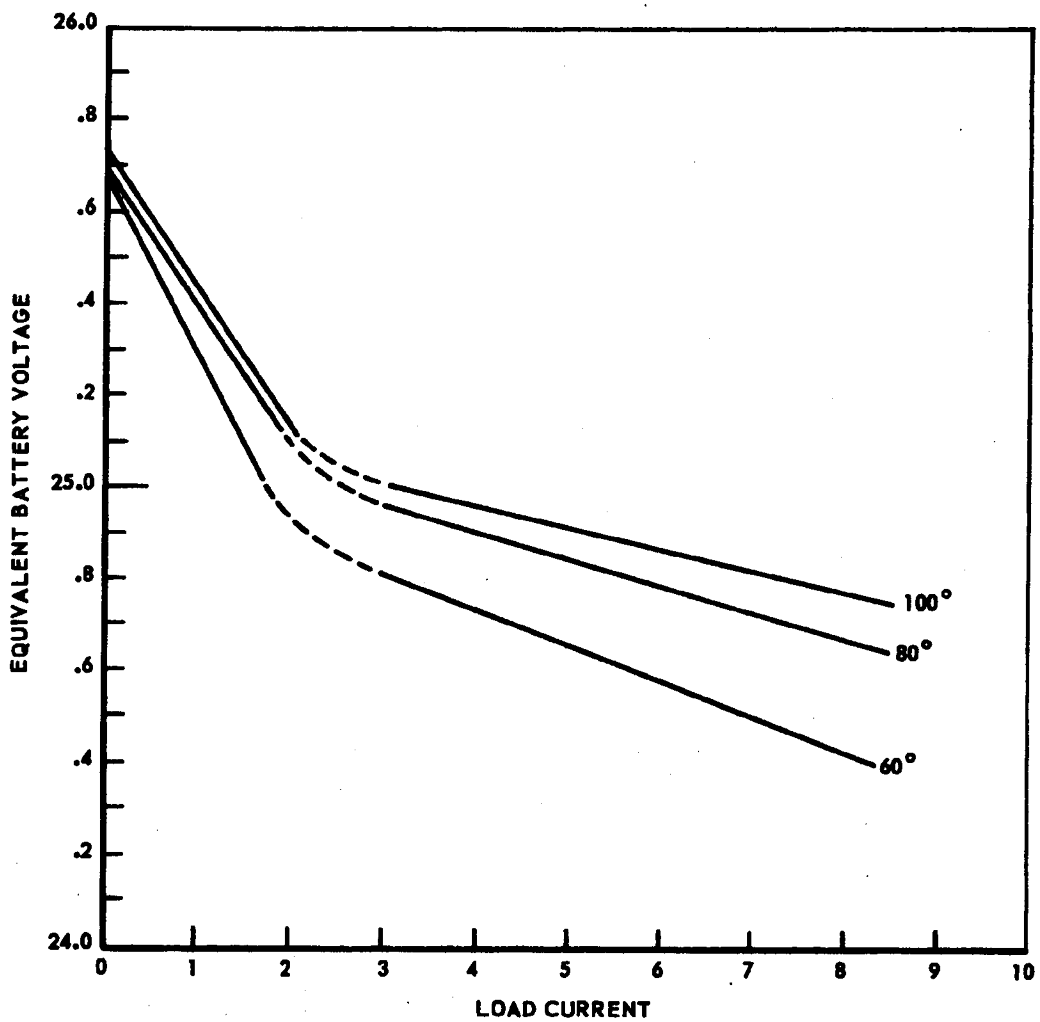

Figure 2.1.2.3 ID Battery Cell Test

batteries were maintained at approximately 70°F to prevent low voltage on the unregulated bus during the payload operation. Special air conditioning requirements were specified during countdown to keep batteries above 60°F at time of launch.

2.1.2.4 Design Change History

The design changes listed below represent significant additions or modifications to the Electrical Power System originated subsequent to initial engineering drawing release. A summary of each change is included, as appropriate.

Relocation of Type VI Battery to BTL Section - The Lifeboat battery was moved to the BTL section at the request of Orbit Thermodynamics. The reason for the move was to improve the thermo reliability of the battery and substantially reduce the Thermodynamics and Engineering effort.

Forward Pyro J-Box Modification (Created -503) - This modification moved the recovery pyrotechnic events from the pyro (payload) battery to the Lifeboat battery. This change would enable a Lifeboat recovery even if the vehicle batteries became depleted.

Forward Pyro J-Box Modification (Created -505) - This change removed parallel relay contacts used for the capsule "Arm" event to avoid a possible failure mode if one relay failed to actuate.

<u>Re-routing of Power Wiring to Reduce Magnetic Moment</u> - This change involved twisting the primary power wiring to reduce the magnetic moment produced during high-current periods of operation.

<u>Addition of Pyro Shield Grounds</u> - This change provided local grounding for pyro shields in the Cylindrical and Conical Racks, reducing the possibility of losing a shield ground through one of the electrical interfaces between the Forward Pyro J-Box and squib functions located in the payload areas.

<u>Addition of C-283 and C-284 Peak-Reading T/M Monitors</u> - The C-283 and C-284 peak-reading monitors are identical units which accept a 0-5 volt telemetry signal as an input and, for an unvarying input, produce a proportional output in the 0-5 volt range. If the input signal to the module contains a positive transient, a condition which would be undetectable on a normal commutated telemetry system, the peak-reading circuit will respond to the peak value of input voltage and decay slowly so that it may be easily detected via telemetry. The time constant of the decay is approximately 3 seconds (63% point).

Examples of input disturbances vs. output are shown below:

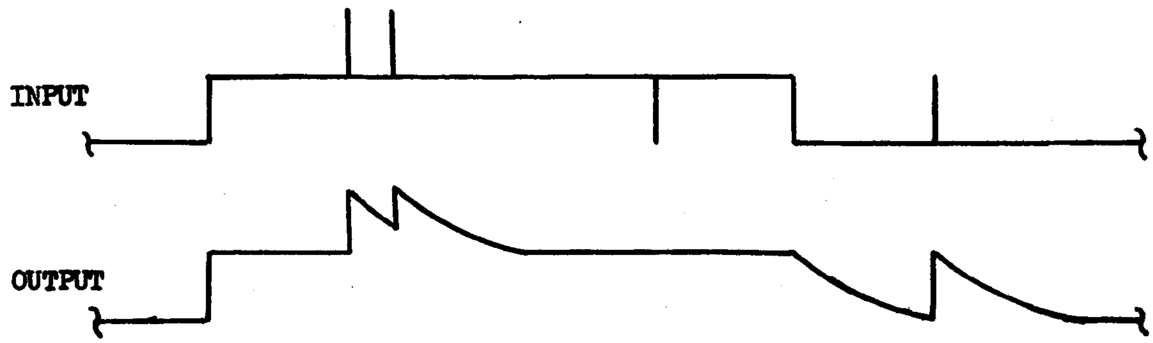

Note that the monitors respond only to positive transients.

The input to the C-283 peak-reading monitor is the output current monitor from the High Voltage Power Supply, C-275. Therefore, it is possible to determine the peak value of current surges drawn from the supply by evaluating C-283 on telemetry.

Similarly, the input to the C-284 monitor is the high voltage monitor, F-14. In the event the High Voltage Power Supply should fail to supply continuous output, and cycle at the normal 5-second intervals, it is possible to determine the voltage level at which the overload is occurring.

Payload Heater Addition - This change added heaters, wiring, temperature monitors for pre-launch temperature conditioning of payload equipment.

<u>Addition of 3Ø Compensating Capacitors</u> - The addition of capacitors to the 400-cycle 3-phase inverter output was required to decrease the waveform distortion to a satisfactory level during operation of the uncompensated payload drive motors. Values of capacity were chosen for a resultant power factor of nearly unity.

<u>3Ø Compensating Capacitor Modification and Addition of Isolation Diode</u> - In the course of altitude testing of the payload section in the TASC Chamber, a recurrence of the waveform distortion occurred. Investigation revealed that the RFI filters wired in series with each phase of the supply, located in payload power supply and recorder were leaking dielectric fluid. The filters, essentially a C-L-C arrangement, were apparently changing in capacitance with altitude. All 400-cycle RFI filters were subsequently removed from these units, which necessitated a realignment of the compensation required because of the removal of the capacitance in the filters.

The addition of a diode was required to isolate the payload and vehicle unregulated busses. In the event the payload buss should seek a level higher than the vehicle buss, excessive current would flow through a diode in the Type XII 3Ø Inverter resulting in failure of the diode. This failure occurred in two inverters prior to incorporation of an additional diode in the vehicle wiring, eliminating the problem.

Type X DC/DC Converter Programming Revision - To increase the reliability of the Type X DC/DC Converter, a revision was incorporated to hardwire the converter on at all times. Formerly it was switched on and off as required for payload operation or telemetry excitation.

2.1.3 Attitude Control Subsystem

2.1.3.1 Attitude Control Requirements - Orbital

Establishment of Attitude Control Requirements - Early in 1963, a number of discussions were held to consider the establishment of orbital attitude control requirements. Representatives of the [redacted] and Goodyear Aircraft Corporation, presented order-of-magnitude estimates of the requirements necessary for successful payload operation. Lockheed representatives presented estimates of the Agena S-01A capabilities in several configurations. The standard Agena, the standard Agena with minor modifications, and a basic Agena type system with major modifications (e.g. new horizon sensor and/or inertial reference package) were considered.

After due consideration of requirements, capabilities and costs it was mutually agreed by [redacted] Goodyear, the Air Force and Lockheed that the basic Agena system had sufficient capability to permit accomplishment of the mission objectives. Minor modifications of the standard system would be permitted to allow the system to be "pushed" to its maximum capability. It should be noted that at this time the magnitude of the problem of horizon sensor susceptibility to cold clouds was not known.

The Attitude Control Requirements - As a result of considerable analysis and analog computer studies the vehicle capabilities (and hence, requirements) were established. These are presented in tabular form.

Payload Operating:

Control Axis			Pitch	Roll	Yaw
Item	Units	Note			
Null Position	degrees	1	0	0	+/- 2.44
Bias Uncertainty	degrees	2	±0.4	±0.4	±0.4
Limit Cycle	degrees	3	±0.25	±0.25	±0.25
Body Rate	deg/sec	4	±0.002	±0.005	±0.003

NOTE 1: Vehicle body axes with respect to orbit reference axes. (See Figures 2.1.3.1 and 2.1.3.2.) The positive yaw bias is for North to South passes and the negative for South to North passes. The tolerance on the yaw bias is ±10%.

NOTE 2: Maximum value - These figures do not include any allowance for horizon sensor noise.

NOTE 3: Maximum value.

NOTE 4: Maximum average value.

Payload Inoperative:

No requirement other than compatibility with the system capabilities and other attitude control requirements.

Payload Duty Cycle and Mission Lifetime - One of the basic ground rules stated by the Customer was that the payload be operated only within the ZI (Continental United States) and within sight (±5° elevation) of either the Vandenberg or New Hampshire Tracking Stations. The mission life was to be four days maximum. For the selected orbit this meant there would be nominally four active (payload operate) passes each day (two each at VTS and NHS) or a total of sixteen passes. The payload operate times would vary from 1.25 minutes to 3.52 minutes with an average value of 2.16 minutes.

2.1.3.2 Program Peculiar Design Features

Payload Antenna Mounting and Vehicle Orientation - Structural interface considerations and the payload system requirements resulted in the payload antenna being mounted on the right side of the vehicle with the antenna boresight axis depressed 55° from the +Y axis. For this configuration a tail first orientation on orbit was desirable so that on the North to South west coast passes (16, 32, 48, etc.) the antenna ground swath would be overland. Additionally, the capsule recovery requires the Agena to be oriented tail first prior to pitch down. In order to minimize the time required for the complete recovery sequence and obtain the added ground coverage it was decided to yaw the vehicle around immediately after injection and fly tail first.

Horizon Sensor Relocation - The payload antenna structure obscured the optical field of view of the right side horizon sensor head in its normal location on the guidance module in the Agena forward rack. It should be noted that due to the physical size of the payload antenna and the geometry of the horizon sensor field of view interference would have occurred for any reasonable antenna mounting. After due consideration Structural Engineering decided to relocate the horizon sensor system in the program peculiar Auxiliary Guidance (BTL) Rack.

Improved Telemetry Resolution - The standard Agena Vehicle provides certain telemetry outputs as tabluated below. The resolution obtainable with these scale factors was not suitable for performance evaluation in view of the narrow deadbands. The addition of an auxiliary signal conditioning package (Secondary Guidance Junction Box) allowed for improvements as tabulated.

Telemetry Output Item	Standard	2355 Program Peculiars
Horizon Sensor - Pitch & Roll	$\pm 5^{\circ}$	$\pm 1^{\circ}$
Gyros - Pitch, Roll & Yaw	$\pm 5^{\circ}$	$\pm 1^{\circ}$
Gyro Torquers - Pitch	$\pm 10^{\circ}$/Min	0 to $+6^{\circ}$/Min
- Roll	None	$\pm 0.5^{\circ}$/Min
- Yaw	None	$\pm 40^{\circ}$/Min
Yaw Steering Monitor	N.A.	3 Levels

This package was available from a deactivated vehicle and required only minor modifications to satisfy the required needs.

Yaw Bias - This mission required a yaw attitude bias of plus or minus 2.44°. This is achieved by applying a torquing signal of proper polarity to the roll gyro in the Inertial Reference Package. Because of the Inertial Reference Package gains, a very low level signal was required to produce the desired yaw offset. This voltage level was 17 millivolts. In order to optimize the signal to noise ratio the attenuator was physically located near the Inertial Reference Package. There was no discernable noise on the signal during flight.

Deadbands - Orbital attitude control requirements dictated that the orbit deadbands not exceed ±0.25 degree. The standard Agena orbit deadbands are optional with the lower limit generally quoted as ±0.25 degree. The actual lower limit is determined by the inherent threshold of the D.C. amplifier in the Flight Controls Electronics Package. This lower limit is nominally ±0.1 degree but is subject to a maximum tolerance of about ±50%. The tolerance is composed of two parts, an uncertainty of about ±20% in the deadband magnitude plus a temperature dependent null shift of about ±30%. A nominal deadband of 0.15 ± 0.07 degrees was specified. The values measured in Vehicle Systems Test fell within the range of 0.14 to 0.19 degrees. The specific values are listed in Section 2.1.3.4. The standard Agena does provide for a coarse and fine (wide and narrow deadband) deadband selection on orbit. This feature is intended to permit the saving of control gas during the coarse mode while making available the tighter control of the fire mode when required. The actual control gas usage for a particular vehicle is dependent upon the mission life, the deadbands required and the fine to coarse duty cycle. For the particular case of vehicle 2355 the planned mission life was relatively short, the duty cycle high and the amount of control gas used in either case low compared to the amount loaded. For these reasons the decision was made to use a fixed deadband.

<u>Torquing Gains</u> - The control system analysis indicated the necessity of changing the horizon sensor torquing gains from the standard Agena settings. The reasons for this are discussed in Section 2.1.3.6. The standard gains are contrasted with the specified nominals below. The units are degrees per minute per degree.

	Standard Coarse/Fine	2355
Pitch	1.00/1.00	1.67
Roll	0.33/1.00	0.33
Yaw	0.67/8.00	1.67

These gain changes were accomplished with a potentiometer adjustment in the Guidance Junction Box.

Magnetic Compensation - Experience with other vehicles alerted LMSC to the necessity for carefully surveying all vehicles for sources of magnetic fields. The reason for this is that any magnetic field within the vehicle will react with the earth's magnetic field and result in a torque on the vehicle. A survey of the FTV 2355 configuration revealed three sources of magnetic fields which were sufficiently large to be of concern. Two of these sources were the permanent magnets in the BTL cannister and the payload Transmitter-Modulator. These sources required the installation of compensating magnets. The third source was a current loop (electro-magnet) in the forward rack wiring. The third source was eliminated by reconfiguring the wiring. An analysis of this situation is contained in Section 2.1.3.6.

Unbalanced Payload Momentum - Unbalanced momenta due to moving masses within the vehicle can result in significant vehicle motion. A survey of FTV 2355 revealed a potential problem due to the film motion. Subsequent analysis (see Section 2.1.3.6) indicated that corrective action was not required.

Horizon Sensor Noise-Horizon Sensor Disconnect - The problem of horizon sensor noise is quite complex and is covered in some detail in Section 2.1.3.6. For the purpose of this present discussion it is sufficient to note that at the inception of this Program LMSC was aware of the problem and the possible resulting degradation of the payload data. As a result of analyzing the situation it was decided to disconnect the horizon sensor outputs to the Inertial Reference Package during the payload operate periods. The disconnect occurred in conjunction with the payload ON command and the reconnect in conjunction with the payload OFF command.

2.1.3.3 The Standard Agena Orbital Attitude Control System

This section is intended to provide a very brief functional description of the standard Agena orbital attitude control system (OACS) for the reader unfamiliar with the system. The program peculiar revisions and additions incorporated in FTV 2355 did not fundamentally alter the system operation.

Axes Systems, Polarities and Vehicle Orientation - In order to minimize explanation of axes rotation and polarities at various points in the text to follow the conventions to be used will be explained. The vehicle body axes are fixed with respect to the vehicle and form an orthogonal right-handed system as depicted in Figure 2.1.3.1. Positive roll, pitch and yaw vehicle motion are defined with respect to these axes. This rotation is consistent with the telemetry output polarities of the three-body axis gyros and the two-horizon sensor outputs. Specifically, a positive vehicle displacement yields a positive telemetry output.

A set of orthogonal local orbit reference axes are depicted in Figure 2.1.3.2. The vehicle flew tail first on orbit with the +Z body axis nominally pointing toward the earth. The plane formed by the +X and +Y body axes was nominally coincident with the plane formed by the local flight direction and the orbital momentum vector. The vehicle was yawed (about the Z axis) either plus or minus 2.44 degrees at all times. The reason for this is explained in Section 2.1.3.6.

<u>Brief System Description</u> - The standard Agena orbital attitude control system (OACS) consists of four major components. They are a horizon sensor, an inertial reference package (IRP), an electronics package and a pneumatic system. See Figure 2.1.3.3. The OACS provides active three-axis control.

The horizon sensor system consists of two heads and an electronics package. Basically, each head contains a drive motor, a prism which is rotated at 30 revolutions per second and an infrared sensitive bolometer. The prism directs the field of view $37\frac{1}{2}^{\circ}$ away from the optical axis of the head. The rotation of the prism causes the field of view to describe a cone in space. The heads are mounted and aligned such that the field of view scans both space and earth on each revolution. The general configuration is depicted in Figure 2.1.3.4. The IR sensitive bolometers are alternately subjected to radiation from the cold space and the warm earth and ultimately provide square wave outputs which are processed to provide pitch and roll attitude information. The attitude determination can be functionally understood with the aid of Figure 2.1.3.5. The earth index (EI) pulse is generated each time the scan crosses the vehicle Y-Z plane. The EI is used to divide the energy in each square wave output into two parts as shown. The four sections can then be compared to yield signals proportional to the vehicle attitude. Referring to Figure 2.1.3.5 it can be seen that

Pitch Error $\propto \frac{1}{2}(B-A) + \frac{1}{2}(D-C)$, and

Roll Error $\propto (C+D) - (A+B)$.

It is also apparent that vehicle yaw motion does not affect the sensor. Yaw motion would rotate the scan patterns about the center of the search circle.

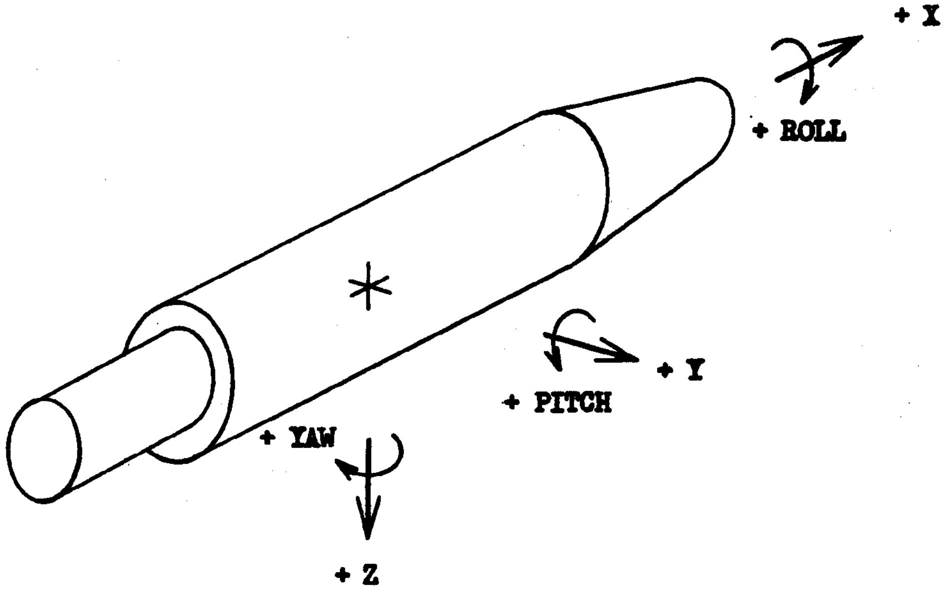

FIGURE 2.1.3.1 VEHICLE BODY AXES

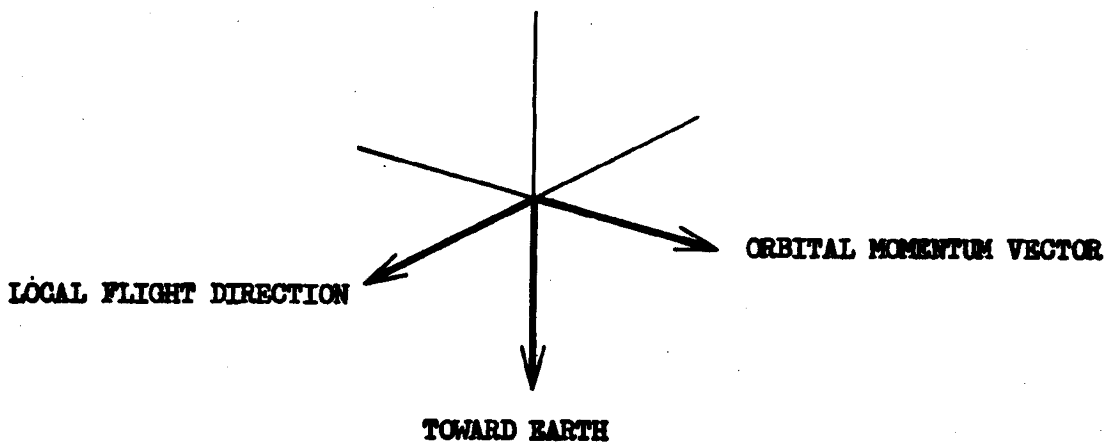

FIGURE 2.1.3.2 LOCAL ORBIT REFERENCE AXES

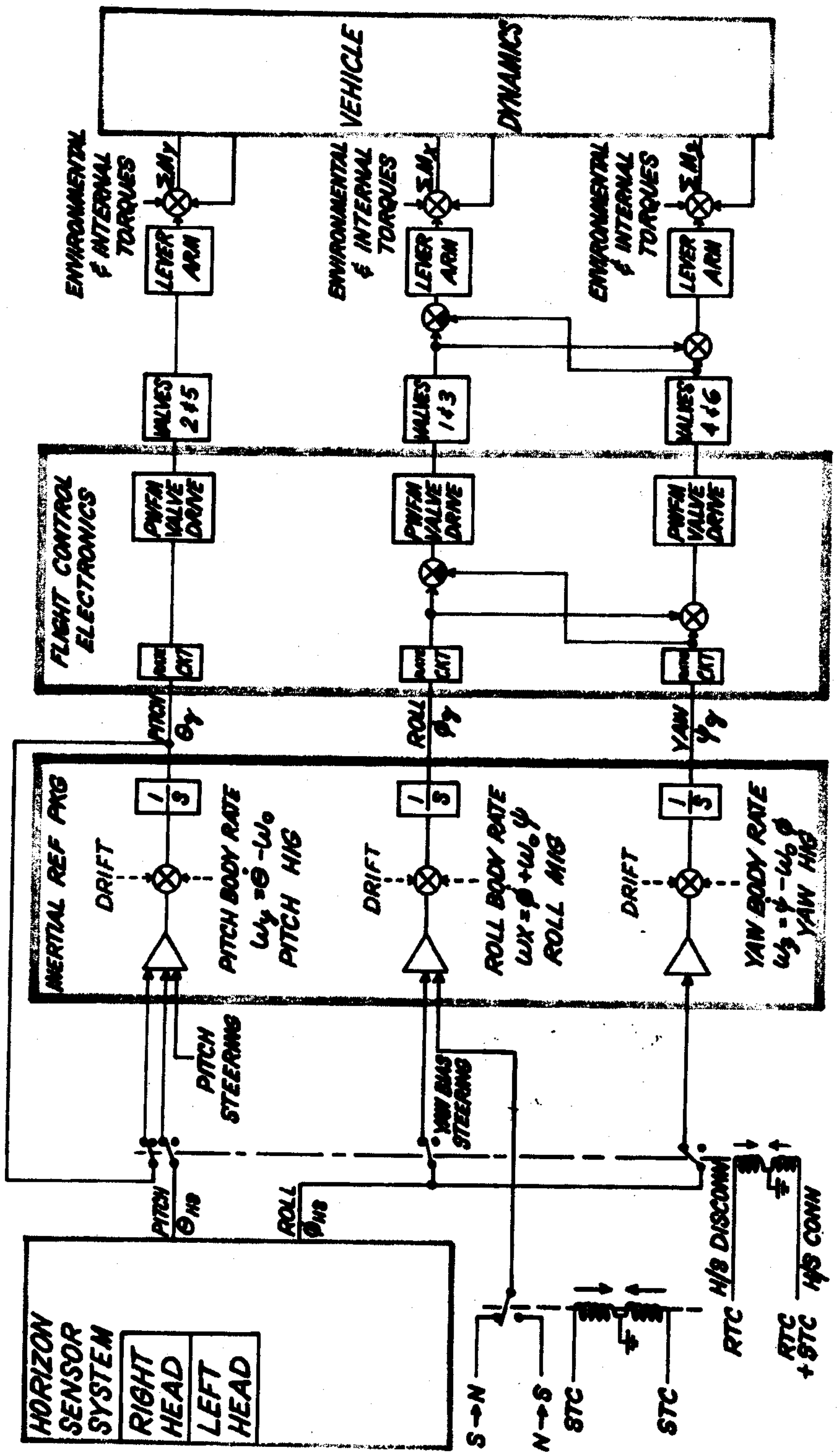

STC = STORED TIME COMMAND

RTC = REAL TIME COMMAND

FIGURE 2.1.3.3 ORBITAL ATTITUDE CONTROL SYSTEM

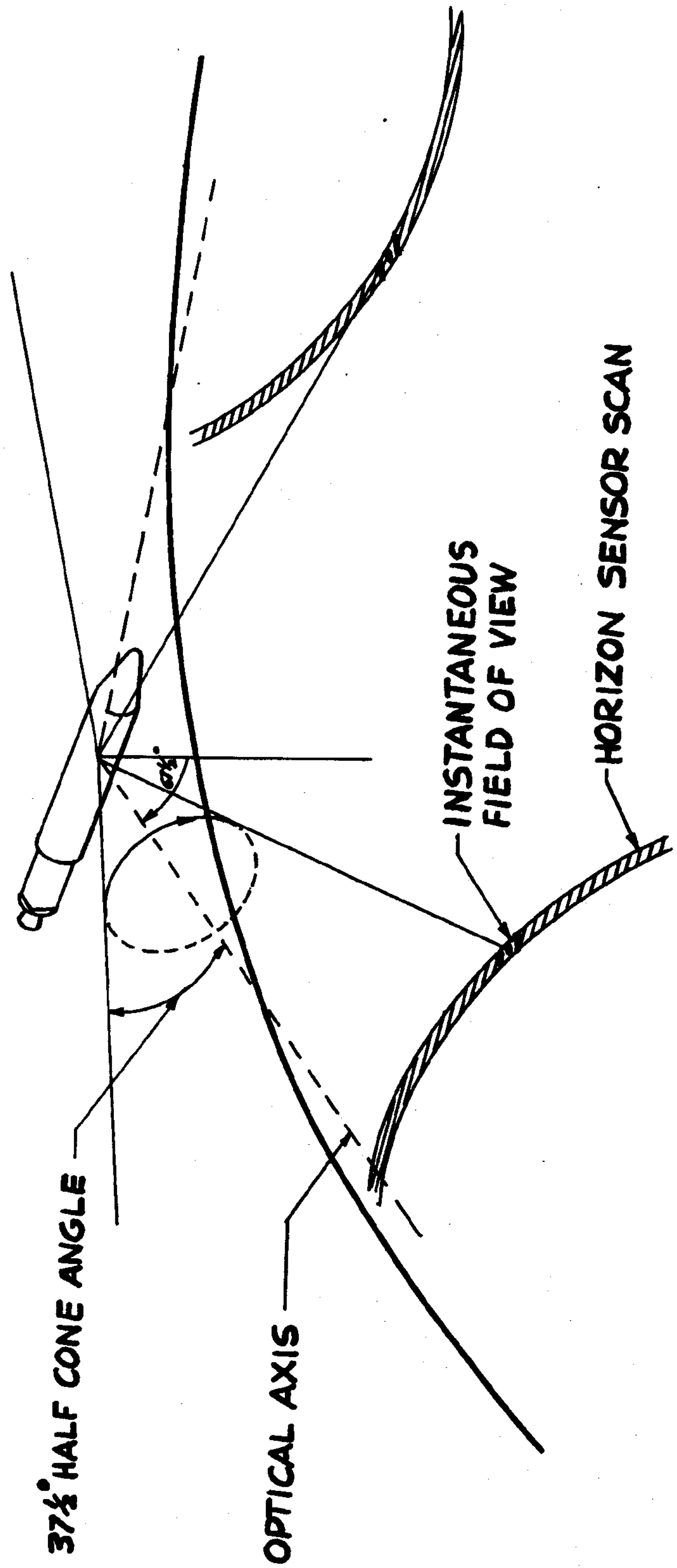

FIGURE 2.1.3.4 HORIZON SENSOR SCANNING

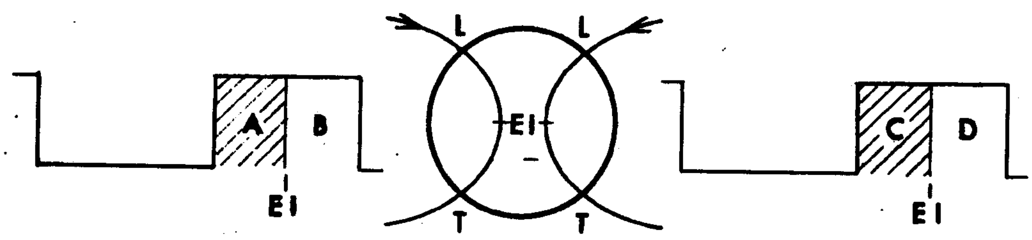

Zero Pitch Error,Zero Roll Error
A = B = C = D

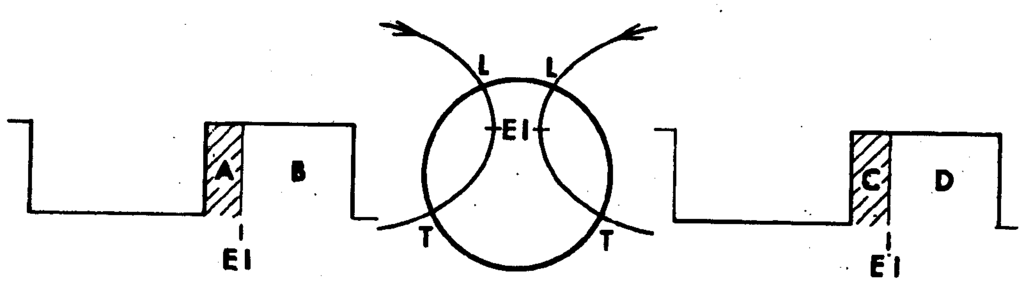

Positive Pitch Error,Zero Roll Error
B A,D C,A + B = C + D

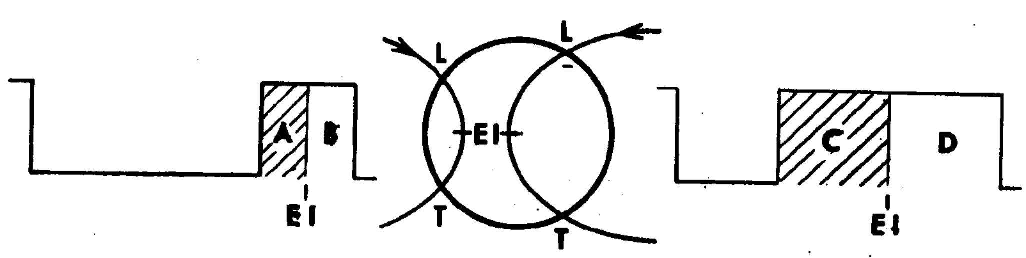

Zero Pitch Error,Positive Roll Error
A = B,C = D,C + D A + B

FIGURE 2.1.3.5 HORIZON SENSOR SIGNAL GENERATION

The inertial reference package (IRP) contains three rate integrating gyros. The three gyros are aligned with their input axes along the roll (X), pitch (Y) and yaw (Z) body axes of the vehicle. This type of gyro is then sensitive to the inertial vehicle body rate (degrees per second) input and yields the integral of rate or attitude (degrees) as an output. The pitch and yaw gyros are HIG (Hermetic Integrating Gyros) gyros and the roll gyro is a MIG (Miniature Integrating Gyro) gyro. Functionally, the three gyros are identical and differ only by their undesired random drifts. The HIG gyros are rated at 6 degrees per hour random drift and the MIG at 1 degree per hour. Each gyro is also provided with an input torquer so that electrical signals for attitude reference correction and vehicle steering may be accomodated.

The flight controls electronics package takes the three gyro output signals, processes them and generates signals to actuate the pneumatic valves. Initially the attitude signals are fed to a rate circuit which yields an output error signal which is proportional to attitude plus the derivative of attitude (or rate). The rate component in the error signal provides system damping. The error signals are then fed to pulse width frequency modulation (PWFM) circuits which in turn provide signals for actuating the pneumatic valves. The error signal mixing in the roll-yaw channel will be explained in a subsequent paragraph. The operation of the PWFM circuits may be understood with the aid of Figure 2.1.3.6. When the error signal value falls within the deadband there is no output from the PWFM circuit. When the error signal just exceeds the deadband the PWFM circuit supplies

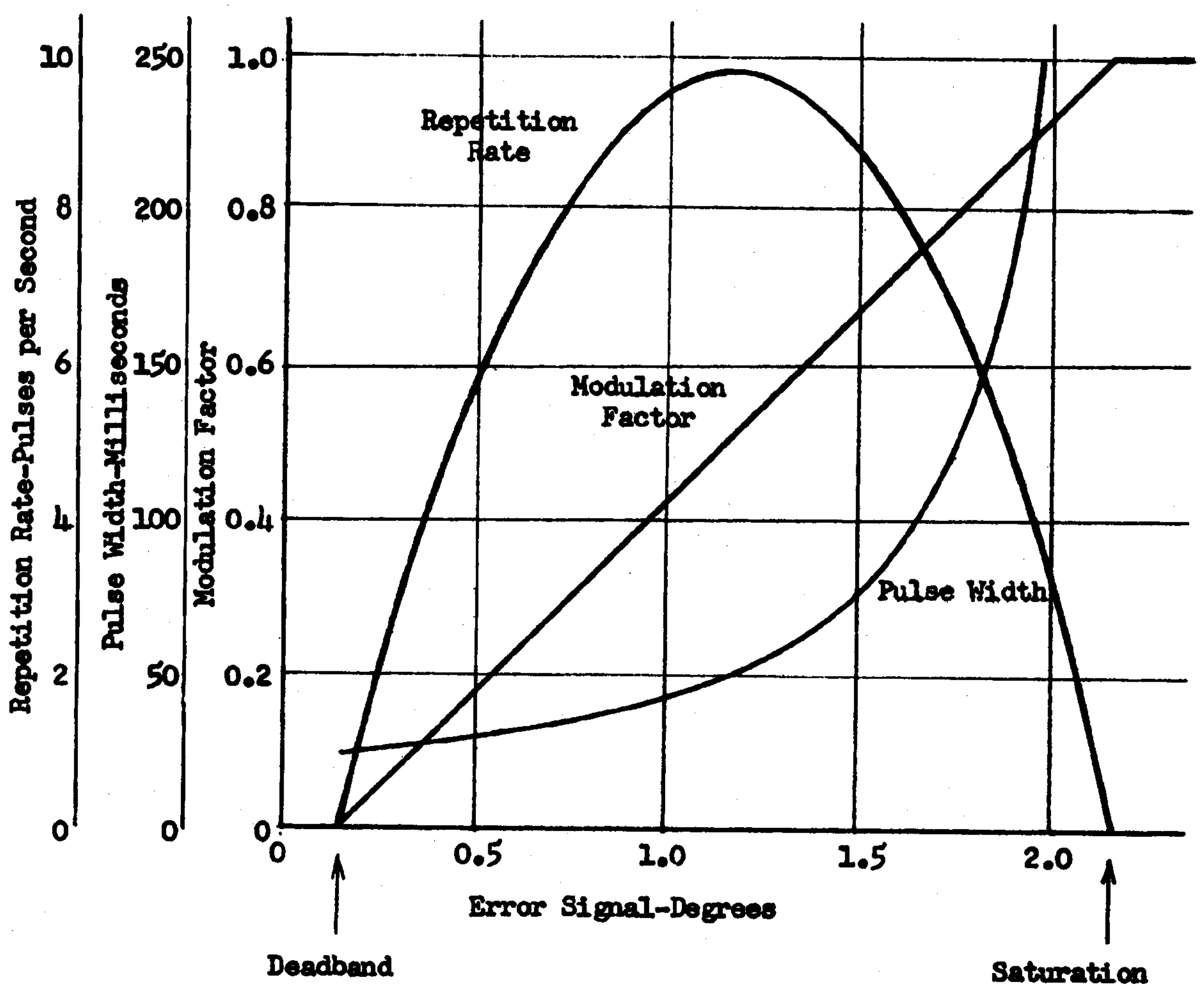

FIGURE 2.1.3.6 PULSE WIDTH-FREQUENCY MODULATION CIRCUITRY CHARACTERISTICS

narrow pulses (approximately 23 milliseconds wide) to the valve at a low repetition rate (one pulse every two seconds). As the error signal increases the pulse width increases and the repetion rate varies as shown. The error signal has a maximum effective value which corresponds to the valve being full ON continuously (saturation). The Modulation Factor is simply the product of Pulse Width and Repetition Rate. The Modulation Factor is proportional to the average valve thrust for any given error signal and thus the system is quite closely equivalent to a porportional system even though the valves operate as ON-OFF valves. While this is true for large disturbances (large error signals) it is not necessarily the case on orbit. In a low torque-low rate limit cycle design the error signal will not exceed the deadband by more than a few hundredths of a degree. In this situation the system appears as one with a constant pulse width and linear repetition rate.

The signal mixing in the roll-yaw channel is part of a system concept intended to reduce attitude control gas consumption and reduce the amount of pneumatic system hardware required. Consider the satellite configuration depicted in Figure 2.1.3.7. In this configuration the valves are positioned on the vehicle such that the reaction torque from any valve is solely about the control axis of interest, i.e.; there is no coupling. This configuration is not practical due to the structural design problems in locating the roll valves on the vehicle midbody. Secondly, the vehicle center of gravity shifts during the design phase and during the actual flight operation as well. Placement of the roll valves on the aft rack

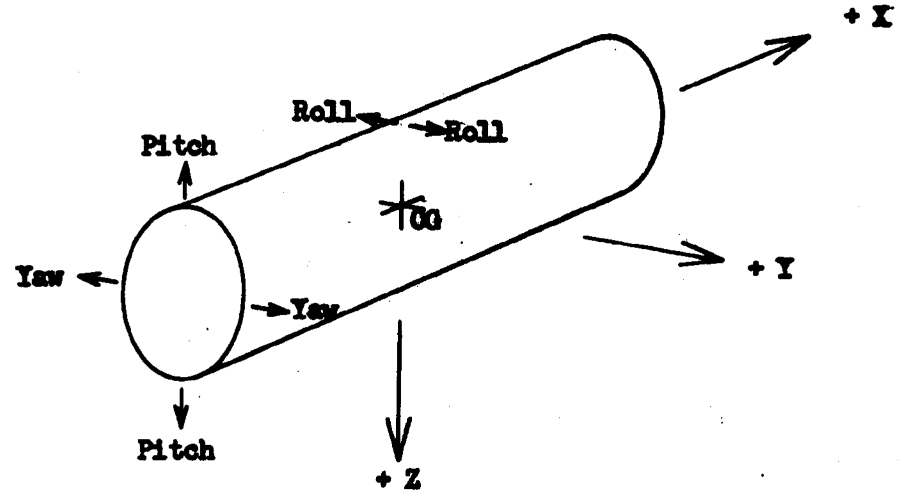

FIGURE 2.1.3.7 UNCOUPLED CONTROL TORQUE CONFIGURATION

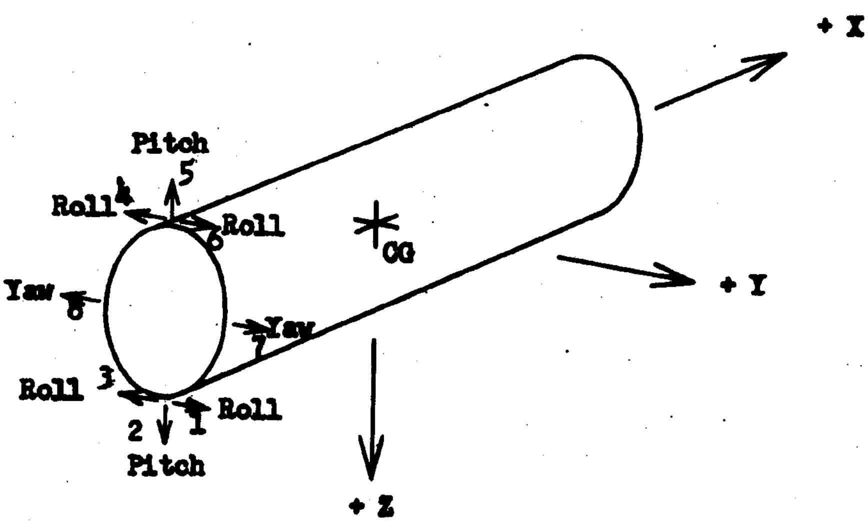

FIGURE 2.1.3.8 UNCOUPLED CONTROL TORQUE CONFIGURATION-AFT RACK MOUNTING

would require two additional valves if coupling is to be avoided. This configuration is depicted in Figure 2.1.3.8. In this configuration it is immediately apparent that the two yaw valves (7 and 8) can be eliminated if the parallel (1 and 6 or 3 and 4) roll valves can be actuated by the yaw error signal when required. This can be done and results in the standard Agena configuration where valves 1, 3, 4 and 6 are designated as roll-yaw valves. Direct actuation of the valves by the roll and yaw error signals independently could result in the unnecessary expenditure of control gas. This is illustrated by the following table:

Attitude Error	Valve(s) Actuated	Net Value Action	Value(s) Wasted
+Roll	3 & 6	3 & 6	0
-Roll	1 & 4	1 & 4	0
+Yaw	3 & 4	3 & 4	0
-Yaw	1 & 6	1 & 6	0
+Roll & +Yaw	3, 4, & 6	3	4 & 6
+Roll & -Yaw	1, 3, & 6	6	1 & 3
-Roll & +Yaw	1, 3, & 4	4	1 & 3
-Roll & -Yaw	1, 4, & 6	1	4 & 6

Simply stated the conclusion drawn from this table is that if both valves of an opposing pair are actuated simultaneously the net result is zero. This problem is precluded in the standard Agena by the signal mixing in the roll-yaw channel. Though this possible saving of gas may not be realized on any particular flight, the hardware simplification is significant.

The pneumatic system consists of two gas storage bottles, a two-stage gas pressure regulator, two-valve clusters of three valves each and the associated plumbing. The components are connected as shown:

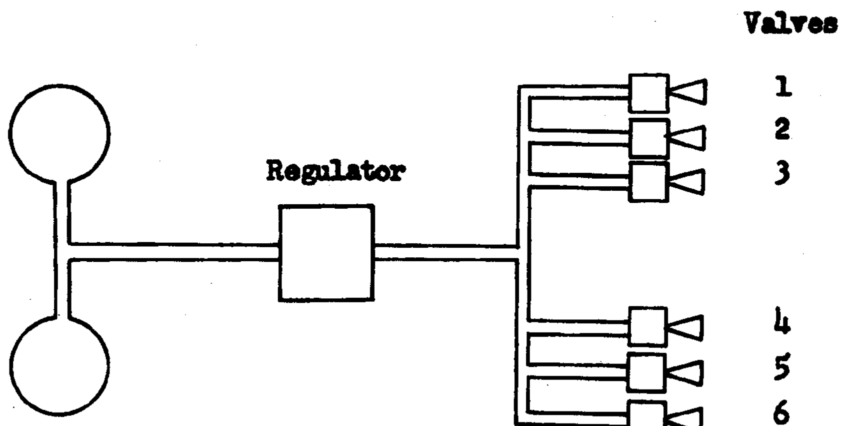

The storage spheres have a volume of 2200 cubic inches each and may be pressurized to 3600 psi. The regulator high pressure stage is used during ascent and provides a regulated output of 20 psi. The low pressure stage is used on orbit and provides a regulated output of 5 psi. The valves are of the ON-OFF type and are individually controlled by solenoids. The solenoids are energized as required by the outputs from the PWFM circuitry.

2.1.3.4 System Parameters

The following tables provide a listing of significant values. The measured values were obtained during Task III of the Vehicle Systems Test on 27 August 1964. The nominal values are from the Detail Specification "Guidance and Control Subsystem, Model 45205, Serial 2355" LMSC 416544A.

Ascent Deadbands and Saturation Levels

Channel	Valve	Nominal D.B. Deg.	Nominal Sat. Deg.	Measured D.B. Deg.	Measured Sat. Deg.
Roll	3	0.25-1.00	11.65	0.620	12.50
	6		to	0.709	13.20
	1		16.80	0.760	13.25
	4			0.760	13.25
Yaw	3	0.07-0.32	3.47	0.192	3.82
	6		to	0.215	3.83
	1		4.92	0.215	3.98
	4			0.222	3.96
Pitch	2	0.08-0.34	1.78	0.204	2.04
	5		2.64	0.202	2.10

Ascent Roll Torquing Gain

Nominal Deg/Min/Deg	Measured Deg/Min/Deg
+9.0 ± 1.4	+9.05

BTL Steering Rates

The nominal value in each case was 120 deg/min ± 5%.

Channel	Measured Value Degrees/Min.
Pitch	+120 -121.5
Yaw	+119.8 -119.8

Programmed Vehicle Rates

Name	Nominal Deg/Min.	Measured Deg/Min.
Engine Burn Pitch Rate	9.24 ± 5%	9.18
Yaw Around	43.0 ± 10%	42.5
Orbital Pitch Rate	4.03 ± 10%	3.97
Pitch Down-Recovery	43.0 ± 5%	42.2
Pitch Up	120.0 ± 10%	128
Yaw Bias Roll Rate +	0.172 ± 5 %	0.177
-	0.172 ± 5%	0.177

Orbit Deadbands and Saturation Levels

		Nominal		Measured	
Channel	Valve	D.B. deg.	Sat. deg.	D.B. deg.	Sat. deg.
Roll	3	0.08	3.55	0.155	3.81
	6	to	to	0.185	4.08
	1	0.022	4.94	0.194	4.05
	4			0.187	4.09
Yaw	3	0.08	3.55	0.137	3.90
	6	to	to	0.188	4.07
	1	0.22	4.94	0.188	4.10
	4			0.179	4.08
Pitch	2	0.08	1.82	0.170	2.10
	5	to	to	0.159	2.10
		0.22	2.57		

Orbit Torquing Gains

Torquing Gain	Symbol	Nominal Deg/Min/Deg.	Measured Deg/Min/Deg.
Pitch	H_θ	$+1.67 \pm 0.25$	+1.81
Roll	H_ϕ	$+0.33 \pm 0.05$	+0.319
Yaw	H_ψ	-1.67 ± 0.25	-1.885

Horizon Sensor - Gyro Decoupling Gains

Gyro Out-Gyro In	Symbol	Nominal	Measured
Pitch to Pitch	$H_{r\theta}$	1 ± 0.30*	1.10
Roll to Roll	$H_{r\phi}$	0 ± 0.03**	0
Roll to Yaw	$H_{\phi\psi}$	0 ± 0.07**	0

*Deg. Gyro/Deg. H/S

**Deg/Min/Deg.

Vehicle Weight, Inertias and Lever Arms

Condition	Weight Pounds	Yaw Lever Arm-Feet	Roll Inertia Slug Ft.^{2}	Pitch Inertia Slug Ft.^{2}	Yaw Inertia Slug Ft.^{2}
Launch	152,922	-	33,122	1,554,062	1,554,137
Solid Booster Burn-out (40 sec)	103,307	-	9,348	1,199,131	1,199,206
Booster After Jettison (65 sec)	81,562	-	3,420	1,053,445	1,053,520
MECO	25,389	-	2,362	494,385	494,457
VECO	25,315	-	2,347	490,010	490,069
Separation	16,836	10.52	309	12,022	11,988
First Ignition	16,738	10.54	288	11,796	11,770
First Burnout	3,535	14.31	285	7,245	7,217
On-Orbit Dry with Gas	3,256	15.00	285	6,594	6,566
On-Orbit Without Gas	3,172	15.34	278	6,130	6,108
On-Orbit Less Capsule	2,866	14.11	272	4,729	4,706

Pitch Lever Arm = Yaw Lever Arm + 0.19 Ft.

Roll Lever Arm = 2.17 Ft.

2.1.3.5 Operational Sequence

The significant operational events as related to the attitude control system are listed sequentially from engine burnout on. The actual times are taken from LMSC/B110236, "Flight Test Engineering Analysis Report(U)" (Secret).

Actual Time from Liftoff (Seconds)	Event
432.75	Engine Burnout (70% Thrust-Decaying)
439.27	Horizon Sensor Pitch Output connected to Pitch Gyro. Horizon Sensor Roll Output transferred to Low Gain.
447.39	Yaw around initiated (-43°/min.). Engine Burn Pitch Rate removed.
698.28	Yaw around terminated. Orbital Pitch Rate initiated. Gyro Compassing initiated. Pitch Gyro Decoupling initiated. Horizon sensor Pitch output transferred to Low Gain. Flight Controls to Orbit Mode. Pneumatic Regulator to Low Pressure Yaw Offset initiated.

At the completion of the foregoing sequence, the vehicle control system was in the orbital mode and the yaw bias for the first active payload pass (Pass 8 at NHS) was initiated. From this time on the significant events were the switching of the yaw bias and the disconnecting of the Horizon Sensor during the Payload Operate period. The yaw bias switching for the passes prior to recovery are shown in the following table.

Pass	Station	Direction	Bias Initiated
8	NHS	S - N	Shortly After Injection
9	VTS	S - N	
14	NHS	N - S	Shortly After Pass 9
16	VTS	N - S	
24	NHS	S - N	Shortly After Pass 16
25	VTS	S - N	
30	NHS	N - S	Shortly After Pass 25

The yaw bias switching after recovery was accomplished in the same manner.

In conjunction with the Payload Operate ON command, the following operations took place:

o) Horizon Sensor Pitch Output to Pitch Gyro was disconnected.

o) Horizon Sensor Roll Output to Roll Gyro was disconnected.

o) Gyro-compassing (Horizon Sensor Roll Output to Yaw Gyro) was disconnected.

o) Pitch Gyro Decoupling was disconnected.

In conjunction with the Payload Operate OFF command these four signals were reconnected.

2.1.3.6 Orbital Attitude Control System Analysis

<u>Basic Mission Outline</u> - This mission shall utilize an SS-01A vehicle with attached payload and a TAT-Thor booster. Shortly after injection the

vehicle will be yawed 180° and will fly tail first and horizontal throughout its useful life. Steady state yaw attitude offsets will be required when the payload is operating. Reorientation for the separation of a recoverable capsule is required. The Agena pneumatic system will be the primary system for attitude control. A secondary, independent back-up stabilization system will be available for recovery control.

Attitude Control Requirements-Payload Operating

Control Axis	Null Position	Bias Uncertainty	Limit* Cycle	Body* Rate
Pitch	0°	± 0.4°	± 0.25°	± 0.002°/sec
Roll	0°	± 0.4°	± 0.25°	± 0.005°/sec
Yaw	± 2.44° ± 10%	± 0.4°	± 0.25°	± 0.003°/sec

* maximum values

Attitude Control Requirements-Payload Inoperative - No requirement other than compatibility with the system capabilities and other attitude control requirements.

Design Approach and Constraints - The basic SS-01A control system will be utilized to fulfill the mission requirements. Minor modifications of the standard system will be permitted but not encouraged. The synthesis, analysis and development of advanced attitude control system components and concepts is beyond the scope of this mission.

Gyro Torquing Gains - The steady state attitude bias uncertainties may be obtained using the following relations. Pitch, roll and yaw are denoted by the symbols θ, ϕ and ψ respectively.

$$\theta_{ss} = -\theta_{hse} - \dot{\theta}_d/H_\theta + (\omega_o - \omega_{op})/H_\theta$$

$$\phi_{ss} = -\left[H_\psi/(\omega_{ot}H_\psi)\right]\phi_{hse} - \dot{\psi}_d/(\omega_{ot}H_\psi)$$

$$\psi_{ss} = \left[H_\phi/(\omega_{ot}H_\psi)\right]\phi_{hse} - \left[H_\phi/(\omega_{ot}H_\psi)\right]\left[\dot{\psi}_d/\omega_o\right] + \dot{\phi}_d/\omega_o$$

where

$\theta_{ss}, \phi_{ss}, \psi_{ss}$ = steady state attitude bias

θ_{hse}, ϕ_{hse} = horizon sensor bias errors

H_θ, H_ϕ, H_ψ = gyro torquing gains

$\dot{\theta}_d, \dot{\phi}_d, \dot{\psi}_d$ = gyro drifts

ω_o = average orbital rate

ω_{op} = programmed orbital rate

The bias uncertainties are calculated from the given expressions by taking the root-sum-square of the individual terms (RSS method). Thus, if $A = B + C$ then $A_{rss} = (B^2 + C^2)^{\frac{1}{2}}$. The values used for the various parameters were:

$$\omega_o = 4.03^\circ/\text{min} = 0.0703 \text{ rad/min}$$

$$\omega_{op} = \omega_o \pm 4.36\%$$

$$\theta_{hse} = 0.37^\circ$$

$$\phi_{hse} = 0.34^\circ$$

$$\dot{\theta}_d = 6^\circ/\text{hr} = 0.1^\circ/\text{min}$$

$$\dot{\psi}_d = 6^\circ/\text{hr} = 0.1^\circ/\text{min}$$

$$\dot{\phi}_d = 1^\circ/\text{hr} = 0.0167^\circ/\text{min}$$

Using the $\pm 0.4^{\circ}$ bias uncertainty allowed and the values of the parameters as stated the given relations yield the following bounds on the gyro torquer gains.

$$H_{\theta} \geq 1.36 \text{ deg/min/deg}$$

$$H_{\psi} \geq 0.27 \text{ deg/min/deg}$$

$$H_{\psi} \geq (4.54 H_{\phi} - \omega_{o}) \text{ deg/min/deg}$$

The gyro compassing time constant is approximately equal to $2/H_{\phi}$. In order to maintain a reasonably low time constant H_{ϕ} must be large. The effect of any noise present in the horizon sensor outputs will be proportional to the torquer gains. Thus, the gains should be kept as low as possible. A reasonable compromise between these conflicting requirements is:

$$H_{\theta} = 1.667 \text{ deg/min/deg}$$

$$H_{\phi} = 0.333 \text{ deg/min/deg}$$

$$H_{\psi} = 1.667 \text{ deg/min/deg}$$

The standard tolerance on these gains is $\pm 10\%$.

The roll torquing gain of 1/3 deg/min/deg results in a gyro compassing time constant of 6 minutes. This is high but tolerable if sufficient time is allowed when switching the torquing signal to the roll gyro to obtain a yaw offset. The bias uncertainties which result from the chosen torquing gains are:

$$\theta_{ss} = 0.39^{\circ}$$

$$\phi_{ss} = 0.33^{\circ}$$

$$\psi_{ss} = 0.37^{\circ}$$

<u>Error Signal Deadbands</u> - The required deadbands can be achieved although a rather high tolerance is indicated. This is discussed in Section 1.4.3.2- "Program Peculiar Design Considerations".

Limit Cycle Rates - For an uncoupled, linearized, single axis system the net change of rate during a turn-around is:

$$\Delta \omega = (nNFW)57.3R/I \quad \text{deg/sec}$$

Where:

n = number of pulses per valve

N = maximum number of valves which may pulse

F = valve thrust in pounds

W = pulse width in seconds

R = valve lever arm in feet

I = vehicle inertia in ft-lb-sec^2

The product nNFW represents the total impulse (lb-sec) imparted to the vehicle during the turn-around and the quantity 57.3R/I represents the change in vehicle rate per impulse imparted (deg/sec/(lb-sec)). In the absence of disturbing torques the vehicle will damp down to a low rate one pulse per valve limit cycle. For a balanced limit cycle the rate will be equal to one half the rate change per turn-around. In the pitch channel only one valve may pulse in response to an error signal whereas in roll and yaw two valves may respond. Due to the electronic coupling of roll and yaw and imbalances between the two roll-yaw channels it is quite likely, but not certain, that only one valve will respond. The two valve responses will be used as a "worst" case.

A determination of the impulse obtained per pulse per valve is rather complicated. The low pressure mode regulation level is specified as 5, +1.0 to -1.5 psi. However, this figure is for full flow through the regulator. The regulator exhibits a lock-up phenomena which results in a higher output pressure under zero or extremely low flow conditions. The specification value for the low pressure mode lock-up pressure is 6.0 psig. In a low rate limit cycle a pulse is required every 50 to 100 seconds or so. This condition should prevail for the vehicle in question. Thus, the actual regulator output pressure will be the lock-up pressure. Data derived from laboratory tests (1) indicates that under these conditions the impulse per pulse for a -5 mixture will be about 0.011 lb-sec.

(1) "Investigation of Specific Impulse Attainable in an Attitude Control System Using Freon-14 - Nitrogen Mixtures", Report Number 16214, Reference 61-2944-1101, 12 September 1962, Lockheed California Co., Mechanical Systems Research Dept.

Based on the current (September 1963) vehicle parameters, the rates for a single pulse per valve limit cycle are as follows:

$$= \frac{1}{2} N(FW) 57.3R/I \text{ deg/sec.}$$

	N Valves	FW lb-sec/value	57.3R/I deg/sec/(lb-sec)	Rate deg/sec
Pitch	1	0.011	0.124	0.0007
Roll	2	0.011	0.418	0.0046
Yaw	2	0.011	0.124	0.0014

The pitch and yaw rates are well below the required levels. The roll rate is 92% of the specific maximum. The only reasonable change which would increase the roll rate margin would be to modify the regulator to lower the output pressures. While it might be physically simple for the vendor to do this the attendant effort would be costly. All things considered it does not appear that any design changes are warranted.

Yaw Steering - Steady state yaw offsets of plus and minus $2.44^\circ \pm 5\%$ will be required when the payload is operating. Positive offsets (nose right) are required on southbound passes and negative offsets on northbound passes. Yaw offsets can be developed by torquing the roll gyro with a signal equivalent to the product of the orbital rate and the offset desired. The roll gyro torquing signal then is:

$$\phi_{gc} = \omega_o \psi_{os} = 0.0703 \text{ (rad/min)} \times 2.44^\circ = 0.1718^\circ\text{/min}$$

The application of these signals will be effected by a brush on the orbital programmer. The gyro compassing time constant is six minutes and the steering program should be initiated three to four time constants before the steady state offset is desired. In order to maintain the desired vehicle orientation the net vehicle body rate must be equal to and coincident with the orbital angular velocity ω_o. The following figure illustrates the situation with an exaggerated offset.

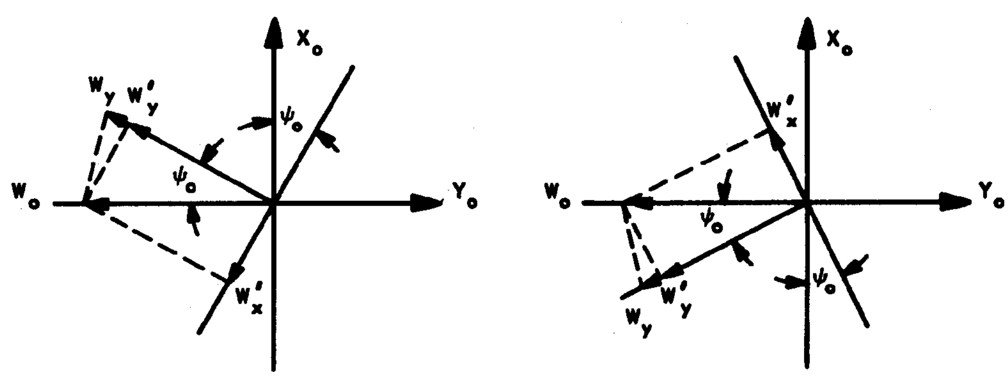

ψ_o = yaw offset = 2.44° = 0.0426 rad (steady state)
ω_o = orbital angular rate = 0.0673°/sec
$\omega_x^1 = W_o \sin \psi_o$ = roll body rate required
$\omega_y^1 = W_o \cos \psi_o$ = pitch body rate required
ω_y = actual pitch body rate (= ω_o for zero yaw)

For the small offset being used the required body rate can be expressed as:

$$\omega_x^1 = \omega_o \psi_o$$
$$\omega_y^1 = \omega_o (1 - \psi_o^2/2)$$

The change in the pitch body rate is:

$$\Delta\omega_y = \omega_o - \omega_y^1 = \frac{\omega_o \psi_o^2}{2} = 0.000061 \text{ deg/sec}$$

This represents a change at 0.091%. As the tolerance on the torque program is 4.36% it is not worthwhile to change the programmed rate. The pitch attitude error required to offset the torque program error is:

$$\Delta\theta = \frac{\Delta\omega_y}{H_\theta} = \frac{0.00366^\circ/\text{min}}{1.67^\circ/\text{min}/^\circ} = 0.0022^\circ$$

This added error is negligible compared with RSS bias errors of ± 0.39 degrees. If the horizon sensor is disconnected after the yaw offset is established a pitch attitude error will accumulate.

$$\Delta\theta = 0.00366 \ (^\circ/\text{min}) \times t$$

For a maximum run of three minutes the accumulated error will be 0.011°. Compared to the bias error and limit cycle excursions, this added error is negligible.

Horizon Sensor Anomalies-Nature of the Problems - Flight test data from a number of vehicles which carried the Model 2-A Horizon Sensor has shown anomalous sensor output signals. This "noise" is attributed to "cold clouds" and may take a number of forms. Long-termed steps, short-term pulses and sinusoidal noise has been observed. The magnitude, form, frequency, frequency of occurrence and duration of this noise varies from flight to flight. The data from a recent flight showed sinusoidal noise of $\pm 1/4$ degree amplitude and a period of 100 seconds. Some of the factors which seem to influence the sensor susceptibility to this phenomena are the time of year, individual sensor head temperature, sensor slicing level and the geographical location of the scan pattern. Department 62-21, Guidance and Controls Equipment Engineering, has performed some analysis of flight data and has stated that anomalous outputs in excess of 1/2 degree will not exist more than 1% of the time. Unfortunately, this bound is too high with respect to the attitude control requirements for this mission. Modifications have and may be made to the sensor to reduce the problem. Additionally, analytical effort is being expended in an attempt to develop a method of determining true vehicle attitude; i.e., separate the noise from the signal. However, due to the "poor" quality of the telemetered data (poor with respect to the accuracy of the desired results) and the lack of any compelling requirement to solve the problem, any optimism regarding the results of the effort would be premature.

Recommended Action - Because of the uncertainty of the magnitude of the horizon sensor noise problem and the general acceptability of operating with the sensor disconnected for short periods of time it was recommended that the sensor be disconnected during the payload operate period. This mode was mechanized as explained in Section 2.1.3.2.

<u>Effects of Horizon Sensor Anomalies</u> - For anomalous pitch and roll sensor outputs of the form $\theta_n = \sin \omega_{nt}$ and $\phi_n = \sin \omega_{nt}$ the resulting gyro outputs will be:

$$\theta_g = \frac{H_\theta \theta_n \sin \omega_{nt}}{s + H_{f\theta}} \quad , \quad \phi_g = \frac{H_\phi \phi_n \sin \omega_{nt}}{s + H_{f\phi}} \quad , \quad \psi_g = \frac{H_\psi \phi_n \sin \omega_{nt}}{s + H_{f\phi}}$$

For the chosen torquing gains and the range of known noise frequencies the effect of the pitch and roll gyro feedback terms is negligible. Thus

$$\frac{1}{s + H_{f\theta}} \doteq \frac{1}{s} \quad \text{and} \quad \frac{1}{s + H_{f\phi}} \doteq \frac{1}{s}$$

The gyro outputs and rates then become:

$$\theta_g = -\frac{H_\theta \theta_n}{\omega_n} \cos \omega_{nt} \quad , \quad \dot{\theta}_g = H_\theta \theta_n \sin \omega_{nt}$$

$$\phi_g = -\frac{H_\phi \phi_n}{\omega_n} \cos \omega_{nt} \quad , \quad \dot{\phi}_g = H_\phi \phi_n \sin \omega_{nt}$$

$$\psi_g = -\frac{H_\psi \phi_n}{\omega_n} \cos \omega_{nt} \quad , \quad \dot{\psi}_g = H_\psi \phi_n \sin \omega_{nt}$$

For a noise signal of 0.5° peak amplitude and period T (sec) the peak gyro attitudes and rates are:

$$\theta_g = 0.0022 \text{ T deg} \quad , \quad \dot{\theta}_g = 0.0139 \text{ deg/sec}$$

$$\phi_g = 0.0004 \text{ T deg} \quad , \quad \dot{\phi}_g = 0.0028 \text{ deg/sec}$$

$$\psi_g = 0.0022 \text{ T deg} \quad , \quad \dot{\psi}_g = 0.0139 \text{ deg/sec}$$

For a step change in the sensor output of θ_s and ϕ_s:

$$\theta_g = \theta_s\left(1 - e^{-H_\theta t}\right) \quad , \quad \dot{\theta}_g = H_\theta \theta_s e^{-H_\theta t}$$

$$\phi_g = \phi_s\left(1 - e^{-H_\phi t}\right) \quad , \quad \dot{\phi}_g = H_\phi \phi_s e^{-H_\phi t}$$

$$\psi_g = \frac{H_\psi}{H_\phi} \phi_s\left(1 - e^{-H_\phi t}\right) , \quad \dot{\psi}_g = H_\psi \phi_s e^{-H_\phi t}$$

For a 0.5° step:

$$\theta_g = 0.5 \left(1 - e^{-t/36}\right) \text{ deg} \quad , \quad \dot{\theta}_g = 0.0139\, e^{-t/36} \text{ deg/sec}$$

$$\phi_g = 0.5 \left(1 - e^{-t/180}\right) \text{ deg} \quad , \quad \dot{\phi}_g = 0.0028\, e^{-t/180} \text{ deg/sec}$$

$$\psi_g = 2.5 \left(1 - e^{-t/180}\right) \text{ deg} \quad , \quad \dot{\psi}_g = 0.0139\, e^{-t/180} \text{ deg/sec}$$

These calculated values do not represent the net closed loop system response but are indicative of the possible magnitudes which may occur.

Effects of Disconnecting the Horizon Sensor - The horizon sensor provides vehicle pitch and roll attitude signals with respect to the desired control reference; i.e., the earth. The IRP gyros cannot be used alone as an attitude reference source. Even if the gyros could be initially oriented along the desired control axes, they would accumulate errors due to gyro drift torques and programming errors. In the normal system configuration the vehicle will respond to the accumulated gyro errors and eventually reach a steady state equilibrium position such that the horizon sensor provides gyro torquing signals to balance out the drifts and program errors. This steady state equilibrium position plus the sensor accuracy result in what is generally referred to as the bias uncertainty. If the horizon sensor is disconnected the vehicle null position will then drift at a rate determined by the gyro drifts and programming errors.

Pitch Axis:

The pitch axis reference null will drift due to pitch gyro drift and orbital rate programming errors.

$$\dot{\theta} = \dot{\theta}_d + (\omega_{op} - \omega_o) +/- \omega_o (1 - \cos \psi_s)$$

where

$$\dot{\theta}_d = \text{pitch gyro drift} = 6^\circ/\text{hr} = 0.1^\circ/\text{min} = 0.00167^\circ/\text{s}$$

$$\omega_{op} = \omega_o (1 \pm 0.0436)$$

$$\omega_o = \text{average orbital rate } 1 \; 4.03^\circ/\text{min} = 0.0672^\circ/\text{s}$$

$$\psi_s = \text{desired yaw bias} = + \text{ or } - \; 2.44^\circ = \pm 0.0426 \text{ rad}$$

$$\cos \psi_s = 0.999092$$

The term $\cos \psi_s$ represents the amount by which the pitch body rate should be reduced when the vehicle is yawed off the zero null position. For the yaw bias being used the magnitude of the term is negligible compared to the other terms.

$$\dot{\theta} = 0.001667 + (0.0672)(\pm 0.0436) \pm (0.0672)(0.000908)$$

$$= 0.001667 \pm 0.00293 \pm 0.000061$$

Evaluating the drift as the RSS of the augend and addends yields:

$$\dot{\theta} = \pm 0.00337 \text{ deg/sec}$$

Roll Axis:

The roll axis reference null will drift due to roll gyro drift and orbital rate programming errors. When the vehicle is yawed off from the zero null position a roll body rate program equivalent to $\omega_o \psi$ is required. The tolerance on the roll program will be assumed to be the same as that for the pitch program (4.36%).

$$\dot{\phi} = \dot{\phi}_d + \omega_o \sin \psi_s (\pm 0.0436)$$

where

$$\dot{\phi}_d = \text{roll gyro drift} = 1^{\circ}/\text{hr} = 0.01667^{\circ}/\text{m} = 0.000277^{\circ}/\text{sec}$$

$$\omega_o = \text{orbital rate} = 4.03^{\circ}/\text{min} = 0.0672^{\circ}/\text{sec}$$

$$\psi_s = \text{desired yaw bias} + \text{ or } - 2.44^{\circ}$$

$$\sin \psi_s = 0.04258$$

$$\dot{\phi} = 0.000277 + (0,0672)(0.04258)(0.0436)$$

$$= 0.000277 + 0.00125$$

The RSS is

$$\dot{\phi} = \pm 0.00128 \text{ deg/sec}$$

Yaw Axis:

The yaw axis reference null will drift due to yaw gyro drift only.

$$\dot{\psi} = \dot{\psi}_d = \pm 6^{\circ}/\text{hr} = 0.1^{\circ}/\text{min} = \pm 0.001667^{\circ}/\text{sec}$$

In the presence of anomalous horizon sensor outputs the initial attitude may exceed the bias uncertainty. Thus, disconnecting the sensor will not improve the attitude accuracy, but will eliminate the associated high vehicle body rates.

Unbalanced Momentum - Each time the payload was activated film was driven from the payload Recorder Unit (Box #7) supply cassette to the take-up spool in the recovery capsule. The complete data track is functionally depicted below. Each time the spools are accelerated to steady state speed a torque is developed which results in a change in vehicle body rate.

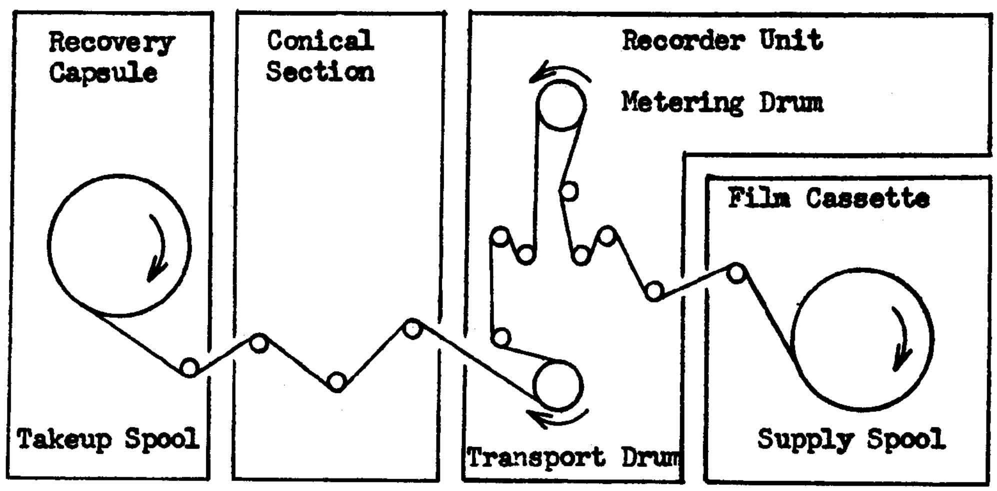

Each of the smaller rollers (including the metering and transport drum) can be viewed as one half of a counter rotating pair. The net unbalance resulting from these pairs is negligible. This leaves the supply spool, take-up spool and the film. The net unbalanced momentum then is

$$h = I_s W_s + I_{fs} W_s + I_t W_t + I_{ft} W_t \, .$$

Where:

I_s = inertia of supply spool

I_{fs} = inertia of film on supply spool

I_t = inertia of take-up spool

I_{ft} = inertia of film on take-up spool

W_s = angular velocity of supply spool

W_t = angular velocity of take-up spool

h = net unbalanced momentum

The units of inertia (I), angular velocity (W) and momentum (h) are foot-pound-seconds squared, radians per second and foot-pound-seconds respectively.

For the particular conditions existing on 2355 this unbalanced momentum is plotted below.

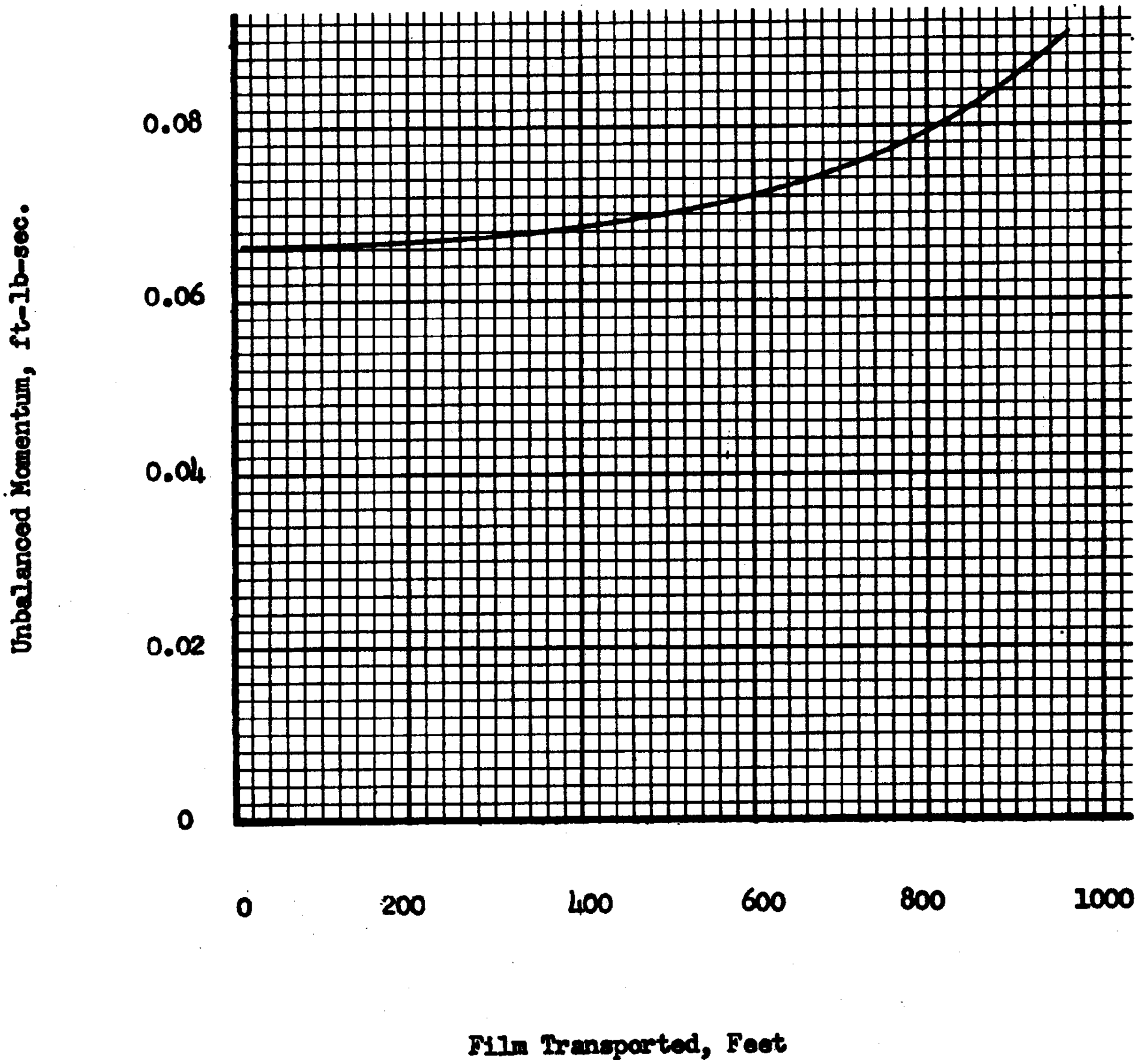

To obtain the resulting vehicle body rates this net momentum must be resolved into body axis components. The Recorder Unit is mounted as shown below and the components of the unbalanced momentum are as shown.

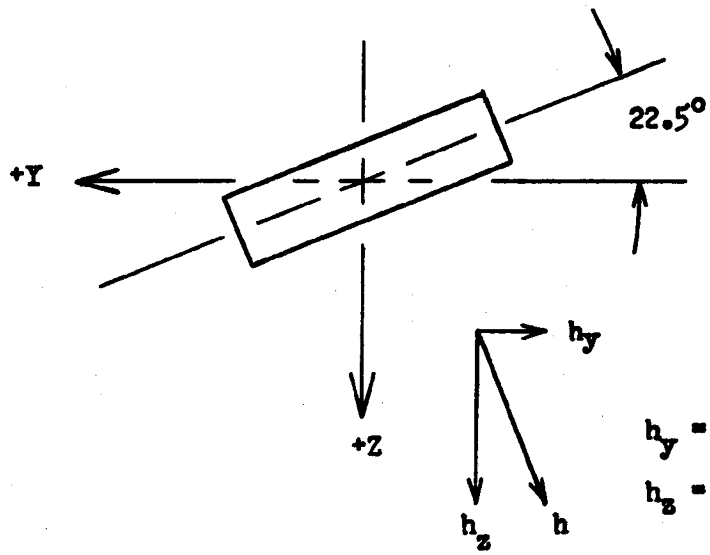

$h_y = h \sin 22.5^\circ = 0.383\ h$

$h_z = h \cos 22.5^\circ = 0.925\ h$

The corresponding body rates at turn on may be computed using the following relations.

$$W_{pitch} = + h_y/I_y \text{ and } W_{yaw} = -h_z/I_z$$

The pitch and yaw inertia are almost equal and are equal to 6580 ft-lb-sec^2 before recovery and 4718 ft-lb-sec^2 after recovery. Using an average unbalanced momentum of 0.075 ft-lb-sec the body rates are:

Before Recovery: $W_{pitch} = 0.00025^\circ/\text{sec}$, $W_{yaw} = -0.00061^\circ/\text{sec}$.

After Recovery: $W_{pitch} = 0.00035^\circ/\text{sec}$, $W_{yaw} = -0.00084^\circ/\text{sec}$.

Though these rates are significant compared with the pitch and yaw requirements of 0.002°/sec and 0.003°/sec it was decided that corrective action was not warranted. The normal vehicle body rates will have a random distribution and thus the probability of the rates being additive is 50%. It should be noted that if the supply and take-up spools had been made counter rotating these rates would be about 1/5 of the given values.

Magnetic Compensation - Any magnetic field contained within the vehicle will in general interact with the earth's magnetic field and produce a torque on the vehicle. This torque must be counter balanced by an average torque produced by the pneumatic system. The magnetic torques are essentially constant for short periods of time while the pneumatic system delivers discrete impulses. With regard to the 2355 payload it was desirable to minimize the numbers of gas valve fittings to avoid degradation at payload data. This required the installation of permanent magnets to compensate for the permanent magnets in the BTL cannister and the Klystron Tube in the Transmitter-Modulator. The compensating units were composed of an assembly of small bar magnets to allow for tuning the unit to achieve a magnetic moment equal to the magnetic moment to be compensated. The assemblies were then mounted in the vehicle with their moments directed opposite to the moments to be compensated. It has been estimated that the method and equipment used permit at least 95% compensation. The following table lists the components of body torque that would generate by the Klystron Tube magnet during typical active payload passes for 0% (no compensation) and 90% compensation. The units of torque used are millifoot-pounds.

Pass No.	0% Roll	0% Pitch	0% Yaw	90% Roll	90% Pitch	90% Yaw
8	6	3	1	0.6	0.3	0.1
9	5	5	4	0.5	0.5	0.4
14	6	5	0.5	0.6	0.5	0.5
16	8	4	2	0.8	0.4	0.2

In roll each valve firing produces a momentum of about 0.024 ft-lb-sec. The uncompensated roll torque on Pass 16 would be 0.008 ft-lbs. The time interval between valve firings is then:

$$T = \frac{0.024}{0.008} = 3 \text{ seconds}$$

For the 90% compensation case the time interval will increase by a factor of ten to 30 seconds. For 95% compensation the interval would be 60 seconds.

For either pitch or yaw the momentum imparted by a single valve firing is about 0.15 ft-lb-sec. Consider an uncompensated torque of 0.003 ft-lb about either axis, the time between firings would be:

$$T = \frac{0.15}{0.003} = 50 \text{ seconds}$$

For 90% compensation the interval is 500 seconds and for 95% compensation it becomes 1000 seconds. These increased time intervals were judged to be satisfactory for payload operation.

2.1.4 Command and Control Subsystem

2.1.4.1 Systems Requirements

The C&C Subsystem for Vehicle 2355 is required to perform the following functions:

- Data Link Operation (VHF and UHF)
- Commanding
- Tracking and Acquisition

A block diagram of the subsystem showing the functions of each major component is shown in Figure 2.1.4.1. Subsystem requirements are summarized in Table 2.1.4.1.

2.1.4.2 Data Link System

The data link system consists of the following subsystems:

- Telemetry System (VHF)
- Wideband Data Link (UHF)

Telemetry System - The telemetry system consists of the basic SS-01A telemetry link and an additional link to accommodate Program peculiar on-orbit instrumentation requirements. The basic SS-01A telemetry is used to monitor basic vehicle performance during the ascent phase and for some additional instrumentation on orbit. The Telemeter, Type 5, which is basic equipment, is augmented with additional VCO's for the added on-orbit instrumentation. Telemetry data is transmitted via a VHF Transmitter, Type 4; Multi-coupler, Type 4; and a VHF Antenna, Type 19, during ascent and orbit.

To fulfill the total instrumentation requirements, one additional

TABLE 2.1.4.1

SUMMARY OF
COMMUNICATIONS AND CONTROL SUBSYSTEM
PERFORMANCE PARAMETERS

Tracking Data Accuracy (3)	
A. Retrospect Ground Track	± 1.5 n.m., both axes
Command Functions	
A. Real Time (RTC)	49
1) Maximum Command Rate	One (1) per 4 seconds
2) Secure Functions	2
B. Stored Program (SPC)	24
Telemetry Links (VHF)	
A. 235.5 mc Link (Basic SS-01A)	
1) Output signal-to-noise ratio	35 db (rms-to-rms)
B. 245.3 mc Link (Program Peculiar)	
1) Output signal-to-noise ratio	35 db (rms-to-rms)
Payload Data Links	
A. UHF Wide Band Data - 2.2 KMC	
1) Information bandwidth	7.5 MC
2) Output signal-to-noise ratio	26 db (peak-to-rms) at elevation above 5°

telemetry link is provided for vehicle and payload status in real time and stored time. A Tape Recorder, Type 12, with a Recorder Marker, Type 1, is used for storing telemetry data. This link utilizes the Telemeter, Type 2, a Type 4 transmitter, a Type 4 multi-coupler, and a Type 19 VHF antenna.

Tape Recorder Problems - The Type 12 tape recorder serial number 303 used on 2355 was returned to the Vendor for tie down of the metallic tape leader. It has been found that excessive oxide build-up on the end-of-tape sensor can result in failure to turn off when the end of tape is reached. With the tape tied down, the hysteresis drive motor will stall, but the unit will function properly when commanded to reverse. The recorder was also given a 25-hour burn-in and re-run of the ATS at the factory. No FEDR's were recorded against S/N 303.

Commutator Problems - During tests at the launch pad, one of the commutators failed to start and was replaced with a spare unit. Experience has shown that units that have once failed to start are likely to fail again, so that replacement of the unit was considered necessary

Wide Band Data Link - The WBDL transmitter operates in the 2200 to 2300 mc telemetry band, with power output of ten watts. The transmitter consists of a transistorized exciter driving a travelling wave tube of advanced design. The power supplies for the TWT and exciter operate from the vehicle +28 vdc unregulated supply.

The WBDL Transmitter characteristics are summarized below:

Dimensions:	14.6 X 8.5 X 6.0 inches
Weight:	21 lbs.
Input Power:	+22.0 to +29.5 vdc at 4.8 amperes max.
RF Power Output:	10 watts
Frequency Range:	Fixed-tuned 2.2 to 2.3 gc
Modulation Mode:	FM
Deviation:	$\pm$ 6 mc
Operating Temperature Range:	-30° F to +165°F
Altitude:	Unlimited (operation at critical pressure)
Reliability:	0.96 probability of survival for 728 hours at a 15 percent duty cycle.
Input Impedance:	75 ohms $\pm$ 10% shunted with not more than 30 micro-micro farads capacitance.
Pulse Response:	Shall be capable of deviating 12 mcs with a rise time of 60 nanoseconds from 10% to 90% points.
Frequency Response:	The modulation voltage required for constant deviation (plus or minus 6 mc) referenced to 100 KC shall not vary more than $\pm$ 2 db from 10 cps to 5 mcs.

Although the design information bandwidth of the WBDL is 5 mc, tests have shown that it will meet the program requirement of 7.5 mc for the 2355 series of vehicles over the predicted temperature range.

As a test of linearity, phase shift, and frequency response, a RETMA television test pattern was transmitted by the WBDL. The table below shows the resolution of the received signal for various signal-to-noise ratios:

RETMA PATTERN

	Cam-Mon.	Data Link Best S/N	+12 db IF	+6 db IF S/N
Vert. Res. (Scan Lines	325-350	325-350	325	250
Horiz. Res. (Retma Lines)	675	675	650	400
Bandwidth (mcs) 80 lines/mc of Horiz. Res.	8.45	8.45	8.125	5.00

The following Table shows the degree of linearity of the video portion of the received signal for various signal-to-noise ratios:

	Cam-Mon.	Data Link Best S/N	+12 db IF S/N	+6 db IF S/N
Number of Discernable Grey Levels	9 (All)	9	9	8

Data-to-noise ratio (pk-to-rms) of 26 db or better can be obtained at all elevation angles greater than 5 degrees using the 60' T&D Antenna and receiving system installed at VTS and NHS.

Redundant WBDL Transmitters were installed on 2355 with provision for switching on the standby unit by real time command.

WBDL Development - Original requirements for the WBDL Transmitter, Type 8 specified operation at sea level and at 10^{-5} mm. It became evident that due to outgassing of the equipment there would be formed an atmosphere surrounding the equipment of approximately 10^{-1}, for as long as 24 hours. Therefore, it was necessary to redesign the transmitter high voltage power supply to exist within this critical environment. This was accomplished by potting the high voltage critical areas and conducting extensive tests to determine their operability from 760 mm through 10^{-6} mm without any malfunction. This requirement was subsequently noted in later revision of the transmitter specification.

Antenna Type Re-direction - The orbit antenna originally installed for the 2.2 gc wideband data link was the UHF Antenna Type 7 which is the UHF part of the UHF/VHF Antenna Type 2. The Type 2 antenna is a boom-mounted antenna which has been very successful on a number of nose down attitude vehicles. The boom antenna was not required on 2355 because of the horizontal vehicle attitude, so the Type 7 antenna was installed under an ejectable fairing on the under side of the vehicle. Antenna patterns were taken with the Type 7 antenna in this location and were found to be unacceptable because reflections from the vehicle skin caused serious holes in the pattern. Patterns were then run with a Type 4 antenna which is a flush mounted cavity-backed dipole. The Type 4 patterns were found to meet the requirements and also make a better installation by eliminating the necessity for an ejectable fairing over the antenna, thus saving weight and improving the reliability.

2.1.4.3 Command System

The vehicle command system consists of the following subsystems:

- Real Time Command Subsystem
- Stored Program Command Subsystem
- Secure Real Time Command Subsystem

Real Time Command Subsystem - (Command Function List) - The real time command (RTC) subsystem consists of an S-band VERLORT or PRELORT Radar, the vehicle-borne S-band Transponder, Type 3, and the Decoder, Type 11.

The command transmission format consists of a three-pulse group with the position of the center pulse of a series of pulse groups modulated with a combination of two audio tones. Six tones are used for a total of 15 combinations of two. The decoder recovers the tones from the position-modulated pulse to activate relays in a matrix to generate 15 non-redundant outputs. These outputs are applied to the Power Control Unit(PCU), Type 25, where a relay matrix is used to obtain a total of 49 outputs from selected combinations of two outputs of the 15 decoder outputs.

The format of the decoder outputs consists of an address function and an execute function. Of the 15 outputs available, 6 are designated even-numbered addresses. When an even-numbered address is selected, the odd-numbered outputs constitute the execute functions. This procedure, therefore, provides for 6 possible addresses with 8 executes associated with each address, for a total of 48 possible commands. The 15th output from the decoder is used to reset the relay matrix before a new address is selected.

Stored Program Command Subsystem - The stored program command (SPC) capability is provided by a Fairchild Programmer, Type 7. The programmer is a transistorized switching device with two tape magazines, each of which is capable of 13 momentary contact closures by brushes making contact through holes punched in the 1½ mil thick, 35 mm wide Mylar tape. The length of the tape is divided into subcycles, each of which corresponds to a nominal orbit. Tape drive speed is adjustable by real-time command to reconcile the pre-set speed for a nominal orbit to that speed required for an operational orbit. Since each cycle on the tape represents an actual orbit, a programmed event occurs in relation to a specific latitude. Real time commands are available to cause the programmer to skip to the next subcycle or to repeat the current subcycle to adjust the programmed longitude of the subcycles.

Secure Real Time Command Subsystem - One secure real time command (RTC) is provided by using the S-band VERLORT system in a digital mode with the Decoders, Type 9 and Type 13. The middle pulse of the three-pulse group transmitted by the VERLORT is positioned in discrete positions relative to the other two pulses to indicate binary "one" and "zero" bits. The Type 13 decoder, which is a bit detector, provides binary "one" and "zero" bit outputs to the Type 9 decoder corresponding to the relative positions of the pulses within the three-pulse input groups. The Type 9 decoder generates an output command when the sequence of bits corresponds to a pre-selected sequence.

A back-up secure command system is provided by the VHF "ZEKE" System. This system consists of a VHF Receiver, Type 1, and Decoders, Types 5, 8, and 9. The command transmission is a carrier which is amplitude-modulated by seven audio tones. The Decoder, Type 8, generates three unsecure outputs from three of the tones. The Decoder, Type 5, generates "one" and "zero" bit outputs from the four other tones to operate the Type 9 decoder. The Decoder, Type 9, generates a secure output command when the sequence of bits corresponds to a pre-selected sequence.

2.1.4.4 Tracking and Acquisition Subsystems

Tracking Subsystem - The tracking system consists of a ground-based S-band Radar and a vehicle-borne S-band Transponder, Type 3. The receiver portion of the transponder operates in conjunction with the command decoders to provide real time command functions. The decoder section of the transponder triggers the transmitter section in response to a properly coded interrogation. This coded interrogation is recognized by the decoder from the spacing between the first and third pulse of a three-pulse group. The transmitter transmits a single-pulse reply for each correct interrogation pulse group received by the transponder.

The antenna for the S-band tracking and command systems consists of the Type 3 S-band antenna which is used for tracking during exit and orbit.

The above-noted tracking system components provide data which, when combined with computational programs that have developed from previous flights, permits an ephemeris determination in retrospect with an accuracy of approximately ± 1.25 nautical miles in altitude. This level of tracking accuracy applies for orbits with an eccentricity as required for these vehicles. This ephemeris determination capability is well within the overall tracking system requirements as noted in Table 2.1.4.1.

S-Band Transponder Problems -

SCR Destruction Due to Cold Starts - SCR destruction results from over-voltage produced when the beacon is interrogated before the transmitting tube is warmed up. An SCR protective network consisting of a zener diode and a diode across the SCR was installed in late Philco production units, and other units were retro-fitted. Cold starts are no longer catastrophic, but will result in reduced tube life. Future transponders will have a time delay so that the unit cannot be cold-started.

Lock-up - Lock-up of the beacon has been experienced in flight 2315 and in tests where an extraneous pulse has fired the SCR before the pulse forming network has charged. The lockup was sustained in beacons where the power supply shifts to a higher frequency but does not turn off. Power transformer redesign solved the sustained lock-up problem and all units were fitted with the new transformer.

Momentary lock-up was prevented by converting the over-interrogation circuit to a blanking circuit. The blanking circuit prevents triggering of the SCR during the critical pulse forming network recharge time. The purpose of the over-interrogation circuit was to limit the repetition rate of the beacon to 1600 pps so that the allowable plate dissipation of the transmitting tube would not be exceeded. However, tests have shown no degradation after 150 hours of operation at the maximum repetition rate of 4800 pps.

Pressure Tests - During pressurization tests at Philco, the output R-F connector from the circulator was found to be damaged. The malfunction was caused when internal pressure was increased to 30 psig.

It has been manufacturing practice by the circulator supplier to mill down a standard connector so that it would fit the circulator. This milling procedure weakened the connector walls at the point where the two pieces of the connector were flanged together. Separation of the connector occurred at this point, causing the center conductor to break.

All transponders were retro-fitted with new connectors of greater mechanical strength and it was recommended by Philco that the pressure not be raised above 15 psig.

UHF Acquisition Subsystem - The UHF acquisition subsystem consists of a 40 milliwatt, 400 mc, continuous wave Acquisition Transmitter Type I and a UHF Antenna, Type 1. This transmitter provides a signal which the 60' T&D Antenna at the tracking stations can acquire and auto-track. The 60' T&D Antenna has such a narrow beamwidth at 2.2 gc that acquisition of the WBDL is difficult. Beamwidth is 0.5° at 2.2 gc and 3.0° at 400 mc. The antenna cannot be slaved to the Verlort Antenna with the required accuracy.

The T&D System has a 2.2 gc auto-track capability which can be used once the vehicle has been acquired. Studies have shown that it should be possible to acquire and lock on at 2.2 gc, but until sufficient flight experience has been obtained, the 400 mc acquisition transmitter is a requirement.

2.1.4.5 Reliability

Reliability computations for the C&C Subsystem have been performed based on the following major assumptions:

- Ascent, orbit and recovery phases are all included in the analysis.
- A 10 percent orbital duty cycle for equipment commanded On and Off.
- Two-thirds of the status telemetry is necessary to achieve mission success.
- The Type 8 Wideband Data Link Transmitters are considered to be in a "standby redundancy" defined as warmed up and ready for switching upon command. Other equipments are considered to be "in series".

For the overall C&C Subsystem, including the "ZEKE" VHF Command System, Reliability is computed to be R = 0.938. Required Reliability for mission life has been specified by the Program Office as R = 0.920 (with ZEKE) and R = 0.933 (ZEKE alone).

Basic C&C Functions	Reliability
Tracking	0.995
Command (Including ZEKE)	0.963
Command (Excluding ZEKE)	0.969
ZEKE Command System	0.994
Payload Data Readout	0.987
Telemetry	0.970

2.1.5 Radar Antenna Development

2.1.5.1 Antenna Selection

Several ground rules were established for the design of the antenna. In accord with these it was determined that there would be no special testing devices which would compensate for the earth's gravity field. To maximize reliability there would be an absolute minimum of antenna unfurling, and the antenna would be as simple as possible. The antenna azimuth beamwidth requirement was such that in order to place an antenna on the vehicle without an unfurling operation it would be necessary to utilize a uniform aperture illumination. From an aperture standpoint this is the most efficient antenna design as it will yield the narrowest beamwidth and the highest gain for a given aperture. The resonant array selected laid along the length of the Agena vehicle and required no unfurling.

Resonant arrays offer several advantages. Among these are uniform slot dimensions and spacing throughout the array. From a manufacturing standpoint this yields the lowest possible cost. Arrays offer the greatest flexibility in pattern control to the antenna designer. When the array of slots consist of relatively few, their conductance can be controlled by individual adjustment. Because the number of slots in this array is very large (4,452 slots) this approach was deemed impractical. Therefore, precision machining with tight overall tolerance control, coupled with a precise electrical design procedure, was necessary.

It was decided that the 15' aperture for the array would be broken into four parts which yielded 53 slots to each quarter section element.

Two different types of array elements were investigated; the broad wall shunt slots and narrow wall shunt slots. Narrow wall shunt slots were selected because of their ease in fabrication.

The antenna was located along the side of the Agena vehicle between the Z-axis cable harness fairing and the tank pressure fittings on the starboard side. This held the minimum usable antenna width to 24" and to keep the covering fairing to a minimum height, the height of the antenna at the center was held to 2½". The antenna fairing was programmed to be separated at Thor VECO so that the fairing weight was not a substantial part of the Agena payload weight. This fundamental design approach of placing the antenna on the side of the Agena in horizontal flight resulted from some excellent vehicle design work and represented a considerable change from the original proposal which had a more complex fairing design.

Several unusual design parameters were generated by placing the antenna along the side of the vehicle. Probably the most interesting was the necessity of freeing the antenna from the effects of vehicle deformations due to thermal gradients across it. This is commonly called "vehicle hotdogging" and over the 15' length of the antenna this effect represented an error of over one-fourth of an inch which would be incompatible with the pattern requirements for an antenna of this application. To solve this problem the antenna was allowed to slide along three fixed points during both exit and orbit while a fourth point was affixed to the vehicle. By this approach the antenna was now free of vehicle deflections. It was determined the total deflections of the antenna aperture due to thermal gradients would be less than .026 of an inch.

2.1.5.2 Performance Requirements

The antenna and interconnecting waveguide specification described the original antenna requirement, specifying that the antenna would be a two-dimensional array capable of operation with the associated equipment. The antenna was to operate at 9600 mcs.

The azimuthal beam patterns for the array were defined as follows:

- o Half power beamwidth of .346 ± .02 degrees.
- o Main beam null to null beamwidth of .78 ± .04 degrees.
- o Azimuth side lobes shall not be greater than 12.5 db down with respect to the principle one way pattern.
- o The position of the second and third nulls should be .78 ± .1 degree and 1.17 ± .1 degree, respectively.

The vertical beam patterns would be as follows:

- o Half power beamwidth of 2.9 ± .1 degree.
- o Null to null beamwidth of the main lobe would be 6.5 ± .1 degree.
- o Side lobes would not exceed 12.5 db down from the peak of the main beam.
- o The position of the second null would be 6.5 ± .5 degree from the main lobe.

- o The side lobe level 30 to 35 degrees from broadside would be at least -25 db.

The antenna was to have a gain in excess of 43.0 db and be designed to handle 50 KW peak transmitter power with a PRF of 8736 and a pulse width of 1 microsecond while in orbit. The antenna VSWR would not exceed 1.4:1 over the required RF Band.

The azimuth boresight accuracy would be 0.05° and the elevation boresight accuracy 0.15°.

2.1.5.3 Antenna Design and Fabrication

To meet the thermal requirements with passive thermal control surfaces a careful thermal analysis was made. It was determined that proper surfaces would control the antenna temperatures during the anticipated launch window to temperatures from 0° to 90°F. This involved a more difficult thermal analysis than is normally accomplished for solid metal hardware designs because this temperature variation determined the extreme limits of the antenna bandwidth requirements. This was an unusual position for the thermal engineer and an unusual philosophy was developed between the two design groups to establish the most practical and economical design. The philosophy involved the establishment of probabilities of various temperature gradients. This proved to be very helpful as the normal approach would have had a minimum of an additional 20 to 40° temperature extreme.

The antenna in its final design configuration consisted of eighty-four elements, each of which had fifty-three narrow wall shunt slots and arranged four elements long and twenty-one elements wide. Two cross feeds with narrow wall shunt slots, twenty-one on each side of the narrow wall of the feed waveguide, were used to feed a single grid of forty-two - fifty-three slot elements. The feed waveguide was WR-75 which has inside dimensions of .375 X .750 in., and was available in both copper and aluminum to accuracies of ± .001 on the inside dimensions. This waveguide allowed greater spacing of the 53 slot elements because of the greater guide wavelength. Spacing between the 53 slot elements was 1.073 inches. Use of the WR-75 feed guide resulted in a 20 percent waveguide weight saving by reducing the number of vertical elements from 26 to 21. Of course, the slots on each side of the feed guide are at the same angle. Each element was precisely made and individually tuned for the best VSWR and bandwidth. An empirical design program was undertaken in conjunction with a theoretical analysis to determine the exact slot angle, depth, spacing, and width. It was necessary to design an over-coupled feed in order to obtain the desired antenna bandwidth. A perfect feed would not give as good bandwidth at a VSWR of 1.4:1 as the over-compensated feed.

Each forty-two element grid assembly was designed to be held on five channel cross members with a slot in each end of the cross member for vertical adjustment on the antenna frame. Each grid was affixed to the antenna frame at the center only, and then allowed to slide on eccentric pins in these slots at each eight remaining adjustment points for each grid. Each of these twenty adjusting points were used to produce an extremely flat array surface.

To eliminate residual stresses produced during fabrication which might be released by thermal variations allowing antenna deformations to occur where these stresses were relaxed, it was decided that welding or brazing would not be utilized as a fabrication technique. The elements were joined to their feeds and to support channels by bonding with ductile epoxy adhesive. This had the additional advantage of allowing magnesium to be bonded to aluminum so that no special extrusion dies were necessary to build the antenna. To obtain electrical continuity from the grid to the feed a silver-loaded epoxy was used and to obtain a mechanical joint with sufficient strength and flexibility each of these electrical joints was covered by Shell Development Company's Epon 921 epoxy. While this resin is procurable under Standard LAC Spec other epoxies which meet the same strength requirements could also be obtained. These epoxies lacked the flexibility necessary for this design to survive the exit environment. Considerable evaluation work was performed before adopting either the conductive epoxy or the mechanical epoxy.

The antenna frame consisted of two longitudinal channels which are separated by tubular members and sheet metal arches. These frames were fabricated on a fixture to insure precise alignment and straightness and to further eliminate the possibility of residual stresses being present which might relax under the influence of vibration or temperature variations. The frame contained the members for mounting the antenna to the vehicle. The antenna was mounted to the vehicle with one hard point and then contained by three additional mounting points which allowed the antenna to slide relative to the vehicle but fully contained the antenna. During exit conditions the cantilevered top portion of the antenna was held in place by the spring action of the frame being deflected 1/16 of an inch and contained by two pin pullers. After the fairing was removed the squib-actuated pin pullers were fired by electrical command allowing the antenna to return to a flat shape.

Broached waveguide was used for the fifty-three slot elements. This is a difficult broaching job as the stock was 48" long. The vendor would not certify that these components would have internal accuracies better than ± .003". The LMSC Antenna Laboratory had had considerable experience with this broach and it was known that the E-plane dimension would probably vary .002 to .003 due to the compression of the part during the broaching process; however, the H-plane dimension would be very accurate. (Indeed, it was, having an accuracy of ± .0005 inch). It is the H-plane dimension or wide dimension of the waveguide which was critical for this application. The broached waveguide for the elements almost eliminated fabrication rejects caused by variations of the H-plane dimension.

The slots were machined in the elements using a fourteen gang cutter. Spaces between each individual cutter were made to be twice the spacing between the slots as consecutive slots are at opposite angles. Every other slot is parallel. The cutter spaces were ground to an extreme accuracy of .00005. The machining was done on a large Lucas in the Agena D facility. A slotted waveguide element was placed in a fixture and then the fixture and table were moved through the gang cutter, next the table was indexed over so that the middle slot would pass back through a cutter. The table was then tilted to the proper angle for the alternate slots, indexed one slot, spaced, and moved through the gang cutter, indexed again and brought back through the cutter. Four cutting operations accounting for the fifty-three slots. The slots, however, were not finished to depth on the gang cutter. This was done by hand finishing with a gauging tool. This process of finishing each slot to the precise depth and de-burring was the most time consuming of the fabrication process. The degreasing and cleaning processes were extremely important to achieving good fifty-three slot elements. The influence of dirt and grease in the slots would create erroneous tuning and it was therefore necessary to establish an unusually rigorous procedure for degreasing, cleaning and application of the Dow 17 processing.

A sweep generator was used to produce a VSWR vs. frequency display on an oscilloscope to select the proper end plates and determine the usability of each of the fifty-three slot elements. All elements used had VSWR's better than 1.05:1 at f_o and all elements had VSWR displays superior to a No-Go standard which was imprinted upon the face of the scope. Each individual element was tuned for bandwidth and VSWR by selection of an end plate of proper dimension.

Each feed was checked with a load terminated stub over each of the forty-two slots and Smith Chart data taken to assure that each of the feeds would be able to produce a grid section with a prescribed bandwidth-VSWR relationship.

The grid assemblies were fabricated on a fixture which would locate each fifty-three slot element end over the appropriate feed slot within .005 of an inch. The grid support channels were bonded to the grid elements in this fixture and the end plates for each of the tuned elements were bonded to the elements at this time. Both the electrical conductive epoxy and the mechanical epoxy were applied in this fixture and before the grid was moved from the fixture the epoxies were cured with a baking process which involved placing a cover over the fixture and using heat guns to raise the temperature of the assembly to 145°F for a period of two hours. After the assembly had cooled a continuity check was made to make sure that electrical continuity was obtained. The grid assemblies were now tuned for bandwidth and VSWR with a double stub tuner and the end plate for the feeds. The end plates were then bonded in place, again using first the conductive epoxy and then the EPON 921 epoxy.

The grid assemblies and frame were transported to the antenna pattern range at Santa Cruz where the frame was mounted to the pedestal fixture and a transit used to align the grids on the frame to a flat surface. The grids were adjusted to flatness by locating the eccentric screws and after a flat surface had been obtained each of the eccentrics were drilled and pinned in place.

The two grid assemblies were then phased together using the pattern range and recorder to balance side lobes and nulls by adding or subtracting shims between each grid assembly and the magic T power divider. A magic tee was used instead of a conventional tee so that one arm of the magic tee would be open to allow the waveguide to outgas at this point. When the proper phasing had been obtained an aluminum shim was machined to replace the brass laminated stock. The antenna was tuned for bandwidth and VSWR consideration by selecting end plates for the double stub tuners. This plate adjustment was necessary in order to obtain the proper VSWR over the prescribed bandwidth of 30 mc.

2.1.5.4 Testing Program

Before any antenna testing could be performed, it was necessary to build a pattern range capable of measuring antenna patterns for this application. An extensive site selection study was undertaken and an excellent site was located in the Santa Cruz Mountains. This 17° range was located immediately adjacent to LMSC's Santa Cruz Test Base Facility and offers an excellent growth possibility for a 5° four-mile range. The Santa Cruz Test Base range had many additional advantages due to the close proximity to the facility at Santa Cruz where maintenance department services, equipment and machine shops, and other services were available. 40' towers were used on each end of this 5600' range. The receiving tower consists of a large working platform at the top of an extremely rigid base which mounts a pedestal capable of supporting an Agena vehicle. The remote or transmitting site is operated by radio controls from the receiving site. The receiver, the positioner control, console and the recorder are all located in one convenient cabinet or console in a 20 X 30' building at the base of the receiving tower. Figures 2.1.5.1 and 2.1.5.2 show the antenna on the receiving tower.

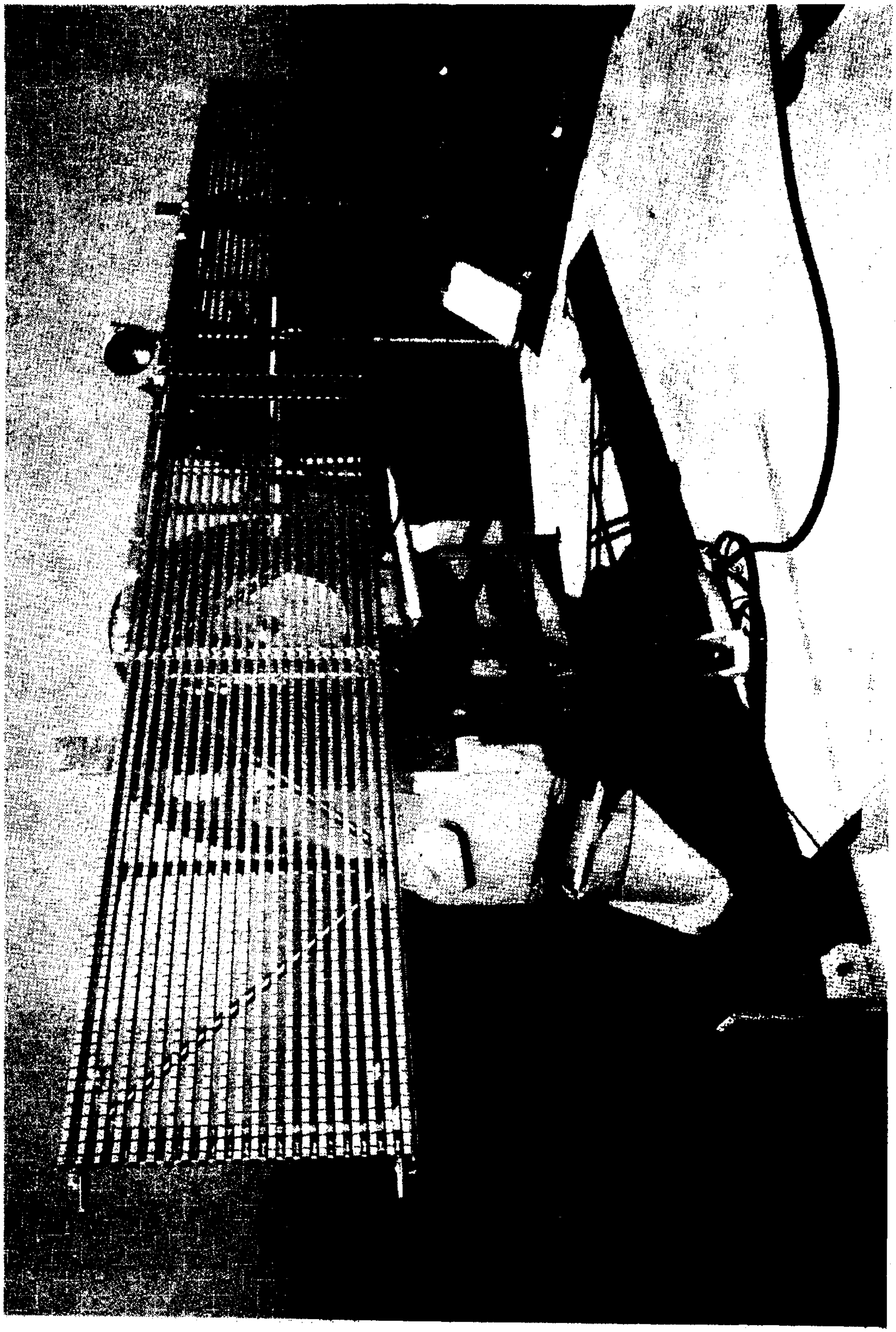

Figure 2.1.5.1 - Radar Antenna on Boresight Tower

Figure 2.1.5.2 - Radar Antenna on Boresight Tower

Patterns taken on this range serve as a method of debugging the antenna design as well as for taking the final patterns.

Two basic testing philosophies were utilized for this program. One was the use of design proof testing to verify the design approach. The second was the more rigorous qualification and acceptance testing required to insure a high quality product capable of successful operation in the space environment after undergoing exit conditions.

Design verification tests were conducted on various epoxy resins to assure that the proper selection had been made. This included hot tests (180°F) and cold tests (-60°F) in which bonded components were drop tested to assure flexibility over the above temperature range. Small scale vibration tests were conducted early in the design stages to verify the bonded design approach.

A quarter-section brass array was tested to verify slot design and to verify that the spacing between the elements in the vertical array was correct. A full scale antenna was fabricated in brass so that design modifications could be made easily, yet a complete electrical antenna assembly would confirm the final design approach.

Feed tests were conducted in the vacuum chamber located in Building 130 to verify the ability of the feed to handle the prescribed power at altitude. Measurements were made of pulsed power breakdown in air at 3.2-cm wavelength in rectangular waveguide through the transition from diffusion-controlled breakdown. The range of pressure for these measurements was between 1 and 10^{-3} Torr. The mean-free-path limit defined by Brown and MacDonald [1] corresponds to about pd = 0.06 cm-Torr, where p is the pressure and d the narrow dimension of the waveguide. Results of the measurements are shown in Figure 2.1.5.3.

The measurements were made using a magnetron modulated by 1-usec pulses at 1000, 2000 and 5000 pulses/sec. No pulse-rate effect was observed. Measurements were made in reduced-height sections of waveguide tapered down from standard 1 X ½ in. (2.54 X 1.27-cm) rectangular waveguide. Two sections were used: one with d = 0.63 cm, the other with d = 0.25 cm. The data were normalized to standard waveguide. A polonium source was placed over a small hole in the waveguide broad face to obtain consistent results.

By curve fitting to the data of Gould and Roberts[2], an expression for the diffusion-controlled breakdown was obtained to extend the curve marked I in the figure to the mean-free-path limit. The expression for this curve is

$$18.4 = \left[\tfrac{1}{4}\,(E_e/p - 26)^2 - 100\,(E_e/p)/p^2d^2\,(1 + w^2/v_c^{\,2})^{\frac{1}{2}}\right] p_t\ , \qquad (1)$$

where E_e is the effective electric field strength, iven by

$$E_e = E_o / \left[2(1 + w^2/v_c^{\,2})\right]^{\frac{1}{2}}\ , \qquad (2)$$

w is the radian frequency, and v_c is the collision frequency.

The portion of the curve marked II, to the left of the transition, was calculated by means of the formula

$$n/n_o = \exp\left[(v_{net}/p)\, p_t\right]\ , \qquad (3)$$

- - - - - - - - - - -

1) S. C. Brown and A. D. MacDonald, Phys. Rev. 77, 1629 (1949)

2) L. Gould and L. W. Roberts, J. Appl. Phys. 27, 1162 (1956)

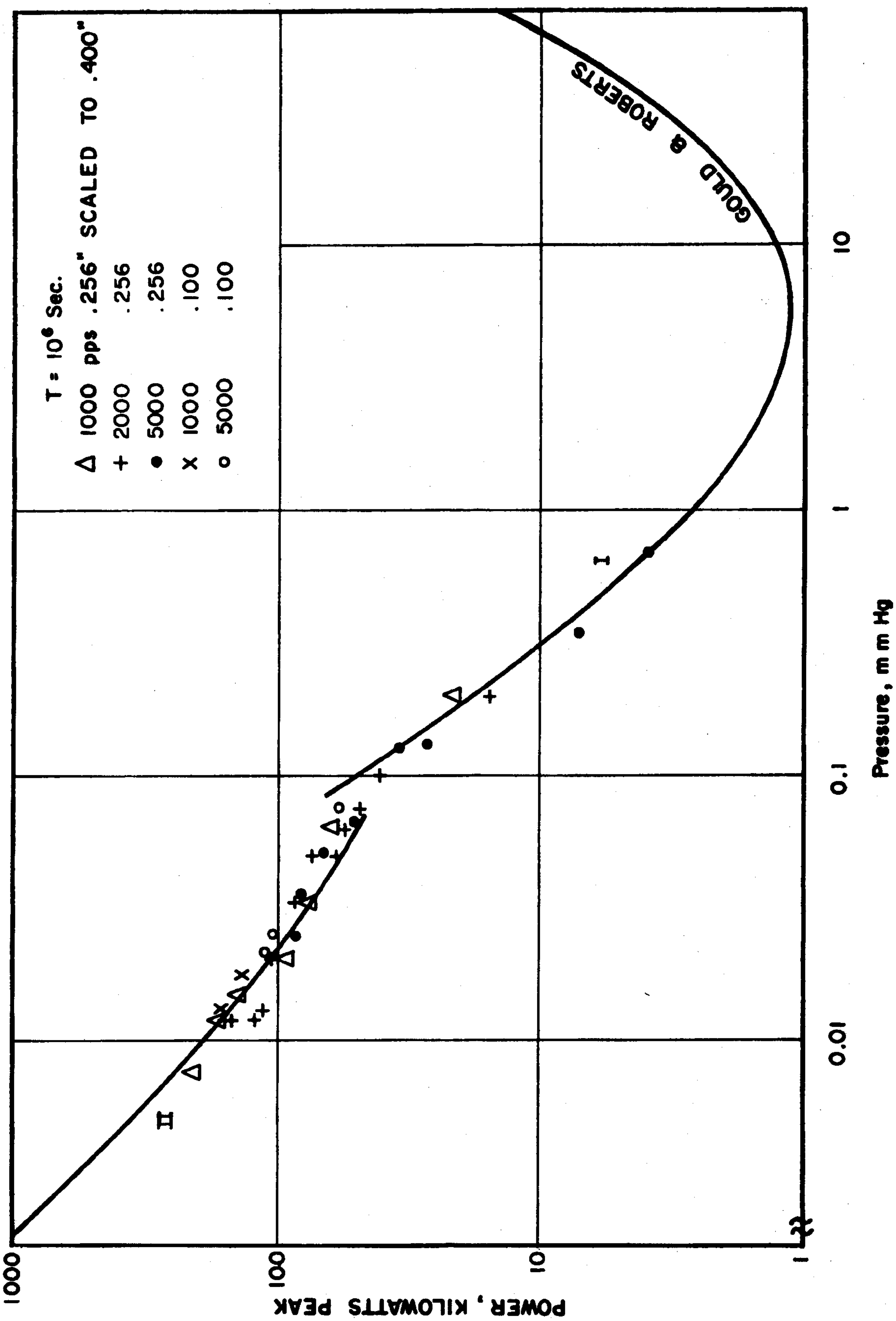

FIGURE 2.1.5.3 BREAKDOWN POWER IN 1 X ½-in. (2.54 X 1.27-cm) WAVEGUIDE AS A FUNCTION OF AIR PRESSURE

where V_{net}, the net ionization frequency, is given by extrapolation of the data of Gould and Roberts by the expression

$$V_{net}/p = \tfrac{1}{4} (E_{e/p} - 26)^2 \times 10^4, \tag{4}$$

and $n/_{no}$ is the ratio electrons produced in time t, the duration of a single pulse, to the initial number n_o. Following Gould and Roberts, $n/_{no}$ is assumed to be at least 10^8. The interpretation of the expression is simply that, although the mean free path of the electron is greater than the waveguide dimension d, the electron makes many oscillations in the field before it can drift to the wall. Consequently, frequent collisions occur that may produce ionization. If the ionization rate is sufficiently great to yield $n/_{no} > 10^8$ before electrons can be lost by drifting to the walls in time t, breakdown will occur.

Multipacting is not indicated. These tests were performed to verify the ability of the entire system to pass 30 KW peak power thru X-band waveguide.

Qualification tests were performed on a quarter-scale model to determine the ability of the antenna to successfully survive the exit environment. Three axis vibration tests were conducted. Resonant searches were conducted in all three axes. Sinusoidal sweep levels of ½" dynamic amplitude from 5 to 9 cps, 2 g load from 9 to 200 cps, 5 g load from 200 to 2000 cps, were conducted in all three axes, together with random vibration levels of 0.01 g^2/cps for 20-200 cps, 0.03 g^2/cps for 200-400 cps, 0.08g^2/cps for 400-2000 cps. These random vibration levels are unusually severe.

Also, during the random vibration in the Z-axis one of the bonds of an element to the waveguide support channel broke and during the Y-axis random vibration a different bond broke to the center waveguide support channel. No additional damage occurred because of these failures. The bonding procedure was improved because of the failures. Before bonding the flight antennas the waveguide support channels were cleaned of their iridite surface finish and the Dow 17 was removed from an area adjacent to the channel on the waveguide element. This procedure had not been used in fabricating the $\frac{1}{4}$ scale model. Patterns which were taken before the vibration test agreed with the patterns taken after the vibration test, therefore confirming that no substantial damage was inflicted to the test mockup by the vibration test.

A full-scale antenna was subjected to static load tests in such a way as to reproduce the maximum possible load levels which the antenna would be required to withstand. Three different structural level tests were conducted with various different loads applied. Deflection of the antenna was recorded for each of the tests before, during and after the tests. In each case, the antenna withstood these tests very easily. Two dynamic tests were conducted on the full-scale model. The first was a squib firing test in which the antenna was deflected as it would be in flight to the proper position for the pin pullers and the squibs were fired. This test was conducted both with one and two squibs in each of the pin pullers. No damage to the antenna was noted. A cyclic load or forced vibration test was conducted in which the antenna was vibrated at the center of the mounting span. The displacement of $\frac{1}{2}$" at 5 cps, a 4 g load or $\frac{1}{2}$"

displacement at 12 cps, and 2 g load from 15-1200 cps. The antenna successfully passed this test without any physical damage. Antenna patterns taken at the Santa Cruz Test Base range before and after these tests verified that the antenna was completely undamaged even though the vibration levels were considerably above expected vehicle requirements.

Feed tests similar to those performed in the vacuum chamber, Bldg. 130, were done with the entire system in the TAS Chamber in Bldg. 104 to verify that a power breakdown problem did not exist in the feed slots nor the input waveguide.

Acceptance tests were conducted on each of the three antennas to show that each had been properly fabricated. A forced vibration of ± .125" deflection at 5 cps, 2 g load at 12 cps and 2g load from 15-1200 cps was imposed on the antenna. The first two tests were of five-minute duration and the last ten from 10 to 20 minutes duration. The antenna was patterned before and after this series of tests and the boresight alignment was checked before and after each of the tests. Figures 2.1.5.4 and 2.1.5.5 are principle plane patterns for the array.

2.1.5.5 Alignments

The first of the alignment procedures took place at the antenna pattern range. This operation was essentially one of locating an optical line of sight parallel to the electrical line of sight. To perform this, a boresight bracket which was capable of adjustment in two planes, was affixed to the antenna frame at the center of one of the channel members.

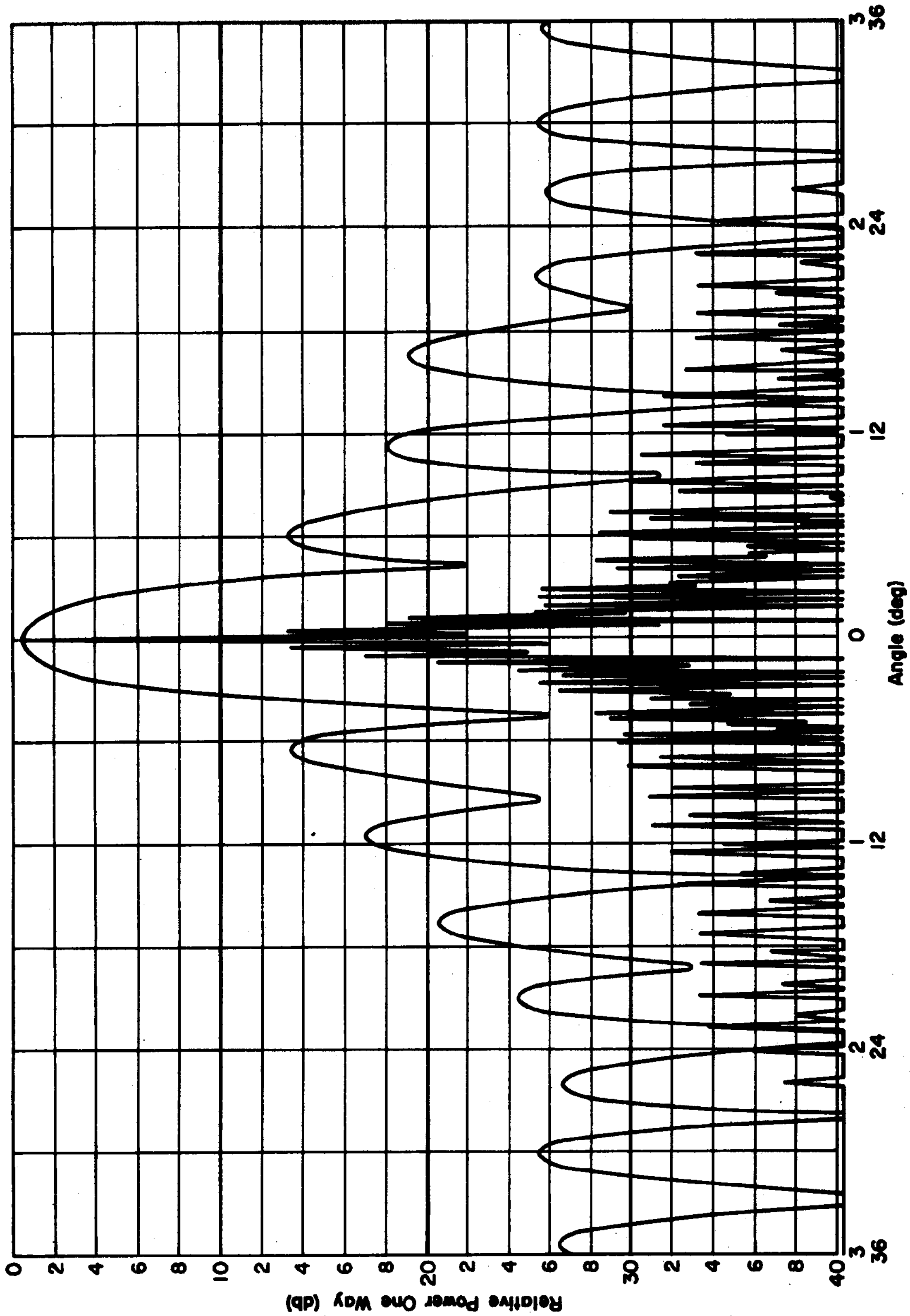

UNIT 101 E-PLANE PATTERN

Figure 2.1.5.4

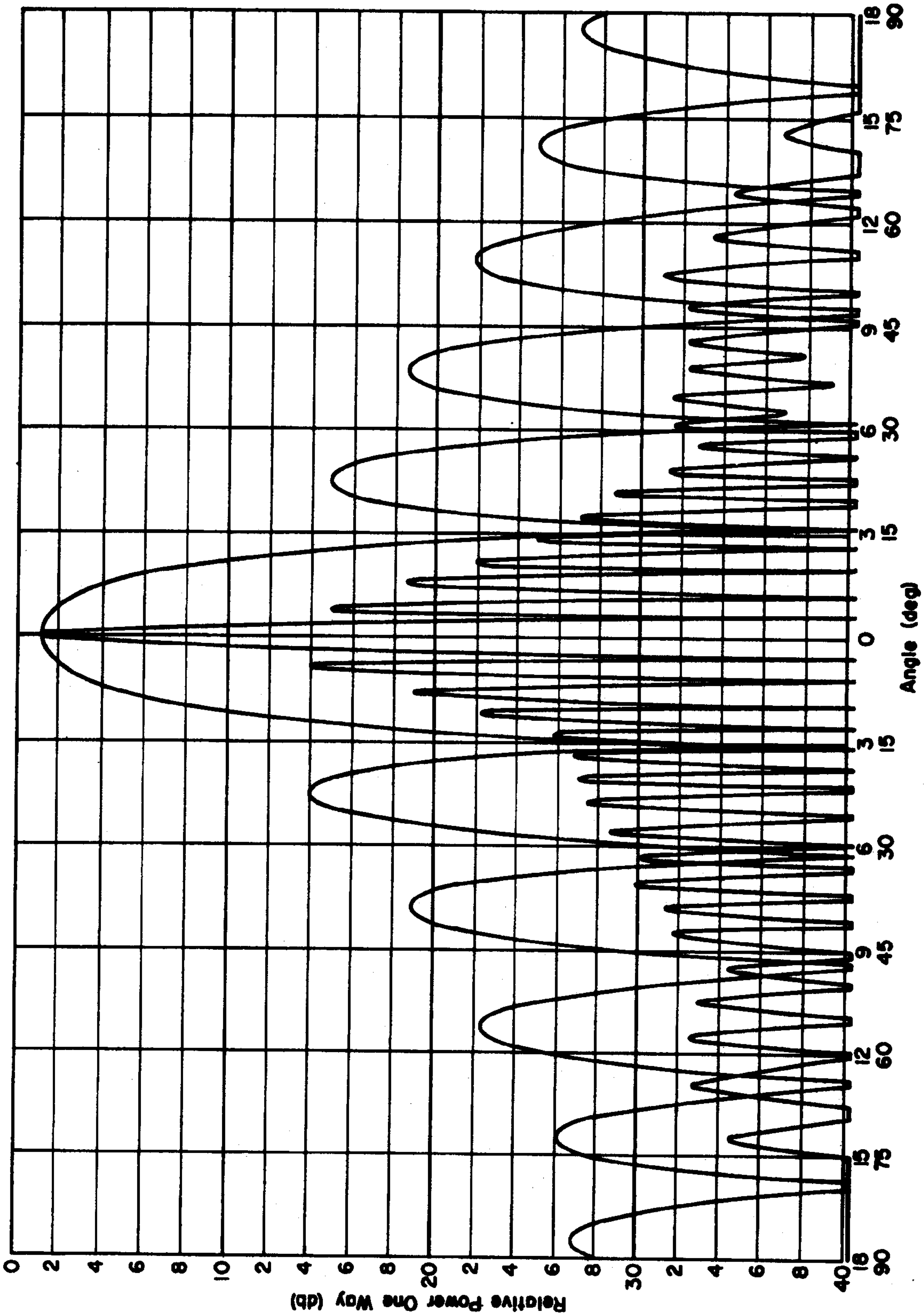

UNIT 101 H-PLANE PATTERN

Figure 2.1.5.5

A telescope was mounted to this bracket and the antenna was positioned for electrical boresight. The optical axis was adjusted by positioning the bracket until the cross hairs of the telescope aligned with a properly positioned target at the transmitting site. The boresight bracket was then drilled, reamed and doweled and repeatability checks made to assure that a proper boresight had been obtained.

The second part of the alignment procedure took place at Vandenberg Air Force Base. The vehicle was mated in a vertical position. The antenna was installed and the vehicle rechecked for its vertical position. A theodolite was positioned on the 35° line from the -Z axis. A second theodolite was positioned in approximately its proper position for alignment with the boresight telescope. The angular position of the second theodolite with respect to the theodolite on the 35° line was established and this theodolite was then set parallel to the 35° line and in a horizontal position. The vehicle mounting eccentrics were adjusted to achieve the best alignment. Perfect alignment was not obtainable because of irregularities in the vehicle greater than the .032" allocated for this error. The error in the azimuth or long dimension was 0° 2' 0". The elevation or short dimension error was 0° 1' 17". Several rechecks were made before the eccentrics were drilled and pinned. A recheck was made after the drilling and pinning operation and the error was the same. The pins were then removed and the eccentrics rotated several turns and then repinned to assure repeatability. The angular errors at the completion of this operation were identical and since this is essentially the same as taking the antenna physically down and putting it back, that specific operation was not performed. Had some error been induced by turning the eccentrics, the antenna would have been removed and re-installed until acceptable; however, the repeatability was excellent. A vertical transit was set up so that it would sweep the four mechanical reference alignment points. A sweep of these points indicated that the boresight scope was pointing high with respect to the mechanical reference plane and this agreed with our check at the antenna range. Our repeatability checks on the antenna range also showed that the boresight itself was pointing slightly higher than the electrical axis so that in the azimuth plane the errors are subtractive and our actual alignment error would be slightly less than 0° 2' 0". Conversely, the errors in alignment in the elevation axis showed that it was slightly less than 0° 2' 0". The specification allowed for errors of 0° 3' in azimuth and 0° 9' in elevation.

A vertical transit was set up to sweep the antenna surface to confirm that the antenna surface was still flat. These measurements showed the antenna was flat within .016 inch over the entire surface when mounted to the vehicle. This confirmed the original fabrication tolerance obtained at the antenna range.

2.1.6 Thermodynamics

2.1.6.1 Introduction

The purpose of this section is to review unique or important thermal-control problems that have been encountered in the utilization and adaption of an airborne radar system to a satellite payload. The general engineering area considered is temperature control of equipment, structure, and the over-all satellite vehicle. Parameters affecting equipment thermal behavior are described; the effects of spacecraft environment and orbit geometry are discussed; problems associated with equipment design, environmental testing, ascent analysis, and orbit analysis are reviewed.

2.1.6.2 Definition of Terms

Understanding of this section requires definition of the basic concepts, quantities and terms used. These are defined in the following paragraphs:

Thermal Radiation   Thermal Radiation is defined as radiation emitted from a body by virtue of its temperature. A blackbody or ideal radiator, absorbs all incident radiant energy and radiates energy at the maximum rate possible per unit area. The Stefan-Boltzman Law states that the total radiant emission of a blackbody is proportional to the fourth power of its absolute temperature.

Emittance, ϵ , of a body is the ratio between the energy emitted by the body and that which would be emitted by a blackbody at the same temperature. Solar absorbtivity, α_s, refers to the fraction of the sun's radiant energy incident on a body which is absorbed and transformed into internal thermal energy of the body.

Thermal Conduction Internally, all solid objects transfer heat solely by conduction, and the property of a substance that expresses this ability is called thermal conductivity, k. The rate equation for conduction heat transfer states that the heat flowing across an area is equal to the thermal conductivity times the temperature gradient at the point of interest.

Thermal Convection In the case of liquids and gases, conduction heat transfer often plays a relatively small part in the transfer of energy, the greater influence on heat transfer being the gross motion of the fluid itself. The fluid in these convection systems may be moved by buoyancy in a gravity field by pumps, or by fans. Convection systems fall into two categories: Free convection and forced convection. Free convection heat transfer results when the fluid to be heated or cooled is stagnant before heat is added or removed. When the fluid begins to change temperature, its density also changes and it will rise or fall in the main body of fluid, owing to local buoyancy forces. As is implied, in a forced convection system the fluid is forced to move by the use of pumps or fans. The rate equation for convection heat transfer states that the heat flowing across an area is equal to the convection heat transfer coefficient, h_c, times the controlling temperature gradient. Whereas thermal conductivity, k, is a property of the material, h_c is a property of the system and depends on a large number of parameters.

Power Dissipation Internal power dissipation in electronic equipment refers to the rate with which thermal energy is added to the equipment during its operation. In the case of an electrical power supply, this energy rate will be the difference between input and output electrical power and is a measure of the equipment's efficiency. For a storage battery, this energy comes from both heat producing chemical reactions and electrical power losses due to the battery's internal resistance.

Launch Window and Orbit Geometry External heat fluxes incident on a spacecraft are a function of the orbit geometry. For nearly circular orbits, these energies can be adequately determined knowing only the mean orbit altitude and the Solar Incidence Angle, Beta (β). Verbally, β is the angle whose magnitude is the complement of the acute angle between the earth-sun direction and a normal to the satellite orbit plane. Since orbit altitude and the satellite orbit inclination angle are mission parameters which do not normally change for any given payload system, external orbital heat fluxes for that system then become only a function of the time and date of launch.

Thermal window refers to the allowable range of Beta angles over which orbital temperature control of spacecraft equipment can be insured. Orbit plane regression due to earth, orbit, and sun geometry also causes Beta to change. For example, at inclination angles of 70° Beta changes approximately 4° per day. For a given mission duration, the regression of Beta must be accounted for to determine the thermal launch window. Considering the following conditions -

- Thermal Window, $30° > \beta > -30°$
- Satellite Orbit Inclination Angle, +70°
- Mission Duration, 5 days
- Launch, June 15 from VAFB

the thermal launch window would be $10° > \beta > -30°$ and would correspond to a launch time (Pacific Standard Time, PST) of 1054 to 1412. To show the effect of date of launch, on December 15 the thermal launch window would be 0930 to 1236 PST.

Active versus Passive Thermal Control Passive control of the thermal behavior of a system and its components is attained wholly through geometrical design and the selection of materials with the requisite thermophysical properties. Neither power nor moving parts are employed. Techniques for passive thermal control include use of -

- Materials with desired thermal radiation properties
- Geometrical design
- Materials with desired values of thermal conductivity
- Utilizing materials as heat sinks

Active thermal control of a system and its components is attained through a feedback control system, with temperature as the controlled variable. Generally, either power or moving parts are employed. Techniques for active thermal control include the use of:

- Thermostats and Heaters
- Shutters to control variable α_s/ϵ devices
- Fluid transport cooling systems
- Variable thermal - resistance techniques
- Thermoelectric cooling

Passive thermal control systems have certain advantages over active systems in regard to reliability. They employ no moving parts or switches which may malfunction and generally require less weight. Active thermal control systems can correct for environmentally induced alterations in the thermal behavior of a vehicle. Extremely accurate knowledge of thermal radiation characteristics is not mandatory for active systems as it is for passive; hence, successful operation of a given vehicle is less likely to be jeopardized by the various factors of the prelaunch environment. In addition, active control can provide much more precise control of temperature than is possible with passive control.

2.1.6.3 General Statement of Work

The primary objective of thermal-control is to maintain satellite components - either mechanical or electrical - within temperature ranges which will insure satisfactory operation. This control must be provided during a variety of environments from component testing to launch countdown, and finally to orbital flight. Thermodynamic investigation of Vehicle 2355 was initiated 26 months before launch and centered around these major items:

- Recognization of thermal-control problem areas
- Internal thermal design of the radar payload
- Coordination between the Payload Associate Contractor and the Systems Associate Contractor
- Determination of equipment temperature limits and duty cycles
- Environmental testing of components and systems
- Orbit analysis of the complete satellite vehicle with resulting temperature predictions
- Temperature control of primary batteries

The radar payload is an adaption of an airborne system to a satellite. Since the airborne system used forced air cooling, it was capable of continuous operation even though the level of internal power dissipation was high. Most orbital temperature control schemes can not afford the luxury of an active control system nor can they add excessive weight to the equipment. Initial meetings between Lockheed and the Payload Associate Contractor resulted in guidelines being set which made passive temperature control feasible. Significant guidelines were the establishment of temperature limits, duty cycle and thermal window.

The normal method of specifying orbital temperature limits for spacecraft equipment is to refer to the maximum and minimum allowable base plate or mounting surface temperatures. For small electronic equipment, where all internal components are mounted on the base plate and the remaining sides act only as a cover, this method is adequate. However, for equipment where sides other than the mounting base may be structural or component mounting surfaces, the method is inadequate since it defines only the allowable temperature environment on one face of the equipment. Additionally, specifying only the base plate temperature environment, causes confusion during qualification testing, since the question arises as to the temperature environment of the remaining sides.

Temperature limits imposed on payload components were unique in that they did not refer to equipment temperatures but rather were limits on the environment in which the equipment must operate. For example, the Transmitter-Modulator would have to operate in an environment that was between 0°F and +100°F - this meant that the surroundings with which all external surfaces of the transmitter exchanged thermal energy would be between 0°F and +100°F. The equipment itself would be at least as warm as its surroundings with some internal components being hundreds of degrees hotter. Setting equipment temperature limits in this manner, in effect, provided the division of responsibilities between Lockheed and the Payload Associate Contractor: the Associate Contractor would provide equipment capable of operating in a specific thermal environment while Lockheed would be required to provide the proper environment in the satellite.

Mission parameters dictated that the payload system would have to be capable of at least 5 minutes of operation each orbit. The maximum duty cycle per orbit was set at 5 minutes of warm-up followed by 5-1/2 minutes of combined pre-operate and operate. Passive internal thermal design of the payload could be accomplished with this relatively short duty cycle even though the internal power dissipation associated with the operate mode was in excess of 2 kilowatts. The design approach would be to store this thermal energy during operation, and then during the off cycle to provide for energy removal from the equipment to the spacecraft structure and eventually to outerspace.

The initial thermal window determined for the satellite gave a Solar Incidence Angle (β) of $30° > \beta > -30°$. Considerations effecting the establishment of this window were:

- Its compatibility with a requirement for daylight recovery.
- The Agena vehicle had previously been analytically and flight qualified to operate within this external environment.
- Considering the 4 day duration of the mission, the launch window would be at least 3 hours wide.
- Lockheed Thermodynamics felt confident that, for this thermal window, passive thermal control would be adequate for all vehicle and payload equipment.

2.1.6.4 Internal Thermal Design of the Radar Equipment

Thermal design of the radar equipment was the responsibility of Goodyear Aerospace Corporation. The following discussion of Goodyear's Thermal Evaluation was abstracted from Section IV of the Goodyear Report.

General - Thermal studies were conducted to determine the requirements for adequate environmental protection to the electronic equipment associated with the KP-II radar system. Analyses were also made to evaluate the adequacy of the equipment to meet these requirements. The studies and analyses included a review of the basic thermal design philosophy, investigation of ascent heating conditions, orbital temperature studies, and a study of the thermal characteristics of the equipment during ground operation. Unit design was based upon the requirements of satisfactory operation for three successive orbit duty cycles and five-minutes of operate per orbit with the environmental conditions specified below. These temperatures are average temperatures which are applicable to the vehicle skin with which the units exchange thermal energy during orbit.

	Temperature Range (F)	Pressure Range (mm Hg)
Units (other than Recorder)	0-100	10^{-1} to 10^{-8}
Recorder	32-130	10^{-1} to 10^{-8}

Thermal Design Philosophy - The KP-II radar system was adapted from the AN/UPQ-102 (RF-4C) Doppler Radar which used internal forced air cooling. Use of forced air or similar active cooling systems in the KP-II system was not considered since thermal control of electronic equipment in space is most efficiently accomplished by passive means. The thermal design of the KP-II system was therefore based upon radiation thermal interchange which is the primary available mode of heat transfer. Thermal control of the various units occurred by radiation to the vehicle skin. Components within these units experienced thermal interchange with the unit walls and structure by radiation and conduction.

Space stable thermal coatings having desirable emittance characteristics were used on the equipment to obtain maximum thermal interchange. To assure high emissivities, black paint or black anodizing was used on the units which comprise the system. Care was taken in selecting paints which, by decomposition while in space, would not create a pressure environment in the equipment or vehicle. It should be noted that proper thermal treatment of the vehicle skin was also required for maximum thermal interchange between the system units and the vehicle. Thermal analyses presented herein pre-supposed such vehicle thermal coating.

The electronic equipment experienced transient heating and cooling conditions, with the maximum and minimum temperatures depending upon the particular orbit geometry. Heat sinks were used in the equipment where local heating conditions of particularly temperature-sensitive components indicated the necessity. Foils and highly conductive silicon grease were used extensively to reduce thermal contact resistance in these applications.

Method of Analysis -

- Radiation - Thermal analysis in many cases was based solely upon radiation thermal interchange (either to a unit case or to the vehicle skin). The following expression for radiation thermal balance was used:

$$Q = \sigma E_c F_c A_c (T_c^4 - T_s^4) + (WC_p)_c \frac{dT_c}{d\theta} \qquad (1)$$

where

Q = Energy Rate (Btu/hr)

σ = Stefan-Boltzmann constant

(0.1714×10^{-8} Btu/hr ft^2 degrees R^4)

E_c* = emittance

F_c = radiation view factor

A_c = radiating area (ft^2)

W = weight (lb)

C_p = specific heat (Btu/lb degrees R)

θ = time (hr)

T_c = temperature of component - emitting (degrees R)

T_s = temperature of component - absorbing (degrees R).

* Subscript "c" denotes properties of the component.

For the steady state, Q can be expressed as:

$$Q = E_c F_c A_c (T_\infty^4 - T_s^4) \; . \qquad (2)$$

Where T_∞ is the steady-state component temperature, Equations (1) and (2) combine to form:

$$\sigma E_c F_c A_c (T_\infty^4 - T_s^4) = \sigma E_c F_c A_c (T_c^4 - T_s^4) + (WC_p)_c \frac{dT_c}{d\theta} \; . \qquad (3)$$

The variables T_c and θ can be readily separated and for a differential time interval, $d\theta$, Equation (3) becomes:

$$\frac{dT_c}{(T_\infty^4 - T_c^4)} = \frac{\sigma E_c F_c A_c}{(WC_p)_c} \, d\theta \; . \qquad (4)$$

With an initial component temperature T_o and a temperature at time θ of T_c as limits, integration of Equation (4) yields:

$$f\left(\frac{T_c}{T_\infty}\right) = f\left(\frac{T_o}{T_\infty}\right) + \frac{4 E_c F_c A_c \sigma T_\infty^3 \theta}{(WC_p)_c} \qquad (5)$$

where

$$f\left(\frac{T_c}{T_\infty}\right) = 2 \tan^{-1}\left(\frac{T_c}{T_\infty}\right) - \ln \pm \frac{(T_c/T_\infty) - 1}{(T/T\quad) + 1} \quad . \qquad (6)$$

It is noted that, for analytical purposes, heating is assumed to be periodic each orbital cycle. For repetitive cycles the component temperatures, therefore, vary between T_{c1} and T_{c2} at the beginning and end of the operate period, respectively.

Equation (6) can then be written as:

For Heating:

$$f\left(\frac{T_{c2}}{T_\infty}\right) = f\left(\frac{T_{c1}}{T_\infty}\right) + \frac{4\, E_c F_c A_c \sigma T_\infty^3\, \theta}{(WC_p)_c} \qquad (7)$$

For Cooling:

$$f\left(\frac{T_{c1}}{T_\infty}\right) = f\left(\frac{T_{c2}}{T_\infty}\right) + \frac{4\, E_c F_c A_c \sigma T_\infty^3\, \theta}{(WC_p)_c} \quad . \qquad (8)$$

For heating, T_∞ is equal to the steady-state component temperature found in Equation (2). For cooling, T_∞ is essentially the skin temperature T_s. The radiation parameter $f\left(\frac{T_c}{T_\infty}\right)$ for both cooling and heating is plotted in Figure 2.1.6.1. Temperatures T_{c1} and T_{c2} can be found by solving Equations (7) and (8) simultaneously.

o <u>Conduction</u> - Maximum temperatures of components mounted on large radiating heat sinks were found by assuming that all heat dissipation was conducted directly into the sink and from there

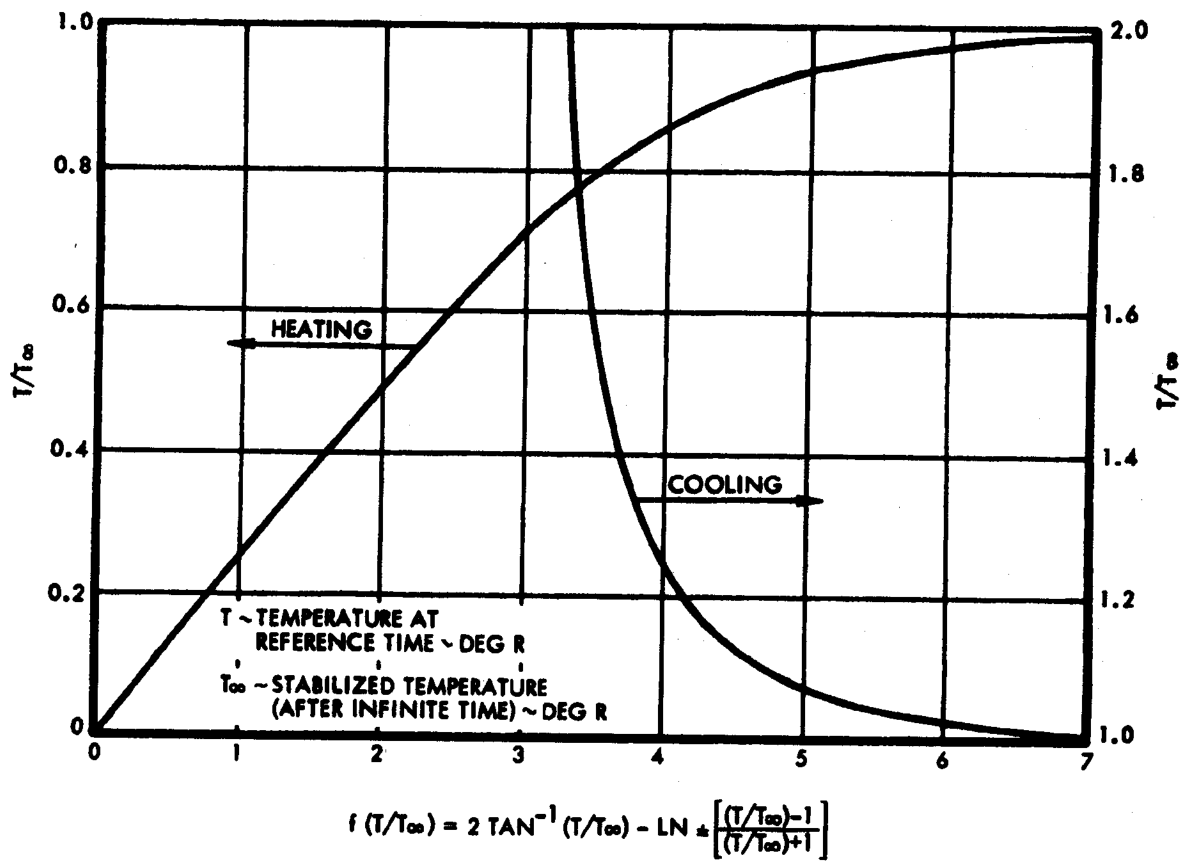

FIGURE 2.1.6.1 - RADIATION PARAMETER

radiated to an absorbing skin (vehicle or case). The sink temperature was then calculated by the method outlined above. The temperature difference between the component and the radiator was found from:

$$Q = U_{c-r} (T_c - T_r) \tag{9}$$

where U_{c-r} is the surface conductance (in Btu/hr degrees R) between the components and the radiator.

In other cases the maximum component temperature was obtained by assuming that all heat dissipated during the operating cycle was fully absorbed by the component thermal mass. This approach was used where the component had a fairly large mounting area and where the thermal contact resistance between the component and the radiating heat sink or mounting plate was small. Under these conditions, the component temperature at the start of the operating cycle is essentially the sink temperature. Since the heat sink or base temperature can be found by considering the radiation thermal balance, a conservative value for maximum component temperature (T_{c2}) can then be found from:

$$Q_c \theta = (WC_p)_c \quad (T_{c2} - T_{c1}) \quad . \tag{10}$$

where T_{c1} is the component temperature at the start of the operating cycle.

Equipment Thermal Analysis - Detailed thermal analyses were conducted on each unit comprising the radar system to determine the unit thermal characteristics while operating in a space environment. Studies were also made on component parts and individual electronic modules to determine heating and cooling response in a vacuum. Experimental investigations of techniques to enhance thermal interchange were also made.

Results of the analyses conducted on the various units are presented in Tables 2.1.6.1 through 2.1.6.5. Maximum predicted orbital temperatures are given for high heat dissipating or temperature sensitive components. Unit average temperatures are also given.

Results of the analyses and investigations indicate that in every instance the thermal design of the equipment was more than adequate to assure proper temperature control of all system components while operating in an orbiting vehicle. In each case maximum expected component temperatures were below acceptable specification limits. Furthermore, temperatures given in the individual analyses are generally conservative and are based, for the most part, on an average vehicle skin temperature of 100 degrees F (Recorder analyses were based on an average vehicle skin temperature of 130 degrees F). Results of the computer analyses conducted on the Agena vehicle by LMSC indicated that the average vehicle skin temperatures in the conical and barrel sections of the vehicle were found to be 80 degrees F and 73 degrees F, respectively. Minimum temperatures were 67 degrees F and 39 degrees F. Expected component temperatures can thus be reduced accordingly.

The analyses were based upon operation during each consecutive orbit. Actual duty conditions were not this severe. Operation would not be required for more than two consecutive orbits. In view of this fact an additional margin of safety was indicated.

Results of the computer analysis further indicated that no thermal problem should be anticipated at the low temperatures encountered during the orbital cycles. Minimum vehicle skin temperatures and unit temperatures would be sufficiently warm for reliable operation of all components used within the KP-II radar system.

TABLE 2.1.6.1 - SUMMARY OF ANALYSES: TRANSMITTER - MODULATOR

T/M Signal Number	Component	Calculated Maximum Orbital Temperature (° F)	Maximum Allowable Temperature Limit (° F)
F 34	Klystron collector	452*	572
F 35	Klystron body	240	250
F 36	Unit case	158	-
-	Pulse-forming network	164	185
-	Power resistors	365	527
F 37	Pulse transformer	159	185
-	Thyratron	386	752

* See Figure 2.1.6.2

TABLE 2.1.6.2 - SUMMARY OF ANALYSES: R-F/I-F UNIT

T/M Signal Number	Component	Calculated Maximum Orbital Temperature (° F)	Maximum Allowable Temperature Limit (° F)
	Unit average temperature	102	-
F 33	Transmit-receive tube	180	185
F 31	Traveling wave tube	135	185

TABLE 2.1.6.2 - SUMMARY OF ANALYSES: R-F/I-F UNIT (Continued)

T/M Signal Number	Component	Calculated Maximum Orbital Temperature (° F)	Maximum Allowable Temperature Limit (° F)
F 32	Frequency multiplier	116	149
-	RE75 power resistors	278	350

TABLE 2.1.6.3 - SUMMARY OF ANALYSES: REFERENCE COMPUTER

T/M Signal Number	Component	Calculated Maximum Orbital Temperature (° F)	Maximum Allowable Temperature Limit (° F)
F 27	Unit case	110	-
-	Printed circuit board (heat density - 20 watts/ft^2)	123	-
F 22	Video amplifier	173	212
F 23	Gate sequencer	165	212

TABLE 2.1.6.4 - SUMMARY OF ANALYSES: CONTROL UNIT

T/M Signal Number	Component	Calculated Maximum Orbital Temperature (° F)	Maximum Allowable Temperature Limit (° F)
F 20	Power supply	165	-
-	Transformer (-23.5 VDC)	141	185
F 21	Unit case	130	-

TABLE 2.1.6.5 - SUMMARY OF ANALYSES: RECORDER UNIT

T/M Signal Number	Component	Calculated Maximum Orbital Temperature (° F)	Maximum Allowable Temperature Limit (° F)
F 30	Unit case	134	-
F 28	Deflection amplifier		
	(Heat sink)	175	-
	(Power transistors)	243	257
F 29	High voltage power supply	145	185
-	Drive motors	204	300

Ground Operation - Thermal design of the units comprising the KP-II radar system was based upon operational cycling in a space environment with a comparatively short duty period per cycle. Thermal conditions encountered during ground operation or bench testing for periods which exceeded the normal space duty cycle were therefore considered.

Analytical studies were conducted to determine the time period that each of the KP-II system units could be operated during testing or other ground operations without exceeding the component design temperature limits. The analyses were based upon operation at full design power levels in the "buttoned-up" condition. Heat transfer was assumed to be accomplished by radiation and by free or forced-air cooling. The analyses showed that the Recorder, Reference Computer, Control and R-F/I-F units could be operated continuously in a laboratory environment using only natural radiation and free-convection cooling, without exceeding temperature design limits.

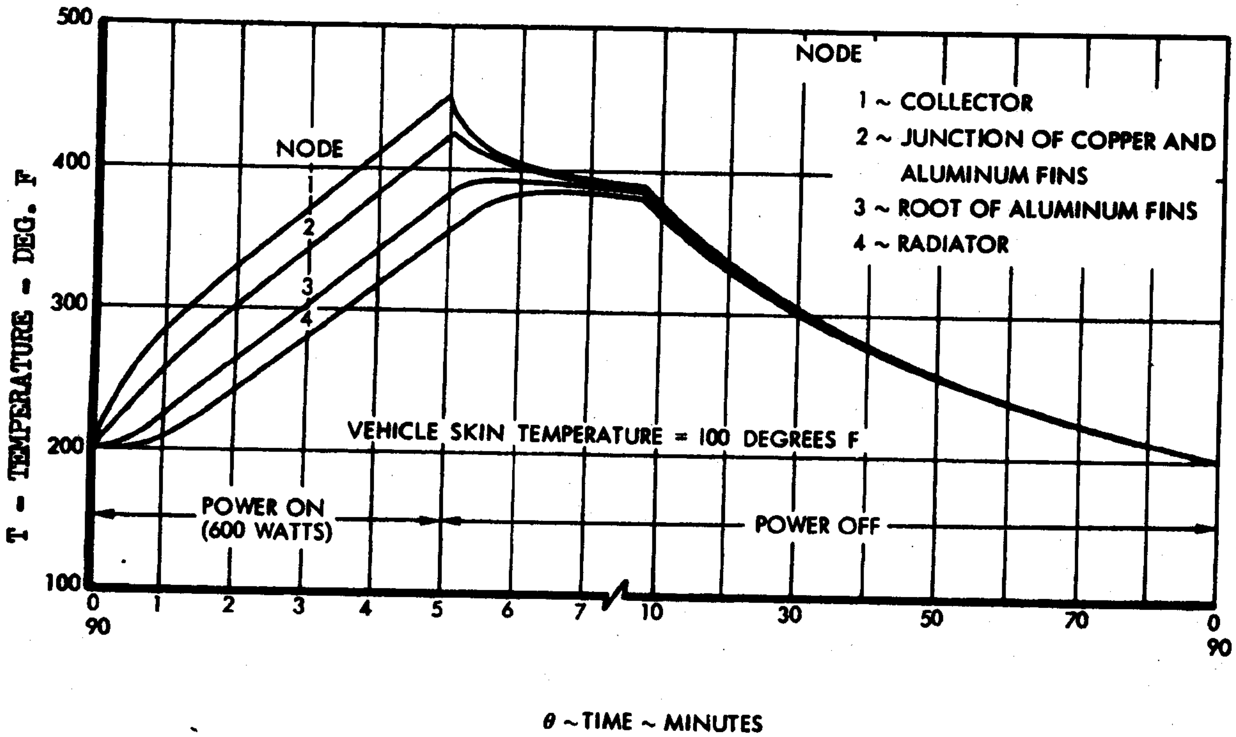

FIGURE 2.1.6.2 - KLYSTRON COLLECTOR AND HEAT SINK TEMPERATURES VS. TIME

Analysis of thermal conditions encountered during ground operation of the Transmitter-Modulator Unit indicated, however, that radiation and free-convection heat transfer would not be adequate to maintain critical component temperatures below design limits. Studies showed that the klystron tube and several pulse components would exceed acceptable temperature limits if operated continuously without additional cooling protection.

As a result of the analytical studies, a duplex squirrel cage blower was added as a part of the unit test apparatus. Forced-air cooling was therefore provided for the klystron and pulse components. A side cover on the unit was removed for cooling access to the pulse components.

Furthermore, analyses showed that cooling air supplied to the vehicle on the launch pad (40 to 60 degrees F air temperature) was adequate to maintain the equipment to an acceptable temperature level while operating during ground checkout.

2.1.6.5 LMSC Preliminary Thermal Design

Thermodynamic capabilities of satellites are strong functions of the location and temperature limits of equipment they are made to carry. If all equipment temperature limits were -30 to +165°F, then the vast majority of satellites could be provided with passive temperature control without having thermal window restrictions. On the other hand, with present equipment temperature limits (including primary batteries), if equipment locations are allowed to be specified by thermodynamic personnel, then most thermal window restrictions would also be removed. This point can best be shown by considering that at least 75% of the thermal window restrictions imposed on Agena vehicles are required because the primary batteries are in the worst possible location within the Agena forward equipment rack. The point of this discussion is that one of the most important aspects of thermal design is interfacing with other design areas to insure that temperature-critical equipment is located in thermally preferred locations. However, it is recognized that equipment locations can not be based solely on thermodynamic criteria but must consider these requirements with both structural and electrical interface requirements.

Preliminary thermal design and analysis of Vehicle 2355 was accomplished during the structural design phase. Equipment locations within the various vehicle and payload equipment compartments were approved based on the existing thermal design window. Considering the nature of the external heat fluxes that would fall on the satellite, the resulting equipment space allocations were nearly ideal. Additionally, a preliminary analysis considering payload parameters such as internal power dissipation and weight, demonstrated that passive thermal control could provide a temperature environment that was compatible with the thermal design of radar equipment.

Preliminary ascent phase temperature predictions were made in support of structural design. The analysis included the effects of vehicle dynamics (angle of attack during the dogleg maneuver) and provided circumferential temperature distributions on both payload and vehicle sections. The effects of vehicle dynamics on aerodynamic heat transfer to the vehicle was included by applying to the zero angle of attack heat rates an empirical factor, equal to the ratio of the heat rate at angle of attack to the heat rate at zero angle of attack. This factor was obtained from data that was not strictly applicable to ascent phase convective heating of Satellite Systems vehicles; however, this analytical techniques had been shown to be conservative on other satellite programs using similar trajectories. A separate ascent heating analysis was made for the magnesium fairing covering the radar antenna to aid in thermal simulation for the fairing separation test.

Potential problem components like the Lear Siegler power supply, primary batteries and radar antenna were reviewed during the early development of Vehicle 2355. To accommodate the high internal power dissipation of the power supply, its external surfaces were coated with a high emittance paint. Flush mounting in a favorable location within the cylindrical payload equipment compartment also minimized the weight of the power supply's heat-sink base plate. These measures were intended to minimize the resistance to heat transfer between the Lear Siegler power supply and its spacecraft environment. Thermal analysis of the batteries and the antenna will be described in Para. 2.1.6.7.

In addition to equipment temperature instrumentation, four sensors were added to monitor structural temperatures in the conical and cylinderical payload equipment compartments. Sensors were intended to give both design and diagnostic data during orbital flight. This instrumentation would augment payload instrumentation and would be used to verify the thermal environment that the spacecraft structure provided for radar equipment.

2.1.6.6 Qualification Testing of the Radar Equipment

Many qualification test procedures do not adequately subject equipment to the thermal environment that they are supposed to operate within. Reasons for this are:

- Thermal testing is performed in an air atmosphere where internal component temperatures are strongly influenced by free convection heat transfer.
- Equipment temperatures are not allowed to stabilize before operational tests are performed. This refers to the amount of time equipment is allowed to "soak" within the test chamber.
- The temperature environment of only a small portion of the

equipment (mounting base) is controlled.

The objective of qualification testing of the radar equipment was to demonstrate the equipment's ability to function within the thermal environment (temperature limits and duty cycles) that had been used as design criteria. Testing of individual boxes was performed in Lockheed's High Altitude Thermal Simulation (HATS) Chamber. Thermally instrumented boxes were mounted on a temperature controllable plate in a manner that simulated the satellite mounting configuration. This plate was placed in the HATS chamber whose wall temperatures could also be controlled. After evacuation of the chamber, the walls and mounting plate temperatures were controlled to one end of the equipment's environmental temperature limits. Internal and external thermal instrumentation was used to determine when the equipment had stabilized at the chamber temperature. This stabilization was assumed when all instrumentation indicated temperatures that were within 5°F of the chamber temperature. Depending on the weight density of the equipment, stabilization required from 4 to 11 hours.

When the equipment's temperature stabilized, it was operated at maximum duty cycle for 3 consecutive simulated orbits. The same operational test was performed at both ends of the equipment's temperature limits. All of the Payload Associate Contractor's equipment was tested in this manner and there were no equipment malfunctions that were attributable to adverse temperature levels.

Qualification testing actually subjected equipment to a duty cycle which was significantly greater than that programmed for orbital flight. During the test equipment was placed in the operate mode a total of 15 minutes in 3 hours while orbital operation required only 30 minutes of the operate mode in 80 hours.

2.1.6.7 Final Spacecraft Thermal Design

The preceding discussions focused attention on the design and testing of equipment and on the importance of equipment location with a satellite. The next step was to identify the specific nature of the orbit environment, provide the methods for predicting its effects, and then generate a passive environmental control system to maintain the required limits of the internal environment as demanded by payload and vehicle equipment. The succeeding paragraphs will discuss the nature of the various environments, indicate the complexity of the attendant problem areas, and describe some of the unique approaches used in obtaining passive thermal control for Vehicle 2355. These discussions are not intended to be technically complete but only to indicate Lockheed's approach to the temperature control problem.

Basic Concepts

Except for periods of exit and entry through the earth's atmosphere, an earth satellite operates in an environment of such low pressure that thermal radiation is the predominant mode of heat transfer between the vehicle and its surroundings. The source-vehicle geometry causes this radiation to fall into three general categories:

- Radiation from the sun.
- Emission of radiation by the earth and its atmosphere.
- Reflection by the earth of radiation from the sun.

The geometry of the vehicle and its relation to these energy sources (generally varying with time) determine the magnitude of the total irradiation. Radiation characteristics of the external surfaces determine the absorbed energy and affect the reradiation from the vehicle surfaces. These factors - the absorbed energy and reradiation, together with internal conduction, radiation and power dissipation effects - determine the temperature boundary conditions upon which the internal thermal control is based.

Regardless of the degree of internal temperature control required, the internal design controls the choice of "external surface" finishes for the vehicle ("paint pattern"). Stable finishes, for which the radiation characteristics and the effect of prolonged exposure to the environment on these characteristics are known, must be used. The function of internal thermal design can be simply stated, "It is required to dissipate power on the average through some heat-flow path to a sink at some temperature while maintaining the power-generating units and other components within a given temperature range". Although it is feasible in some cases to use power as a means of control, it is generally required that the heat-flow path and the sink temperature be passively controlled to yield the required temperature regulation.

The thermal analysis problem in a satellite is typified by the system shown in Figure 2.1.6.3. The basic elements of thermal capacity, heat-transfer paths, and external radiating surfaces are shown together with the analogous electrical circuit. The solution for such a circuit is relatively simple. However, a space vehicle must be represented by many such systems, all interconnected to form a single network or "Thermal Model". Discrete equipment or structural items in these networks are referred to as "Nodes" and are assumed to be a uniform temperature. Each node has an associated value of thermal capacity, and many have a time-dependent electrical power dissipation. The radiant interchange of the skin with internal equipment and structure must also be accounted for. Solution to the equations describing these networks must be obtained through use of digital computers. Thermal Analyzer Network programs have been developed at Lockheed as a means of solving such problems.

Analysis of Payload and Agena Equipment Compartment

Vehicle 2355 had five basic equipment compartments as shown in Figure 2.1.6.4. The standard method of analysis is to determine external paint patterns and make temperature predictions for the individual equipment compartments. The use of this technique is often justified since it minimizes both computer time and complexity of the analytical thermal model; however, temperature predictions are often strongly influenced by the boundary condition assumptions. For example, during analysis of a short equipment rack like the BTL guidance rack, it would

(a) SIMPLE THERMAL SYSTEM

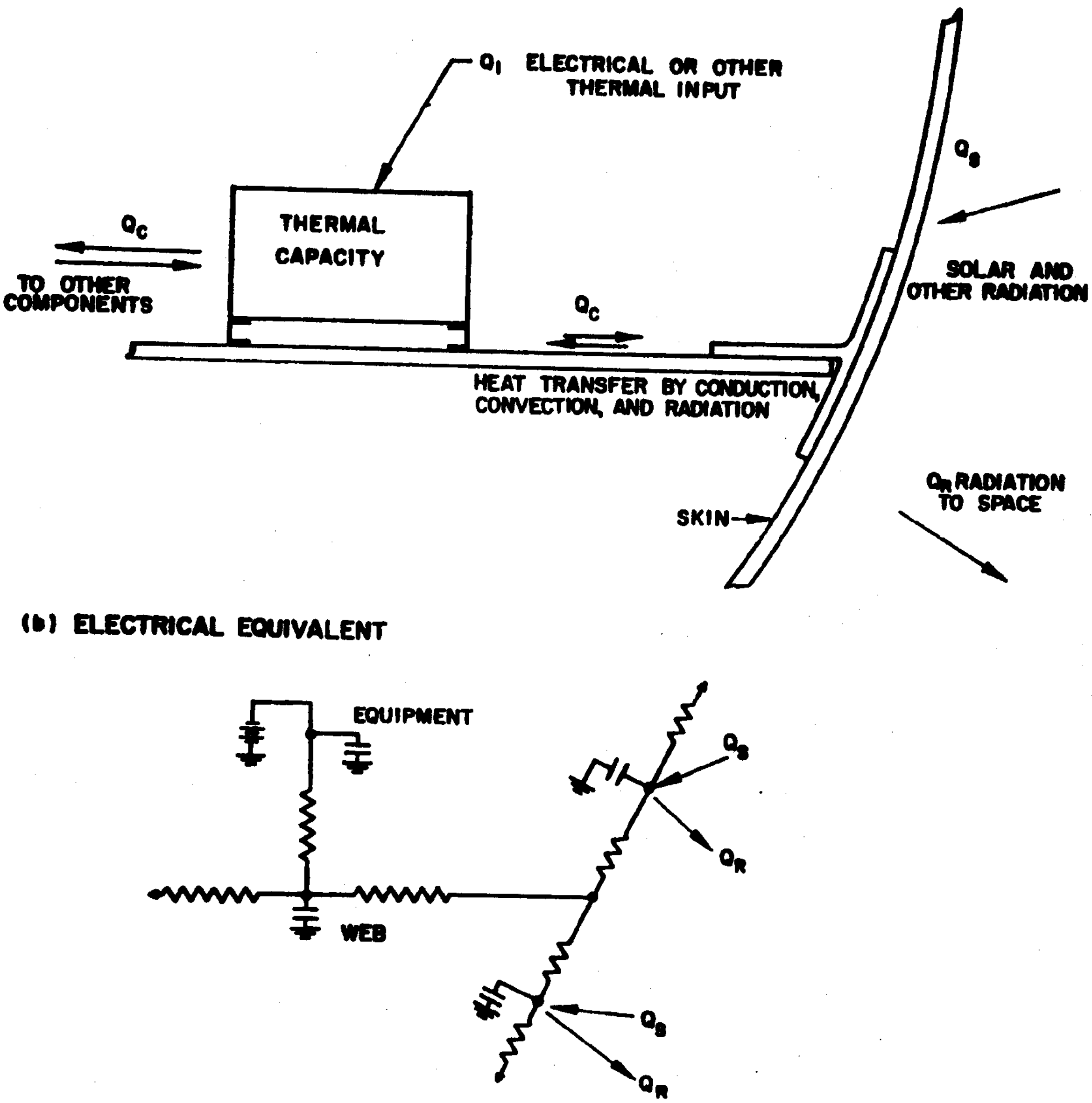

BASIC THERMAL SYSTEM

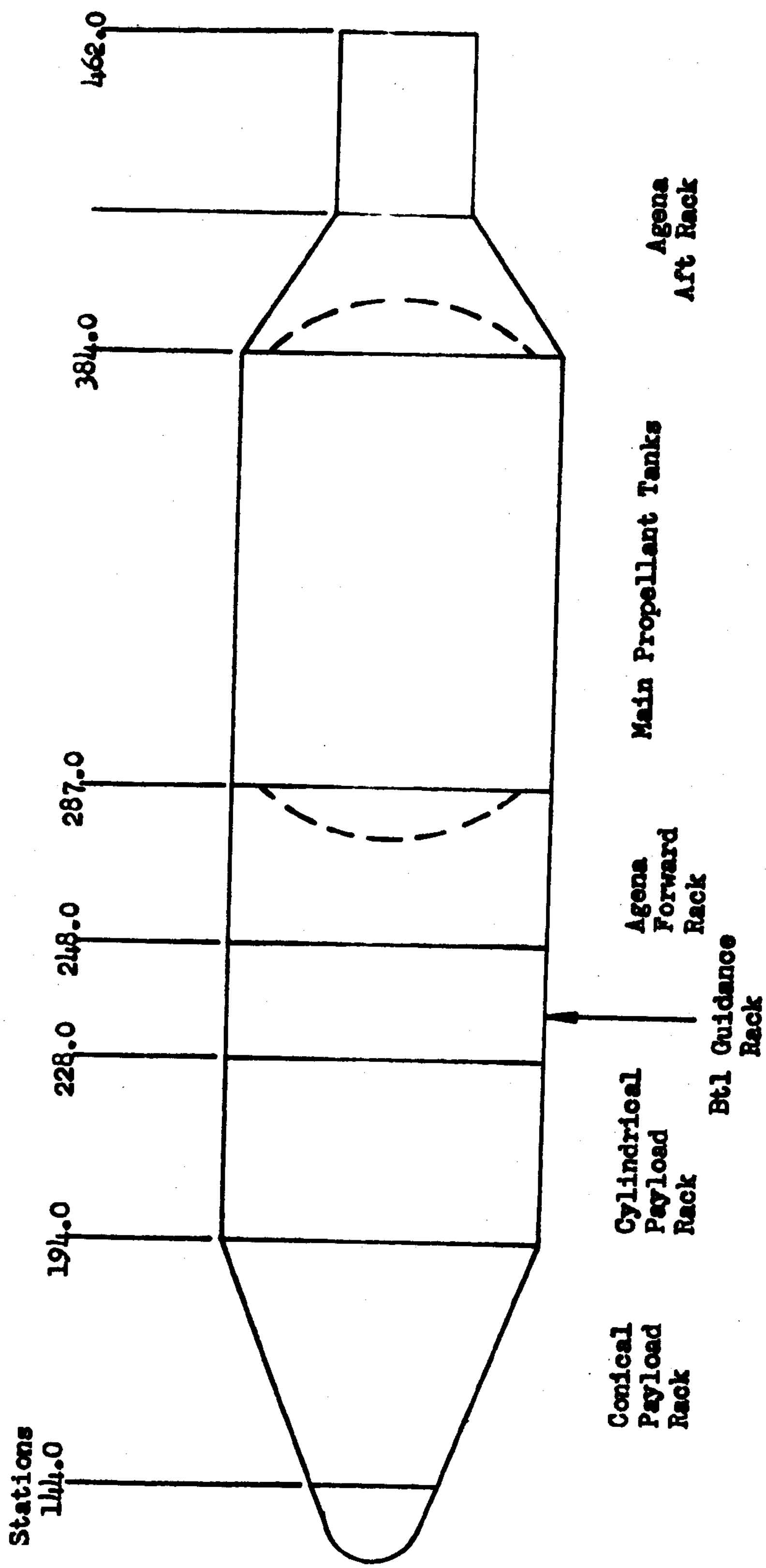

EQUIPMENT COMPARTMENTS VEHICLE 2355

Figure 2.1.6.1

be necessary to assume environmental temperatures for both the Agena forward rack and the cylindrical payload section. For this case, the assumed temperatures would represent over 60% of the boundary temperatures of the equipment compartment. In using this technique of separate equipment compartment analysis, it is necessary to exercise great care in establishing boundary temperatures. Preliminary thermal analyses for Vehicle 2355 used this separated rack technique.

As a result of a number of battery failures on Agena Vehicle during 1964, thermal design criteria for Vehicle 2355 primary batteries was substantially restricted in November, 1964. These restrictions, especially narrowing of battery temperature limits, made it clear that the inherent inaccuracies in separated rack thermal analysis could not be tolerated. The recently developed thermal model of the [redacted] Agena forward equipment rack, including the main propellant tanks, was felt to be the "best" model available of that section. This model was modified to the Vehicle 2355 configuration and combined with the existing models of the BTL guidance and payload equipment racks. The interaction between the various equipment compartments could now be accurately calculated since the thermal model included all sections of the vehicle from Station 144.0 to 384.0.

The complexity of this combined model can best be demonstrated by considering the following network parameters:

Equipment and structure within the equipment compartments were divided into 968 discrete elements or "nodes". To account for heat transfer between the various nodes it was necessary to describe 5,377 radiation resistances and 1,715 conduction resistances. To solve this network on a computer, the existing thermal network analyzed program had to be streamlined to make available additional storage.

These parameters describing network size are cited only because it is felt they represent a "State-of-the-Art" advancement in both spacecraft thermal analysis and thermal network analysis computer programs.

Battery Thermal Analysis

Vehicle 2355 carried three primary batteries of the 1-D Type. As shown in Figure 2.1.6.5, one battery was mounted in the Cylindrical Payload Equipment Compartment with the other two batteries being mounted in the standard location in an Agena Forward Equipment Rack. The extensive thermodynamic analysis of these battery installations fall into three categories:

- The First Analysis used internal power dissipations of 1.0 to 3.5 watts per battery over an operational temperature range of +55°F to +130°F.
- The Second Analysis considered internal power dissipation up to 14 watts per battery over an operational temperature range of +55°F to +130°F.
- The Final Analysis considered internal power dissipations up to 35 watts per battery over an operational temperature range of +60°F to +100°F.

a) One battery located in cylindrical payload equipment compartment

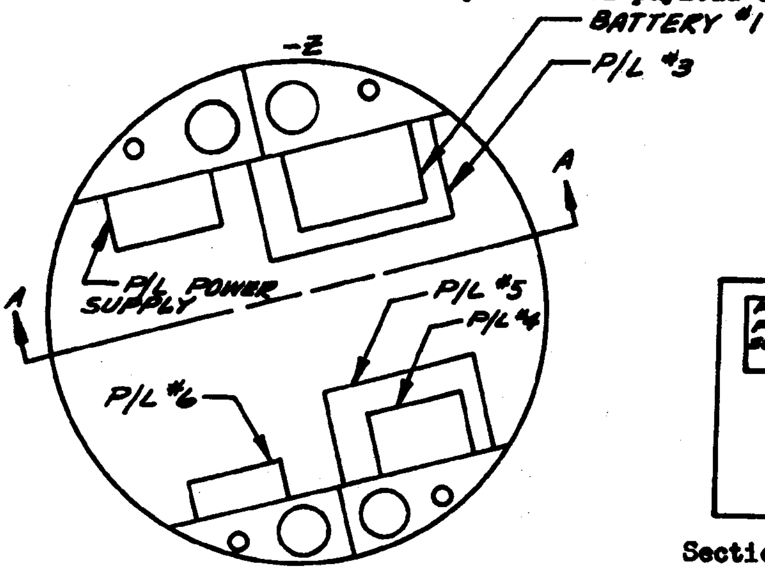

View Looking Fwd At Sta. 228.0

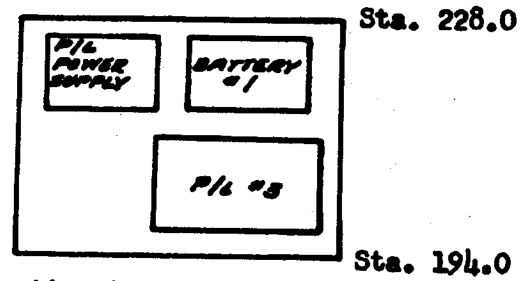

Section A - A Web only

b) Two batteries located in Agena forward equipment rack

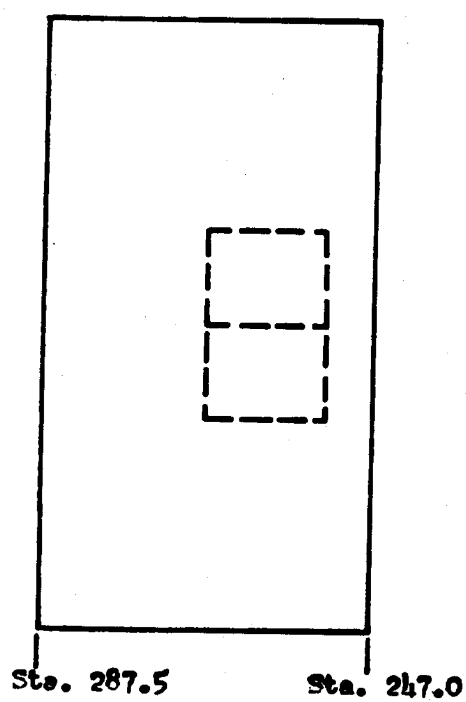

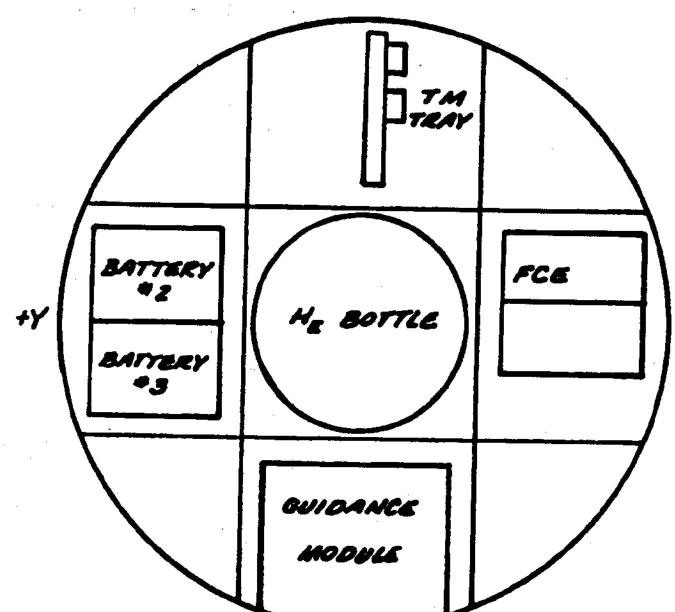

View Looking Aft At Sta. 247.0

LOCATION OF PRIMARY BATTERIES VEHICLE 2355

In all of these analyses, the thermodynamic design considered average internal power losses per battery only to center the expected operational temperatures within the allowable temperature range. Temperature predictions were then made with internal power dissipation as a variable. In each case, the thermal design allowed the batteries to operate within temperature limits even though their internal power dissipation might vary significantly from what was expected for an equal load sharing condition.

Orbital temperature limit requirements for the first analysis could be met passively by providing maximum thermal isolation between the batteries and their equipment compartments and by using the internal battery power losses to control battery temperatures. This isolation scheme places phenolic fiberglas pads between batteries and their mounting structure and covered the batteries with a radiation shield. Figure 2.1.6.6 presents typical battery temperature predictions for the first analysis. Slopes of this equilibrium battery temperature versus power dissipation curve were used to obtain the dependence of temperature upon power dissipation. For example, a one-watt change in power dissipation would result in approximately a 20°F change in the predicted payload rack battery temperature. It is noteworthy that this dependence of temperature upon internal power dissipation was an order of magnitude higher for the payload battery than it was for most other vehicle and payload equipment. This high dependence resulted since the temperature control scheme required thermal isolation between the batteries and their surroundings.

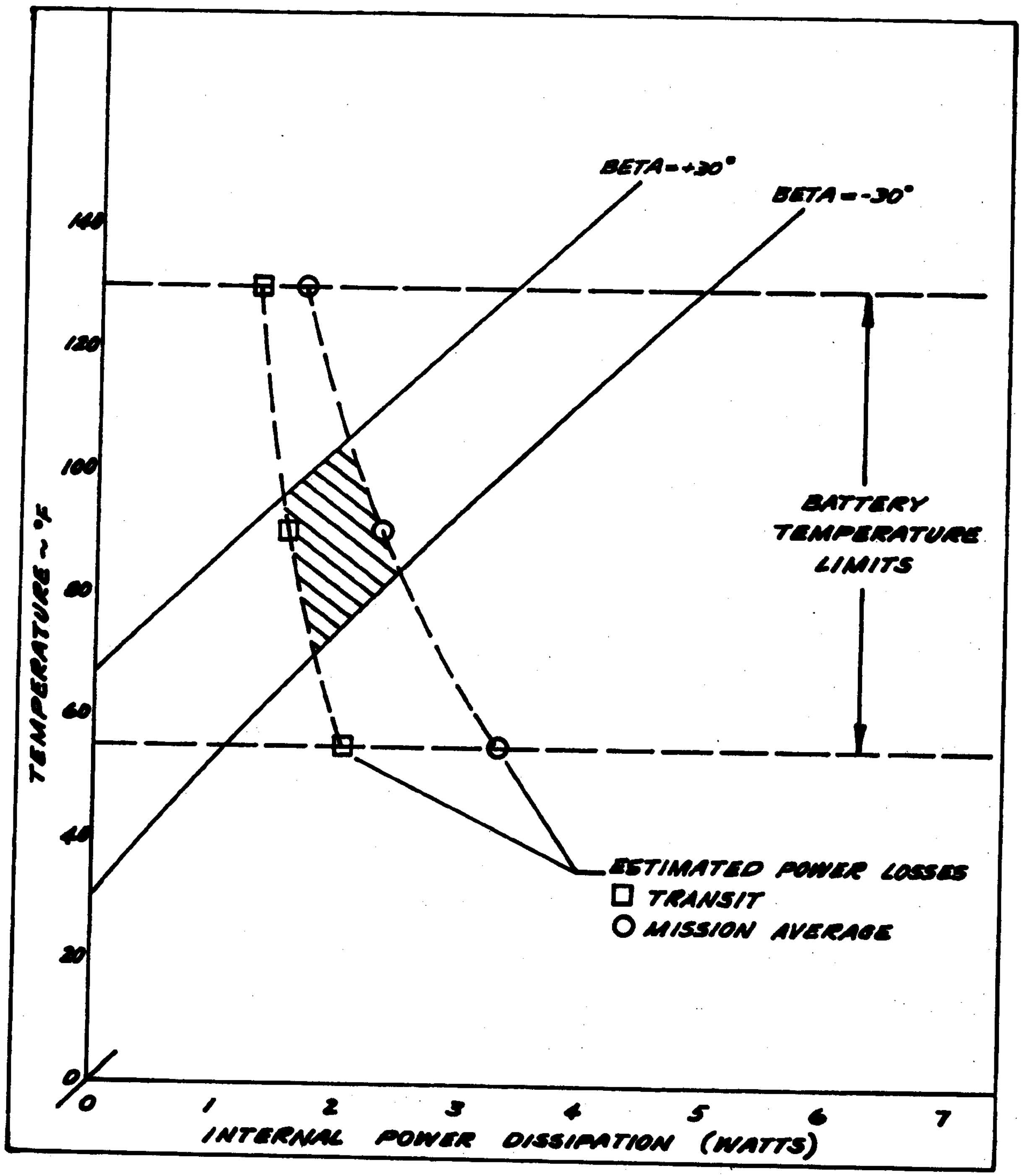

PAYLOAD BATTERY TEMPERATURES
VS.
INTERNAL POWER DISSIPATION
(Preliminary 1-12-64)

Since primary battery power losses were apparently not accurately known and this parameter was critical for battery temperature control, an activated 1-D battery was included in the TASC test of the 2355 FTV.

The test was accomplished by installing a 1-D battery in the payload equipment rack using the flight item battery brackets. A flight hardware battery radiation shield was also installed during this test. Battery voltage leads were brought outside the TASC facility to an external load where orbital power requirements were simulated by using three levels of current drain--2 amps for transit, 8 amps for 12 to 20 minutes during active orbits, and 50 amps for the programmed payload on time. This loading profile resulted in an average current of 2.8 amps. During 30 hours of testing, battery temperatures rose from 74°F to 116°F. The internal power dissipation required for this temperature response was calculated to be 14 watts.

This experimentally determined battery dissipation was six times greater than the estimated internal power losses used as thermal design criteria. It is noteworthy that a low power dissipation of 1.5 to 2.0 watts per battery had traditionally been used in the thermal analysis of Agena vehicles. These estimated levels of dissipation had been provided by SS/C personnel associated with each project. Additionally, all environmental tests on equipment compartments had used external power and batteries, although installed, were never operated under an electrical load.

Analysis of battery failures during recent flights had shown that there could be unequal load sharing by batteries during orbit flight and that this condition was aggravated by having different thermal environments for the batteries. Additionally, the flight failures occurred at temperatures below 130°F but above 100°F. The knowledge of primary batteries of the Type 1-D and 1-C, although greatly increased before the launching of Vehicle 2355, was still far from complete. The following was known about the Type 1-D battery and other primary batteries:

- Temperature limits specified by the battery manufacturer were +30°F to +100°F.
- Voltage regulation data on the Type 1-D battery showed that battery temperatures would have to be above 60°F to provide radar payload power requirements while maintaining the vehicle BUSS above 22.0 volts.
- Recent heat dissipation test on both 1-C and 1-D batteries had shown that internal power losses were approximately 3.5 watts per amp of discharge.
- During the simulated flight operation of 2356 in the Anechoic Chamber, the average amperage load was 8.5 for the total vehicle and payload.

On 19 November 1964, the following proposal for battery thermal design on Vehicle 2355 was outlined to the Project Office:

Considering battery temperature limits as +60°F to +100°F, the battery temperature control scheme should be redesigned to accommodate unequal load distribution and also to provide an identical thermal environment for the two different battery locations.

These objectives were met by a narrowing of the launch window and by a redesign of the vehicle and payload external paint pattern. The resulting thermal window was $-21° < \beta < 13°$.

Figure 2.1.6.7 presents the final battery temperature predictions. Dependence of battery temperature on its own internal power dissipation had been reduced by minimizing the thermal resistance between the batteries and their satellite environment. As can be calculated from the equilibrium temperature predictions, this dependence was now only 0.9°F per watt, whereas it was 20°F per watt for the first battery thermal analysis.

Battery thermal design for Vehicle 2355 had compensated for the apparent unknown battery performance data by a design and analysis which allowed for unequal battery load sharing without having battery temperatures above 100°F or below 60°F. The design technique was to minimize the dependence of battery temperatures on their own internal losses. Analytical techniques removed nearly all the uncertainties associated with spacecraft temperature control by 1) demanding near perfect optical properties for thermal control surfaces, and 2) by use of a mathematical model which accurately accounts for the

NOTES: 1) TOTAL POWER DISSIPATION FOR THE 3 BATTERY SYSTEM ASSUMED TO EQUAL 30 WATTS.
2) POWER LOSSES ASSUMED TO BE IN ONLY ONE OF THE AGENA BATTERIES (LOWER DASHED LINE REPRESENTS BATTERY WITHOUT LOSSES).

LEGEND: ———— PAYLOAD BATTERY
– – – – AGENA BATTERIES

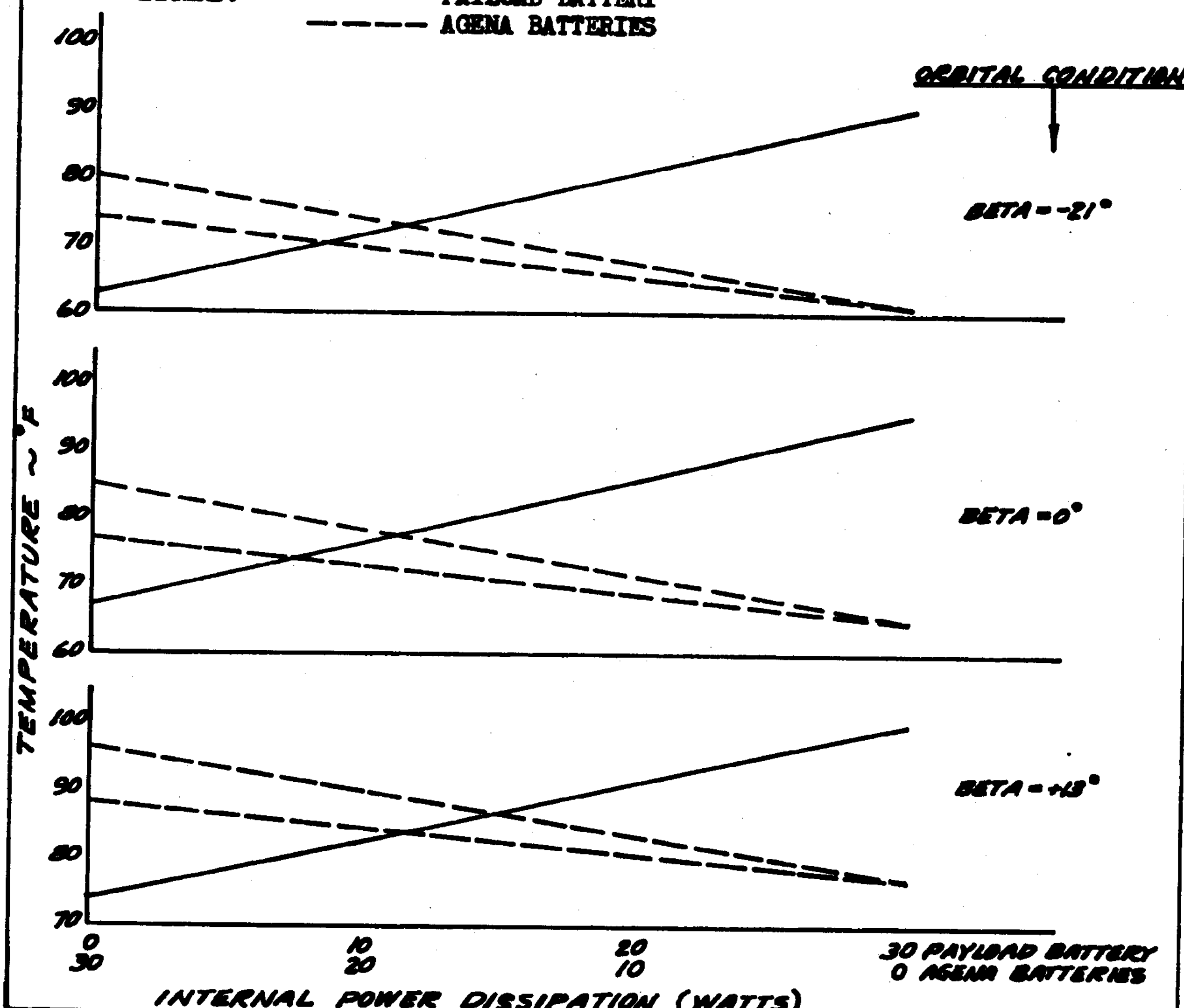

FINAL BATTERY TEMPERATURE PREDICTIONS
VS.
INTERNAL POWER LOSSES

Figure 2.1.6.7

exchange of thermal energy between all sections of the vehicle. The penalty paid for this conservative approach was a launch window restriction.

Thermal Analysis of Radar Antenna

Requirements for dimensional stability of the antenna made it necessary to impose the following operational temperature criteria:

- Waveguide temperature levels had to be between 0°F and +90°F.
- Temperature gradients across the waveguide (measured perpendicular to the antenna plane) could not exceed 2.0°F per inch.
- Temperature gradients in the supporting longitudinal side beams (LSB) could not exceed 0.5°F per inch.

These striengent orbital requirements were met by 1) integrating the thermal analyses of both the antenna and the vehicle, 2) specifying acceptable thermal control surfaces for the entire antenna structure, and 3) providing uniform vehicle surface temperatures underneath the antenna. The antenna's influence on the thermal performance of the vehicle was found to be negligible since it covered only 1/9 of external vehicle surfaces and also was a relatively open structure.

The surface selected for controlling temperature levels of the antenna waveguides was a non-leafing aluminum lacquer. This thermal control surface provided acceptable orbit average temperatures due to its low value of α_s and ϵ (α_s/ϵ = $.41/.48$). Temperature gradients, induced by non-uniform heating due to direct and reflected solar energy, were reduced to acceptable levels by covering portions of the LSB with an adhesive-backed aluminum tape which would absorb only 12 percent of the incident solar energy.

2.1.6.8 Environmental Testing of Flight Payload

Test objectives, configuration, instrumentation, and procedures which were necessary to produce the satisfactory high altitude and temperature simulation for the 2355 Payload are briefly discussed in this section. Evaluation of test results is also presented. Objectives of this testing were, 1) to subject the radar payload and associated equipment to simulated orbital thermal environments at high altitude, 2) to experimentally determine the operating temperature levels of thermally critical components, and 3) to determine the validity of temperature predictions by comparing predictions with results of environmental test.

The facility used for these tests was Lockheed's Thermal/Altitude Simulation Chamber (TASC) which is a high vacuum chamber using a sink/source technique for external heat flux simulation. The radiation heat transfer sink is the liquid nitrogen filled internal chamber walls which average a temperature of -300°F. Sources for external heat fluxes are quartz lamps arranged on a "birdcage" structure which is suspended 8½ inches from the test specimen. The TASC facility was designed to accommodate 60 inch diameter cylindrical sections up to 9 feet in length plus conical sections having 15 degree half-cone angles and up to 6 feet in length. The spectral energy distribution available at the specimen surfaces is in the infrared spectrum and can have intensities up to 185 watts per square foot (1.5 times the intensity of the sun's radiant energy).

The 2355 flight payload, including the recovery capsule and the conical and cylindrical payload equipment compartments, was the test specimen. Flight thermal control surfaces had been applied to the external equipment compartment surfaces. A radiation shield, attached to the aft end of the payload (Station 228.0), was used to minimize heat transfer across this boundary. Thermal instrumentation consisted of 48 thermocouples connected to continuous recorders. Thermocouple locations coincided as much as possible with the node center designations of the thermal network used to predict payload temperatures.

Lamps comprising the external heat flux simulator are divided into 12 peripheral and 2 end zones with each zone having independent voltage control. Orbital simulation was achieved by specifying a voltage program for these zones which duplicated the absorbed orbital heat flux on the payload. Heat fluxes absorbed by the payload in the test chamber were dependent on, 1) the mean spectral emittance of the payload surface finishes, 2) the spectral radiance of the quartz lamps for a given voltage setting, and 3) the geometric relationship of the simulator-payload configuration. Items 1) and 2) were determined in LMSC's Thermophysics Lab. Item 3) was determined using previous TASC simulator calibration test data.

TASC environmental testing of the 2355 payload simulated the conditions existing in an orbit whose Beta angle equals +30° since this simulated orbit provided the hottest environment for the 1-D battery, the Transmitter-Modulator, and the Recorder unit. Both dynamic and orbit average voltage programs were analytically developed for the heat flux simulator. During the initial TASC test, accurate external heat flux simulation could not be achieved using these analytically developed voltage programs. The analysis which generated the thermal control surface requirements for the payload as well as the techniques which result in a voltage program for the simulator were checked and found to be correct. Calibration data for incident flux on the payload versus lamp voltage was suspected of being inaccurate. This suspicion was verified by installing heat flux calorimeters on the external payload skins during subsequent TASC testing. It is noteworthy that although this inaccurate calibration data resulted in nearly 150 percent of the calculated incident energy on the test specimen, it had previously been used many times for TASC testing of other payloads.

Lamp voltages for the orbit average program were ratioed down by a factor of 0.8 and used during all but the first TASC test of the 2355 payload. It is unfortunate that time varying or dynamic external heat flux simulation could not be accomplished since temp data taken from this type of simulation could have been used to better verify the validity of analytical temperature predictions. The modified orbit average voltage program did provide adequate simulation with an average difference between predicted and actual temperatures of less than $5^{\circ}F$ and a maximum deviation of $15^{\circ}F$.

From a thermodynamic viewpoint, the most significant result of the TASC environmental testing was the determination of internal power dissipation for type 1-D batteries. Accurate knowledge of this power dissipation was instrumental in determining the successful battery temperature control scheme for orbital flight of Vehicle 2355.

2.1.6.9 Special Considerations

This section presents a discussion of unique temperature control considerations and problems encountered during the thermal design of Vehicle 2355.

__Analysis Verification__ Structural design is verified by qualification testing on structural mockups or substantiated by low level testing of flight hardware. Electronic design is verified almost continuously from systems test to launch countdown. Unlike these and other engineering disciplines, the thermodynamics design of a satellite does not usually receive experimental verification before the actual orbital flight. Hence, the analysis resulting in the thermal design should be meticulously checked and/or be overly conservative in its design approach.

The narrow temperature limits on Vehicle 2355 batteries left no room for a conservative design approach and it was necessary to subject the analysis, which resulted in the passive temperature control of the entire spacecraft, to extensive checking. Objectives of this checking were:

- To substantiate the validity of thermal design driteria such as power dissipation, temperature limits and thermal capacity.
- To verify that the thermal model adequately described the spacecraft.
- To verify the accuracy of calculated parameters such as 1) heat transfer coefficients for radiation and conduction and 2) external heat fluxes incident on the spacecraft from the sun and earth.

The majority of this checking was accomplished after completion, on 30 November 1964, of the final orbital thermal analysis and resulting external paint pattern for Vehicle 2355.

A review of thermal design criteria such as equipment power dissipation and temperature limits revealed no anomalies between this criteria and actual test or design specification data. Of greatest importance was the internal power dissipation of the Type 1-D batteries and this had been assumed to be a total of 30 watts. Additionally, it was assumed that battery temperatures would respond to their average internal power losses and would not be significantly influenced by the higher dissipations during payload operation. These assumptions could be substantiated by considering that, 1) during the testing of 2356 in the Anechoic Chamber, the amperage load for the entire spacecraft averaged 8.5 amps for 64 orbits of simulated flight, 2) heat dissipation test on the Type 1-D and similar batteries (Type 1-C) had shown that internal power losses were approximately 3.5 watts per amp of discharge, and 3) during both Anechoic and TASC testing, the high thermal capacity of the Type 1-D battery was sufficient to damp out the effects of high internal power dissipation during payload operation.

It was not feasible to check all the network parameters comprising the system thermal model of Vehicle 2355 equipment compartments. Instead, the temperature predictions of this model were compared against other prediction techniques. The validity of the portion of the thermal model describing the payload equipment compartments had been adequately demonstrated during the TASC environmental testing. Validity of the Agena forward equipment rack portion of the model was substantiated in the following manner:

> An existing thermal model of the Agena rack used for thermal analysis of Program 241 Vehicles was modified to the Vehicle 2355 configuration. Considering the time available, these

modifications could only be partial but did include changing the network parameters describing external paint pattern, battery installation, and equipment power dissipation. External heat fluxes from the sun and earth were recalculated and programmed into this check model. Differences between predicted equipment temperatures from the two models averaged less than 5°F and were well within the allowable uncertainties associated with this type of spacecraft thermal analysis. Battery temperature predictions from these two independent analyses were less than 6°F apart.

Internal equipment temperatures are strongly influenced by the orbit average skin temperatures of a spacecraft. The final method of substantiating the validity of Vehicle 2355 equipment temperature predictions was, therefore, to independently evaluate these skin temperatures. A relatively simple thermal model, including all external skin structure from stations 144 to 384 was analytically constructed. Node breakdown of the external skin was identical to the breakdown in the complete systems model. External radiation heat transfer and conduction between the various skin elements was accurately calculated. For simplicity, internal equipment power dissipation and heat transfer had to be accounted for in an approximate method. External heat inputs were also recalculated. Orbit average skin temperature predictions generated by this simple model agreed very favorably with predictions from the complete systems model. The maximum deviation between predictions for individual skin elements was less than

10^oF and differences in the average skin temperature in each equipment compartment did not exceed 5^oF. This simple thermal model had demonstrated that no gross errors had been made in evaluating external heat inputs and that the larger systems thermal model did not violate the law of conservation of thermal energy.

Verification of the orbital thermal design of Vehicle 2355 was far more complete than it had been for other LMSC designed satellites. The value of this verification can best be shown by considering the resulting successful battery temperature control during orbital flight. These techniques of verification by constructing a simple model of the skin structure and by correlation of predictions against similar equipment compartment thermal models have now become a standard technique in the LMSC Thermodynamics organization.

<u>External Paint Pattern</u> The 60^oF lower temperature limit of the Type 1-D batteries made it necessary to develop a paint pattern which would maintain a relatively high mean skin temperature even though Vehicle 2355 would spend up to 40 percent of the orbit in the earth's shadow. This was accomplished by, 1) using a black paint on portions of the vehicle ($\pm$ Z axis) which received direct or reflected solar energy and, 2) placing adhesive-backed aluminum tape (Mystik Tape) on sections of the vehicle ($\pm$ Y axis) receiving little external energy from the sun and earth. Nominal optical properties of these thermal control surfaces are shown below:

Surface	Solar Absorptivity (α)	Infrared Emittance (ϵ)
Black Lacquer LAC 37-4033, Class II	.93	.88
Aluminum Tape LAC 24-4199	.12	.04

Of the 225 sq. ft. of external skin area enclosing the forward equipment compartment of Vehicle 2355 (Station 287.0 to 140.0), 104 sq. ft. were covered with Mystik tape. This tape had been used externally on other LMSC vehicles but had never comprised more than a few percent of the total thermal control surface area. Mystik tape has three basic limitations:

- The design specification for the tape states that it may be used externally in areas where ascent temperatures do not exceed 750°F. However, due to outgassing of the adhesive, it will rise from a surface whose temperature is only 300°F. This fact was first discovered two weeks before the launching of Vehicle 2355.
- Incorrect removal of the backing from the tape can increase its solar absorptivity by 100 percent.
- Being a highly polished aluminum surface, it is susceptible to optical degradation caused by inadequate protection or handling.

In light of these limitations, it would not seem wise to use Mystik Tape as a thermal control surface: however, its optical properties make it one of the most useful thermal control surfaces available to the designer. The following paragraphs describe the manner in which Mystik Tape was successfully used on Vehicle 2355.

With the exception of the conical equipment compartment, Mystik Tape was only used on removable panel sections. Width of the tape varied from 2 to 6 inches and it was tucked around all edges of the panels. Additionally, tape was overlapped approximately ¼ inch. These measures were intended to minimize the free edges of the tape and thereby reduce the possibility of aerodynamic shear loads removing the tape during the ascent phase of flight. On the conical equipment compartment, tape had to be used on sections where there were no removable panels. The design approach was to overlap 6 inch wide tape and place a stainless steel strap over the leading edges. Since the greatest angle of attack and associated high aerodynamic heat loads occurred on the +Y axis the tape was overlapped from this axis in a manner that simulated shingles on a roof.

A technician at VAFB, after applying tape to one of Vehicle 2355's removable panels, placed the panel under a nearby heat lamp and noticed that the tape began to "blister". Similar qualitative tests at Sunnyvale showed that the tape would lift off its mounting surface at moderately low temperatures. When blisters became large enough to reach a free edge of the tape they would collapse. Upon cooling, a blister would disappear and the tape would re-attach itself to the surface. These phenomena had not previously been noted or suspected since the adhesive properties of the tape were quoted to be adequate up to 750°F. Test presently being conducted in Lockheed's Thermophysics Lab shows that Mystik Tape will remove itself from surfaces whose temperatures are as low as 300°F. This has been explained by concluding that outgassing of the tapes adhesive can cause pressure differences large enough to lift or blister the tape. Additional tests are planned and will undoubtedly result in the recommendation being made that if Mystik Tape is exposed to ascent heating and aerodynamic shear loads, it should be tucked around all leading edges or be mechanically held against the surface.

Although Mystik Tape had been used for two years, it was not determined until early 1964 that the method of removing the backing from the tape could have a significant effect on the ultimate optical properties of this thermal control surface. This fact was first discovered on [redacted] where Mystik Tape, installed on the Agena aft rack, was so badly degraded due to the method of application that the resulting orbital temperatures actually caused the failure of a solar array drive motor. Recently a Lockheed Process Bulletin (PB-105) was written on the application of Mystik tape which, if followed, reduces the possibility of installation procedures causing degradation of optical surface properties. When this type of degradation does occur, its main effect is to increase the solar absorptivity of the aluminum surface. Degradation often becomes visible to the eye and shows itself as a dulling of the surface caused by a stretching or wrinkling of the aluminum.

Visual inspection of Vehicle 2355's thermal control surfaces at VAFB, showed that all Mystik taped surfaces were either physically damaged or had been improperly applied. Since much of this tape had been installed eleven months before flight, its degradation was anticipated and replacement (as required) had been planned. With the exception of the aft rack surfaces, all areas covered with Mystik tape were stripped and new tape installed. Aft rack surfaces were not replaced, since an analysis had shown that all aft rack equipment would operate within allowable temperature limits even if the Mystik taped surfaces were degraded. After replacement of the taped surfaces, an optical inspection was made of all external thermal control surfaces on the forward equipment compartments. The device used for this inspection was Lockheed's Optical Surface Comparator (OSC) which compares the emittance and reflectance of applied surfaces against known standards. Over 200 individual measurements were made and it was concluded that optical properties of the thermal control surfaces were within acceptable limits. VAFB personnel were commended on their application of Mystik tape on Vehicle 2355 since all of the 104 sq. ft. of tape they replaced had been properly applied and exhibited nearly nominal optical properties. It is noteworthy, that plans are being initiated to install the majority of required Mystik tape surfaces at VAFB on future vehicles of [redacted] In addition to minimizing the possibility of degrading the tape, this procedure will simplify vehicle handling and reduce cost.

Being a highly polished aluminum surface, Mystik tape is susceptible to optical degradation caused by handling or inadequate protection. On R-2 the Gantry was removed from around Vehicle 2355 and since it was raining, a "protective" polyethylene cover was placed over the forward sections. High winds caused this cover to repeatedly slap against the external thermal control surfaces. When the Gantry was reinstalled on R-1 and the covering removed, it was found that the majority of the Mystik tape surfaces had been abraded. The abraded tape had the appearance of dull rawstock aluminum and in some areas was so degraded as to appear black. Additionally, finely divided aluminum had been transferred to adjacent painted surfaces. As the Optical Surface Comparator was in the Gantry, it was used to determine the degree to which the thermal control surfaces had been degraded. Solar absorptivity of Mystik tape surfaces on the cylindrical sections of the vehicle had been increased by up to 300 percent (0.12 to 0.35). Fortunately, tape on the conical section had not been degraded beyond acceptable limits. The degradation of tape on the cylindrical section could not be tolerated. Between T-15 and T-10 hours, approximately 75 percent of the tape on removable panels was replaced. Additionally, painted thermal control surfaces were cleaned using distilled water and a mild abrasive soap. By checking the cleaning procedure with the OSC it was determined this mild abrasive could be used to remove the finely divided aluminum from painted surfaces without altering their optical surface properties. The OSC was also used to examine the retaped panels.

Panels which were retaped where chosen in an orderly manner, starting first with Quad. III and IV and then proceeding to the Quad I and II panels closest to the $\pm$ Z axis. At T-10 hours, the Gantry was removed and it was no longer possible to remove additional panels for retaping. At that point all but approximately 15 sq. ft. of the degraded Mystik tape had been replaced. By controlling the order in which the panels had been retaped, all degraded thermal control surfaces which would have a major effect on the Type 1-D battery temperatures had been replaced. Degraded surfaces not replaced were those nearest the +Y axis and their effect could be reduced by a narrowing of the thermal window. The revised launch window became 11:15 to 12:03 PST whereas the previous window was 10:30 to 12:03 PST.

This page intentionally left blank.

2.1.7 High Voltage Operation in a Space Vehicle Environment

2.1.7.1 Introduction

The voltage necessary to cause breakdown or sparking between electrodes in air is a function of the density or pressure of the air. Ionization of the air between the electrodes is the primary mechanism of voltage breakdown. Thus, at lower pressures (high altitude) air is more easily ionized and breaks down at a much lower potential than at sea level. Paschen, using calculations of the mean free path and ionization potentials, predicted that in a uniform field the breakdown potential of a gas (air) varies as a function of the gas pressure (mmHg or torr) times electrode spacing (cm). A Paschen Curve (Figure 2.1.7.1) which he verified experimentally, has a minimum breakdown potential of approximately 300 volts DC when the pressure-spacing product is around 0.6 cm torr. Later investigators have established that lower breakdown potentials can be expected in non-uniform fields such as are commonly found in actual equipment. Likewise, high frequency alternating fields and/or pulsed DC further lowers breakdown potentials.

Upon examining Paschen's Curve, it would seem reasonable to assume, in a space vehicle operating at altitudes in excess of 300,000 feet (10^{-4} torr & below), that there would not be a voltage breakdown problem. However, this assumption that equipment pressures will be the same as the ambient atmospheric pressure at a given altitude is unwarranted since it completely ignores the effect of the vehicle on the ambient environment. A considerable amount of volatile matter

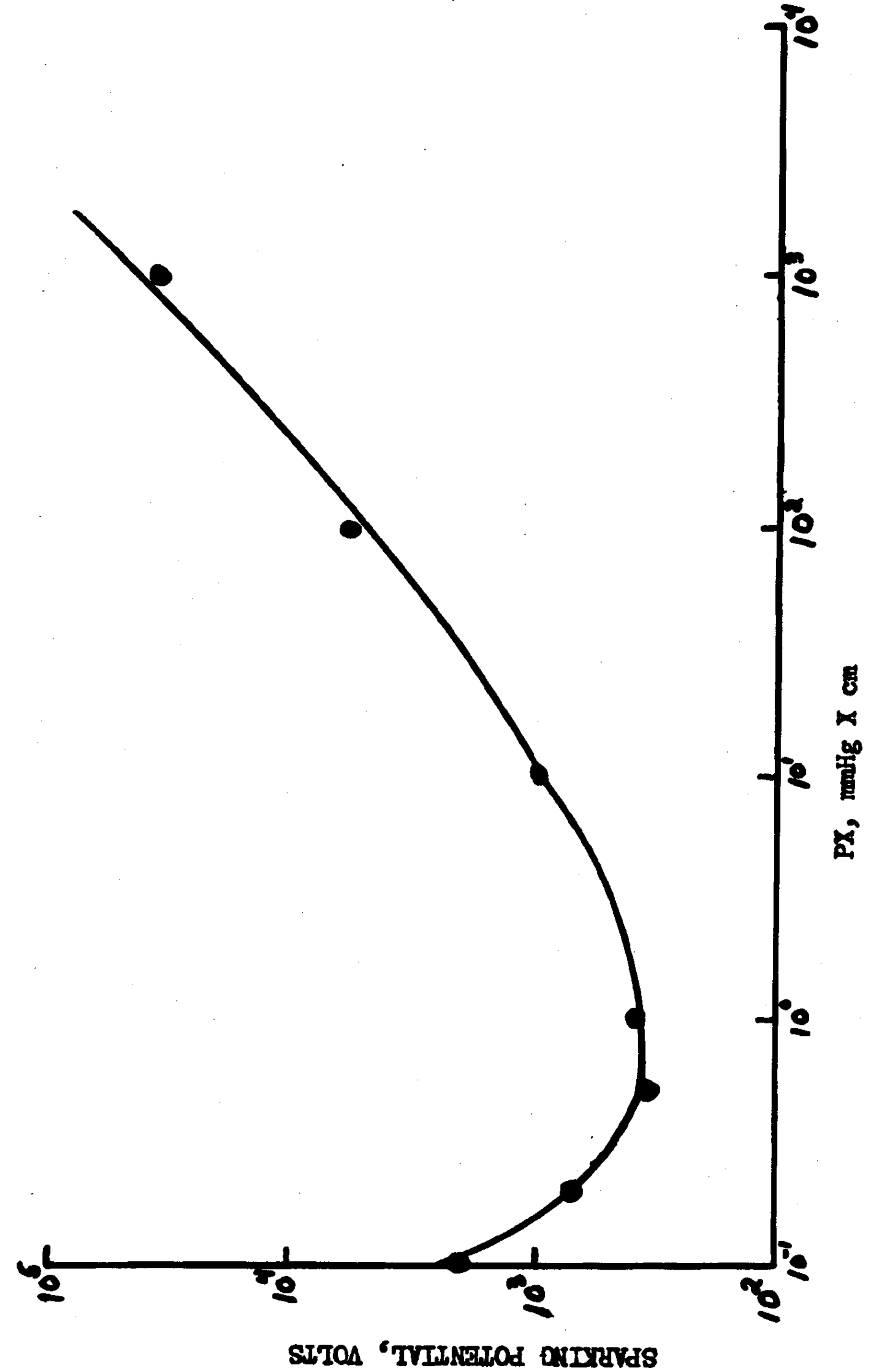

Fig. 2.1.7.1 PASCHEN'S SPARKING POTENTIAL PX CURVE FOR AIR

(gas) is given off by the vehicle and its equipment due to liberation of occuluded gases and sublimation of materials. This outgassing, which is time and temperature dependent, raises the local pressure and may bring the pressure into the critical range, i.e., between 1 and 10^{-3} torr.

Thus, high voltage equipment intended to be flown in a space vehicle must be examined in detail and proper assessment made of the breakdown and corona hazards. Equipment operating voltages, frequencies, temperatures and outgassing rates must be considered and provision made for insulating where needed against voltage breakdown. Gaseous, liquid, and solid insulation systems as well as hard cacuums have been used successfully to insulate high voltage equipment in space vehicles and missiles.

2.1.7.2 KP-II Radar System

The KP-II radar system is based upon an existing AN/UP Q-102 airborne doppler radar system. In order to assess the effects of operation at reduced pressures, it is necessary to examine each of the components in each of the boxes making up the complete system. Voltage levels, frequency, operating temperatures, existing high voltage insulation (if any) and interconnection methods for all of the high voltage components or circuitry are outlined in Table 2.1.7.1.

2.1.7.3 Space Vehicle Gaseous Environment

During ascent and orbit a space vehicle will encounter an ambient

TABLE 2.1.7.1

KP II SYSTEM CONFIGURATION PRIOR TO INSULATING FOR SPACE VEHICLE OPERATION

Box #	Component or Circuit	Voltage, Frequency and/or Wave Shape	Operating Temp.	Existing High Voltage Insul.	Interconnection Method	Interconnection Term. Potting
	Transformers	825 AC, 2 KC sine	160°F	Epoxy Products TC 2417	Polyolifin HV cable	Dow Corning RTV 882
	Rectifiers	5KV DC with 2 KC ripple	160°F	Potted in epoxy by Supplier		
2	HV Filter		160°F	None		
	HV Capacitor	5KV DC pulsed at 8800 CPS	160°F	Potted in epoxy by Supplier		
	HV Cable (Burndy)		160°F	Rubber	- -	
	Thyratron	10KV DC pulsed at 8800 CPS	500°F	None		None
3	Pulse Forming Network		180°F		Silicone rubber insulated high voltage cable	None - AMP Connectors (PT output - none)
	Pulse Transformer	10 KV Input - 30 KV output pulsed at 8800 CPS	180°F	Oil filled		
	Charging Choke	5 KV DC pulsed at 8800 CPS	160°F			

TABLE 2.1.7.1 (Continued)

Box	Component or Circuit	Voltage, Frequency and/or Wave Shape	Operating Temp.	Existing High Voltage Insul.	Interconnection Method	Interconnection Term. Potting
	Plate Choke	10 KV DC pulsed at 8800 CPS	160°F	None		
	Charging Diodes		160°F	Potted in epoxy by supplier	Silicone rubber	
3	Inverse Diode		160°F		insulated	
	Inverse Resistor	5 KV DC pulsed at 8800 CPS	270°F	None	high voltage cable	
	Klystron	30 KV DC pulsed at 8800 CPS	250°F	Base potted by supplier in silicone rubber		Silicone HV cable potted to base by supplier
	Avalanche Circuit	300V DC input 100V DC pulsed at 8800 CPS	160°F	None	Teflon hookup wire	
	Grid Choke	250V DC pulsed at 8800 CPS	160°F	None		None
	Power Supply		140°F	Sylgard 182		None
4	H.V. Divider	2 KV DC	140°F	Hermetic seal	Silicone HV cable	Amp connectors
	TWT		180°F	Potted in silicone by supplier		Silicone HV cable potted in place by supplier

TABLE 2.1.7.1 (Continued)

Box	Component or Circuit	Voltage, Frequency and/or Wave Shape	Operating Temp.	Existing High Voltage Insul.	Interconnection Method	Interconnection Term. Potting
4	Freq. Multiplier	50 V at 100 to 9600 mc	140°F	None	Teflon hook-up wire	None
5	All	300 V DC (Max.)	160°F	None	Teflon hook-up wire	None
6	All	300 V DC 115 V 2 KC 115 V 3Ø 400 CPS	110°F	None	Teflon hookup wire	None
7	HV	10 KV DC	240°F	None	Silicone HV cable	None Amp Connector
		and				
	CRT	2 KV DC	160°F	Potted in silicone by supplier		

atmosphere that varies in composition and density (pressure). The variation of pressure with altitude is well documented and the ambient pressure at altitude may be obtained from the latest (1962) U.S. Standard Atmosphere. However, the presence of the space vehicle itself modifies the ambient atmosphere to a considerable degree. Material outgassing, the release of occuluded gases from all surfaces, and the gas from the control system all have their effect on the induced atmosphere surrounding a space vehicle. In an early Russian experiment where pressure gauges were flown at short distances from the vehicle, pressures of 10^{-5} torr were read all the way to the moon and back. Figure 2.1.7.2 shows the time history of pressure in the forward equipment chamber of an early Discoverer Satellite (1062) as measured by an inverted magnetron gauge. As can be seen from the figure, the pressure is several orders of magnitude higher than the ambient corresponding to an altitude of 115 nautical miles (10^{-7} torr). In addition, the pressure curve appears to be approaching a lower limit of 2×10^{-4} torr. A later vehicle (1102) measured pressures of 10^{-3} torr just inside the horizon sensor doors (30 sq. in. opening). The pressure at any given point in a particular vehicle will of course depend not only on the quantity and types of materials present but also on the equipment temperature and on the degree of surface contamination such as finish, dirt, grease, cutting oils, finger prints, etc.

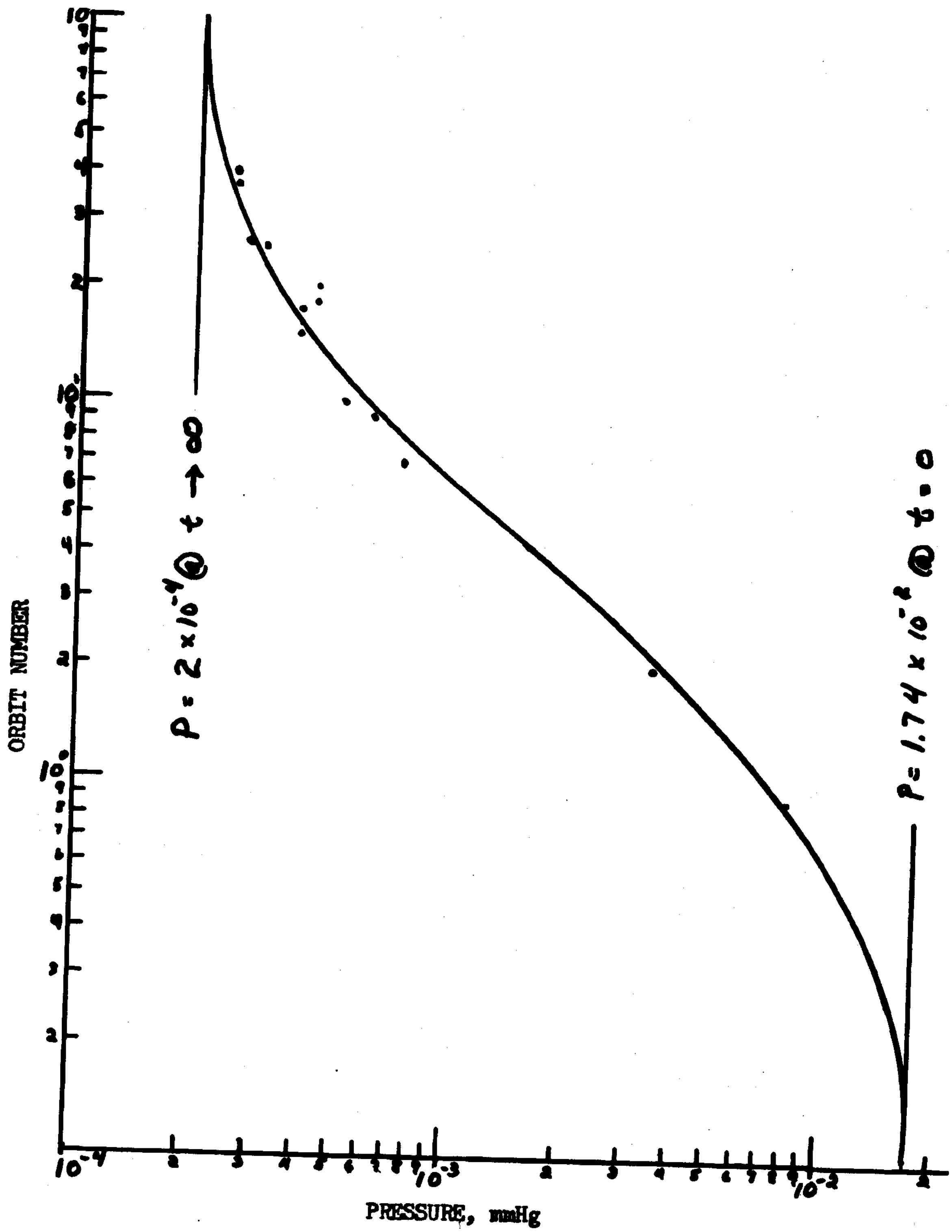

Fig. 2.1.7.2 TIME HISTORY OF PRESSURE IN DISCOVERER SATELLITE FORWARD EQUIPMENT CHAMBER

Pressures within the equipment boxes are again a function of materials, surface areas, temperatures, contamination, and sizes of openings or vents in the boxes. Incorporation of vent holes in equipment boxes (properly screened for EMI) should have a marked effect on internal box pressures. The instantaneous pressure for a given outgassing rate, external pressure, and enclosure volume can be determined by the number, size, spacing and distribution of vent holes. As can be seen from the data in Table 2.1.7.1 the Transmitter/Modulator (Box 3) contains the highest voltages, frequencies and operating temperatures. Because of the spacing, compartmentation and temperature levels in this box, the local pressure rise (even with venting) due to outgassing would be 10 to 100 times higher than the ambient vehicle compartment pressure of 10^{-3} to 10^{-4} torr. Thus, internal high voltage components could see local pressures of 10^{-1} to 10^{-2} torr and if this condition existed, would undoubtedly arc over at the voltage levels present.

2.1.7.4 Breakdown and Corona at Reduced Pressures

a) Uninsulated Electrodes

Paschen's Curve (Figure 2.1.7.1) predicts, for electrode spacings commonly found in electronic equipment, that breakdown and corona will most likely occur as pressures of 10 to 10^{-2} torr. As mentioned previously, Paschen's Curve applies specifically to uniform fields and to DC or low frequency alternating fields. In general the breakdown will be the same for DC as AC provided the positive ions have enough time to travel between electrodes during a half cycle. However, if the ions cannot bridge the gap in time, a space charge will build up between electrodes causing a field distortion. In a similar manner, non-uniform fields give rise to space charge and field distortion effects. Field distortion will in turn cause breakdown to occur at a lower potential than a uniform DC field. There are indications from the literature that breakdown potentials decrease with frequency such that at 20 KC, breakdown values are 15% lower; at 5 - 15 MC, 30 - 40% lower; and on into the microwave region where even lower breakdown values have been observed. Ambient ionization and elevated temperatures further lower breakdown potentials.

Under changing field conditions, with AC or when DC is being raised or lowered, a localized gas discharge called corona usually occurs just before breakdown. Corona type streamer discharges are characterized by low-conduction currents in the microampere range and usually by a visible glow in the vicinity of the electrodes and sometimes by emission of noise in the audible range. This localized discharge indicates that complete breakdown of the gap will occur at a slightly higher voltage.

b) <u>Insulated Electrodes</u>

Corona may also occur on the surface of insulated electrodes when there is a gas gap in series. Discharges in series air gaps are promoted by two factors: the lower dielectric strength of air and the electric stress concentration on the air due to its lower dielectric constant ($k \approx 1.0$). The electric stress in the air is higher than in the adjacent series solid by the factor K_s, which is the dielectric constant of the solid insulation. The corona threshold voltage for a simple series air gap may be calculated. Since the total voltage is distributed between the gas and the solid, the calculation results in the relation: $V_{threshold} = E_{gb}\, d_b \left(\frac{ds}{K_s} + 1\right)$, where E_{gb} is the gas breakdown stress for the gas spacing dg. Lowering the dielectric constant and increasing the thickness of the insulation will lessen the stress on the air gap, lower corona intensity and increase corona threshold voltages.

2.1.7.5 Design Options for High Voltage Protection

a) Maintain Pressure Below the Critical Range

To maintain the pressure below the critical range requires that the high voltage equipment be adequately vented to the space vacuum so that the pressure in the vicinity of the most critical element does not rise above the lower limit of the critical range, regardless of the amount of outgassing from components and materials. This has the advantage of using sea level hardware with a minimum of modification. However, vent holes must be adequately screened for EMI which cuts down the effective pumping speed of the vent and large vented areas are impractical from a structural integrity standpoint. In addition, venting imposes severe problems in predicting outgassing rates of all components within the boxes. This condition can be eased by warming up the boxes (increasing outgassing rates) before applying voltages to elements sensitive to breakdown. The outgassing and pumping characteristics of the high voltage assemblies are difficult to predict and accurate values can only be obtained by a long and careful testing program of each and every possible source of gas, plus rigid control of materials, finishes and contamination. Moreover the best available information indicates that pressures in the forward barrel section will be in the 10^{-3} to 10^{-4} torr range (Figure 2.1.7.2) which would impose a lower limit on pressures available through venting. It appears from Paschen's Curve (Figure 2.1.7.1 that operation at 10^{-3} to 10^{-4} torr would not present breakdown problems. However, it is not known what derating factors have to be applied to this curve to take into account non-uniform fields and square wave pulse conditions as in the Transmitter/Modulator. If it is assumed that venting can reduce ambient pressures within the box to 10^{-3} to 10^{-4} torr there is still the probability that when certain high voltage elements are energized that copious amounts of gas would be given off due to thermal rise causing local pressures possibly in the 10^{-1} to 10^{-2} torr range.

b) <u>Maintain Pressure Above Critical Point</u>

Since the KP-II system operates at atmospheric pressure without breakdown, the hazards of a low pressure environment can be eliminated by maintaining the pressure, in the payload equipment section or in the individual equipment boxes making up the system, above the pressure at which breakdown would occur. This approach necessitates the construction of pressure vessels and the determination of leak rate. Pressure vessel design dictates the use of shell type curved surface construction and the elimination of large flat areas. Existing equipment boxes, which are essentially rectangular sheet metal boxes, would have to be replaced, and pressure vessels designed and fabricated. Accessibility and maintainability are sacrificed and sealing becomes a major problem. Elastomeric seals (O-rings) have finite leak rates and deteriorate in hard vacuum due to loss of plasticizers and low molecular weight constituents. Soft and hard metal seals have poor compressibility and sealing properties and require hard flat container flanges which are easily damaged. For extended missions, welded leak checked seals are preferable. Access to welded boxes can only be accomplished by grinding away the weld which means that maintainability and trouble shooting problems would be severe.

c) Insulate with a Liquid Dielectric

Immersing high voltage components in a dielectric fluid so as to eliminate air or other gases will provide voltage protection at altitudes. Two of the high voltage components, namely the pulse forming network and the pulse transformer are insulated in this manner. In addition to the increased weight of liquid insulation there are problems in accommodating the large volume expansion of the dielectric liquid over a wide temperature range and in maintaining a pressure on the liquid so that it will not gas and breakdown at reduced pressures. The thermal expansion problem requires that an expansion chamber be provided for high temperature operation and the reduced pressure requires that the sides of the containers be rigidly reinforced to prevent expanding or bowing out.

d) Insulate with a Solid Dielectric

Embedding or potting of high voltage components, and the termination of interconnections in organic resins provides high voltage breakdown protection under any pressure conditions. Potting also provides design advantages such as improved heat transfer and a means of mounting and supporting components during vibration and shock. In many cases, existing components and circuitry may be simply embedded with a minimum of design changes and testing time, whereas liquid and gaseous insulation requires extensive redesign and fabrication of structural hardware such as expansion devices and pressure vessels. Failure modes do exist in solidly insulated components but they are predictable and, through proper design, selection and testing of materials, may be eliminated.

Internal Corona and Treeing Potted components may fail due to corona and/or treeing in entrained air bubbles, in cracks that may develop due to mechanical or thermal stresses or in interface separation caused by non-adhesion or incompatibility of materials.

Voids or cracks containing air would have dielectric constants of approximately 1.0 while the surrounding potting would have a dielectric constant of approximately 3 to 4. The field concentration in the void or crack thus would be 3 to 4 times higher than in the insulation resulting in probable corona in the void. Whether corona existed in the void would depend on the size of the bubble and on the gradient in the insulation. The immediate effect of internal corona is to decrease the thickness of the insulation which may result in immediate breakdown. Long term corona frequently results in a phenomenon called "treeing" in which tree-like corona paths continually erode their way through the insulation until failure occurs. Treeing is believed to result from corona degradation which tends to form isolated conductive areas in the voids or cracks resulting in field concentration effects which locally exceed the dielectric strength of the material.

Voids and bubbles can be avoided by selecting materials with low enough viscosity and long enough "pot life" so that vacuum inpregnation techniques can be effectively used to insure their absence. Non-adhesive problems can be eliminated by selecting potting materials that adhere and are compatible with all the materials in the component or device. Mechanical and thermal stresses can be eliminated by proper design of the potting configuration and by selecting materials that do not crack or degrade at the thermal extremes encountered.

External Corona As discussed previously, external corona may exist between insulated electrodes. Low dielectric constant, high resistance, and high dielectric strength materials and increased thickness will minimize external corona. Because of the spacing, voltage levels, pulse and frequency conditions peculiar to the KP-II system, the extent and intensity of external corona can only be established through altitude tests on the system. However, there are the design options of decreasing dielectric constants, increasing thickness, potting solidly and shielding (elimination of air gap) to prevent corona.

The direct impingement of corona discharges on insulation surfaces will cause slow or rapid (varies among different insulators) decomposition of all organic plastic materials. Corona bombardment generates a multitude of active molecular atomic and ionic species such as ions, free radicals, electrons and high energy ultraviolet light which depolymerize and decompose organic plastics to low molecular weight fragments which evaporate. The rate of attack depends on corona intensity and on the rate of discharges. Corona intensity will depend on the ratio of operating voltage to corona starting voltage and the rate will be proportional to pulse rate or frequency. Insulation exposed to corona will eventually fail due to corona erosion of insulator surfaces. High reliability electronic equipment for space vehicles demands that corona be considered as dielectric breakdown and eliminated.

2.1.7.6 Insulation of the KP-II System

As can be seen from examination of Table 2.1.7.1 the Transmitter/Modulator (Box 3), presents the greatest challenge in the selection of an insulating method. Figure 2.1.7.3 is a view of the high voltage components in Transmitter/Modulator prior to insulating for space vehicle operation. The second most complex insulation problem is in the Recorder, (Box 7); however, here the CRT is already insulated and tested to pressures of 8.4 torr by the vendor. The third most complex problem is with Lear Siegler Power Supply, Box 2, followed by the RF-IF Box 4, and then the Control Unit, Box 6 and finally the Reference Computer, Box 5. In the latter two units only the 300 volt circuitry presents problems and this can be handled by the application of a void free insulating conformal coating.

Each of the high voltage components and each circuit listed in Table 2.1.7.1 was initially examined in detail as to temperatures, voltages, frequencies and to the difficulties of providing insulation at possible box pressures of 10^{-1} to 10^{-2} torr. Redesign problems, fabrication, maintainability and testing difficulties as well as weight penalties and the effect of all these problems on schedule were taken into consideration before the insulating system was selected. In each case the relatively uncomplicated solution, with minimum design changes, fabrication costs, maintainability and testing difficulties is to pot or embed the high voltage components and circuitry in an organic

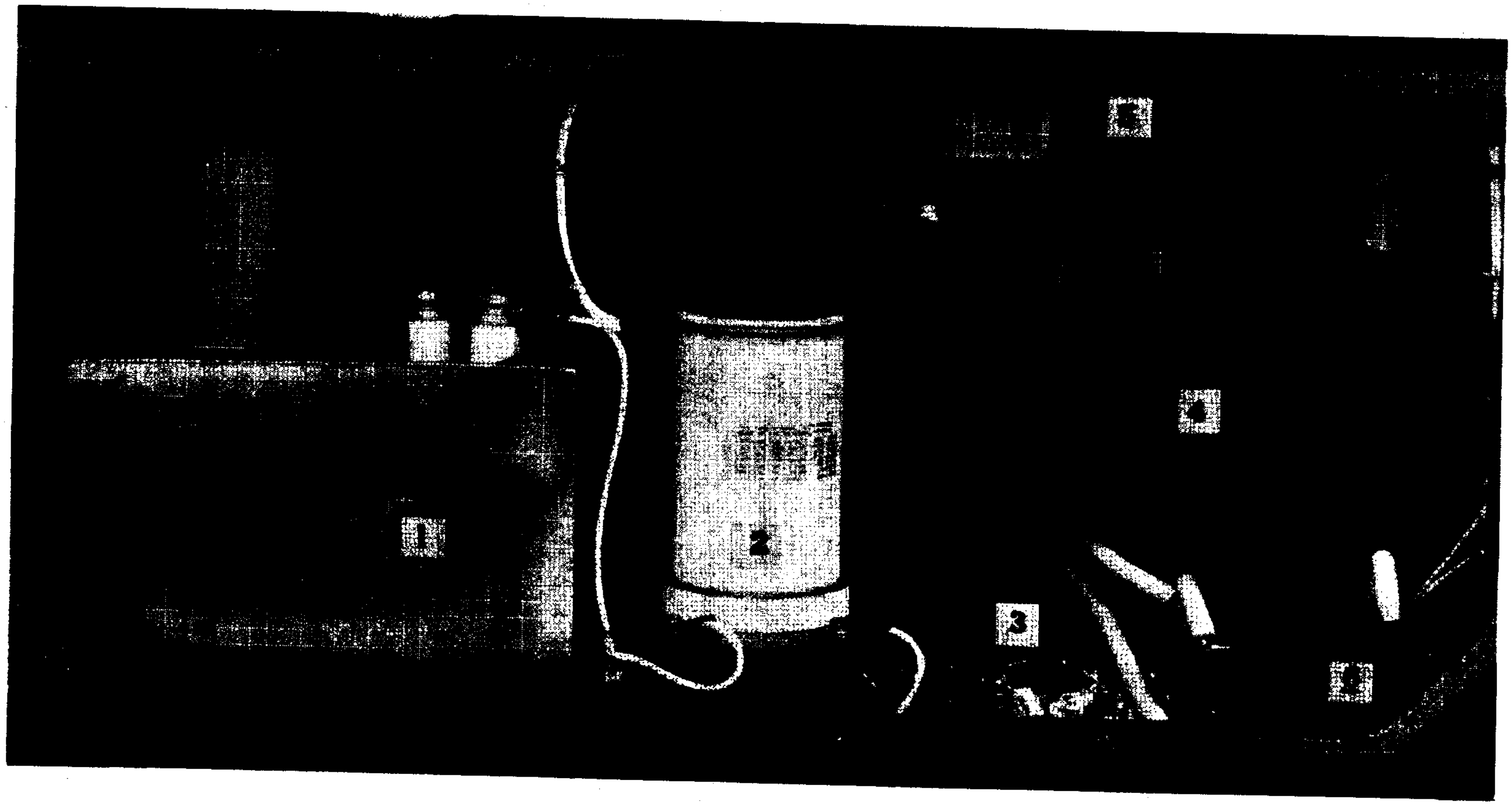

(1) Pulse Transformer
(2) Thyratron
(3) Diode
(4) Pulse Forming Network
(5) Plate Choke
(6) Inverse Resistors

Figure 2.1.7.3 View of High Voltage Components in Transmitter-Modulator (Box 3) Prior to Insulating For Space Vehicle Operation dielectric solid. For each device that needed to be insulated, there were known proven materials available that had the intrinsic dielectric properties and the required temperature resistance. The problem of insulating the components was reduced to the evaluation and selection of suitable materials and development of suitable application and testing techniques for each specific component or circuit.

A potting evaluation and selection program was initiated by Lockheed, with Goodyear's cooperation, to develop potting materials and techniques for insulation of the KP-II high voltage components. Testing of potted components was conducted by Goodyear over the pressure range of 2 to 10 torr to insure that the completed system would operate at any pressure. In addition, Goodyear felt that for Box 3, a pressure vessel could be designed and tested within the same time scale as the potting and would provide a backup solution in case the potting development proved to be unsolvable.

2.1.7.7 Development of Potted High Voltage Components

a) Initial Potting Material Selection Criteria

Electrical insulating and potting materials were selected on the basis of an analysis of the engineering requirements applicable to each specific component or device to be insulated for high altitude operation. Potting materials were selected on the basis of:

- o High dielectric strength at operating temperatures.
- o Lower dielectric constants to minimize stress on air gaps.

- Low dissipation factor to prevent dielectric heating problems.
- High resistivity to minimize leakage currents.
- Stability at operating temperatures, i.e., no change in properties with time at operating temperature.
- Resistance to thermal cycling, i.e., no cracks developing during exposure to thermal extremes.
- High thermal conductivities and low coefficient of expansion.
- Sufficient mechanical strength to provide support to components during shock and vibration.
- Low viscosity, i.e., can be cast void free using vacuum degassing techniques.
- Forms an adhesive bond to and is chemically compatible with the materials to be insulated.

Interconnection of High Voltage Components Silicone rubber insulated high voltage cable was used extensively throughout the KP-II system to interconnect high voltage components. Many of the components in the system such as the klystron base, the CRT, and the TWT already had the silicone high voltage cable potted in place and other components such as the pulse foaming network and pulse transformer had AMP connectors installed which were designed for the H.V. cable. In addition, the high temperatures/high voltages existing at the thyratron anode, the klystron base, and the inverse resistors, precluded the use of any other type of H.V. cable. This requirement, that silicone rubber H.V. cable be used, placed severe restrictions on the selection of materials for potting components and terminating the H.V. cable since only silicone potting materials will bond to silicone rubber cable. Silicone rubbers require primers for bonding to other materials and special cure schedules for high temperature operation and, in addition, exhibit inhibition problems when in contact with certain organic materials.

Thyratron Potting   Initially, anode temperatures on the thyratron were expected to be in the 500°F range. The H.V. cable termination at the anode would be the most critical potting problem.

An evaluation of cleaning methods, primers, cure schedule, materials inhibition and high temperature exposure tests were conducted on suitable silicone potting materials specifically for the thyratron potting but also generally applicable for termination of the H.V. cable to other components.

Two inch lengths of white silicone H.V. cable were abraded (not primed) and potted in five different materials. Adhesion to wire and potting cup were checked, specimens were then postcured and subjected to high temperatures. Results of these initial tests are contained in Tables 2.1.7.2, 2.1.7.3, and 2.1.7.4.

TABLE 2.1.7.2

SILICONE RUBBER ADHESION TESTS

Materials*	Cure	Primer	Adhesion to Cable	Adhesion to Cup
RTV 501	24 Hrs./RT	AC-7000**	Yes	Yes
RTV 503	" "	Q2-1011*	Yes	No
RTV 521	" "	AC-7000**	Yes	No
RTV 601	" "	Q2-1011*	Yes	No
Sylgard 103	" "	Sylgard*	Yes	Yes
Sylgard 103	" "	None	No	No

*Dow Corning Corp. ** Hysol Corp.

TABLE 2.1.7.3

RESULTS OF EXPOSURE TO 500°F FOR 28 HOURS

Material	Cure Schedule	Results of Exposure to 500°F for 28 Hours
RTV 501	Note 1	Passed - No damage
RTV 503	" "	Failed - Blown into sponge
RTV 521	" "	Passed - No damage
RTV 601	Note 2	Passed - No damage
Sylgard 183	Note 3	Passed - No damage

TABLE 2.1.7.4

RESULTS OF EXPOSURE TO HIGH TEMPERATURES

Material Note (1)	Post Cure	500°F/1 hr.	600°F/1 hr.	700°F/1 hr.	750°F/1 hr.
RTV 601	None	No damage	No damage	Delayering	Delayering & blowing
RTV 601	500°F/1 hr.	----	No damage	----	----
RTV 601	500°F/1 hr. plus 600°F/1 hr.	----	----	Delayering	----
RTV 601	600°F/1 hr.	----	----	Delayering	----
Sylgard 182	None	No damage	No damage	Cracking	Cracking & disintegrating
Sylgard 182	500°F/1 hr.	----	No damage	----	----
Sylgard 182	500°F/1 hr. plus 600°F/1 hr.	----	----	Cracking	----
Sylgard 182	600°F/1 hr.	----	----	Cracking	----
Sylgard 183	None	No damage	No damage	Surface hardening	Surface hardening & delayering
Sylgard 183	500°F/1 hr.	----	No damage	----	----
Sylgard 183	500°F/1 hr. plus 600°F/1 hr.	----	----	Surface hardening	----

TABLE 2.1.7.4 (Cont.)

Material Note (1)	Post Cure	500°F/1 hr.	600°F/1 hr.	700°F/1 hr.	750°F/1 hr.
Sylgard 183	600°F/1 hr.	----	----	Surface hardening	----

Note: (1) Test specimens consisted of 50 grams of material cured in an aluminum weighing dish (approximately 1/2 inch depth). All specimens initially cured at 150°F/4 hours.

Based on the results of these tests, Dow Cornings RTV 501 with Hysol AC-7000 primer was selected for termination of the H.V. cable. A thyratron was obtained from Goodyear, along with a section of bright yellow silicone H.V. cable and these were potted using RTV 501. Upon completion of the cure, it was noted that the potting was inhibited by the cable and not bonding to it. A new batch of a light yellow silicone H.V. cable was received from the AC abraded (not primed) and tested using the RTV 501 and some additional primers. Results of these tests are contained in Table 2.1.7.5.

TABLE 2.1.7.5

ADHESION TESTS TO SILICONE H.V. CABLES

Material	Primer		Adhesion to Cable	Adhesion to Cup (Rating)	
RTV 501	General Electric	S-4004	Yes	Yes	1st
RTV 501	Hysol	AC7000	Yes	Yes	2nd
RTV 501	Products Research	PR1902	Yes	Yes	3rd
RTV 501	Dow Corning	4094	Yes	No	

The H.V. cable is purchased by Goodyear from AMP, Inc. in 18 inch lengths with a female connector fabricated on one end and are identified by AMP as No. 832692-22. AMP confirmed that they did not manufacture the cable itself and bought cable from different cable manufacturers, which would account for the inhibition encountered with some samples. At this time information was received from the AC that thyratron anode temperature would be approaching 700 F. Additional samples of silicone materials were prepared and tested. Test results are contained in Table 2.1.7.6.

TABLE 2.1.7.6

RESULTS OF ADDITIONAL TESTS AT HIGH TEMPERATURES

Material	Additional Post Cures	RESULTS OF EXPOSURE TO— 550°F/ 45 min.	600°F/ 35 min.	650°F/ 15 min.	700°F/ 20 min.
RTV 501 (1) RTV 521 (1) RTV 601 (2) Sylgard 183 (3)	500°F/ 28 hrs.	No Damage	----	----	----
RTV 501 (1) RTV 521 (1) RTV 601 (2) Sylgard 183 (3)	500°F/28 hrs. plus 550°F/45 min.	----	No Damage	----	Blown into sponge Hardening & delayering Hardening & delayering Surface hardening
RTV 501 (1) RTV 521 (1) RTV 601 (2) Sylgard 183 (3)	500°F/28 hrs. plus 550°F/45 min. plus 600°F/35 min.	----	----	No Damage	----

Note: (1) R.T./7 days plus 150°F/4 hours plus 300°F/3 hours plus 400°F/3 hours plus 450°F/16 hours.

(2) R.T./7 days

(3) 150°F/4 hours

A silicone H.V. cable was potted into the top section of the thyratron using Sylgard primer and Sylgard 183 potting. A potting procedure was written up and delivered to Goodyear with the potted thyratron for further testing. Sylgard 183 was selected for this application because it has the highest temperature resistance of the silicone potting materials and does not have to be extensively post cured at higher and higher temperatures to obtain the high temperature resistance. This potted thyratron was satisfactorily tested at altitude by Goodyear without breakdown.

Potting of Other High Voltage Components - Goodyear evaluated silicone potting materials and selected Hysol's RTV 211 (equivalent to Dow Corning's RTV 521 tested by LMSC), for the potting of the pulse transformer bushing, inverse resistors, avalanche circuit, grid choke, plate choke and for the termination of the silicone H.V. cable on other components. Sylgard 182 (a clear version of the Sylgard 183 used on thyratron) was selected by Goodyear to pot the RF-IF power supply and high voltage divider. An epoxy resin was selected by Goodyear to pot the 2 to 10 KV supply in the Recorder.

Conformal Coatings - As mentioned previously, the insulation of circuitry with voltage up to 300 volts could be accomplished by the application of a void-free insulating coating to all terminals, printed circuit traces and component leads. In addition, this conformal coating, when applied to components, provides mechanical support for shock and vibration protection. The conformal coating must be capable of being applied void free and in sufficient thickness (approximately 0.010 inches) for voltage protection with 100% coverage and must form an adhesive bond to all lead materials. Epoxy resins are usually used for this type of application because of their electrical properties, mechanical strengths and their adhesion to components, leads, terminal boards and most wire insulations. However, in this case, the requirement that all terminal edges and cut leads be coated to a void free thickness of 0.010 inches was very difficult to meet since low viscosity coatings drain off from sharp edges and high viscosity resins cannot be applied without voids. An evaluation of conformal coatings that could be vacuum degassed in place without excess run off was initiated by LMSC. As the result of this evaluation, an experimental resin system Scotchcast XR 5072 (3M Co) was selected as a conformal coating. This material is a heatcuring, controlled flow epoxy resin that can be applied, degassed and cured without voids and with a buildup of approximately 0.010 inches on leads and terminals. Additional quantities of this material along with processing instructions were passed on to the AC for further evaluation on actual circuits.

<u>Teflon Insulated Hook Up Wire</u> A surface treated (for adhesion and marking) teflon insulated wire, HiTemp B (HiTemp Wires), was used extensively by Goodyear in the KP-II system. The adhesion of the Scotchcast XR 5072, Sylgard 183 and Hysol RTV 211

to this treated wire was unknown and an investigation of the adhesive bond strength of these materials to surface-treated teflon was conducted by LMSC. Results of these tests are contained in Table 2.1.7.7.

TABLE 2.1.7.7

ADHESION TO TEFLON INSULATED WIRE

Test Specimens: 22 AWG Teflon Insulated Wire:
Nominal 10 Mil Wall; OD 0.050 inches;
Potting Depth 0.5 inches;
Three specimens per test.

Potting Material	Pull Out Force (PSI)				
	Surbond	HiTemp A	HiTemp B	Virgin	Etched
Scotchcast XR 5072 (No Primer)	121	85	81	0	122
Sylgard 183 (Sylgard Primer)	85	5.5	35	0	91
Hysol RTV 211 (Primer AC7000)	19	5.8	84	0	87

<u>Results of Initial Altitude Tests on KP-II System</u> Altitude testing over the range from 2 torr to 10^{-4} torr was conducted by the AC on all boxes comprising the KP-II system. As the voltages were raised on the T/M, the insulation flaws were uncovered and corrected until the box could operate at full voltage without breakdown. However, there was extensive corona around all potted

H.V. components and all H.V. cable. In the RF-IF box, breakdown was experienced in a 100 mc varactor multiplier at 30 - 50 volts.

b) Corona Suppression Techniques

Foams Light weight (2 lbs. per cubic foot) closed cell polyurethane foams with dielectric constants of approximately 1.2 and dissipation factor of 0.001 have been extensively used to insulate and support high frequency components. Several such foam systems have been extensively used by LMSC on varactor multipliers similar to the AC's without experiencing any altitude breakdown or corona problems. This material, along with processing instruction was supplied to Goodyear and successfully eliminated corona and breakdown in the varactor multiplier in Box 4.

The 2 lb/ft^3 foam has a dielectric breakdown strength of approximately 50 volts/mil at ambient pressures. The individual cells are formed initially by either the expansion of freon or carbon dioxide caused by the exothermic resin reaction. Upon cooling to room temperature a partial vacuum exists in the cells and air eventually diffuses in. Under vacuum conditions, of course, the diffusion would be in the other direction with the foam cells eventually going through the critical range; however, there are indications from the literature that if the cell size is small enough the mean free path of electrons and ions would be reduced and Paschen's Curve would be raised to much higher voltages. While foams do not have sufficient dielectric strength to be used as the primary insulation in the

T/M, they may have some merit as a corona suppression medium. Accordingly, an evaluation of foams for corona suppression was initiated by LMSC.

The main problem in applying foams to the T/M is in obtaining wetting and adhesion of the foam to the silicone insulated lead wires and high voltage components. Various silicone primers and adhesives were applied to samples of Sylgard 183, H.V. cable, RTV 211 and several other RTV silicones but none of these primers were effective in creating an adhesive bond between silicone and polyurethane foam. Several lengths of H.V. cable were terminated in a block of silicone rubber, primed, foamed and tested at pressures of 2 torr to 10^{-1} torr in a vacuum chamber using a Tesla coil as a high frequency high voltage source. Corona was produced along the H.V. lead and was also evident at the foam-lead interface but not around the block of silicone rubber. This test proved that an adhesive bond must exist between foam and silicone insulation and that if insulation thickness is increased significantly corona will not be present. Experiments with polyurethane foam were abandoned because of the adhesion problems. A H.V. cable specimen was prepared using a closed cell 10 lbs/ft^3 silicone rubber foam, 3 M's Scotchcast XR 5017; however, because of high viscosity, this foam did not flow readily and wet the cable. When this foam was tested at 10^{-1} torr using Tesla coil, it exhibited corona between the foam and the cable.

<u>Shielding</u> As mentioned previously, external corona problems can be eliminated by applying a grounded conductive coating (shield) to the insulation or by potting high voltage components in metal cans thus eliminating the series air gap. The decision was made to put high voltage components in metal cans and LMSC investigated methods of shielding the H.V. cable which was not available shielded. Samples of conductive silicone rubber, Dow Corning Q92-005, were procured and samples of the H.V. cable were coated. A section of H.V. cable was also shielded by slipping on a section of Belden braid and potting it in place void free using Hysol RTV 211. These samples and processing data were forwarded to Goodyear to test. The braid shielded H.V. cable performed satisfactorily at altitude. The decision was then made to pot all H.V. components in metal cans with AMP type connectors and to use the braid shielded H.V. cable to interconnect these components using an AN type nut and ferrule and a conductive epoxy to properly terminate the braid mechanically and electrically at the can.

<u>Lear Siegler Power Supply</u> As can be seen from Table 2.1.7.1, the voltage and temperature levels in the Lear Siegler are below those in the T/M. The initial method of interconnection between the transformers and rectifiers and between rectifiers was accomplished with polyolifin insulated H.V. cable with the ends of the cable being potted in place and no connectors being

used. Recommendations on potting materials, shielding methods, and processing techniques were forwarded by LMSC to Lear Siegler. At the request of the customer, a personal visit by LMSC personnel was made to Lear Siegler to pass on the design, materials selection, and processing philosophy that had developed concerning high voltage breakdown. During this visit, a partial assembly consisting of three transformer-rectifiers was tested at altitude and extensive corona was observed. One of the transformers was shielded using a conductive paint and a marked reduction in overall corona resulted. Specific recommendations were made to Lear Siegler on a better transformer potting material (Scotchcast 281), a better H.V. lead adhering potting (Furane Plastics Epocast 202/9615) and a better conformal coating (Hysol 12-007) for low voltage areas. An evaluation of conductive paints suitable for shielding the epoxy potted transformers and the polyolifin insulated wire was begun by LMSC. Several samples of epoxy resin were coated with various silver filled conductive paints and resistivity measurements taken at elevated temperatures. In addition, similar tests were performed on polyolifin insulated wire but the rigidity of the conductive paints are such that the wire insulation could not be flexed without cracking the coating. Recommendations were made to Lear Siegler that they shield the polyolifin wire with braid and bond the braid in place with Epocast 202/9615. The question of silver migration into the potting was raised and a test was made to evaluate this problem.

A 0.125" slab of a flexible epoxy, i.e., Epocast 202/9615, at a one to one mix ratio was cast and conductive silver electrodes of approximate 1-1/4 inches in diameter painted concentrically on both sides. A flexible epoxy was chosen because it is not highly crosslinked (large spaces between crosslinks) and if silver migration was a problem it would occur in this type of epoxy much faster than in a rigid, highly crosslinked system.

Two specimens were prepared and placed in an oven at 165°F and the initial volume resistivity, dielectric constant and dissipation factor measurements taken when samples reached oven temperature. One sample was held at temperature as a control and did not exhibit any changes in electrical properties during a five hour test. The other sample was held at 500 volt DC potential (4 volts/mil) for 1 hour with a slight increase in volume resistivity. This sample was then held for two hours without voltage and no changes noted. Voltage was increased to 2000 VDC (16 volts/mil) and held for an hour during which time the volume resistivity increased from 9×10^8 ohm-cms to 3×10^9 ohm-cms. After voltage was removed sample remained at 3×10^9 while control sample still remained at 6.5×10^8. No variation in dielectric constant or dissipation factor was recorded in either specimen during the test. Insulation resistance of the test specimen was 2×10^{12} ohm at room temperature and did not exhibit any detectable change after three hours at 15 KV (120 volts/mil) at room temperature. It was concluded from these tests that silver migration would not be a problem. A literature search revealed that the only reported cases of silver migration occurred in porous insulation at humidities above 50% RH and under a constant DC voltage stress of many months' duration. High humidities and porour insulation both were required before migration occurred.

Lear Siegler had decided to place the transformer-rectifier in a single metal can thus eliminating the need for the silver paint and for shielding the interconnection between transformers and rectifier. Rectifier interconnections were made in an open metal channel with the epoxy potting being thick enough so that corona was not present. The polyolifin wire connecting the rectifiers to the H.V. choke exhibited corona during altitude and had to be shielded. This was accomplished with Belden braid which was bonded in place with Epocast 202/9615.

<u>Venting</u> As a further precaution against H.V. breakdown and corona, it was decided by LMSC that the boxes would be vented. Laboratory experiments were conducted by LMSC on a small conformally coated electronic module (resistor board, 18 sq. inches in area) contained within typical electronic boxes of 226 cubic inches and 396 cubic inches volume. Tests were performed in a vacuum chamber with the internal module and the external chamber pressure being monitored during pump down. Parameters studied included the effect of module box vent diameters, (1/16, 1/4 and 1 inch) and the effects of materials outgassing (at module tempera-

tures of 75°F, 125°F and 200°F), on the internal box and external chamber pressures.

Test results indicated that even with a 1 inch diameter vent hole and an external pressure of 10^{-6} torr or below that the internal box pressure cam up from 1-1/2 (on 396 in^3 box) to 2 (on 226 in^3 box) orders of magnitude into the 10^{-4} torr range as module temperature came up to 200°F. The peak pressure occurred between 10 and 20 hours after power was applied to the resistors, and external chamber followed a parallel curve that came up slightly over one order of magnitude (i.e., 10^{-5} range) even though chamber was continuously being pumped.

As a result of these tests it was decided by LMSC that one inch diameter properly screened vent holes be installed in each of three sides on each box.

c) Potting Problems Encountered

Adhesion of Silicone Potting The adhesion of silicones to other materials can only be accomplished through the use of primers. Surface preparation, cleaning and the uniformity of the primer application are critical in obtaining adhesion. Many of the potting failures on the thyratron, klystron, diodes, H.V. divider, PT bushing, and plate choke were caused by poor surface preparation, cleaning and primer application techniques. Extensive surface preparation such as sandblasting, and liquid honing were found to be required on ceramic surfaces (PT bushing and AMP connectors) metal surfaces (potting cans) and plastic surfaces. Primer uniformity was also critical and techniques had to be refined to prevent buildup which resulted in non-adhesion.

Once surface preparation, cleaning and primer application parameters were established, components were potted on a batch basis with adhesion being verified by dissection of an operable unit.

Inhibition of the Sylgard 182 by the epoxy fiberglass laminates in the H.V. divider resulted in non-adhesion of the Sylgard to the epoxy which caused a failure at altitude. Potting was changed to Hysol RTV 211 which is not inhibited by epoxy curing agents.

Potting Expansion Problems on Thyratron Potting of the thyratron into a metal can (for corona suppression) introduced problems in accommodating the large volume expansion of the Sylgard 183 potting due to thermal rise during operation. The initial potting can was cylindrical and enough pressure was generated by the expanding potting to split the seam on the can. Goodyear changed the potting can to a square configuration to allow movement of the can's sides during thermal expansion and contraction (oil can effect) and started experimenting with expandable top cans. LMSC started an investigation into reducing the coefficient of expansion of the Sylgard through the use of fillers and evaluating high temperature epoxies for potting the thyratron.

Low coefficient of expansion inorganic fillers are commonly used to lower expansion coefficients in polymer systems. However, the amount of filler needed is greater than 50% by volume before any reduction is noted. The addition of such a large amount of filler to the already viscous Sylgard 183 would raise the viscosity and make the polymer unsuitable for H.V. applications. Another technique to reduce expansion is to use a coarse filler, 20 to 40 mesh, and impregnate it in place with the Sylgard 183. This gives volume percentages of 85 to 90% and marked reduction in expansion and some reduction in dielectric strength. The bulk of the potting in the thyratron is in the anode cup and dielectric strength in the cap itself is not of importance since the inside of the cup is all at the same potential. Several commercial resin systems are on the market that use this fill in place technique and the coarse fillers from these systems were evaluated with Sylgard 183 using metal cups approximately the same diameter and depth as the thyratron anode. Measurements on the test specimens at elevated temperature indicated that the coefficient of expansion was cut in half. Dissection of the specimens indicated incomplete impregnation and that even coarser fillers would be needed.

Concurrently with the filler investigation on the Sylgard, LMSC was also investigating high temperature epoxies. The silicone H.V. cable was no longer being embedded in thyratron potting but was terminated at an Amp connector and adhesion to the silicone cable was no longer the governing parameter. In addition, Goodyear had taken thermocouple measurements on a potted thyratron that established the anode temperature at a maximum of 400°F and external can temperature (at top) of 250°F after several operating cycles. A filled epoxy resin would have a coefficient of expansion at least an order of magnitude less than the Sylgard 183, would bond without primers and would eliminate the potting can since conductive epoxies could be utilized as corona shield. Filled rigid high temperature epoxies would have less dielectric strength and increased leakage at elevated temperatures than the Sylgard 183 and are notorious for their poor thermal shock resistance at low temperatures. The rigid low coefficient ceramic and metal thyratron would impose severe mechanical stresses on the resin during curing and exposure to low temperatures. A fixed air capacitor with plate spacing of 0.125 inches and mounted on a ceramic plate was totally embedded in various high temperature epoxies. Elevated temperature dielectric strength and leakage were measured between capacitor plates and the embedded ceramic plate made a good thermal shock specimen.

The best filled high temperature epoxies were evaluated first using the air capacitor specimen but upon removal from 400°F post curing oven, these specimens either cracked around ceramic or around the edges of the metal capacitor plates. Additional high temperature filled resin systems with increasing degrees of flexibility or increased filler loading (less shrinkage and lower expansion coefficient) were evaluated until a resin system was found that would not crack around the embedded capacitor when placed in a freezer at -20°F and would withstand 15 KV DC between the embedded plates at 400°F. Of the six resin systems evaluated only a blend of 60% Scotchcast 281 (a semiresilient filled resin) and 40% Scotchcast 251 (a rigid filled resin) would pass these screening tests. A rejected thyratron (open cathode) was mounted in an open-top cylindrical potting can with an AMP connector and potted in the resin blend (SC 281/SC 251). This thyratron was tested at 300°F with voltage applied between the H.V. connector and the can and a breakdown at 4 KV DC was experienced. At room temperature, breakdown occurred at 7 KV DC. Upon peeling off the aluminum can, it was discovered that the can was inadvertently touching the grid ring and no breakdown had occurred through the resin. Further removal of the can resulted in breakage of the base of the thyratron. A voltage of 5 KV DC between grid ring and H.V. connector resulted in internal breakdown of thyratron. The outside of the potting was wound with a bare copper wire and covered with a conductive epoxy. Potted thyratron was tested at 300°F with DC voltage up to 20 KV without breakdown or corona. At 25 KV a sizzling noise was heard which is evidence of corona. At 10 KV and 300°F the DC leakage between H.V. connector and shielding was one microamp. Nothing further was done on epoxy-potted thyratrons, since in the interim Goodyear had perfected the braided expandable top can and had added an aluminum sling in the anode area to reduce the bulk of the potting. These techniques solved the thyratron expansion problems and no further trouble was experienced with the thyratron.

Potting Problem on Diodes   Sporadic diode failures continued to occur even after rigorous surface preparation, cleaning, priming, and strict processing controls were instituted by LMSC and Goodyear. Dissection of operable diodes right after potting and testing indicated perfect adhesion and no voids, yet after sometime at altitude a separation would occur usually at the H.V. connector interface. A reject diode and metal potting can were obtained from Goodyear and a diode was potted by LMSC using the resin blend, i.e., 60% SC 281 and 40% SC 251 that was evaluated for the thyratron potting. This diode was checked out by the AC at voltage and altitude without any problems. This diode was dissected and examined for internal voids, adhesions and corona, none of which were present. Additional silicone rubber potted diode failures occurred and further analysis of the problem indicated that because of the geometric configuration of the potting and the excellent bond to the potting can, the only way that the Hysol 211 silicone could accommodate any thermal expansion and contraction forces or increased curing shrinkage was to split itself (cohesive failure) or to part from a bonded surface (adhesive failure). The lowest strength most highly stressed area in the diode was the bond to the ceramic H.V. connector. When this bond failed, a direct short would occur to the grounded can. Diode failures always occurred in this area.

When there appeared to be no way out of the problem except to redesign the diode potting configuration, additional operable diodes were potted by Goodyear in the epoxy and successfully tested and dissected. The epoxy offered several advantages over the silicone in that its thermal expansion characteristics were at least an order of magnitude lower, it could be easily and rapidly post cured to a stable condition without time dependent shrinkage problems, and it was physically much stronger and formed a strong adhesive bond to the ceramic H.V. connector. The decision was made to pot diodes in the epoxy blend and no further trouble was experienced with the diodes.

Lear Siegler Power Supply Two potting failures occurred on the Lear Siegler during altitude testing at LMSC after the Acceptance Test Procedure altitude tests had been completed. Dissection and analysis of the first failed unit revealed several contributing factors were involved. The ceramic bushing on the H.V. capacitor did not have the glaze removed resulting in non-adhesion, and an air containing adhesive used to bond the potting cup to the capacitor was in the field and the resulting corona in the voids contributed to the lifting of the non-adhering potting causing an arc along the ceramic potting interface. The potting material (Epocast 202/9615) used was not suitable for this application. This resin was originally recommended for the individual wire terminations and because of short pot life, high viscosity and high exotherm, large amounts of this material (such as used for the capacitor potting) are difficult to degas. The capacitor potting was repaired by LMSC because of a plant vacation shut down at Lear Siegler, using a lower viscosity longer pot life epoxy resin Scotchcast XR 5073. Potting cup redesign eliminated the need for adhesives in the field. The second failure was analysed as being caused by voids in the Epocast 202/9615 in the channel potting that interconnected the rectifier-transformer modules. This potting was changed to SC XR 5073 for the same reasons previously noted. After these changes were incorporated, no further breakdowns were experienced on the Lear Siegler power supply.

2.1.7.8 Final Potting Configuration on Vehicle 2355

The final potting configuration for each H.V. component that was successfully flown in Vehicle 2355 is shown in Table 2.1.7.8. Figure 2.1.7.4 shows the final flight configuration of the insulated and shielded high voltage components in the Transmitter/Modulator.

TABLE 2.1.7.8

KP II SYSTEM CONFIGURATION AFTER INSULATING FOR SPACE VEHICLE OPERATION

Box #	Component or Circuit	Peak Operating Temp.	Potting Material	Interconnection Method	Interconnection Termination Potting	Remarks
	Transformer Rectifier Modules	160°F	Scotchcast 281	Polyolifin HV cable	Scotchcast XR 5073	
2	HV Filter	160°F	Scotchcast 281	Shielded Polyolifin HV cable	Epocast 202/9615	Braid impregnated with Epocast 202/9615
	HV Capacitor	160°F	Potted in epoxy resin by supplier	Polyolifin HV cable	Scotchcast XR 5073	
	HV Cable (Burndy Termination	160°F				
		160°F	Scotchcast XR 5073			
	Thyratron	400°F	Sylgard 183			
	Pulse Form. Network	110°F		Braid shielded silicone HV cable	Amp Connector with HV shielded cable bonded in place with Hysol 211	
3	Pulse Transformers	180°F	Oil filled	Braid impregnated and coated with Hysol 211		Output of pulse transformer potted to Klystron base with DC RTV 501
	Charging Choke	110°F				

TABLE 2.1.7.8 (Continued)

Box #	Component or Circuit	Peak Operating Temp.	Potting Material	Interconnection Method	Interconnection Termination Potting	Remarks
	Plate Choke	110°F	Hysol 211	Braid shielded silicone HV cable	Amp Connector with HV shielded cable bonded in place with Hysol 211	Output of pulse transformer potted to Klystron base with DC RTV 501
	Inverse Resistors	270°F		Braid impregnated and coated with Hysol 211		
3	Inverse Diode	110°F	Molded in epoxy and then potted in Scotchcast 281/251			
	Changing Diode	110°F				
	Klystron	250°F	Potted by supplier in silicone rubber	Silicone HV cable	RTV 501 (Base)	
	Avalanche Circuit	110°F	Hysol 211	Teflon hookup wire	Hysol 211	
	Grid Choke	110°F				
	Power Supply	140°F	Sylgard 182	Silicone HV cable	Amp connector with HV cable potted with Hysol 211	

TABLE 2.1.7.8 (Continued)

Box #	Component or Circuit	Peak Operating Temp.	Potting Material	Interconnection Method	Interconnection Termination Potting	Remarks
	High Volt. Divider	140°F	Hysol 211	Silicone HV cable	Amp connector with HV cable potted with Hysol 211	
4	TWT	180°F		Silicone HV cable		
	Prog.Multiplier	140°F	Polyurothane foam		Teflon hookup wire	
5	All	160°F	Scotchcast XR 5072 on 300 V Ckt. & Humiseal 1B12 on low voltage circuits	Teflon hookup wire		
6	All					
	HV Supply	240°F	Filled epoxy formulated by AC	Silicone HV cable	Amp connector with HV cable potted with Hysol 211	
7	CRT	140°F.	Potted by supplier in silicone		Hysol 211	

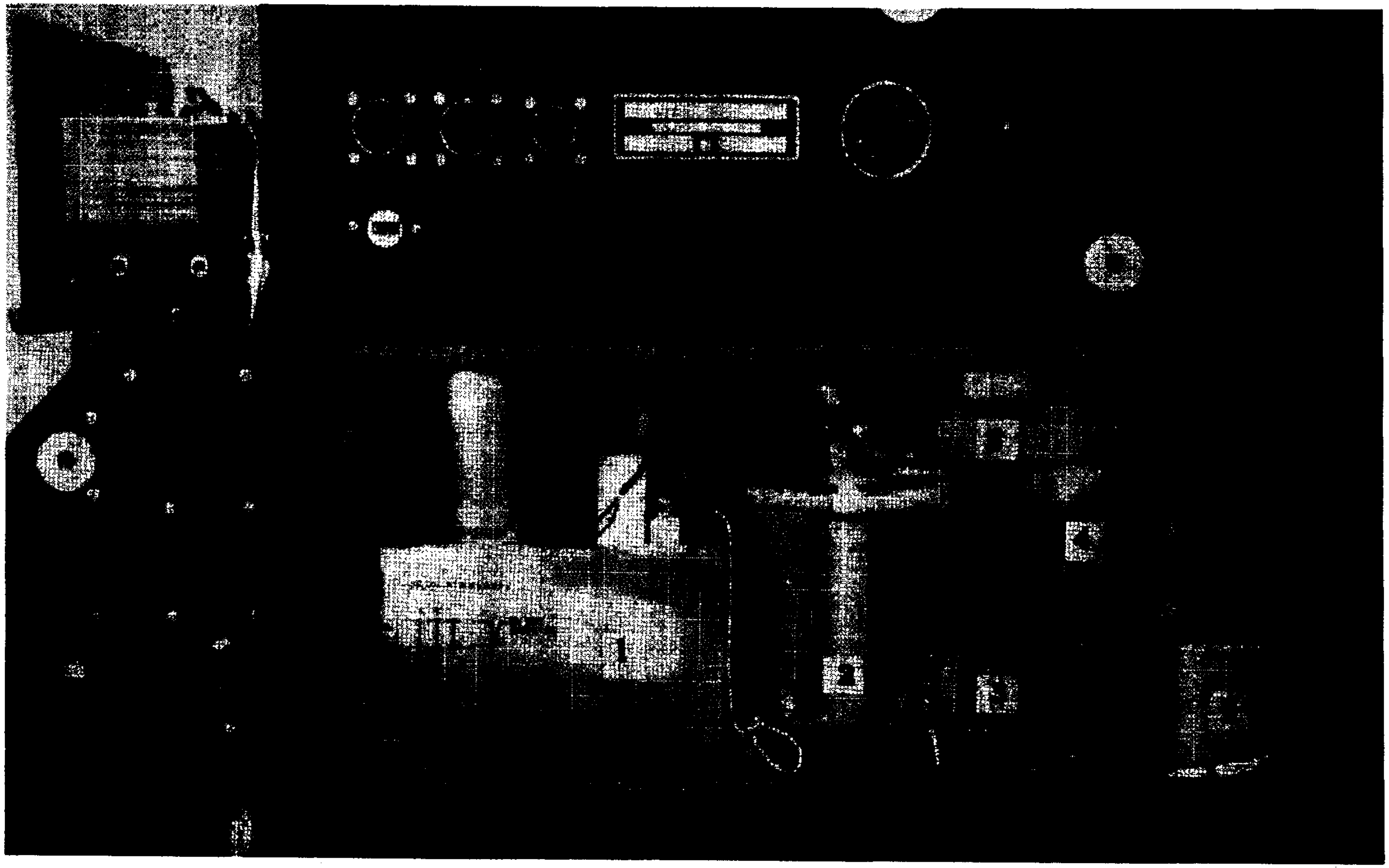

(1) Pulse Transformer
(2) Thyratron.
(3) Diode
(4) Pulse Forming Network
(5) Plate Choke
(6) Inverse Resistors

View of High Voltage Components in Transmitter-Modulator

Figure 2.1.7.4 (Box 3) Showing Final Insulated and Shielded Configuration.

2.1.8 Vacuum Measurements

2.1.8.1 High Voltage Breakdown

As illustrated in Figure 2.1.8.1, the Paschen Curve - Air, a voltage breakdown or arc-producing condition exists when there is a potential of 350 volts or greater across a .10 centimeter gap and in a pressure environment between 10^{-3} and 10 millimeters of mercury. For a 1 centimeter gap the condition exists in a factor of ten higher pressure environment. Since the payload system on 2355 uses voltages around the 4400 volt level, which is much greater than the minimum mentioned the probability of a breakdown occurring is very high if the pressure range as shown on the curve is transgressed. This pressure range is experienced normally during the ascent phase of the vehicle where a pressure of 10^{-3} mm Hg is attained at approximately 300,000 feet altitude. Most components are not pressure sealed and therefore will vent at a rate slightly less than the vehicle itself. If the box has vents it will follow the vehicle vent rate. A pressure rise in a component can be caused by outgassing as discussed in the following paragraph.

2.1.8.2 Outgassing

Outgassing is a well known phenomena and is a function of pressure, temperature, and chemical composition of the material in question. All material under the proper conditions of pressure and temperature can be caused to vaporize with a resultant rise in local pressure. If the outgassing rate of the material in a component is greater than the venting rate of the box, the box pressure will rise. This pressure may rise to a level greater than 10^{-3} mm Hg which is the area discussed above. A complete treatise on the

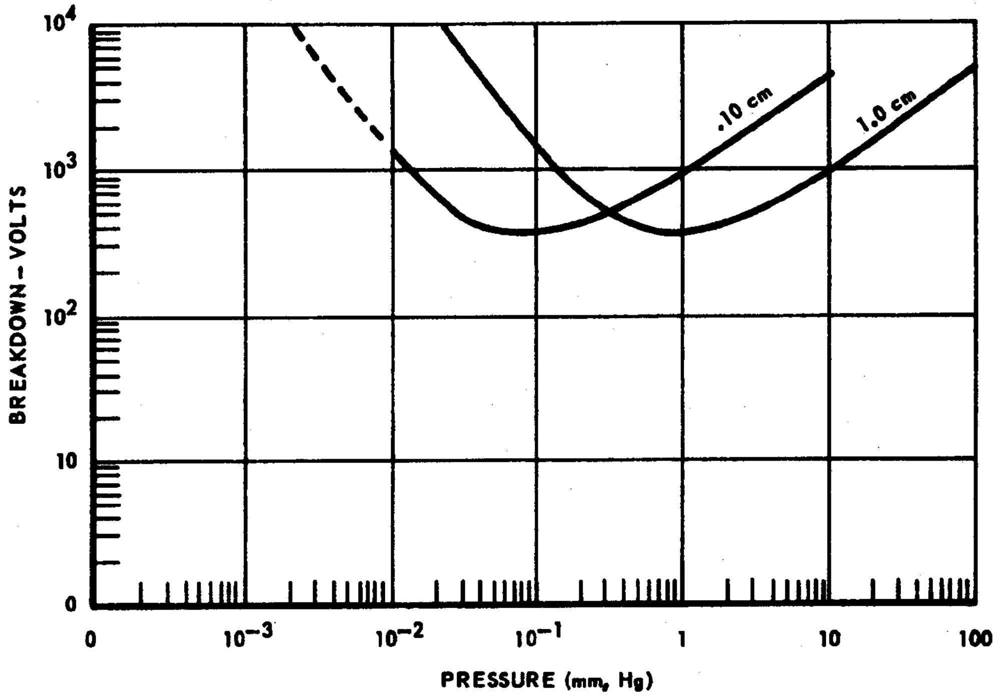

Figure 2.1.8.1 Paschen Curve - Air

subject of outgassing can be found in "Scientific Foundations of Vacuum Techniques" by Dushman and Lofferty, as published in 1962 by John Wiley and Sons, Inc.

2.1.8.3 Vacuum Measuring Requirement

A Program directive entitled "Requirement for Orbit Pressure Measurements" was issued on 8 October 1963. The directive discussed the problems in voltage breakdown due to voltage versus pressure relations and requested that two classes of experiments be conducted. First was to be the measuring of internal rack pressure and internal typical box pressure on an early vehicle. Second was to be a correlation of this data with data obtained by measuring internal box pressure in controlled laboratory conditions at simulated altitudes. Proceeding with this direction, research into vacuum gages was started. After selecting an ion gage, built by Lockheed's Physical Science Lab, arrangements were made to build not only the ion gages but an experimental black box to be entitled a "typical box". The gages and black box were to be installed on [redacted] Due to schedule impact and cost, the complete endeavor was stopped and redirection was given by the Program Office. The new requirement was to provide a minimum of five gages to measure selected box pressures and internal rack pressures in the barrel and conical sections of Vehicle 2355 and up. This still met the requirement for flight and ground test data correlation as the qualification payload vehicle system (with gages installed) would be tested under laboratory conditions in the Temperature and Altitude Simulation chamber. All subsequent work was performed under these requirements.

2.1.8.4 Types of Gages Researched

Under the original requirements two types of ion gages were considered. One, designated the Model 1-B was a Lockheed Physical Science Lab design that covered the range of 10^{-2} to 10^{-4} mm Hg. Power required for this unit is 5.23 watts at 28.3 VDC ± 1 percent. Output of the gage was 0 - 5 volts. The size and weight of this transducer is relatively small, 1.96" dia. X 6.38" long and approximately 1.5 pounds. The second vacuum gage was the Model O-44 designed and built by Alto Scientific Co., Inc. of Palo Alto. This unit utilized a cold cathode Phillips ionization gage tube and therefore could cover the range of 10^{-2} to 10^{-7} mm Hg. The undesirable factor of this gage was that the high voltage was required by the Phillips gage tube. This requirement dictated using a bulky step up transformer in the electronics of the gage which made the size and weight of the assembly comparitively large. The gage was 7.94" long X 5.25" wide X 2.47" high and weighed 4 pounds. The main power input was 115 volt 2 KC with 28.3 VDC ± 1 percent monitor power and 28 VDC unreg. ON-OFF switch power required. The monitor output is 0 - 5 volts over a range from atmospheric to 10^{-7} mm Hg. After redirection was given as discussed above, the requirement to fly five gages made the weight, size, power, and cost of the first two gages prohibitive. From information supplied to Engineering by the Program Office a different type of gage was investigated. This was a Pirani or thermocouple vacuum gage. Although this gage is only good down to 10^{-3} mm Hg it is a very small, light weight unit and very low priced. Two companies, the NRC Equipment Corp. of Newton, Mass., and Hastings-Raydist Inc. of Hampton, Virginia, were contacted and all parameters of the equipment were discussed with their representatives. A decision to buy the Hastings-Raydist units were made and the vacuum measurement system was evolved about these gages as discussed in the following paragraphs.

2.1.8.5 Type of Gage Used

The gage tube, Hastings-Raydist Model DV-6MX (Fig. 2.1.8.2) is a thermopile device that measures the rise in temperature in a constant current heater due to the decrease in the density of the environment in the tube as it is exposed to a decreasing pressure from atmospheric to one micron of mercury (10^{-3} mm Hg). The tube is a ruggedized device able to withstand high shock and vibration levels. It was modified by the vendor to remove an octal tube base and add a four foot cable for electrical connections. The tube less the cable weighed approximately 2.5 ounces. The power to the tube is supplied by the Hastings-Raydist SA-3AE "Sub-Miniature Power Converter" which is a DC to AC converter and current regulating device. It also acts as the controlling unit for the two in combination. The output of the power supply gage tube combination is 0 - 10 millivolts with an output impedance of 18 ohms. A superimposed 1.5 KC signal with an amplitude of 1 to 50 millivolts is on the DC output. The output stability is ± 2 percent over a range of -55° to $+60^{\circ}$C. The power drain is approximately 1 watt at 28 VDC ± 1 percent. The SA-3AE weighed approximately 7 ounces. Each gage tube was matched with a power supply and calibrated by the vendor. A calibration curve was furnished with each matched pair. As mentioned, the DC output of the gage has a 1.5 KC signal superimposed on it. The first units were designed without a filter for this

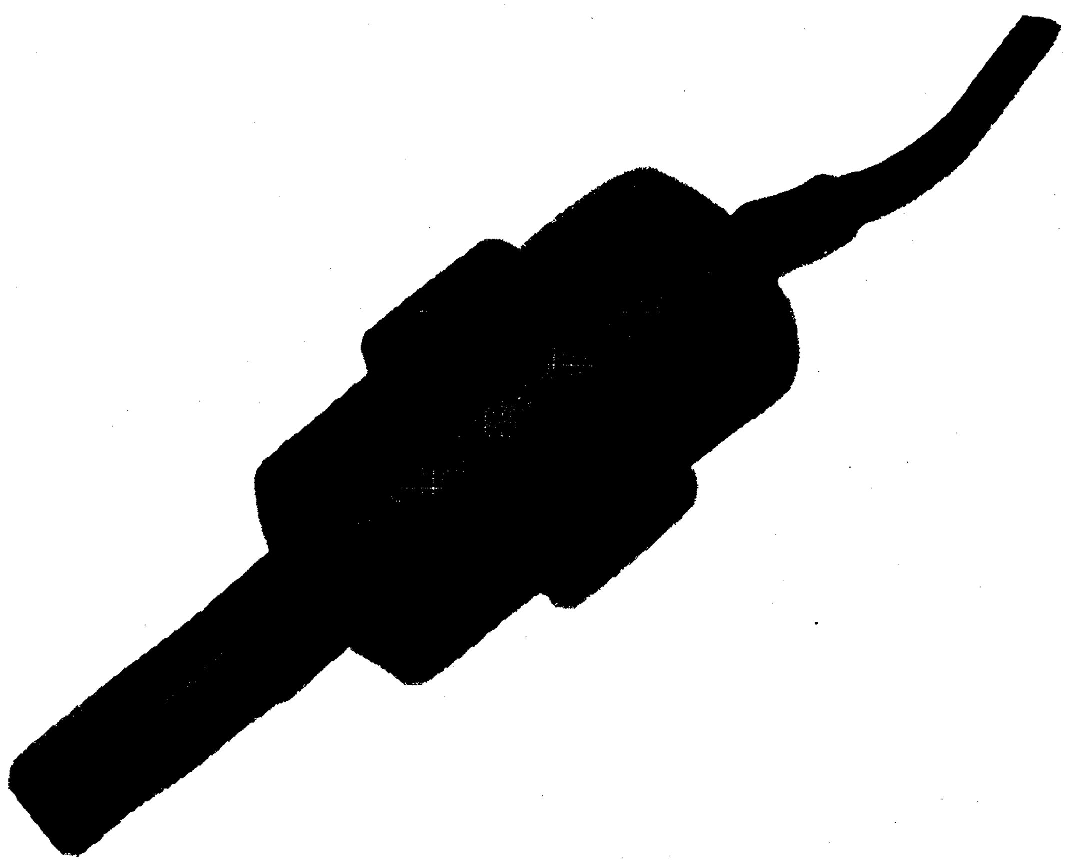

Figure 2.1.8.2 Gauge Tube

noise as it was felt the differential DC amplifier, Lockheed 1461944-1, used to amplify the 0 - 10 millivolt output of the gage to 0 - 5 volts, would filter this out as it has a common mode rejection of greater than 80 db at 1 KC. Preliminary testing revealed this not to be true. A two stage low pass filter was designed, tested, and added between the PS-gage output and the amplifier. This reduced the output noise level from 2 volts down to 10 millivolts on the 5 volt TLM scale which is a very acceptable noise level. The DC amplifier per Lockheed Specification 1414703 has a gain of 50 to 500, continuously adjustable. The PS-gage tube output of 0 - 10 millivolts dictates using the maximum gain setting of 500 to obtain a 0 - 5 volt output acceptable to the TLM. The signal input impedance of the unit is 75 K ohms and relative to the 18 ohm output of the power converter this appears as an infinite load which is the ideal condition. The amplifier will operate on 28 VDC $\pm$ 1 percent and requires 30 milliamperes of current maximum. The part weighs approximately 6 ounces.

2.1.8.6 Gage Assembly Design

The design of the bracket to hold the power supply and amplifier was a simple problem since the parts were small and lightweight. The original assembly did not include the 2 stage low pass filters as this was added after preliminary testing. Three connectors are on the front of the assembly and are used as follows: J1 is the power input and signal output of the PS-gage tube combinations; J2 is the power input and signal input and output of the amplifier; J3 is for the disconnect plug of the gage tube. The addition of the low pass filter was done very simply by utilizing the three screws that held the power supply in place. The final configuration is as shown in Fig. 2.1.8.3

2.1.8.7 Gage Location

The locations of the five gage tubes were selected to meet the requirements criteria. Therefore two of the gages were mounted such that they sampled the interior of the payload barrel section. One of these, designated F100, was located at the +Y axis on the aft ring. The other, F101, was at the -Y axis on the same ring. F102 and F103 was mounted so as to sample the interior of payload boxes numbered 7 and 3, respectively. The fifth gage, F104, was used to monitor the pressure of a section of equipment between payload boxes 3 and 4. The power supply amplifier assemblies were located such that the four foot cable on the gage tube was sufficient to reach them with proper routing and retaining.

2.1.8.8 Preliminary Test Results

Since the gage assemblies are not tested until they are installed on the vehicle it is necessary to set up the gage-amplifier relation. This was accomplished using the vehicle TLM simulator and reading out the individual monitors while adjusting the amplifiers to maximum gain to attain the 5 volt output which is relative to 10^{-3} mm Hg. The 10^{-3} mm Hg level was accomplished by substituting a Hastings-Raydist vacuum gage reference tube number DB-20 in place of the DV-6MX gage tube. This tube is an evacuated tube device (pressure level is marked on the tube) that simulates the DV-6M gage tube. The first test in the TAS chamber showed the gages followed the chamber pressure down through the 10^{-3} mm Hg range. The test also revealed the noise as mentioned in Par.2.1.8.5 was a problem. The filter was

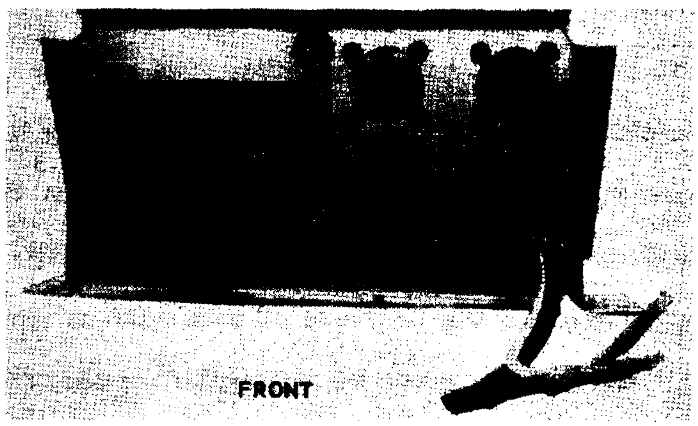

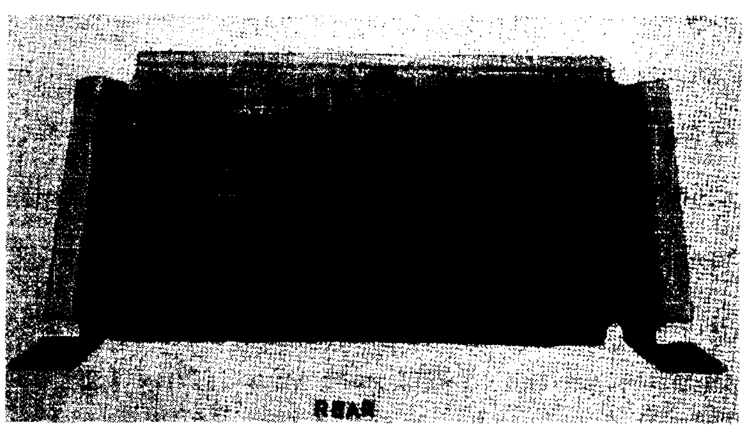

Figure 2.1.8.3 Power Supply - Amplifier Assembly

subsequently designed and installed after this test.

2.1.8.9 Ground Test

During the TASC test of the qualification vehicle no abnormalities were detected. All monitors followed the predicted vent rates or followed the chamber pressure down through the limits of the gages. Chamber testing of transmitter modulator configurations (in the flight vehicle structure) which resulted in breakdowns, caused pressure increases to register on the pressure gages. These pressure rises lasted approximately 15 seconds in the majority of instances, indicating a release of gaseous or volatile substances.

2.2 Radar Payload

Introduction The radar payload furnished by the Goodyear Aerospace Corporation consisted of five components:

Transmitter-Modulator

R.F.-I.F. Unit

Reference Computer

Control Unit

Recorder

This section of the report discusses the radar payload to a limited degree, to permit general understanding of the fundamentals of doppler side looking radar by the reader. As indicated elsewhere in this report, Goodyear maintained full responsibility for the radar when not installed in the system. Accordingly, the complete engineering details of the radar are to be found in the Goodyear report, entitled Program Report, KP-II Orbital Doppler Radar, Thor/Agena Satellite Program, Control Number AKP-II-596, dated 1 March 1965. The contents of this section are generally excerpts from that report, included in the interests of completeness of the system report, and the permission for the use of this materials is gratefully acknowledged. The reader is referred to the above Goodyear Aerospace Corporation report for further information pertaining to the radar payload utilized in this mission.

2.2.1 Basic Doppler Theory

General Concept The beam-sharpening process used in a doppler, high resolution, side-looking radar may be described by means of a physical antenna analog. As the vehicle travels its orbital path a series of pulses is transmitted. Successive pulse transmissions are identified with the elements of an array of dipoles. The spacing between elements is the distance traveled by the vehicle between pulses. Each transmission is made with a controlled phase. The amplitude and phase of the reflected energy from the terrain at all ranges and angles within the physical beam width of the antenna is recorded on the data film.

The length of the antenna synthetically generated is basically limited to the distance instantaneously illuminated on the ground by the physical antenna. By the technique of optical processing, the amplitude and phase of the returns from the successive pulses are vectorially added to create the narrow synthetic beam. The results of these data are then recorded on a final film. Thus, the resolution equivalent to that of an antenna hundreds of feet in length is achieved with a small physical antenna.

Basic Equations The basic equations of a high-resolution radar are most easily developed if the analysis is restricted to the slant-range plane of a single-point target. Figure 2.2.1.1 shows the geometry involved. R is the distance to the target from the antenna at time t. At time $t = 0$, R_1 is the distance to the target. The angle θ_o is measured in the slant-range plane to the center of

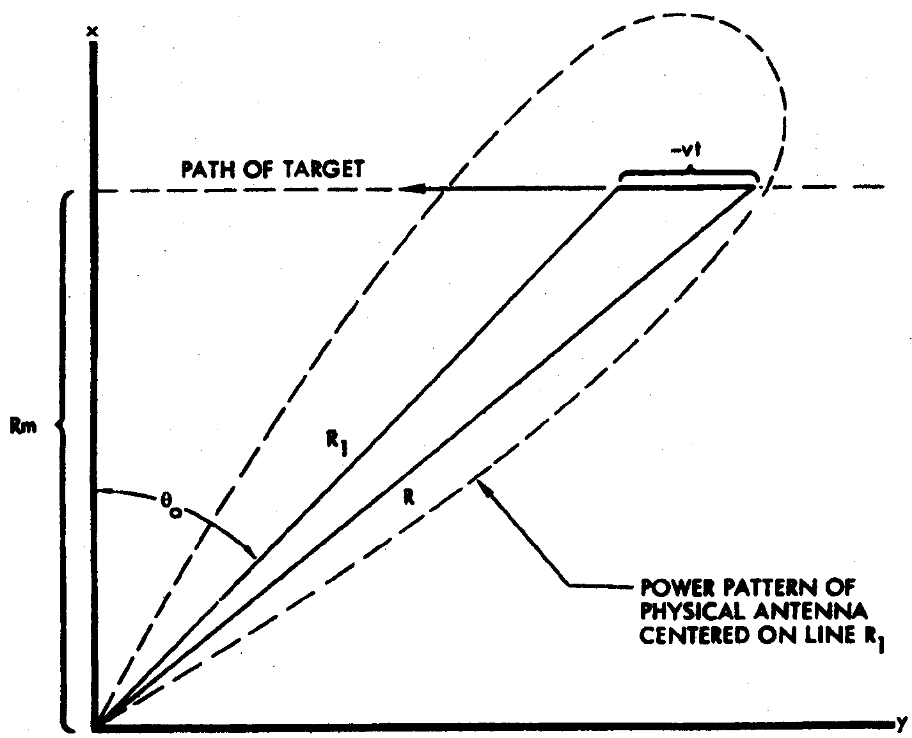

FIGURE 2.2.1.1 - Geometry of a Point Target in the Slant Range Plane

the antenna beam at slant range R_1. Several combinations of pitch and yaw will yield the same angle θ_o. From the geometry of Figure 2.2.1.1 the instantaneous range R to the target is

$$R = \left| R_1^2 + (vt)^2 - 2R_1 vt \sin \theta_o \right|^{1/2} . \quad (1)$$

As the beam width of the physical antenna is small, the range during the period when the target is illuminated may be closely approximated by taking the first few terms of the binomial expansion of Equation (1):

$$R \approx R_1 \left(1 - \frac{vt \sin \theta_o}{R_1} + 1/2 \frac{(vt)^2}{R_1^2} \cos^2 \theta_o \right) . \quad (2)$$

The range dependence on time is reflected in a phase dependence on time of the return signal. The dependence of phase 0 of the return signal on time is

$$\phi = 2\pi f_o t - \frac{4\pi R}{\lambda} + \phi_o \quad (3)$$

where

f_o = the transmitted frequency

λ = the wave length of the carrier

ϕ_o = the phase change caused by reflection.

Equations (2) and (3) may be developed into

$$\phi = 2\pi f_o t + \frac{4\pi}{\lambda} vt \sin \phi_o - \frac{2\pi (vt)^2}{R_1 \lambda} \cos^2 \phi_o + \phi_1 \quad (4)$$

where

$$\phi_1 = \phi_o - \frac{4\pi R_1}{\lambda} \quad .$$

The return signal is synchronously demodulated with respect to some reference frequency to remove the carrier. It is desirable for the reference frequency to be the frequency of the return signal when the target is at the center of the beam. The phase of the return signal when the target is at the center of the beam and at range R_1 is given by

$$\gamma = 2\pi f_o t - \frac{4\pi R_1}{\lambda} + \phi_o \quad . \tag{5}$$

The frequency will be

$$f_r = \frac{1}{2\pi}\frac{d\gamma}{dt} = \frac{1}{2\pi}\left(2\pi f_o - \frac{4\pi}{\lambda}\frac{dR_1}{dt}\right) \quad . \tag{6}$$

From Figure 2.2.1.1, however,

$$\frac{dR_1}{dt} \equiv \left.\frac{dR}{dt}\right|_{t = 0} \quad . \tag{7}$$

Therefore, from Equation (2)

$$\frac{dR_1}{dt} = -v \sin \theta_o \quad . \tag{8}$$

Then, substituting into Equation (6),

$$f_r = f_o + \frac{2v}{\lambda} \sin \theta_o \quad . \tag{9}$$

Therefore, f_r is the frequency that will be used for synchronous demodulation. The synchronous demodulated signal will have the form

$$S(t) = A(t)\mathrm{Re}\left[e^{-j2\pi f_r t}(e^{j\phi})\right] \tag{10}$$

$$= A(t)\cos\left(\frac{2\pi(vt)^2 \cos^2 \phi_o}{R_1 \lambda} - \phi_1\right) \tag{11}$$

where $A(t)$ denotes the amplitude of the return which is a function of the reflectivity of the target and its position in the antenna beam. When

$$\phi_1 = n(2\pi)$$

$$0_o = 0$$

and

$$A(t) = K$$

Equation (12) reduces to the familiar expression

$$S(t) = K \cos\left(\frac{2\pi(vt)^2}{\lambda R_m}\right) . \tag{12}$$

The signal recorded on film at range R_m will be of the form

$$S(x, R_m) = T_b + K' \cos\left(\frac{2\pi x^2}{\lambda R_m}\right) \tag{13}$$

where

T_b = the transmissivity of the film

K' = some constant times K.

From Equation (9) it is seen that all scatterers at an angle θ_o and with velocity v will have the same frequency. It follows that the locus of all possible scatterers whose returns have the same frequency is one nappe of a right circular cone with semi-apex co-angle θ_o whose axis contains the velocity vector.

The locus of points on the earth can be visualized if the intersection of the above doppler cone with a plane tangent to the earth at midmapping range is considered. Since the range interval mapped is small, the mathematical model so described is a good approximation near the point of tangency.

Ambiguities   Two types of ambiguities - range and azimuth - are inherent in a coherent high-resolution radar and provisions must be made to avoid them. The range-ambiguity problem is common to all pulsed radar and is usually avoided by lowering the prf so that the so-called "second-time-around" targets are not seen by the radar. However, the consideration of azimuth ambiguities yields another set of constraints on the choice of prf.

For a processor operating about zero doppler the information spaced at $\pm \Upsilon_n$ from zero doppler is ambiguous. This angular spacing is given by

$$\gamma_n = \frac{n\lambda F}{2v} \qquad (14)$$

where

n = a positive integer, 1, 2, 3, . . .

λ = carrier wave length

F = prf

v = radar velocity.

The focused processor used with this system operates about an offset of prf/4 and is unable to distinguish between positive- and negative-going frequencies so that the ambiguity spacing is given by

$$\gamma_n = \frac{n\lambda F}{4v} \qquad (15)$$

For most high performance radars it is desirable to choose a prf such that the first azimuth ambiguity is placed in the vicinity of the first null of the physical antenna azimuth pattern. This choice of prf places an upper bound on the size of the mapped interval. This constraint in turn dictates the antenna height, since from the range-ambiguity standpoint the vertical antenna pattern is employed to avoid range ambiguities. It is readily deduced that ambiguity constraints are a determining factor in choosing antenna dimensions for a satellite radar. These considerations will be discussed further in Para. 2.2.3.

2.2.2 Data Processors

The most successful type of high-resolution processor thus far is the optical correlator.* Considerable insight into the optical processor is possible if the properties of a sine wave diffraction grating are considered. Figure 2.2.2.1 shows the three principal emergent rays from a sine-wave diffraction grating resulting from an incident plane wave of coherent light. The angle θ is defined thus:

$$\sin \theta = \lambda' f \tag{16}$$

where

λ' = the wave length of the coherent light

f = the spatial frequency of the sine-wave diffraction grating.

Now consider a diffraction grating of the form $\cos\,(2\pi x^2/\,\lambda' R_m)$. This is of the same form as the demodulated return signal from a point target (Equation (13). Assuming a one-to-one scale factor in recording the demodulated return, the spatial frequency is $2x/\ 'R_m$. From Figure 2.2.2.2 the distance r to the crossing of the zero axis is given by

$$r = \frac{x}{\tan \theta}\ . \tag{17}$$

For small angles

$$\tan \theta = \sin \theta = \theta\ . \tag{18}$$

Then,

$$r = \frac{x}{\lambda' f} = \frac{x\lambda' R_m}{\lambda' 2x} = \frac{R_m}{2} \tag{19}$$

*These devices are commonly known as correlators because the original conception, [redacted] was an optical cross-correlator.

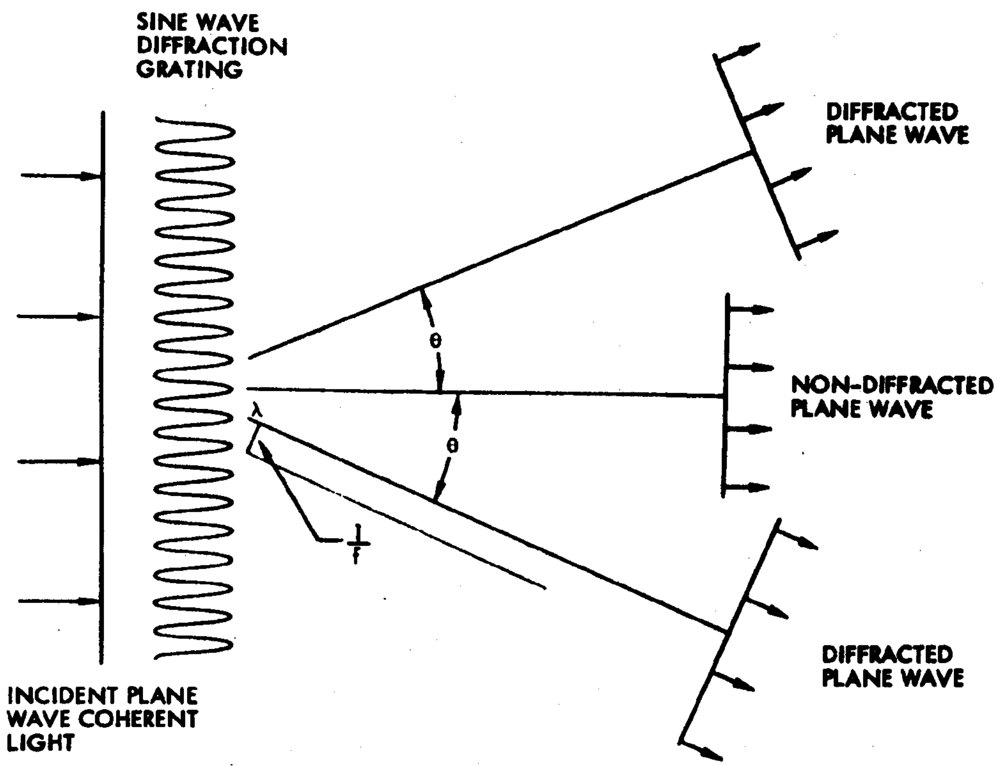

FIGURE 2.2.2.1 - Geometry Illustrating Fraunhofer Diffraction

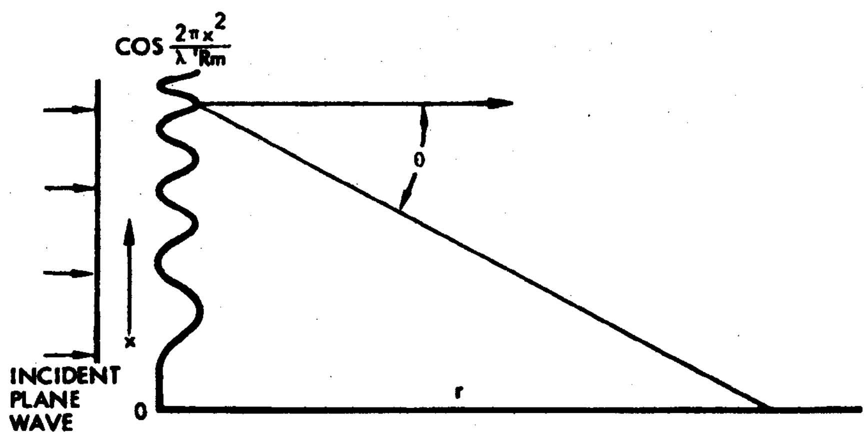

Figure 2.2.2.2 - Diffraction from $\frac{\cos 2\pi x^2}{\lambda' R_m}$ Grating

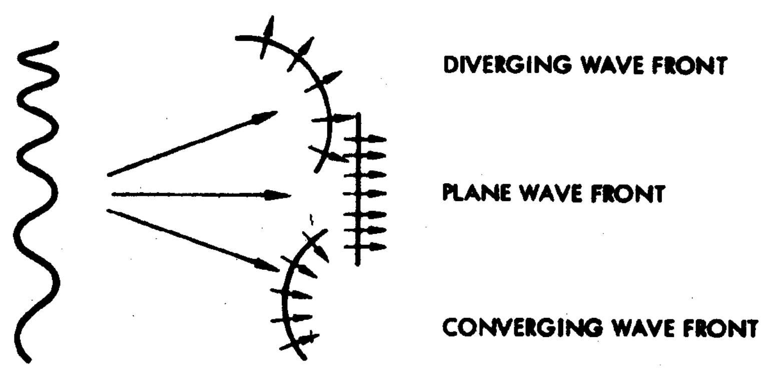

Figure 2.2.2.3 - Three Wave Fronts of a Parabolic Phase History

which is to say that the diffracted light focuses on the zero (doppler) axis at a distance $R_m/2$ from the grating (data film).

From Figure 2.2.2.1 it is recalled that there are three principal emergent waves. For the cosine x^2 grating the three waves are defined thus (see Figure 2.2.2.3):

- o Converging wave front focused at a distance r on the axis
- o Diverging wave front with a virtual image at a distance -r on the axis
- o Plane wave front focused at infinity.

The converging wave front focuses at that angle and at that distance away from the recorded phase history which corresponds to the same angle and the scaled-down distance (proportional to the ratio of light-to-radar wave lengths and aircraft motion-to-film-scale factors) of the radar space where the data were recorded. Unfortunately, in a practical case the ratio is not nearly high enough and a converging lens must be used to bring the desired spot into focus at a convenient distance. Of course the other two wave fronts also come to a focus then but since they lie at different angles they can be blocked off from the final film with an appropriate optical stop. However, from Equation (19), the focal distance is a function of range; therefore, the lens must have a converging power which varies with range, giving rise to a conical shape. A cylindrical lens is also required to maintain target separation in range.

Thus, the basic elements of an optical processor are a coherent light source, optics to focus range and azimuth data onto a single plane, and film drives for transporting both the data and image films.

The optical processor for this system is being provided by the [redacted]

2.2.3 System Analysis

Antenna Length Relationships Equation (9) demonstrated that the basic equation for the doppler frequency of a scatterer is

$$f_d = \frac{2V_r}{\lambda} \sin\theta \qquad (20)$$

where

V_r = relative velocity

λ = radar wave length

θ = angle to scatterer measured from the perpendicular to the relative velocity vector.

Using Equation (20) with Equation (15) and the small angle approximation, the first ambiguous frequency is seen to be F/2. To avoid illumination of this frequency it should be placed at or beyond the first null of the physical antenna pattern. Using this criterion,

$$\frac{F}{2} = \frac{2V_r}{\lambda} \sin \frac{K_a\lambda}{D} \qquad (21)$$

or

$$F \approx \frac{4V_r K_a}{D} \tag{22}$$

where

K_a = constant greater than unity

D = length of physical antenna.

The value of K_a varies depending on the type of antenna illumination used in the horizontal plane and the degree of suppression of azimuth ambiguity that is desired.

The basic equation for conditions of range ambiguity is

$$F = \frac{C}{2\Delta R_s \max} \tag{23}$$

where ΔR_s max - maximum unambiguous slant range interval. Equation (23) assumes a vetical antenna pattern which has a square-shaped beam illuminating only the desired slant range interval. To account for the actual vertical beam shape, Equation (23) may be rewritten as

$$F = \frac{C}{2K_r \Delta R_s} \tag{24}$$

where

K_r = constant greater than unity

ΔR_s = slant range interval mapped.

The value of K_a varies depending on the type of antenna illumination used in the vertical plane and the degree of suppression of range ambiguity which is desired. By using Equations (22) and (24) and solving for ΔR_s, the following relationship is obtained:

$$\Delta R_s = \frac{CD}{8K_a K_r V_r} \quad . \tag{25}$$

This equation shows that the slant range interval which can be mapped is directly proportional to the length of the physical antenna. It is also seen that increasing K_a or K_r to reduce ambiguity levels will reduct the interval mapped.

Because of the physical limitations imposed by the vehicle, the length of the antenna was chosen to be 15 feet. To have as narrow a beam as possible, uniform illumination was chosen for the horizontal plane.

Antenna Height Relationship In this system the vertical pattern of the antenna is used to control the level of the range ambiguities. The geometry of the problem is shown in Figure 2.2.3.1. In this figure, the distance C/2F is the slant range interval between points of ambiguity such as A, A', and B, B'. The angle α is the angle between the ambiguous returns. The slant range to point A is R_1 and to A' is R_2. The slant range to point B' is R_{mid} and is measured along the bore sight of the antenna. The problem is to illuminate as much of the slant range interval from A to A' as possible while maintaining the level of range ambiguity to a reasonable value. The final choice of antenna height must also be within the physical limitations imposed by the vehicle.

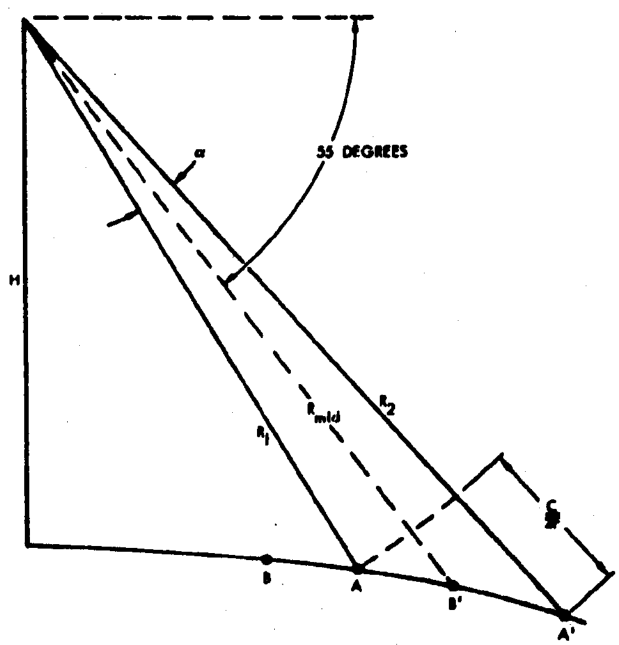

Figure 2.2.3.1 - Range Ambiguity Geometry

A typical two-way power pattern is shown in Figure 2.2.3.2. The dotted lines indicate the useful portion of the beam. This portion was selected to be the 6-db width since this choice leads to a realistic sensitivity time control requirement. There are two types of range ambiguities which can be encountered. The first occurs when targets illuminated by the sides of the main beam are ambiguous with respect to targets in the useful portion of the beam. This type can be referred to as main lobe ambiguity and is illustrated by points C, C' of Figure 2.2.3.2. The second type occurs when targets illuminated by side lobes are ambiguous with respect to targets in the useful portion of the beam. This type, referred to as side lobe ambiguity, is illustrated by points D, D' of Figure 2.2.3.2.

For a given prf or for a given ambiguity angle α , a fixed set of points on the pattern becomes ambiguous with points in the useful portion of the beam. To illustrate graphically an ambiguity situation, the pattern of ambiguous points can be shifted by the angle α or multiples of α so that the ambiguity points are placed directly beneath the useful portion of the beam. This technique is shown in Figure 2.2.3.3. In this figure only the ambiguity caused by the first right-hand side lobe is shown for clarity of illustration. By varying the amount of shift, different amounts of ambiguities are introduced. In the case shown no ambiguity is being caused by the sides of the main lobe.

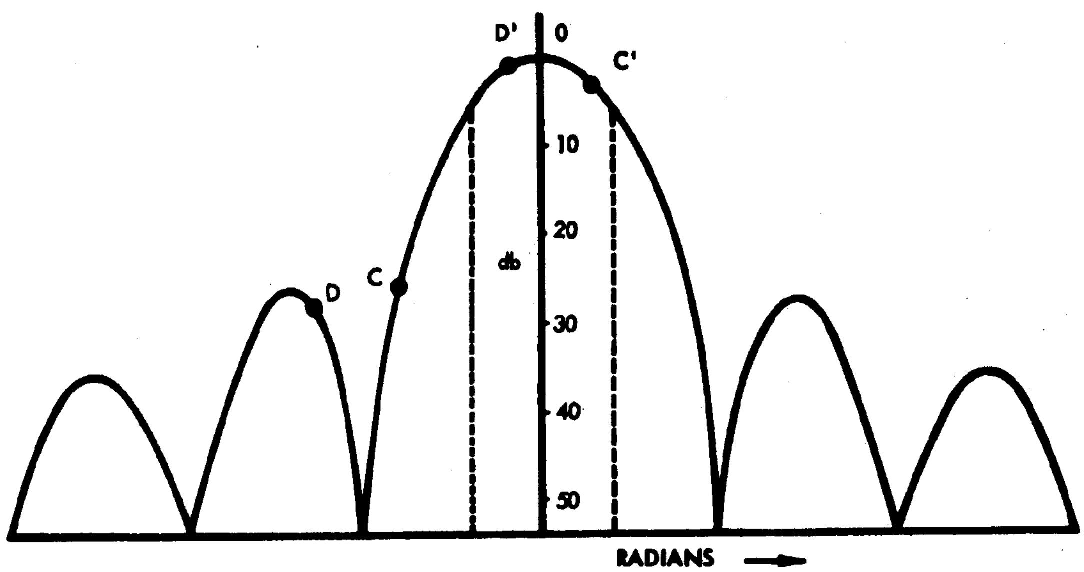

Figure 2.2.3.2 - Typical Two-Way Power Pattern

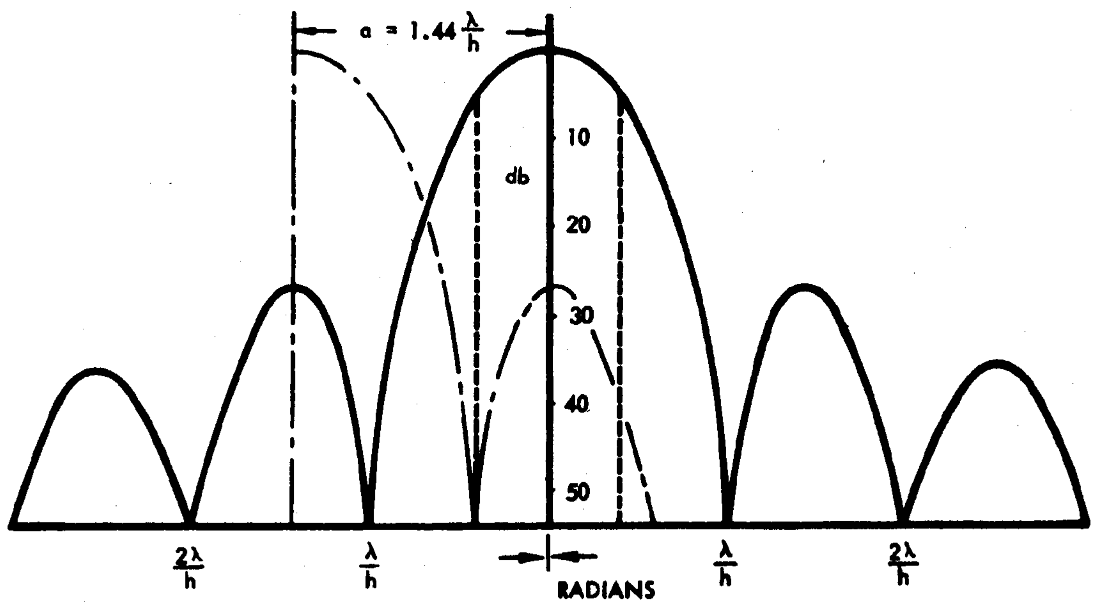

Figure 2.2.3.3 - Two-Way Power Pattern for Uniform Illumination and $\alpha = 1.44\lambda/h$

In the course of the original investigation, a number of types of antenna illuminations were considered and various spacings evaluated. The results of this study showed that by choosing the angle α so that main-lobe ambiguity was minimal, the largest portion of the slant range interval could be mapped consistent with low ambiguity levels. Increasing the ambiguity angle did not rapidly reduce the ambiguity level but did reduce the amount mapped. The results of this study are shown in Table I.

TABLE I

SUMMARY OF AMBIGUITY SPACING REQUIREMENTS

Type of Illumination	Ambiguity spacing	Level of First Side Lobe (Two-way) (db)	Precentage of maximum Interval Mapped
Uniform	$\frac{1.44\,\lambda}{h}$	26.4	0.61
Cosine	$\frac{2.10\,\lambda}{h}$	46.0	0.57
Cosine^2	$\frac{2.72\,\lambda}{h}$	64.0	0.53

Referring to Figure 2.2.3.1, the value of α was calculated to be 0.0801 radian for the nominal altitude of 130 nautical miles, a prf of 8500 cps, and a depression angle of 55 degrees. This value of prf was based upon azimuth ambiguity studies. Using this value of α and the ambiguity spacing relationships shown above, the required antenna heights for the various types of illuminations were found to be:

Uniform	1.8 feet
Cosine	2.7 feet
Cosine^2	3.5 feet

Because of physical limitations of the vehicle, the uniform illumination type was chosen with a heightof 1.8 feet. This choice also allowed mapping of the largest portion of the slant range interval.

Clutterlock Loop Analysis

<u>General Requirements of Clutterlock Loop</u> The clutterlock loop is designed to orient the narrow synthetic array, generated by the coherent radar, along the axis of the physical antenna. It is generally assumed that the exact bore sight of the physical antenna with respect to the velocity vector is unknown and furthermore is changing at some limited maximum rate. The clutterlock must ascertain the antenna bore sight and cause the system to align its own synthetic pattern. Secondly, the clutterlock must follow the physical antenna with a small enough hang-off error to avoid ambiguities in the data and yet move slowly enough to avoid the destruction of coherent buildup in process at the recorder. A moment's reflection will show that complete compliance with these requirements is an impossibility, particularly if the rate of angular rotation of the physical bore sight is large.

Conceptually, the clutterlock operates by measuring the positive- or negative-going phase shift of the targets within the beam on successive returns. This process, of necessity, depends on the statistical nature of the return signals. Error may occur because of a predominance of targets in one side of the physical beam or because of very large targets not symmetrically located. These sources of error are largely eliminated if the time constant of the loop is long compared to the transit time of a single target across the beam. Further help is available in reducing the effect of very large targets by allowing the video used in the clutterlock to be limiting a substantial portion of the time, say 50 percent.

2.2.4 Radar System Block Diagram

Simplified Block Diagram of KP-II Radar System Figure 2.2.4.1 shows a much simplified diagram of the radar system. Block 1 provides the various timing pulses while block 12 generates the required frequencies. During the transmit mode the signal flow is via blocks 1 through 10 inclusive. The modulator trigger pulse triggers the 0.06-microsecond pulser of block 2 and the modulator of block 11. The output of the 0.06-microsecond pulser is filtered and imposed on a 70-mc carrier producing the 70-mc sine x/x pulse. The switches of blocks 4 and 6 are controlled by the On-Gate (present in the transmit mode) so that the sine x/x pulse if passed down the i-f chirp line to the mixer of block 7. Block 7 converts the signal to f_o, at which frequency

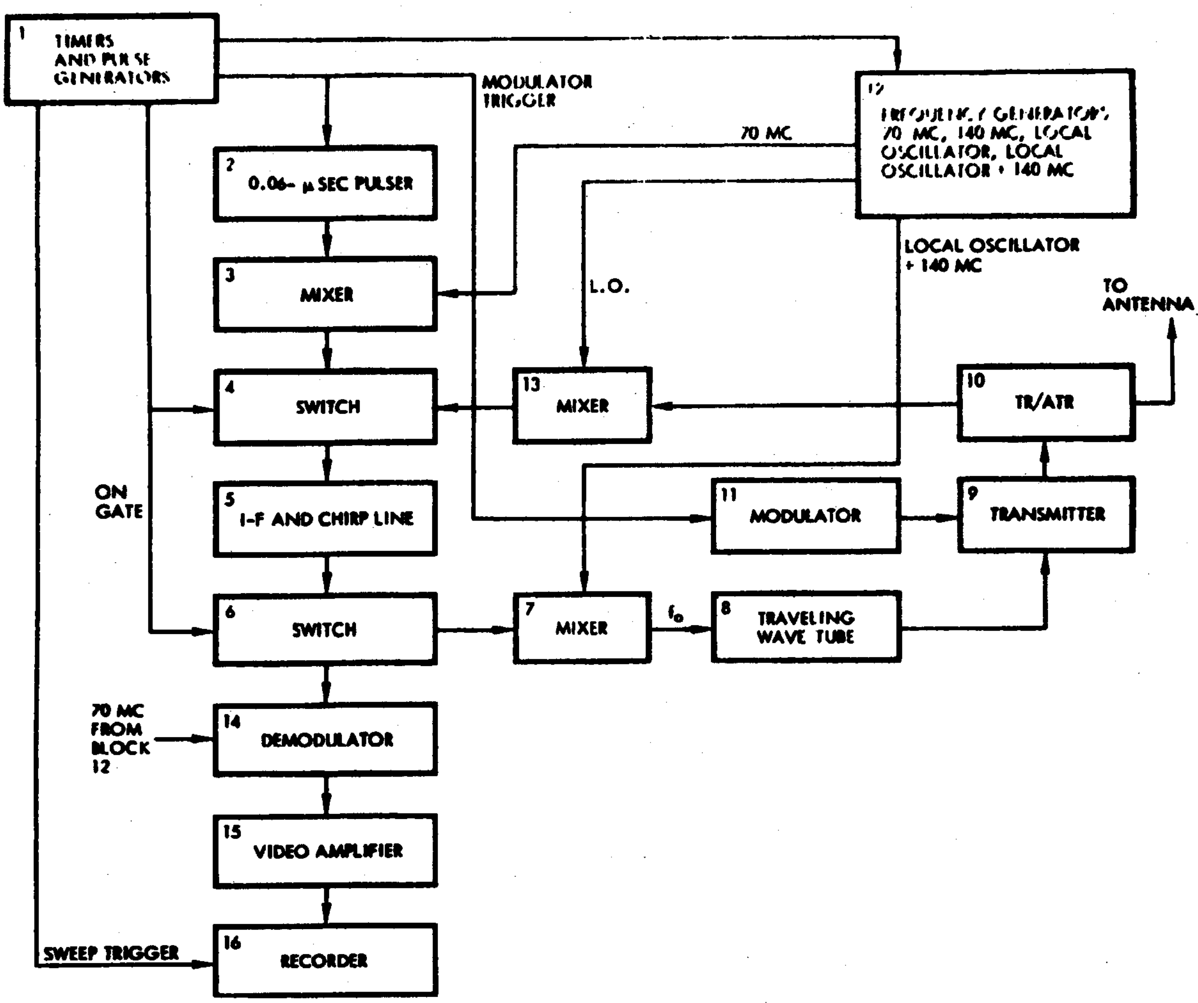

Figure 2.2.4.1 - Simplified Block Diagram of KP-II Radar System

further amplification is obtained in the twt, block 8. Next, the twt output goes to the transmitter (block 9) in coincidence with the high-voltage pulse from the modulator (block 11). The transmitter output passes finally through the TR/ATR box (block 10) and on to the antenna.

With the disappearance of the On-Gate the system reverts to the receive mode. The signal flow in the receive mode is via blocks 10, 13, 4, 5, 6, 14, 15 and 16.

The returning signal passes the TR/ATR box (block 10) and is immediately reduced to 70 mc by the mixer (block 13). The switches (blocks 4 and 6) allow the signal to pass the i-f and chirp line (now a dechirp line) and continue to the demodulator (block 14).

Because of the side band inversion process the output of the i-f line (block 5) is recompressed into a series of 0.06-microsecond target returns. Block 14 reduces these returns to bipolar video which is amplified and recorded. The recorder (block 16) is also the recipient of a sweep trigger which controls all recorder timing and the stc function. The reader is referred to the above referenced Goodyear report for further system details.

2.2.5 Component Description

The radar payload units are described briefly, including weights, photographs and electrical functional descriptions. The radar consisted of five units, of which the design center values of weights and volumes are given in Table I, below.

TABLE I

RADAR UNITS WEIGHT AND VOLUME

Unit	Weight (LB)	Volume (CU FT)
Transmitter	130	2.3
RF-IF	47	1.5
Reference Computer	46	1.2
Recorder	110	2.0
Control	37	0.5
Totals	370	7.5

The actual weight of the equipment flown was 348 pounds.

The payload components, excepting the recorder, were mounted in the cylindrical section of the payload vehicle between Station 228.0 and Station 194.0. The transmitter-modulator was mounted in a Goodyear fabricated cradle, having four side mounts with vibration isolators. The RF-IF was attached at six points - two side mounts and four base mounts. The design center values of system power requirements are given in Table II.

Voltage	Frequency	Power (watts)			
		Off	Warm-Up	Pre-Operate	Operate
115 ± 2 percent (3-ϕ)	400 ± 0.001 percent	0	82	82	122
115 ± 1 percent (1-ϕ)	2000 ± 1 percent	0	97	197	197
28.3 ± 2 percent	DC	5	5	215	215
2850 ± 250	DC	0	0	0	2000
Totals		5	184	494	2534

Table II - System Power Requirements

Basic System Parameters

Frequency - Transmitter Carrier	9600 mc
Pulse Repetition Frequency	8215 to 8730 CPS
IF Frequency	70 mc
Average Power	246 to 262 watts
Peak Power	30 Kw.

Transmitter-Modulator Electrical Design The function of the Transmitter-Modulator (see Figure 2.2.5.1) is to provide a high-power pulse of at least 30-kilowatts peak by amplifying the chirped signal from the RF-IF unit. This amplification is provided by the five-cavity klystron which is cathode-pulsed by a line-type modulator. This klystron provides linear amplification and preserves the amplitude and pulse characteristics of the input drive pulse.

The Transmitter-Modulator will be described by breaking it down into three major divisions: modulator, timing and trigger circuit, and overload and protection circuit. Each of these functions will be discussed in the following paragraphs.

Modulator The function of the modulator is to provide the proper voltage for operation of the klystron r-f amplifier. This voltage is applied as repetitive negative pulses to the cathode of the tube. Each pulse is about 28 to 30 kv in amplitude and approximately 1.2 microseconds in width. The circuit produces

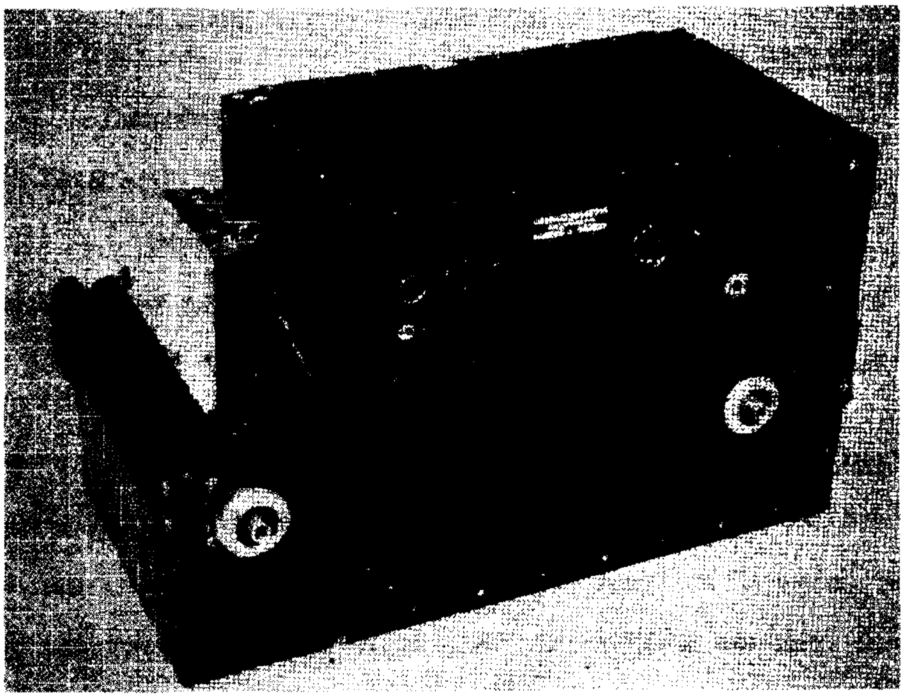

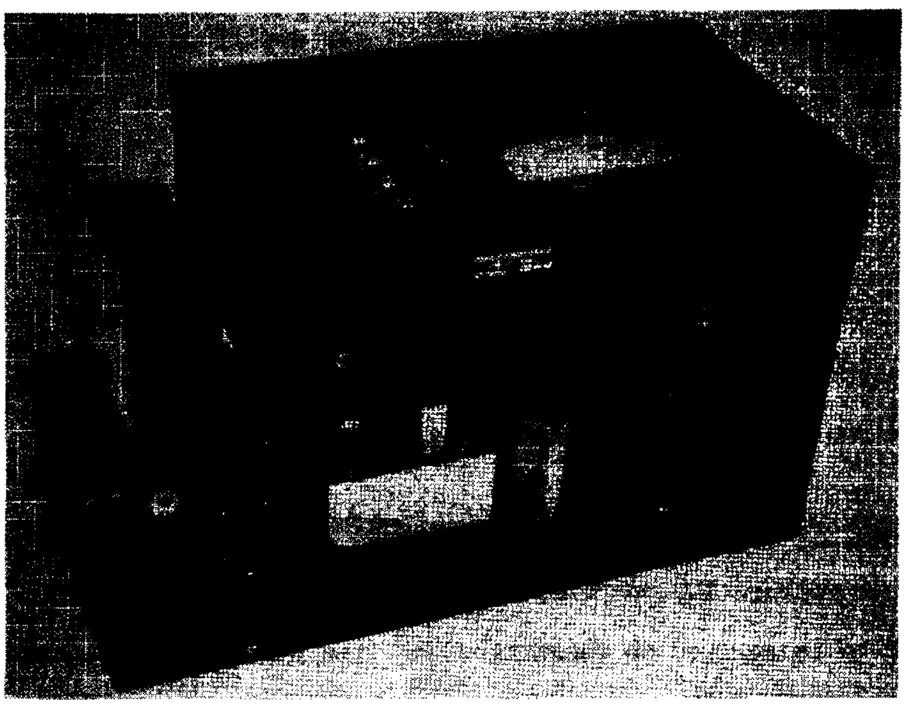

Figure 2.2.5.1 - Transmitter-Modulator

these pulses at a rate of 8215 to 8735 pulses per second.

A simplified diagram of the modulator is shown in Figure 2.2.5.2 along with some of the voltage and current wave shapes. These pulses are produced in the following manner:

At the beginning of the charging cycle the capacitance of the pulseforming network (pfn) is almost completely discharged and the thyratron is cut off. The inductance of the pulse transformer is small compared to that of the charging choke. The constants of the pfn are chosen for the pulse width desired and the inductance of the charging choke is chosen so that it forms a series resonant circuit with the capacitance of the pfn. The resonant frequency is approximately one-half the lowest prf:

$$f \simeq \frac{PRF}{2} = \frac{1}{2\pi\sqrt{LC}} .$$

In the absence of the charging diode CR1, the inrust of current to the pfn would normally cause a damped oscillation to be set up with the voltage E across C rising to approximately twice the power supply voltage (assuming negligible drop across the pulse transformer) and finally approaching the power-supply voltage as a steady-state value. This discharge action is prevented and the charge is maintained on the pfn because of the forward diode in the charging circuit which will not allow the current to reverse.

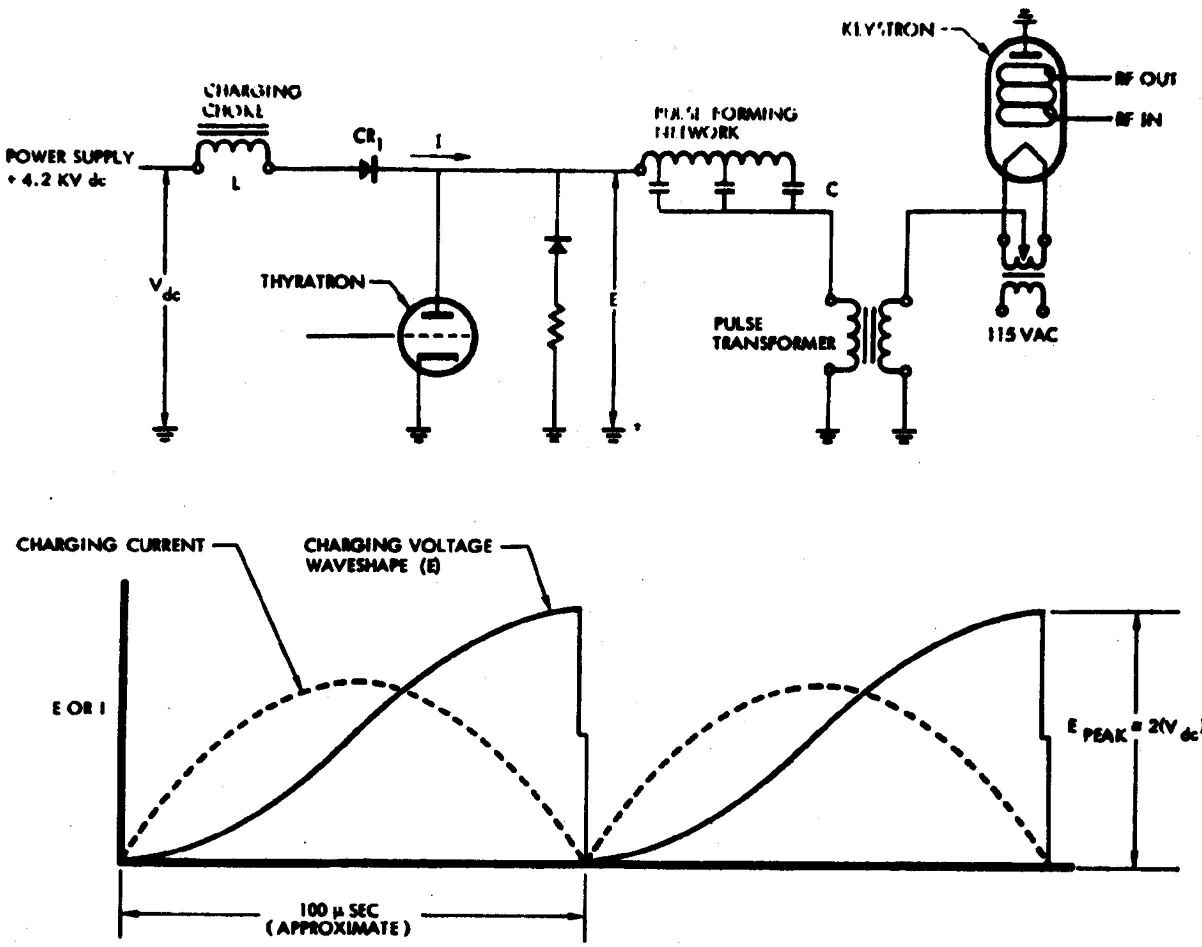

Figure 2.2.5.2 - Simplified Schematic of the Modulator

The timing is such that the peak voltage on the pfn occurs just before the trigger pulse to the thyratron. When the thyratron is triggered it shorts the input of the pfn to ground. The pfn is now directly across the pulse transformer and the energy of the pfn is completely discharged through the pulse transformer to the klystron. Since the characteristic impedance of the pfn is matched to that of the pulse transformer and its load, a voltage pulse approximately E/2 in amplitude and 1.2 microseconds long, is impressed across the pulse transformer. This pulse is stepped up by the pulse transformer to a 30-kv pulse across the klystron amplifier. This causes the tube, during the high-voltage pulse, to amplify the r-f signal being applied to its input cavity.

In practice, the impedance of the pfn is designed to be slightly higher than that of the pulse transformer and its load. This causes the voltage E to go slightly negative at the end of the discharge and effectively cuts off the thyratron.

This charge and discharge process is repeated at the prf rate causing the klystron to amplify the high-power r-f pulse (30-kw peak) each prf period. This pulse is then radiated by the antenna.

<u>Timing and Trigger Circuit</u>

This circuit makes use of a delay line, an avalanche-trigger amplifier, and a blocking oscillator. The function of the circuitry is to properly delay and develop the voltage trigger required by the grid of the thyratron.

The incoming 5-volt modulator trigger is coupled to the delay line which is adjustable from 0 to 0.65 microsecond in 0.05-microsecond increments to a value as required to properly align the system pulses with the inherent delays found in the existing cables and circuits.

The output of the delay line is used to trigger a transistor delay line controlled avalanche stage. The avalanche stage develops sufficient voltage to drive the grid of the cathode follower which in turn triggers the blocking oscillator circuit. The cathode-follower method of triggering the blocking oscillator was chosen since it is adaptable to high prf rates.

The blocking oscillator, which is of conventional design, develops a high-voltage, medium-power pulse to drive the grid of the hydrogen thyratron. The grid pulse amplitude, pulse width, rise time, and driving impedance are specified by the thyratron manufacturer. To assure stable and reliable operation all these conditions must be met, particularly when operating at high prf rates. This blocking oscillator has an amplitude of 250 volts and is capacitively coupled to the thyratron grid. A despiking network in this circuit prevents large voltage spikes produced by the hydrogen thyratron during ionization from being reflected into the blocking oscillator circuit.

Overload and Protection Circuit

This circuit monitors the inverse current, power-supply overload, the time delay, and the temperature of the klystron collector. All of these signals either operate or feed through relays to provide a voltage to turn off the high-voltage power supply in case of malfunction.

RF-IF Electrical Design

General The RF-IF unit (see Figure 2.2.5.3) has two basic functions: it generates the chirped pulse that is amplified by the Transmitter-Modulator, and it serves as the receiver section of the radar system. Since most of the unit concerns itself with chirping and dechirping pulses, it is necessary to explain what these processes are before discussing the detailed circuitry.

In the transmit section of the circuit this unit receives a 0.06-microsecond, sine x/x pulse from the Reference Computer from which it generates a linear sweep-frequency pulse for the r-f drive to the transmitter. This is achieved by feeding the sine x/x pulse through a chirp network where all the frequencies are delayed according to their frequencies. The chirped pulse emerges as a 1.0-microsecond pulse. The rf in the 1.0-microsecond pulse is a linearly frequency-modulated signal with the start of the pulse

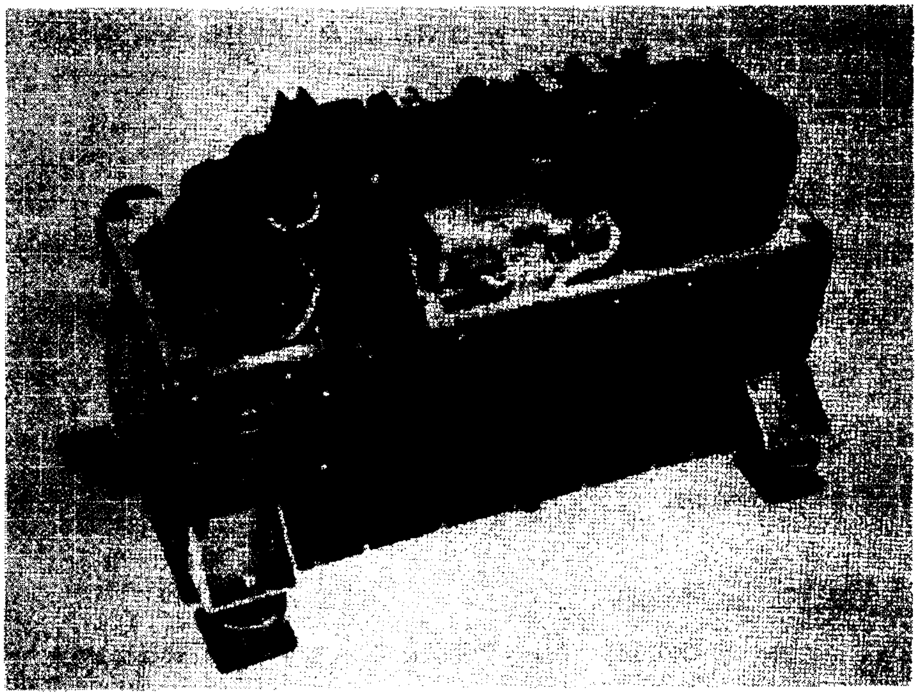

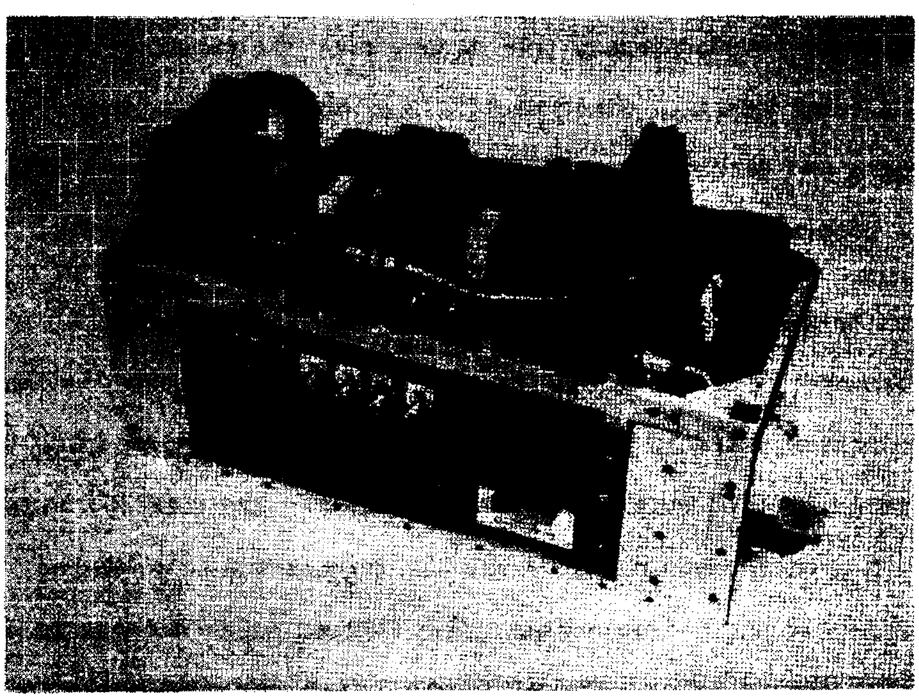

Figure 2.2.5.3 - RF-IF Unit

being f_1 and the end of the pulse being f_2. The frequency content of these pulses requires an information band width of 15 megacycles which is sufficient for the required 50-foot resolution with some additional allowance provided. All of the chirping circuitry is designed around a 70-megacycle frequency. The chirped pulse is later mixed with the appropriate signals to translate it to an X-band frequency. It is then amplified by the transmitter and becomes the transmitted signal. This burst of energy upon being reflected by a target is then detected by the receiver.

The receiver portion of this unit includes X-band wave guide sections, t-r tubes, a microwave mixer, circuits for dechirping the returned signal, and circuits for providing amplification at the i-f frequency. The wave guide and t-r tubes perform the duplexing function of the system and provide protection for the receiver from the high-powered pulse from the transmitter. The losses in this wave guide and the performance of the microwave mixer-amplifier determine the minimum sensitivity of the system. Once a returned signal is detected and amplified it is sent through the chirp network where the linear sweep-frequency pulse is recompressed into the original 0.06-microsecond sine x/x pulse. How well this pulse resembles the original pulse is a measure of proper system performance. In actual operation the returned signal has experienced a doppler shift that results in the sine x/x pulse having slightly different frequency content. In the reference computer this pulse is detected in a synchronous demodulator where it is compared with the reference frequency for determination of the doppler shift.

Transmitter Circuit Function The RF IF unit functional block diagram is shown in Figure 2.2.5.4. The transmitter and receiver sections time-share the center i-f amplifier portion of the circuit. The signal flow through the transmitter section, beginning with the 99-megacycle oscillator, is as follows:

- 99-Megacycle Oscillator

  This oscillator is the stable local oscillator (stalo) of the radar system. It is highly stable over short-term periods and is tuned to a frequency of 99.275 megacycles. This frequency is multiplied to the X-band region in the frequency multiplier.

- Frequency Multiplier

  The frequency multiplier utilizes the harmonic generation property of varactor diodes to multiply the stalo frequency 96 times and provide enough power at this frequency to drive the receiver mixer and the 140-megacycle mixer.

- 140-Megacycle Mixer

  The output of the frequency multiplier is mixed with a 140-megacycle signal from the Reference Computer and forms two side bands in the X-band region. One of these side bands is filtered out before reaching the 70-megacycle mixer. The 140-megacycle from the Reference Computer is derived from the basic 70-megacycle oscillator to maintain phase coherence.

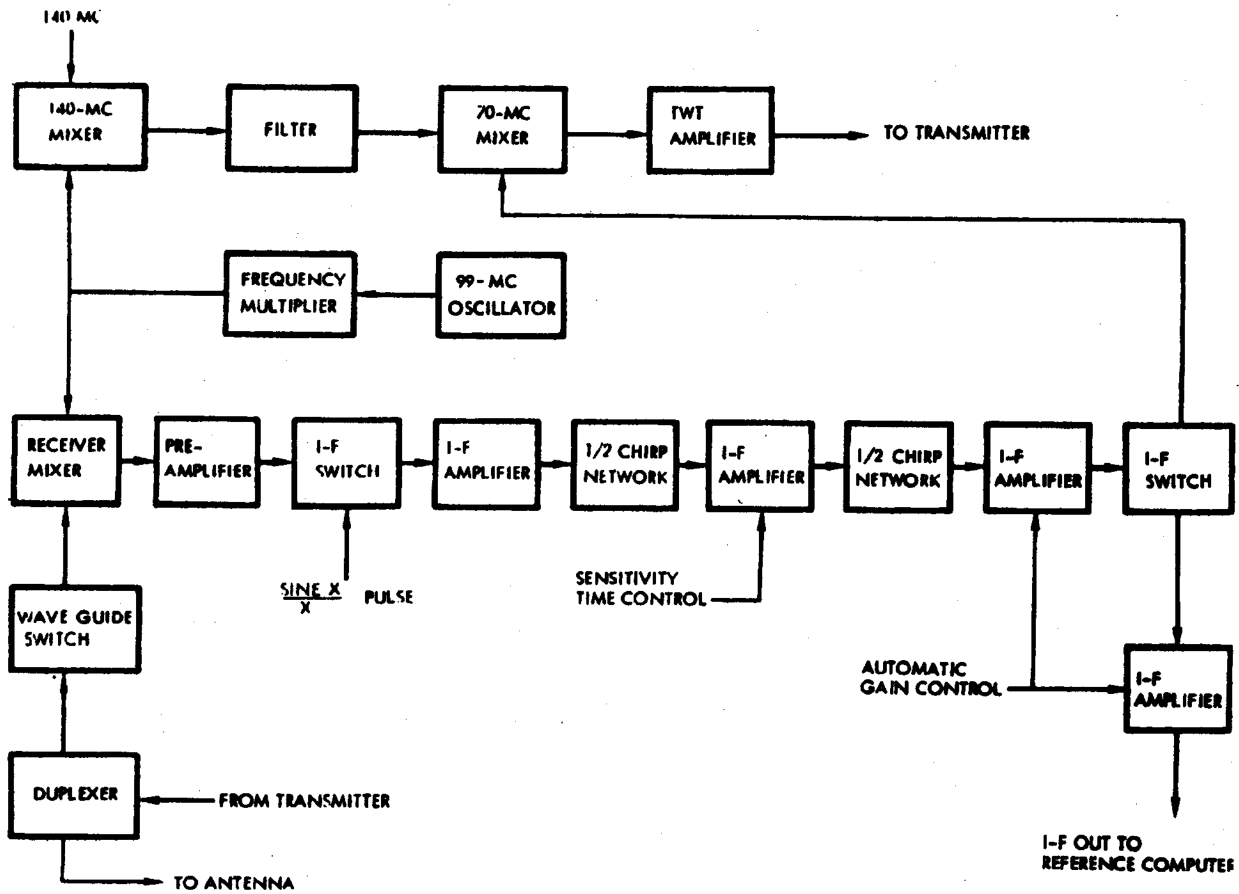

Figure 2.2.5.4 - Functional Block Diagram of RF-IF Unit

This mixing operation is required only in the transmitter chain since the transmitter signal must be frequency-inverted so that is can be sent back through the same chirp network. Otherwise the returned pulse would be further expanded instead of being recompressed.

o <u>Filter</u>

This unit is an X-band wave guide filter that selects the upper side band from the 140-megacycle mixer so that the transmitter signal is frequency-inverted.

o <u>70-Megacycle Mixer</u>

The 70-megacycle mixer, during the transmit period, accepts the 9670-megacycle signal from the filtered 140-megacycle output, and the linearly swept 70-megacycle pulse from the i-f channel, and mixes them. The two resulting side bands are frequency swept, one sweeping from low frequency to high frequency, the other doing the opposite. The lower one, which is in the pass band of the transmitter, is amplified while the undesired side band is reflected from the transmitter and absorbed in a load isolator at the output of the twt amplifier.

o <u>TWT Amplifier</u>

This tube amplifies the relatively small 9600-megacycle power output to about 250 milliwatts which is sufficient to drive the klystron amplifier in the transmitter. Operation of this tube is such that it provides linear amplification of the signals without appreciable phase shift.

Receiver Circuit Function In the preceding transmitter discussion the transmitted pulse generation was discussed. The receiver description will therefore begin with a signal returning to the duplexer:

- Duplexer

  The duplexer consists of wave guide sections, a 3-db hybrid, and a t-r tube. During the transmit period the duplexer protects the receiver from the high-power transmitter pulse and directs the transmitter pulse to the antenna. During the receive period the duplexer allows the low-energy level received pulses to pass on to the receiver.

- Wave Guide Switch

  A wave guide switch is included in the wave guide run to the receiver mixer. This switch provides protection for the receiver crystals when the system is not in operation and might be damaged from high-level pulses from some outside source.

- Receiver-Mixer Amplifier

  This unit has a balanced crystal detector input stage followed by a 70-megacycle preamplifier. The mixer converts the X-band return pulses to the 70-megacycle i-f frequency by mixing with the local oscillator frequency. The design of this unit is such that it will provide a receiver noise figure of 10 db when installed in the unit. There is a gain of about 24 db in the preamplifier which ensures that the noise figure of the amplifiers following the mixer-amplifier will not degrade the over-all noise figure of the system. The output of the unit is an i-f signal (70-megacycles) that is further processed elsewhere in the system.

- <u>I-F Switch</u>

  The i-f switch allows the chirp network to be time-shared by the transmitter and the receiver. During the interval of time that the transmitter is on, the receiver's normal function is disconnected. At that time the sine x/x pulse from the Reference Computer is fed through the i-f amplifiers and chirp networks so that it is changed into a 1.0-microsecond pulse having a linear frequency change during the pulse. At the end of the transmitting period the switch returns the receiver/i-f amplifiers and chirp networks to their normal functions of amplifying and dechirping the return echoes.

- <u>I-F Amplifiers</u>

  These amplifiers are provided to amplify the return signals and to overcome the losses of the chirp network. They operate at a center frequency of 70-megacycles and have a band width of about 15 megacycles, which is the information band width of the amplified pulses. Each amplifier has a gain of about 30 db and has provisions for adjusting the gain by

6 db with a three-position step attenuator on the front of the unit.

- <u>Chirp Network</u>

  The chirp network is divided into halves and interspaced with i-f amplifiers to overcome the losses in the networks and to keep the signal above noise level. These networks are passive filter elements taking the form of a bridged "T". Their design is such that they exhibit a linear phase delay versus frequency characteristics for all frequencies within the pass band. Therefore, whenever a sine x/x band of frequencies, centered at 70-megacycles, is fed into the chirp network, it produces an expanded pulse of nearly constant amplitude with a linear frequency change from the start of the pulse to the finish of the pulse. When the expanded pulse is inverted in frequency and fed back into the network, the original sine x/x pulse is reconstructed by the network. This reconstructed pulse is then amplified and sent to the Reference Computer as a detached target return.

- <u>Automatic Gain Control and Sensitivity Time Control</u>

  These functions are inputs to the R-F/I-F unit from the Reference Computer and Recorder, respectively, and are described in the sections covering these units.

Reference Computer Electrical Design

Operation The operation of the Reference Computer (see Figure 2.2.5.5) is best described by breaking it down into four major divisions: synchronizer, r-f section, clutterlock, and self-verification and signal conditioning.

o Synchronizer

The synchronizer section generates the basic timing and control signals for the radar. These signals are sweep trigger, modulator trigger, on-gate, and unblanking gate. The synchronizer section also generates the following signals for control and timing of the computer: prf/4 and complement, prf/2 and complement, block oscillator trigger and doubler gate.

The synchronizer section consists of a crystal-controlled clock at 2.07065 mc ± 1000 cps and a counter with controlled feedback. The feedback is controlled by four digital-control lines. The state of the four control lines is either +28 or 0 vdc and is determined by the prf selection. The four input-control lines are applied to four control relays. This enables a total of 16 prf selections which vary from 8.735 to 8.215 kc with a separation of approximately 35 cycles. This method of producing a variable prf has proven very successful in minimizing jitter. Jitter is less than 0.01 microsecond.

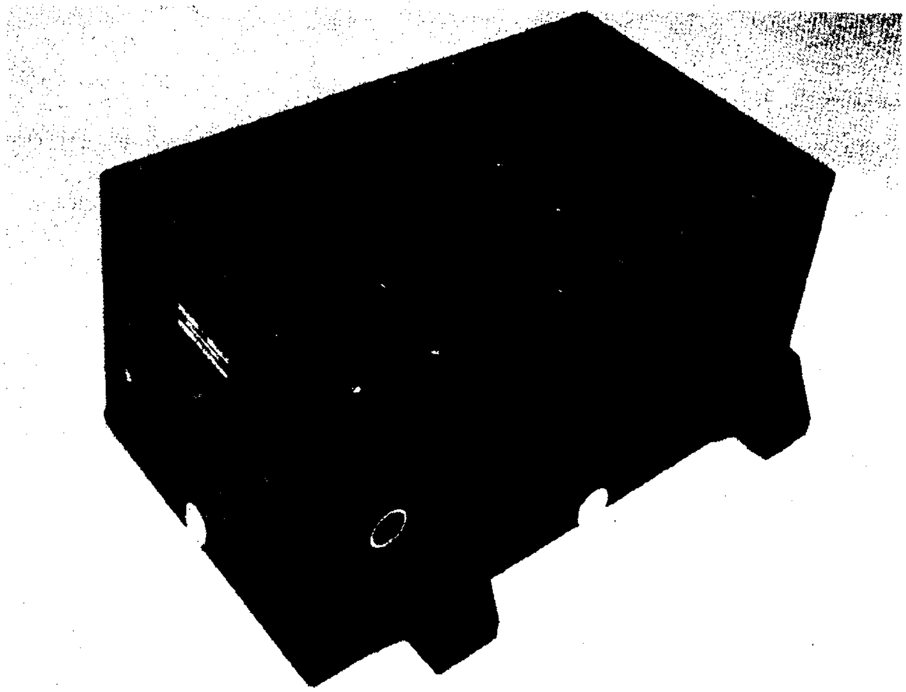

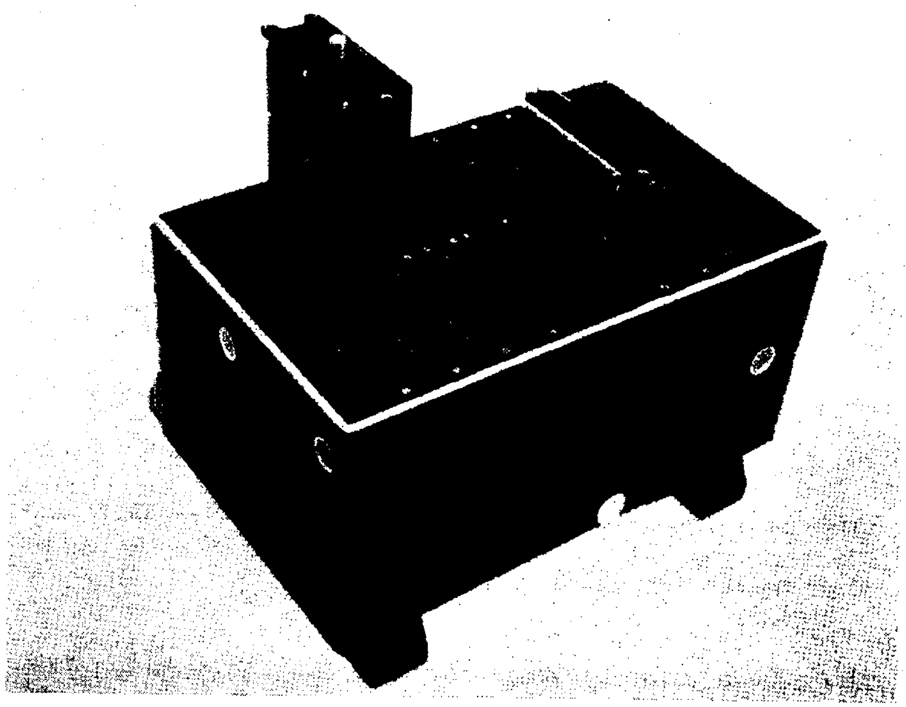

Figure 2.2.5.5 - Reference Computer

During each cycle of the counter, a modulator trigger, on-gate, sweep trigger, unblanking gate, doubler gate and B. O. trigger are generated, using the logic provided by the counters, to trigger the necessary circuitry. (See Figure 2.2.5.6.)

o **R-f Section**

The r-f section generates the following signals: 140-mc pulse; 0.06-microsecond, 70-mc (sine x/x) pulse; 70-mc reference signal offset by 90 degrees each prf; and an age control signal. See Figure 2.2.5.7 for a block diagram of the r-f section.

The r-f section is composed of a crystal-controlled, 70-mc oscillator which has two isolated outputs. One output is fed to a phase-stepper which is also supplied with the logic of prf/4, prf/4 complement, prf/2 and prf/2 complement which causes the reference signal to be stepped 90 degrees in phase each prf. The output of the stepper is the offset 70-mc reference supplied to the doubler and to the balanced modulator. The logic lines supplied to the stepper are generated in the gate sequencer by counting down from the prf. This logic is also fed to the video gate board.

The 140-mc pulse is generated by a doubler circuit from the 70-mc reference and is gated by an inverted on-gate.

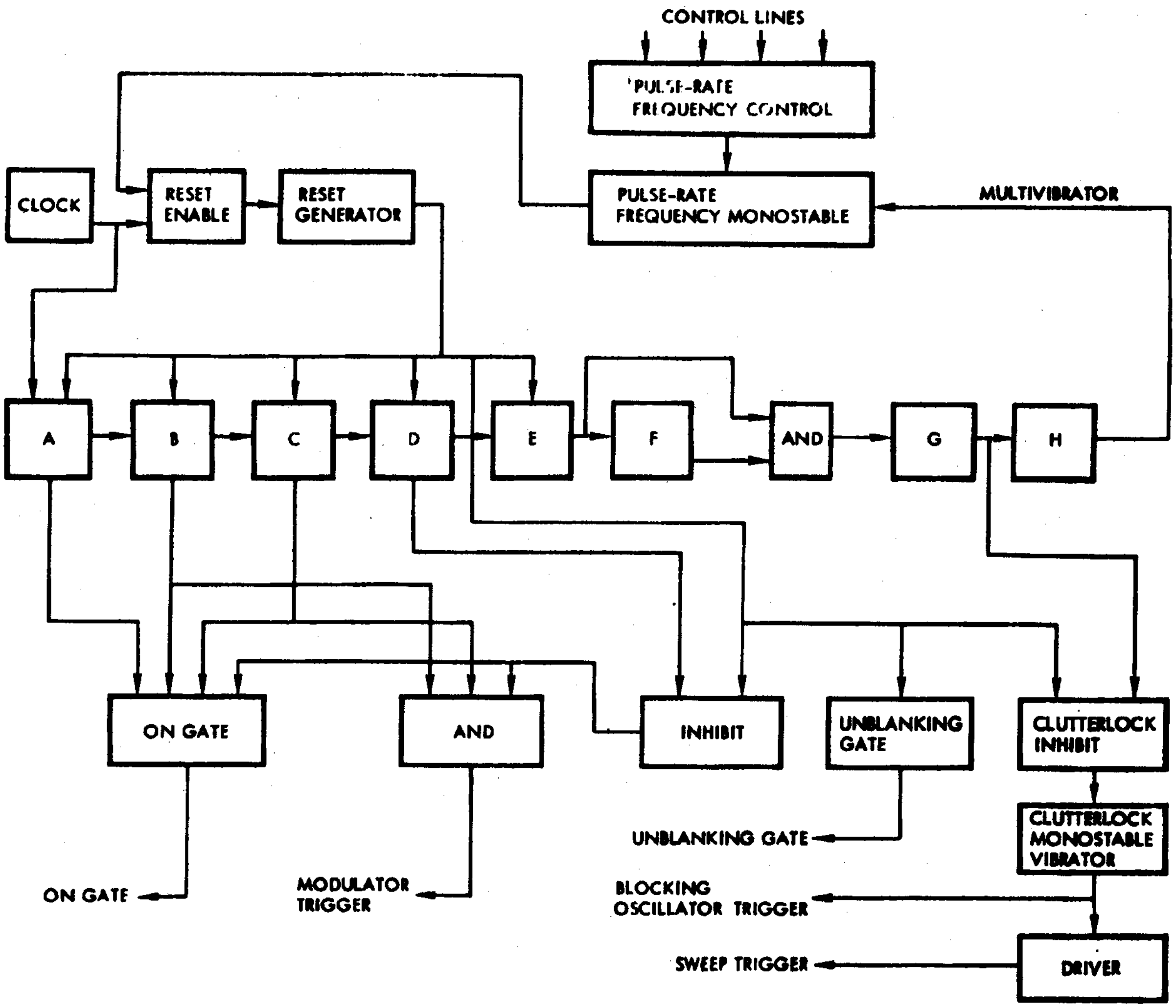

Figure 2.2.5.6 - Synchronizer Timing Logic

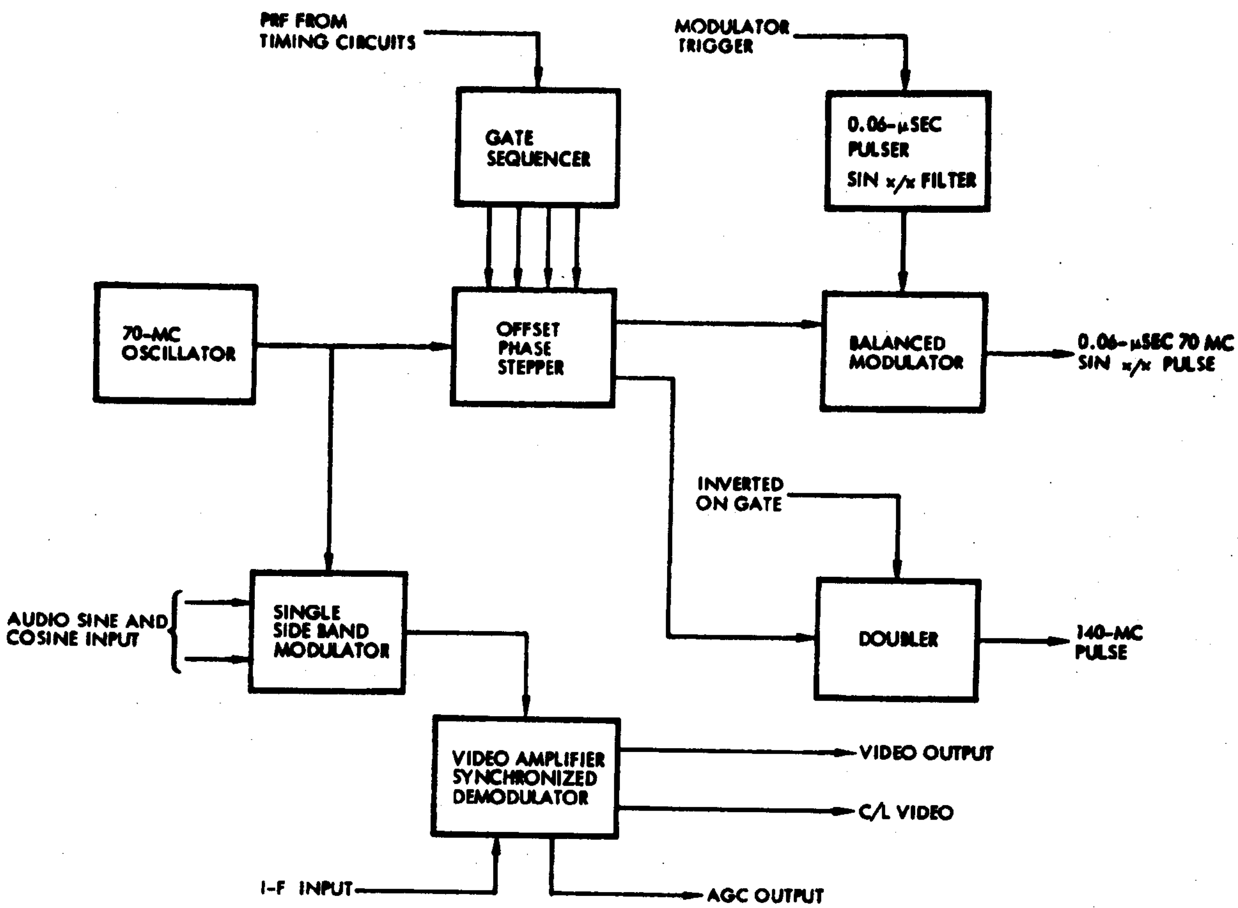

Figure 2.2.5.7 - Block Diagram of R-f Section

The 0.06-microsecond, 70-mc pulse is generated by first triggering a blocking oscillator circuit which utilizes an avalanche transistor to produce a 0.06-microsecond square wave. The 0.06-microsecond square wave is fed to a special Fourier transform filter designed for a flat pass band and linear phase shift between limits of 0 to 7.5 mc. The output from the pulser, a classical sine x/x time domain spectrum distributed symmetrically about the Y-axis center frequency, is fed to a balanced modulator where the 70-mc offset reference is modulated by this signal producing a 0.06-microsecond, sine x/x, 70-mc suppressed carrier signal to the radar.

The r-f section also has a high-resolution synchronous demodulator which demodulates the i-f input using as a reference the output of the single side-band (ssb) modulator whose output is offset from the 70-megacycle reference by the audio frequency from the clutterlock section. An agc voltage of 0 to -6 volts is produced as a function of the i-f input signal.

- <u>Clutterlock Section</u>

  The basic purpose of the clutterlock section is to generate sine and cosine error signals to the ssb modulator to compensate for angular displacement of the antenna beam with respect to the zero doppler direction.

The clutterlock section (see Figure 2.2.5.8) consists of a video amplifier, video gate, storage and switching module, approximate multiplier, audio synchronous demodulator, audio filter, 50-kc reference generator, voltage-controlled oscillator, and an integrator reset.

An output from the synchronous demodulator (Figure 2.2.5.7) is amplified and fed to the video gate. The video gate transfers the signal to the approximate multiplier and the storage and switching module. The signal transferred by the video gate is 60 microseconds of information following the blocking oscillator trigger. The information transferred to the storage and switching module is stored on eight sampling capacitors. Following the next blocking oscillator trigger these capacitors are sampled and the output is fed to the approximate multiplier through the video gate.

In the approximate multiplier the phase difference between the transferred and the stored video is detected. This means that the phase of the return from consecutive pulses is compared. Because of the 90-degree offset between prf's (providing the synthetic beam is centered with respect to the zero-doppler plane) the video signals will be 90 degrees out of phase and will be zero. The detector output will be one polarity for a

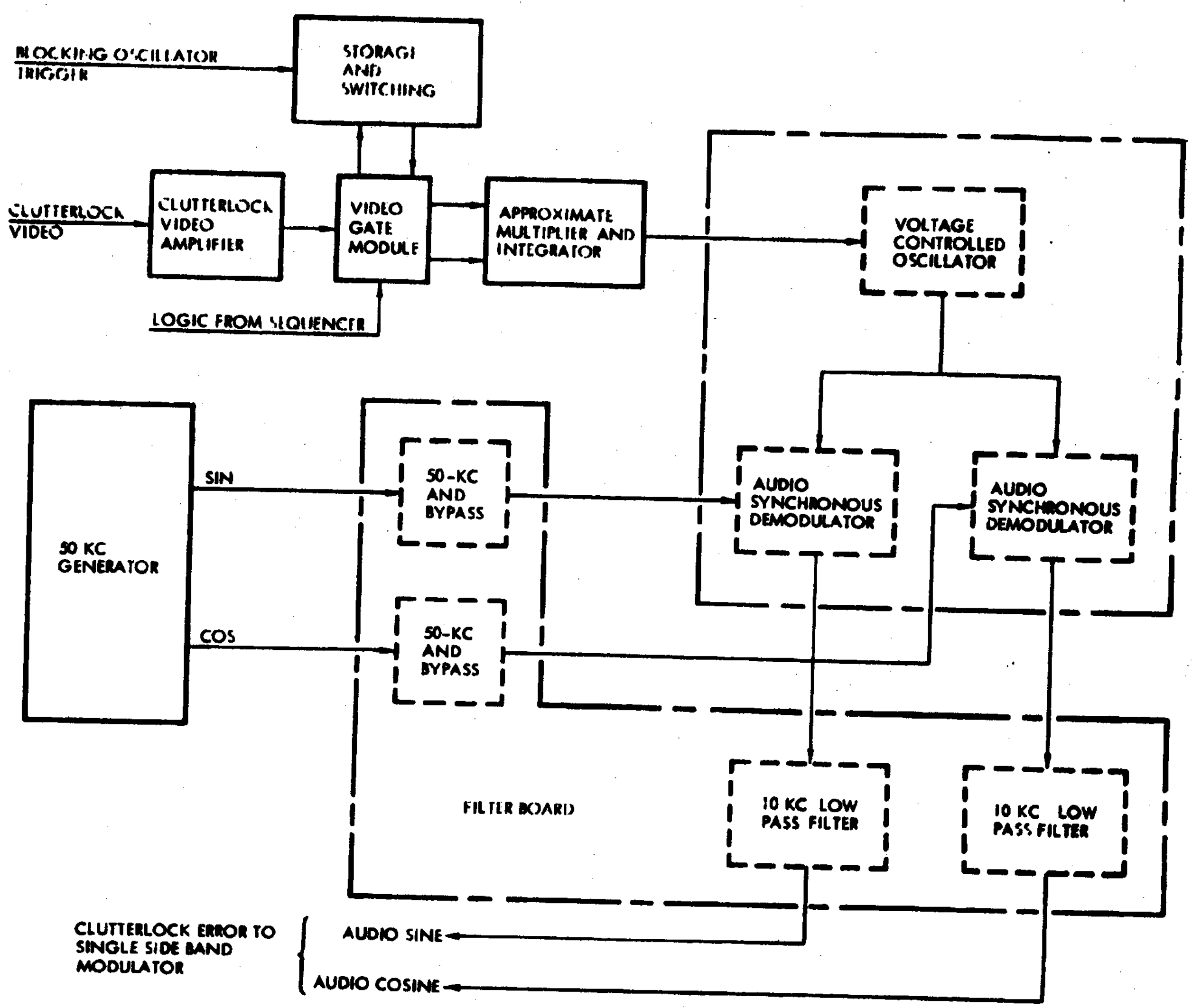

Figure 2.2.5.8 - Block Diagram of Clutterlock

forward misalignment of the antenna beam and of opposite polarity for an aft misalignment.

The output of the integrator is fed to a voltage controlled oscillator (vco) whose output is from 40 to 60 kc, depending on the output of the integrator. The output from the audio synchronous demodulator module is then two quadrature sinusoidal signals chopped at the vco rate. These quadrature signals are then applied to a low-pass filter which eliminates all except the difference components. These two signals, sine and cosine, are fed to the ssb modulator.

The inputs to the ssb modulator are the sine and cosine signals and a 70-mc reference signal. The ssb module consists of two balanced modulators which are driven by the sine and cosine signals, respectively. The references applied to the balanced modulators are the 70-mc and the 70-mc pulse shifted by 90 degrees. The output of the two balanced modulators is then fed to a summing network which suppresses the carrier and the lower side band. The upper side band is then amplified and fed to the synchronous demodulator for demodulation against the input i-f signal. The output of the ssb is a 70-mc signal which is offset by an audio frequency which is proportional to the original antenna beam misalignment from the zero doppler plane. The remaining circuitry in the clutterlock section is an integrator reset. The purpose for the reset is to sense the integrator output voltage and to discharge the integrator capacitors when this voltage exceeds +8.5 vdc or falls below -8.5 vdc. These values correspond to approximately ±1 degree of beam displacement and approximately ± 3 prf.

- Self Verification

  The built-in test (BIT) circuit generates a 70-mc signal chopped at a 30-kc rate which is fed to the high-resolution synchronous demodulator when so commanded by the operator. This is used to simulate an i-f input signal. When the BIT loop is closed the clutterlock circuit nulls out at prf/4 and holds in this condition until the BIT switch is opened.

Control Unit Electrical Design

Operation The Control Unit (see Figure 2.2.5.9) serves primarily as a control and junction box. Power from the vehicle system power supplies is distributed to the other side-looking radar (slr) units through the Control unit. It also provides three regulated voltages not otherwise available to the other slr units. The Control unit will be described by breaking it down into five major functions or divisions: control and junction box, -23.5 vdc power supply, +23.5 vdc power supply, +300 vdc power supply, and the timer override circuitry. The Control unit is shown in simplified schematic form in Figure 2.2.5.10.

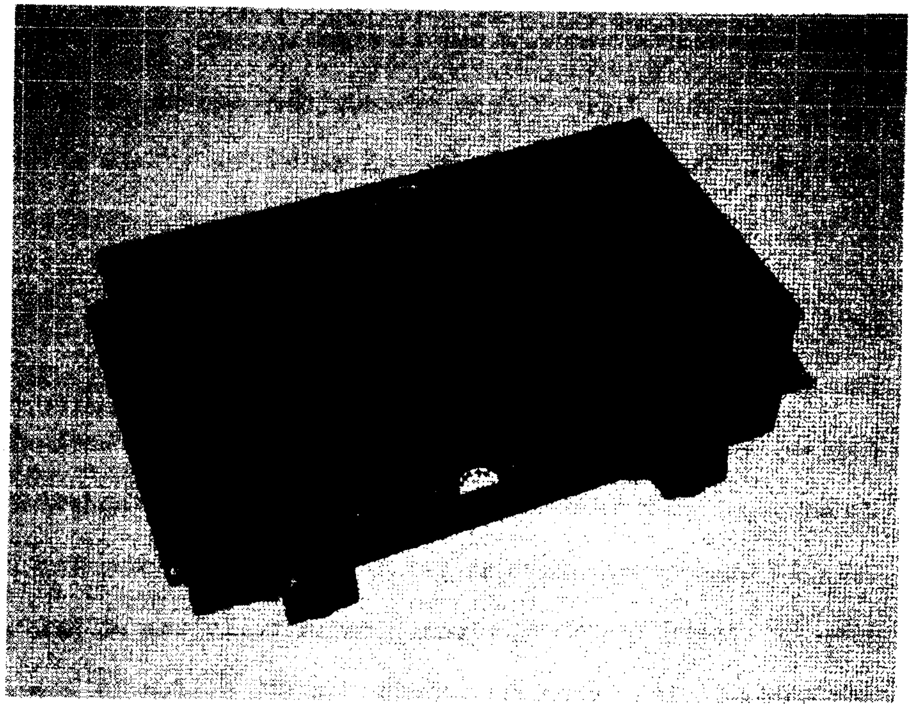

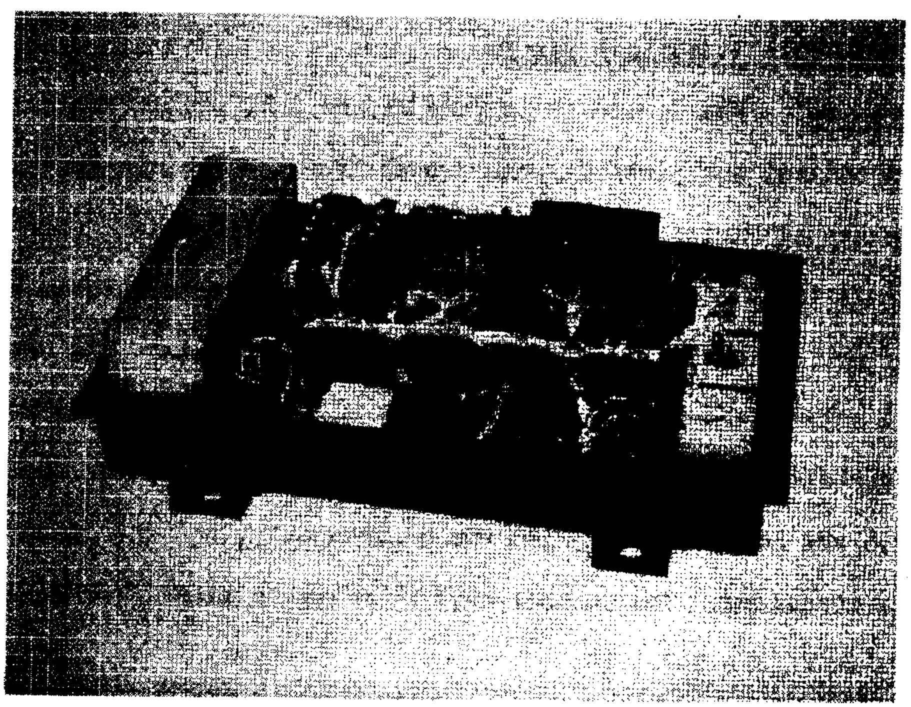

Figure 2.2.5.9 - Control Unit

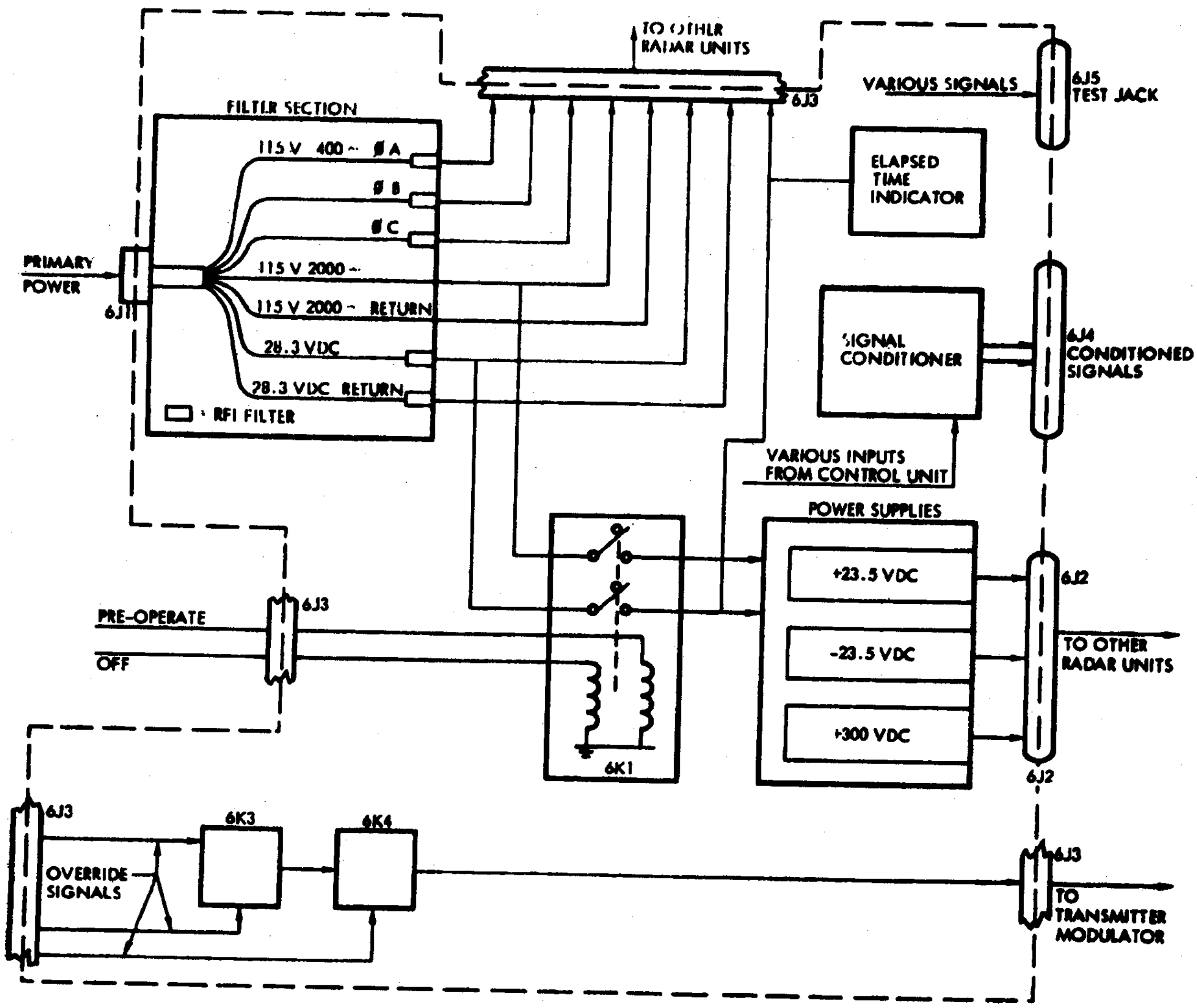

Figure 2.2.5.10 - Simplified Schematic of Control Unit

- <u>Control and Junction Box</u>

  When the slr system is in the warm-up mode, (1) 28.3 vdc, (2) 115 v, 3 phase, 400 cps, and (3) 115 v, 1 phase, 2000 cps voltages are applied to the Control unit from the vehicle power supplies. These voltages are distributed to the other units in the slr system.

  When the slr system is in the pre-operate or operate mode, 28.3 vdc and 115 v, 2000 cps power is applied to the circuits in the Control unit which generate +23.5 vdc, -23.5 vdc, and 300 vdc. This is accomplished with relay 6K1. The relay is of the latching type and is energized from the vehicle command subsystem by applying 28.3 vdc momentarily to the pre-operate input of the Control unit. The Control unit is commanded from the pre-operate mode with the momentary application of +28.3 vdc to the OFF input of the Control unit. The slr is commanded to the operate mode by momentary application of +28.3 vdc to the OPERATE input. In OPERATE, the film drive motor (Box 7), the transmitter high-voltage (Box 3), and the integrator time constant (Box 5) relays are energized. No Control unit functions are involved when the OPERATE command is given.

- <u>+23.5 Vdc Regulated Power Supply</u>

  The +23.5 v power supply (shown in block-diagram form in Figure 2.2.5.11) is a series regulated supply. The regulator

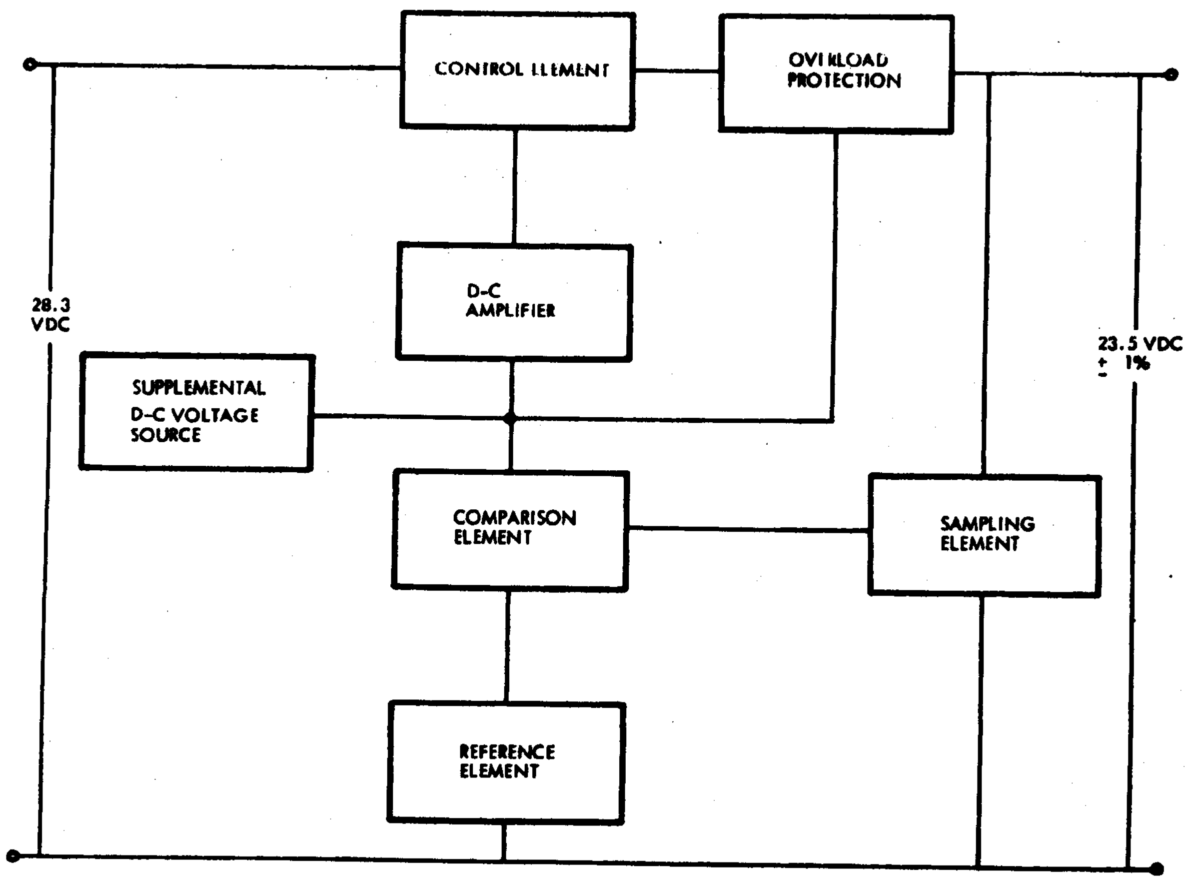

Figure 2.2.5.11 - Block Diagram of +23.5 Vdc Power Supply

was designed to deliver an output voltage of 23.5 v ± 1.0 percent for all load currents from 0 to 5 amperes. The maximum peak-to-peak output ripple at full load is less than 18 millivolts. A series-type regulator circuit was chosen because it is best capable of providing a constant output voltage to a variable load while maintaining a high efficiency. An overload-protection circuit was also incorporated to prevent destruction of the series-regulator transistor for an overload or short-circuit condition on the output. The overload protection operates at a current of 7 to 8 amperes and recovery after overload is automatic.

The regulator is composed of seven functional elements: a sampling element, reference element, comparison element, supplemental d-c voltage source, d-c amplifier, control element, and an overload-protection circuit.

The voltage regulator, like a servoamplifier, uses an error or difference signal to correct any error in the output. The difference between a reference and a portion of the regulated output is detected and amplified by the comparison element and, if necessary, is further amplified by the d-c amplifier. The control element senses the magnitude and phase of the amplifier difference and regulates the load voltage in the proper direction to correct any voltage change.

The series control element regulates the current to the load so that the product of load current and load resistance remains equal to the required output voltage.

- <u>-23.5 Vdc Regulated Power Supply</u>

  The -23.5 vdc regulated power supply is identical to the +23.5 vdc supply with the following exceptions:

  The circuit was designed for a full-load current of 3.8 amperes

  The primary power source for the regulator is 115 v, 2 kc, transformed down and then rectified by a full-wave bridge rectifier

  The positive side of the output line was grounded and the return line used for the negative output voltage.

  The regulator circuits are built on printed circuit cards with the exception of the control element and sensing resistors. Otherwise, being identical, the regulator circuits will operate with either primary source.

- <u>+300 Vdc Power Supply</u>

  The +300 vdc power supply (Figure 2.2.5.12) operates from a +28.3 vdc ±2 percent source. A step-down transformer (located in the +23.5 vdc supplies) is used to supply 10-vrms, 2000-cycle power to the 300-vdc supply. The power drain on the

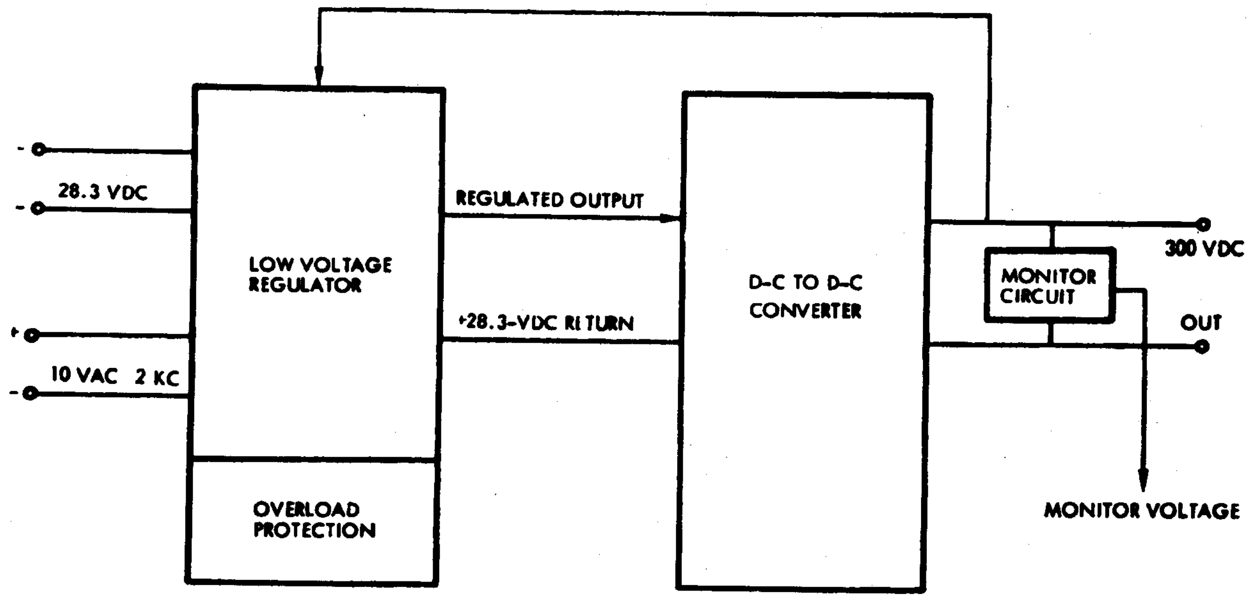

Figure 2.2.5.12 - Block Diagram +300 Vdc Power Supply

115-vac, 2000-cycle power is approximately 10 milliwatts. The supply is designed to deliver 30 watts of power.

The supply can be considered from an electrical viewpoint to be divided into two main sections. The first section is a simple series regulator. A transistor in series with the 28.3-vdc input is used to adjust the voltage level which is fed to the second section. The input voltage to the second section is regulated to maintain a constant (within ±1 percent) output voltage regardless of the 28.3 vdc input voltage.

The second section is a d-c to d-c converter. The converter is based on the "Jensen" circuit and as such employs two transformers. A small saturating transformer is used to set the chopping or switching frequency of the two power transistors which are used in this section. A second, nonsaturating power transformer steps the chopped voltage up to 300 volts. A full-wave bridge converts the square-wave voltage into a d-c voltage. A two-section inductance-capacitance network smooths the output and ensures low ripple on the output.

A resistor divider is used to obtain a sample of the 300-vdc output. This sample is fed back to the series regulator.

Semiconductor circuitry is used to control the base drive to the series regulator transistor mentioned above. The base drive is lowered if the output voltage is high and increased if the output voltage is low. In this manner it is possible to maintain a constant output voltage.

Overload protection circuitry is also employed. If the load current exceeds 120 to 160 milliamperes, a sensing circuit in the series regulator will halt the flow of base drive to the series regulator transistor. The supply is therefore protected from shorts which might accidentally be placed across its output terminals. The supply will function normally after the overload is removed.

- <u>Timer Override Circuitry</u>

  The Control unit provides a means of overriding (by vehicle command) a timer-delay circuit in the Transmitter-Modulator unit of the slr (see Figure 2.2.5.10). When a 28-vdc signal is commanded through time-delay overload no. 2, nonlatching relay 6K3 is energized. When a 28-vdc signal is commanded through time-delay overload no. 3, nonlatching relay 6K4 is energized. The normally open contacts of the two relays form two breaks in a line connecting the time-delay over load no. 1 to an output which goes to the Transmitter-Modulator. When both relays are energized, a voltage level on the input lead is applied to the Transmitter-Modulator unit and the desired override function is accomplished. The two relays can be considered to form a three-input "and" gate.

Recorder Design

Mechanical The recorder (see Figure 2.2.5.13) film transport system is used to regulate accurately the speed of the film as it passes over an exposure drum and is exposed to the light from the crt through the optical system. The film transport system is depicted schematically in Figure 2.2.5.14. Operation of the film transport can be described in five parts: film supply, film drive, film-tension control, film transport drive, and film takeup.

- Film Supply

  The film is stored in and supplied from the film supply cassette. Within the cassette is a film supply-spool brake assembly which contains a friction brake and a magnetic particle brake both in constant mesh with the spool shaft through a reduction gear assembly. The friction brake is applied when de-energized (recorder not operating) and released when energized (recorder operating). The magnetic particle brake is energized with the Recorder system and its braking torque regulated by a potentiometer connected to the pivot shaft of an input tension-control assembly input (refer to paragraph Film Tension Control following).

- Film Drive

  The primary drive for the film is the metering drum. The metering drum drive (Figure 2.2.5.15) is powered by a hysteresis synchronous motor running at a constant 8000 rpm. An input

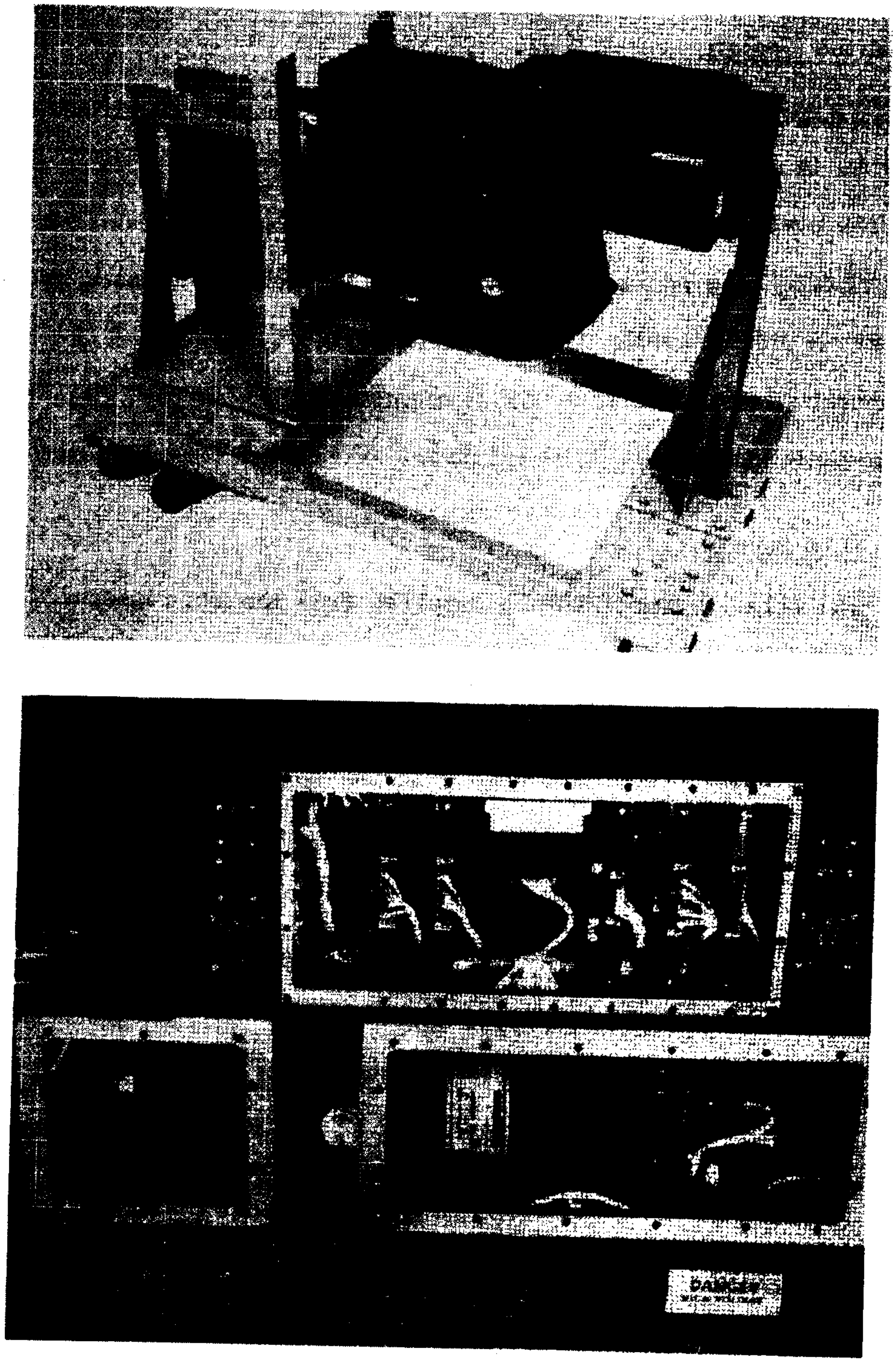

Figure 2.2.5.13 - Recorder

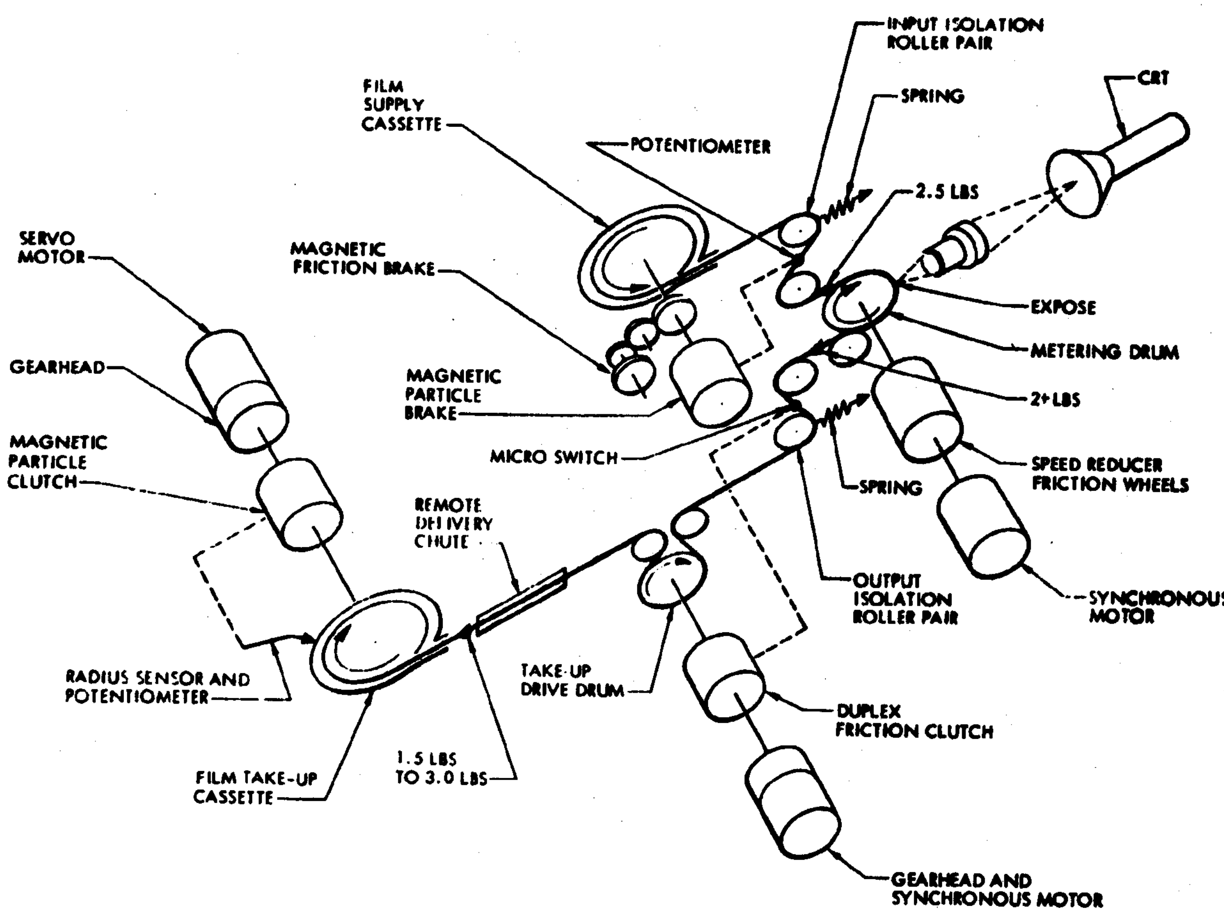

Figure 2.2.5.14 - Film Transport System

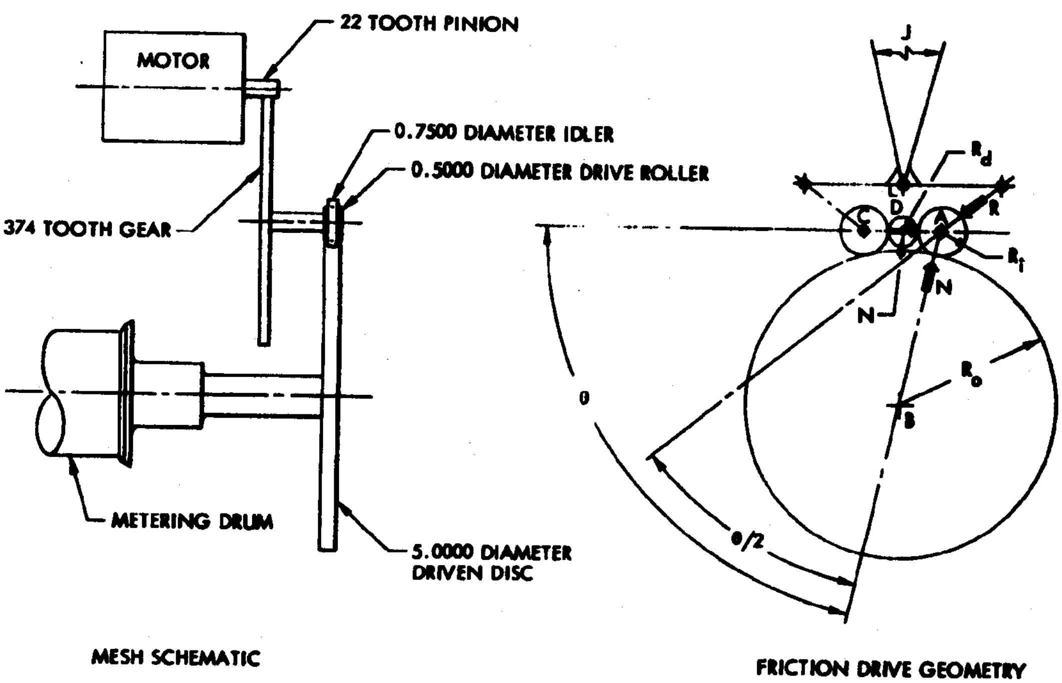

Figure 2.2.5.15 - Metering Drum Drive

roller drives the final friction disc through an opposed set of idler rollers. The final friction disc is keyed to the exposure metering drum which determines the film velocity (5.000 ± 0.050 inches per second) of the system. The friction drive of the final reduction was utilized to eliminate short-term velocity variances which could cause striations on the data film.

- <u>Film Tension Control</u>

  Film tension is controlled (Figure 2.2.5.16) on both the input and output sides of the metering drum. The film tension-control assembly contains an input and an output set of balanced pivoting isolation rollers and three film guide rollers. The input set of isolation rollers (film supply spool control) activates a potentiometer connected to their pivot shaft. A preloaded pair of clock-type springs enable the isolation rollers to pivot as the film-supply tension varies and thus position the potentiometer for a compensating current to the magnetic particle brake. The output set of isolation rollers (film transport drum control) is similar to the input except that a cam is actuated by the pivot shaft to open and close a microswitch which is part of the output tension-control servo loop. The microswitch actuates a duplex friction clutch to change the film velocity as the pivoting rollers reach the limits of a predetermined angular displacement. The output set of isolation rollers (film transport drum control) is

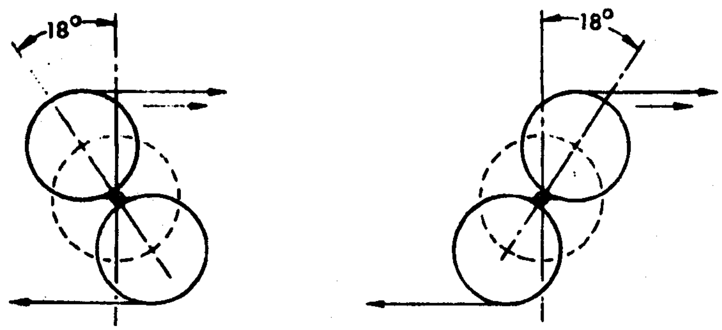

THE SUPPLY SPOOL CONTROL ROLLER ASSEMBLY ACTUATES A POTENTIOMETER WHICH REGULATES THE BRAKING TORQUE OUTPUT OF THE MAGNETIC PARTICLE BRAKE.

INITIAL POSITION (FULL SPOOL) | FINAL POSITION (ALMOST EMPTY SPOOL)

a. FILM SUPPLY SPOOL CONTROL

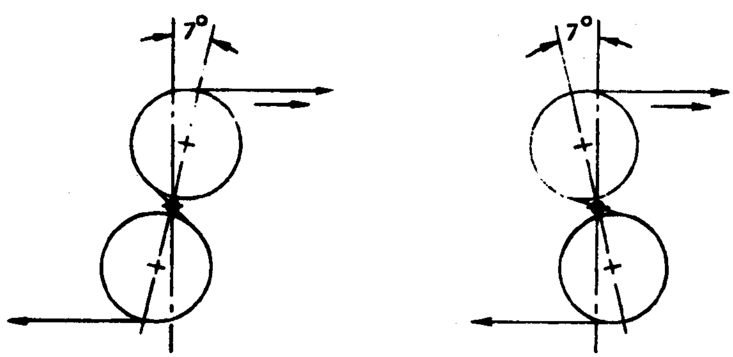

THE FILM TRANSPORT DRUM CONTROL ROLLER ASSEMBLY ACTUATES A MICROSWITCH WHICH SELECTS THE PROPER DUPLEX FRICTION CLUTCH OUTPUT SHAFT FOR EITHER LOW OR HIGH SPEED MESH.

SWITCH TO LOW SPEED | SWITCH TO HIGH SPEED

b. FILM TRANSPORT DRUM CONTROL

Figure 2.2.5.16 - Tension Control Roller Function

similar to the input except that a cam is actuated by the pivot shaft to open and close a microswitch which is part of the output tension-control servo loop. The microswitch actuates a duplex friction clutch to change the film velocity as the pivoting rollers reach the limits of a predetermined angular displacement. The output tension-control servo motor tends to keep the film tension constant (2.0 pounds) on the output side of the metering drum and to isolate the film from changes of take-up tension in the film take-up mechanism.

The output-isolation roller and cam-operated switch operate in conjunction with the film-transport drum drive assembly to control the output tension.

o <u>Film Transport Drive</u>

The film transport drum drive assembly (see Figure 2.2.5.17) contains a hysteresis synchronous motor with an integral 40:1 ratio gearhead with a 200-rpm output. A gear on this output shaft meshes with the input gear on the duplex clutch. This clutch has two independent output gears meshing with 1:1 compounded gears. These gears are in constant mesh with their respective bull gear, one of which has 266 teeth and the other 267 teeth. This one-tooth difference creates a 0.375-percent change in the nominal film velocity to prevent a long-term accumulation of shortening of the film between the exposure metering drum and transport drum for proper isolation roller

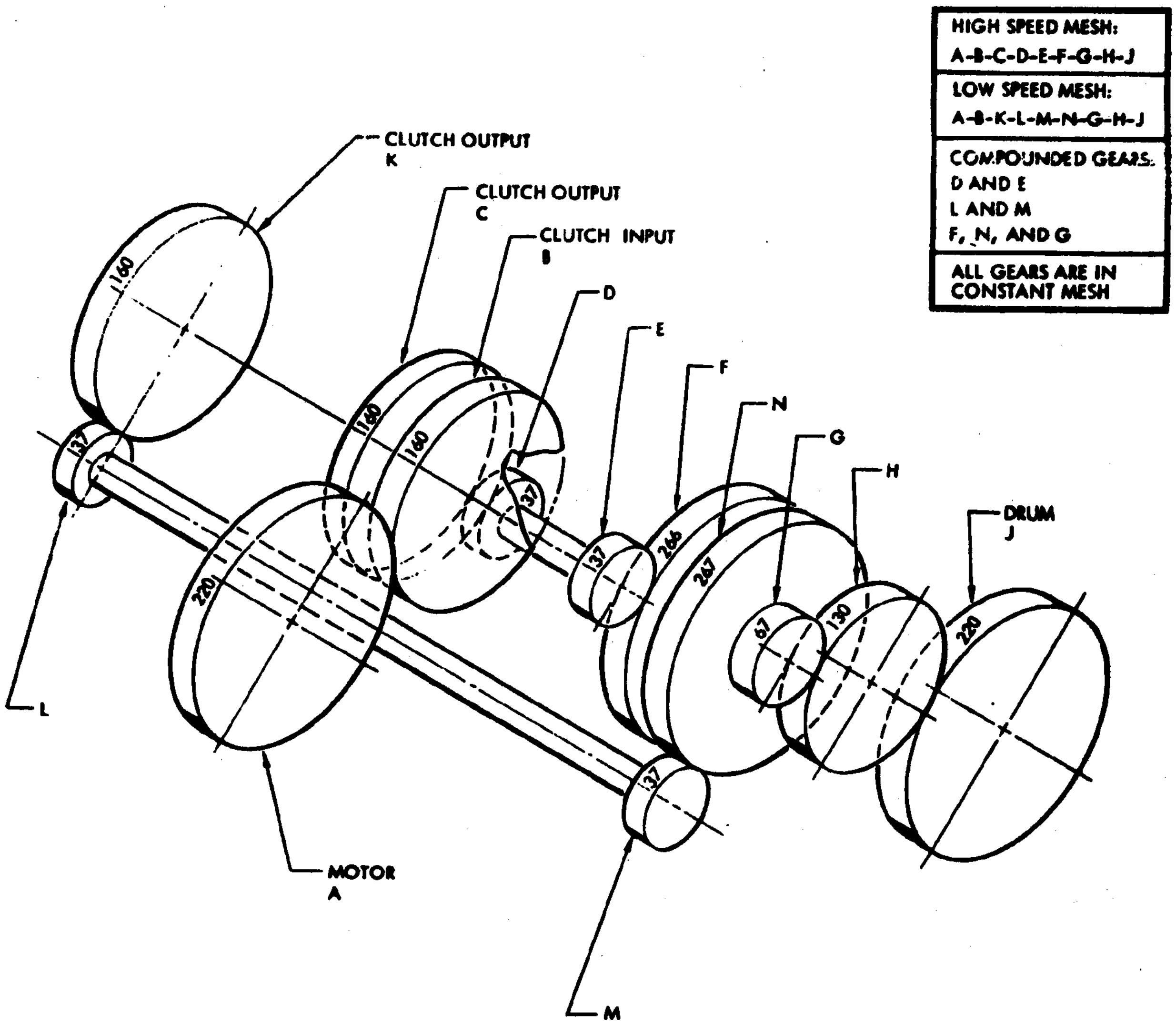

Figure 2.2.5.17 - Schematic of Transport Drum Drive

operation. The two bull gears are compounded on the same shaft with an output pinion gear which meshes with an idler geat which in turn meshes with the transport drum drive gear. As the duplex clutch is energized or de-energized by the micro-swich on the output isolation roller, the power flow is directed through the appropriate gear train to increase or decrease the transport drum velocity. The idle gear train remains in mesh and freewheels in the same direction as it does when it functions as the power train.

o <u>Film Takeup</u>

The film takeup system was contained in the GFE capsule, which is described in Paragraph 2.3.2.10.

<u>Electrical</u>

<u>Operation</u> The operation of the electronic portion of the Recorder will be described by breaking it down into five major divisions: ramp generator, deflection amplifier, focus and intensity circuits, video and vertical-position amplifiers, and magnetic brake amplifier.

o <u>Ramp Generator</u>

The ramp generator (Figure 2.2.5.18) produces a linear voltage ramp which is proportional to the slant range to the target. The accuracy and stability which is required of the output wave form is provided by a stable, high-gain, d-c

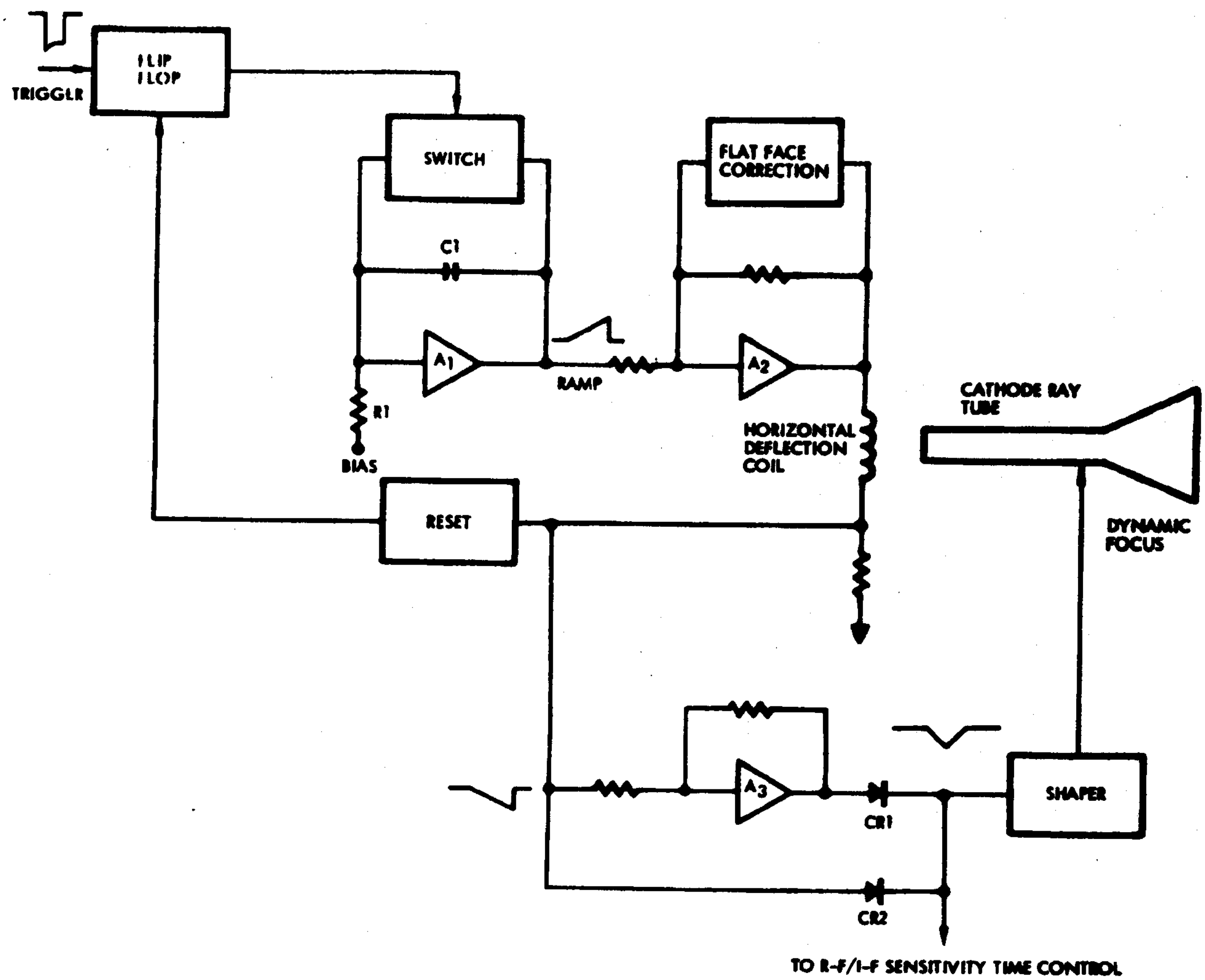

Figure 2.2.5.18 - Recorder Sweep Circuits

amplifier-integrator and controlled bias current.

The sweep trigger causes the bistable multivibrator (flip-flop) to open the switch across integrating capacitor C_1 in the feedback circuit of A_1, which is a three-stage, high-gain d-c amplifier (gain approximately 50,000). This allows the capacitor to charge through R1 and a stable and precise charging current is developed by the bias supply. An internal r-c feedback loop within the amplifier A_1 serves to further stabilize and maintain linearity of the wave form.

- <u>Deflection Amplifier</u>

  The rising linear output from the ramp generator is fed to the deflection amplifier A_2. This amplifier is a stable, high-gain, d-c feedback amplifier that provides deflection signals to the crt yoke. Nonlinear feedback is provided so that the amplifier gain may be varied as the crt spot is deflected from the center of the tube, thereby compensating for the non-linearity introduced because of the flat face of the crt. The nonlinear feedback network which produces the so-called "Flat-Face Correction" is a symmetrical one using diodes (eight) and resistors to provide a linear sweep throughout the entire range. The deflection-amplifier output is used to reset the bistable multivibrator thereby cutting off the sweep and preparing the ramp generator for the next sweep cycle.

o **Focus and Intensity Circuits**

The Recorder crt focus and intensity unit is comprised of two separate functional circuits which provide dynamic focus and a crt intensity gate.

The crt exhibits spot defocusing at the sweep extremities caused by the flat-plane display surface and resulting beam-path length differences. This defocusing effect is eliminated by generating a dynamic focus signal which has a parabolic wave shape and feeding it to the focus anode of the crt.

The required focus control signal must be symmetrical about the sweep center and is derived from the deflection current wave form.

As the deflection signal is symmetrical about zero, the negative portion is passed through diode CR1 and inverted by amplifier A . The positive portion is passed through diode CR2 and added to the inverted signal to provide the V-shaped signal. This signal is used in the R-F/I-F unit as a stc signal. This V-shaped signal is also fed to a biased diode circuit which gives a parabolic shape to the slopes of the V. The parabolic V-shaped wave form is in turn applied to the two-kilovolt focus anode voltage source to compensate for the defocusing at the extreme portions of the sweep.

The crt display is held blanked off at all times except during a deflection sweep. The deflection drive signal generates a voltage gate. This voltage gate signal is fed to the crt cathode, unblanking the crt during the sweep time and intensifying the sweep to the desired viewing level.

- Video Amplifier

The video amplifier, which has a 10-kc to 12-mc 3-db band width, accepts the video output from the Reference Computer and linearly amplifies up to outputs of 6 volts peak-to-peak. For output signals greater than this value, limiting is done by a diode bridge which reduces the gain of the amplifier and prevents excessive swing of the crt grid. The gains in the system, however, are chosen to allow most of the limiting to be done by the data film rather than by this video circuit.

- Magnetic Brake Amplifier

The magnetic brake amplifier assists in maintaining a constant film tension as the film is passed through the input isolation roller assembly. This is achieved by using a d-c feedback amplifier whose load is the magnetic particle brake coil and whose input is approximately proportional to brake tension. This input is from the potentiometer which is mechanically coupled to the isolation-roller assembly so that as the tension is increased, the current is decreased in the brake coil, thereby decreasing the drag and compensating for the change in tension.

2.2.6 Test

The testing which was conducted on a system basis is described in Paragraph 2.3, following. The most significant problem area associated with the testing of the radar payload was in the breakdown of high voltage in a vacuum environment, which was discussed in Paragraph 2.1.7 above. Further details of the testing and associated problems involving the radar payload units are given in the above referenced Goodyear Aerospace Corporation report.

2 .3 Test

2.3.1 Test Philosophy

2.3.1.1 The incorporation of a radar system into a satellite vehicle, while not involving any fundamentally new tenets of a good test philosophy, did necessitate a carefully planned test sequence, guided by certain basic considerations which are an integral part of a proper testing approach. It is the purpose of this discussion to consider, in retrospect, the test philosophy parameters which were implicit in the handling, test and flight preparation of vehicle 2355, and in so doing, to attempt to bring to focus and to record the elements of an effective test philosophy. The launch and orbital performance of this vehicle, or any vehicle, are the result of the design, manufacturing, engineering, test, handling and pre-launch checkout efforts of large numbers of personnel. The resulting quality of performance of the vehicle is therefore determined, incrementally, by each of these endeavors.

2.3.1.2 The roles of the testing organizations in the preparation of a satellite vehicle are to fulfill several very specific requirements, among which are:

a) Prove by <u>demonstration</u> that the hardware, as designed, will <u>perform as expected</u>.

b) Establish, by <u>sufficient operation</u> in the correct test environment, that the hardware will survive and has <u>adequate reliability</u>, when operating as a system, to satisfactorily accomplish the mission requirements.

c) Establish the functional compatibility of all systems and subsystems in all possible operating modes, including specifically the assigned mission.

d) Conduct a mission simulation with the complete launch system in the launch environment.

e) Finalize the flight preparations and conduct the countdown.

The foregoing building block approach to testing, if it is to be thoroughly objective, can accept no prior conclusions as to inherent quality. These conclusions as to quality may be the product of a number of identical or similar systems operations, resulting in some modifications to the test approach on later vehicles, as opposed to the utmost rigour on the first vehicle. The sequence, described above in general terms of the requirements to the test organisations, is more explicitly defined by these respective examples:

a) Proving the design involves principally component or unit tests to exercise every design function to the design tolerances. This was accomplished on every Goodyear Corporation payload unit, as a first article. Tests on each succeeding unit utilized the design approval test parameters to the maximum extent realistically possible.

b) Proving the hardware survivability, repeatability and reliability includes vibration, thermal and vacuum component testing. This was done on the payload unit level in accordance with LMSC 6117D - Environmental Specification. It also fundamentally involves extensive, repeated operation in accordance with the mission profile. This was done at ambient as a satellite system and in a thermal-vacuum environment with the payload vehicle.

c) Establishing the subsystem and system functional compatibility in all modes involves the operation of every possible electrical and mechanical function in all normal and failure mode combinations. This was done on a payload vehicle basis in the test laboratory, and on a satellite vehicle basis in the first systems test, in the Anechoic Chamber, in the second systems test and in the launch complex simulated flight.

d) The mission simulation in the launch environment provides a cross check against all previous testing, wherein a deficiency may have been obscured by virtue of a different test environment, but more importantly, it completely revalidates the satellite system at a late point prior to launch and establishes a new benchmark of confidence in being ready to enter the launch countdown. This test - the pad simulated flight - must produce performance which is completely beyond question or compromise before the vehicle can be considered ready to enter the launch countdown.

e) The launch countdown establishes the flight configuration (propellants, gases, power and guidance settings and program peculiar command and control/payload configurations), rechecks the performance as established during pre-launch tests, and results in lift-off of a flight ready system.

2.3.1.3 The application of this test philosophy therefore produces two primary results:

a) A rigorous proof by demonstration that the design is correct and compatible for the operations of the assigned mission, that the manufactured and assembled system is in strict accordance with the design, that the design and hardware together are compatible with and correct for the operating environment, and that the system reliability is adequate for the mission.

b) The launch of a system which is determined to be flight ready as a result of all prior testing and as a result of a complete and correct system operation in the launch environment.

Each of the above results are necessary if a satellite system is to be realistically considered flight ready. A good test philosophy does not challenge the design - the task is to validate the design. In so doing, it must be able to reveal and identify design weakness or functional incompatibilities. The test sequence is not intended to establish qualification status or provide reliability data for the components, but it must be able to establish system reliability - in a manner which is not possible on a component basis.

2.3.1.4 The test sequence on Vehicle 2355 is discussed against the guidelines of the previous paragraphs - in terms of particular examples where applicable.

The test philosophy attempted to preclude any payload component or system failures by requiring each payload component to pass an Acceptance Test Procedure immediately prior to installation. Each item of LMSC furnished power conversion equipment (inverters, converters, junction boxes, etc.) was installed after a determination that the item had successfully passed the required acceptance tests. The wiring was checked, pin to pin against the wiring drawings, during which manufacturing errors were corrected. The payload as a system was thus brought to a point of readiness for power application. Power loads were applied and measured in increments, and system functional utility was determined - item by item - as further described in succeeding paragraphs.

This approach to establishing correct system operation on a subsystem by subsystem basis was maintained throughout the test span, wherein the system would be exercised first in sequence of testing and recording the engineering parameters in all modes, then proceeding into the operational configuration for operation in all modes. The significant differences between these types of tests are tabulated in the following examples, which assist in the description of the test philosophy.

	Test Item	Engineering Tests	Operational Tests
(a)	Power and Loads	Shunt Boxes - Breakout Boxes and Test Cabling allowed.	Flight Configuration only.
(b)	Unregulated Voltage Range Testing	Electronic Power Supply utilized.	Flight Batteries & Flight Cabling only - Mission simulation.
(c)	Telemetry Checks	Test Plug Hardline Monitoring.	RF Telemetry Links only.
(d)	WBDL Evaluation	RF Coax Monitoring.	RF Link monitoring.
(e)	Command System Checkout	Umbilical and Hardline Command Control.	RF Command Link.
(f)	Orbital Programmer Test Mission.	Test Tape Program.	Flight Tape Program.
(g)	Satellite Vehicle Test	Breakout Cables - Test Complex C-12	Anechoic Chamber - Flight Configuration.

The 2355 test sequence progressed through the detailed engineering tests required to validate the systems functional performance. The principal tests which are termed engineering tests are:

- Payload Laboratory - [redacted]
- Preparations for Altitude Test - Temperature Altitude Chamber
- Preliminary Systems Test - Complex C-12
- Final Systems Test - Complex C-12
- Pad Horizontal Simulated Flight - VAFB 75-1-1

These tests were in some cases conducted in an engineering (breakout) configuration, instead of a more complete operational configuration, as a result of security requirements (Preliminary and Final Systems Tests and Pad Simulated Flight) and because of physical handling limitations (Pad Simulated Flight). In each test of this type, the extent of the required compromise from the operational configuration was carefully evaluated to determine the effect on the test validity.

As a result of the fact that many tests are of necessity conducted in less than the full operational configuration, certain tests were included in the 2355 test sequence which were in the complete operational configuration, to the extent possible. These tests validated the total system, specifically including those interfaces which were non-operational in the engineering tests. These tests are listed and described as follows:

Test

(a) Anechoic Chamber Test (2355 and 2356)

These two vehicles, of identical configuration, were tested in the Anechoic Chamber. Vehicle 2356 was tested prior to the 2355 flight.

Configuration

Flight Batteries
Radar Antenna installed
Flight Cabling
Test Program and Flt. Program (Orbital Pgmr.)
RF Air Link Commands
RF Air Link Data
Flight Pyro Simulators
No Test Plug Umbilicals
No Main Umbilical
Gas Supply - Gas Valve Operation

Results

System compatibility was demonstrated - operating in an orbital configuration.

(b) **Temperature-Altitude Chamber**	**Configuration**
This test operated the payload vehicle in an orbital environment of temperature and altitude programmed in accordance with the mission.	The payload vehicle was in an orbital configuration forward of Sta. 228, excepting for pyros and flight battery. **Results** The temperature altitude testing produced repeated failures of the payload components, which are further discussed in Para. 2.3.2.5. These failure items were redesigned accordingly. The payload vehicle, after multiple component redesigns and component retests, operated through the programmed mission without failure. The payload vehicle was subjected to extensive, repetitive testing - through a failure regime until repeated <u>successful</u> operation was achieved.
(c) **R-3 Launch Stand Payload Vehicle Test**	**Configuration**
This test followed the pad simulated flight.	Complete flight configuration, including batteries and pyros, but prior to final attachment of the radar antenna. **Results** This test successfully exercised every interface function, power, ground, data circuit and command circuit between the payload vehicle and the Agena. It validated the final flight configuration of flight batteries. In the course of performing every payload function, the entire satellite vehicle was essentially validated in the launch configuration.

2.3.1.5 The Associate Contractor (Goodyear Aerospace Corporation) performed a vital role in the test series on this vehicle. An initial procedure was established for acceptance of payloads from Goodyear which involved the participation of LMSC personnel in the final

Acceptance Test Procedure on each system. The data was then reviewed jointly, together with the final deliverable hardware status. Based upon these results, the System Associate Contractor recommended hardware acceptance to the Air Force, or as circumstances dictated, recommended further action and another payload system test prior to acceptance. After receipt of the payload at LMSC, a unit Acceptance Test Procedure was conducted on each payload unit as a final validation on the box level prior to installation in the payload vehicle. Joint responsibilities were defined and documented, briefly as follows:

a) Goodyear maintained responsibility for all payload units when not installed in the payload vehicle, and established an acceptable test status just prior to installation.

b) Goodyear participated in all tests which involved any operation of the payload, during which veto power was in force as to continuance of each test.

c) Goodyear and LMSC jointly conducted test data evaluation and reached a joint determination on test acceptability.

d) Lockheed maintained responsibility for all systems operation, including the operation of the system test equipment.

e) System log books were maintained by Lockheed and individual payload unit log books were maintained by Goodyear. Lockheed Quality Assurance was responsible for both payload and system while at Lockheed facilities.

f) Lockheed provided all necessary support for the Goodyear field operation.

g) Neither system testing nor unit testing were to be conducted unless both contractors were present.

The foregoing operating procedures were defined in a letter dated 8 November 1963, Subject, "Operating Procedures and Responsibilities for the Conduct of P-21 Checkout and Testing".

The Goodyear personnel were included, as a normal function, in all System Associate Contractor-technical reviews, staff meetings and routine testing planning and status meetings. The result of the early planning efforts and of the integration techniques evolved between Lockheed and Goodyear, were very effective and compatible working relationships. It is considered that the Goodyear participation in the testing, and the complete support of the test philosophy described herein, were essential elements in reaching a flight-ready status and in the successful conduct of the mission.

2.3.1.6 Summary

The prior discussion outlines the applicable test philosophy. The implementation of a proper test philosophy involves the intangible aspect of an understanding of the philosophy, and mental acceptance of the objectives, by the personnel accomplishing the tests. Adequate test planning and test execution require stringent disciplines to avoid the acceptance of questionable or unverified results, and the necessity to be sufficiently thorough and methodical to guarantee completeness. In short, testing requires experts in the field, properly trained, experienced and motivated. Certain parameters are considered significant enough to warrant specific identification:

a) Detailed, documented planning, expressed in completely unambiguous terms.

b) Thorough understanding of the technical aspects of the systems involved - termed professional competence.

c) A thorough and direct understanding of that status which is correctly termed launch-ready for a satellite system.

d) The mandatory requirements that each system be operated in the orbital configuration - through representative times and cycles - in the orbital environment - as realistically as is possible.

e) A step by step subsystem to system validation process (building block approach) wherein the thorough engineering tests involving the demonstrated and recorded performance of every design parameter are followed by progressively more complete and realistic operational configuration tests.

f) Rigid configuration control of the components, subsystems and systems, as progressively validated.

The planned and actual test sequences on Vehicle 2355 are further discussed in the remaining sections of Para. 2.3 together with the results. The planned test sequences for Sunnyvale and Vandenberg AFB are pictured in sequential block diagram form in Summary Figures A and B respectively, pages 3-12 and 3-13. Summary Figure C, page 3-14, shows the actual test sequence insofar as it differed from the planned sequence.

~~SECRET~~ SPECIAL HANDLING

AC 04306

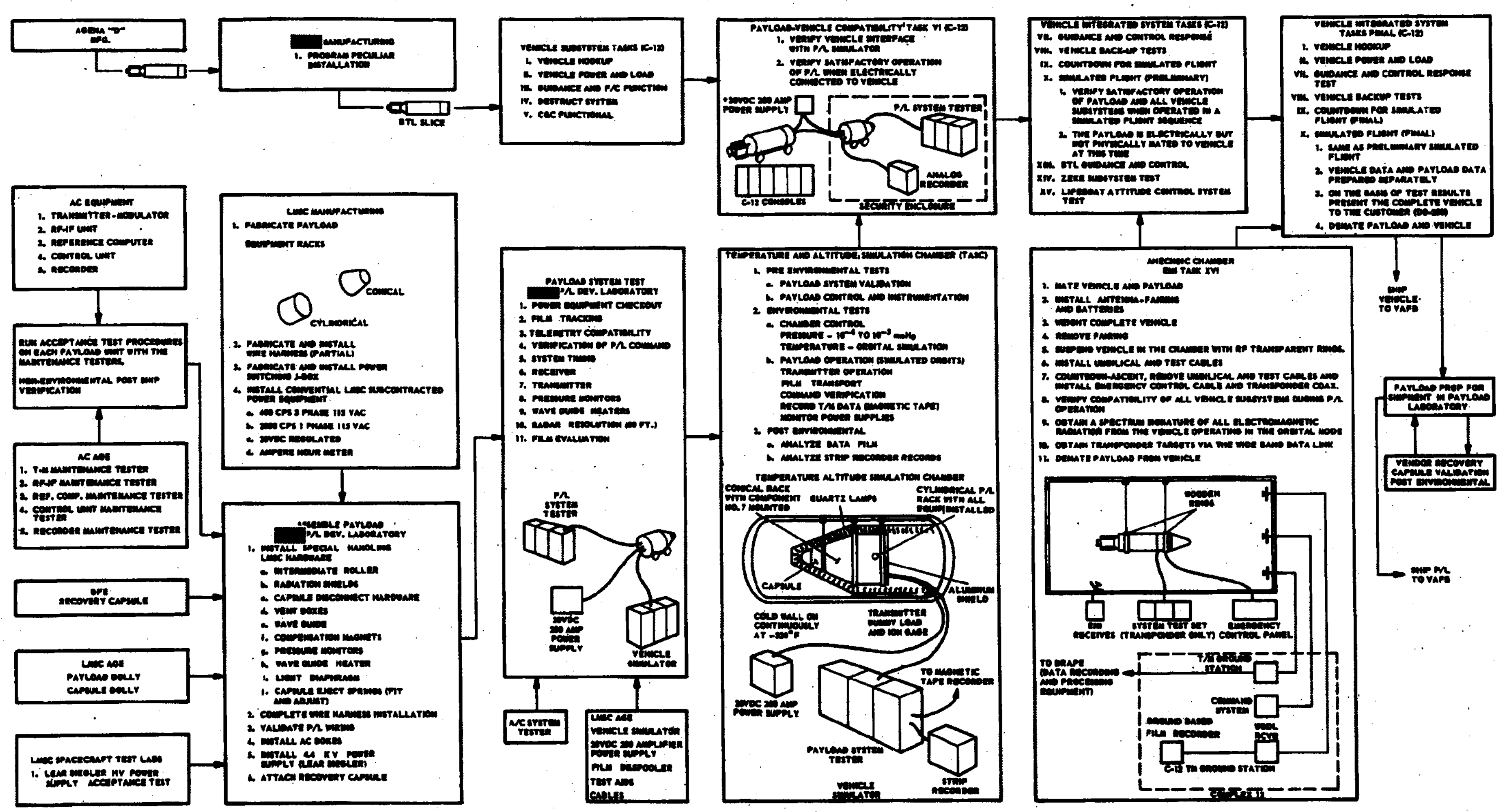

Summary Figure A

~~SECRET~~ SPECIAL HANDLING

NRO APPROVED FOR RELEASE
DECLASSIFIED BY: C/IART
DECLASSIFIED ON: 9 JULY 2012

~~SECRET~~ SPECIAL HANDLING

AC 06306

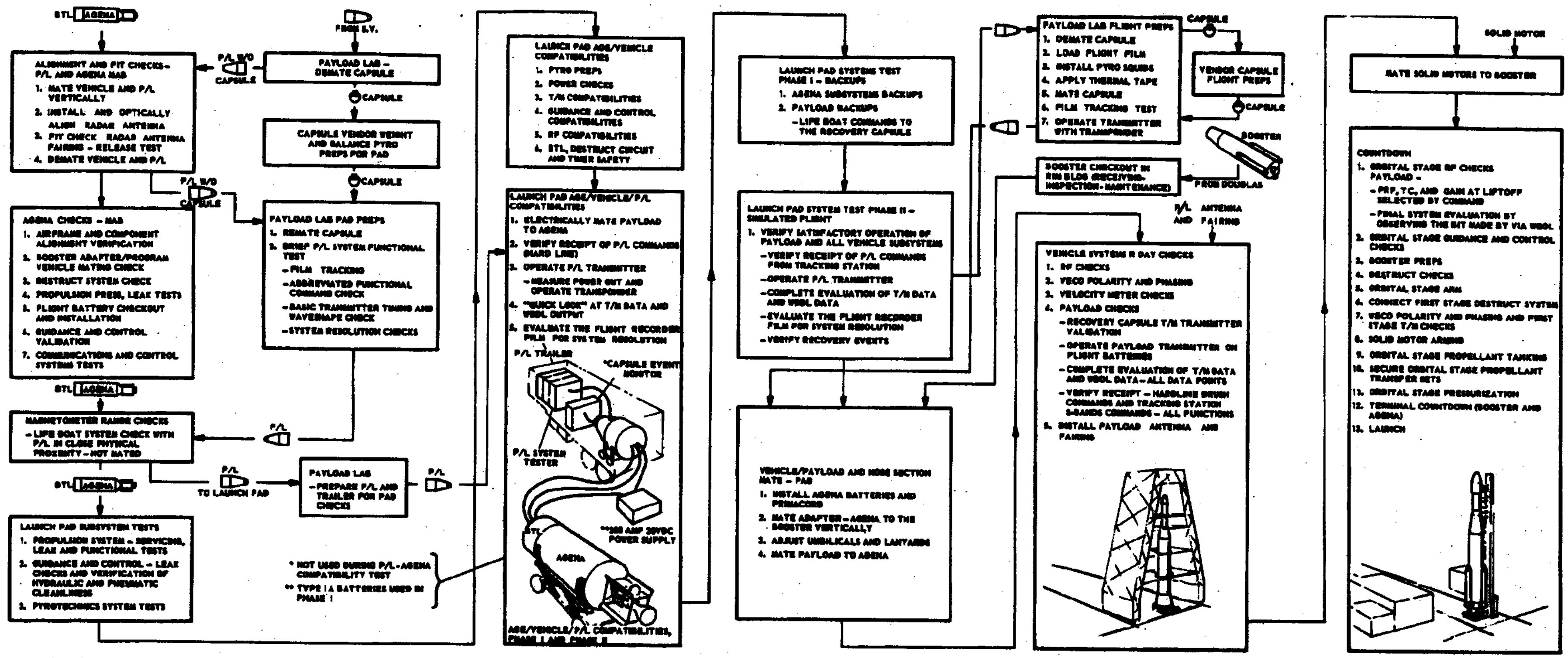

Summary Figure B

3-13

~~SECRET~~ SPECIAL HANDLING

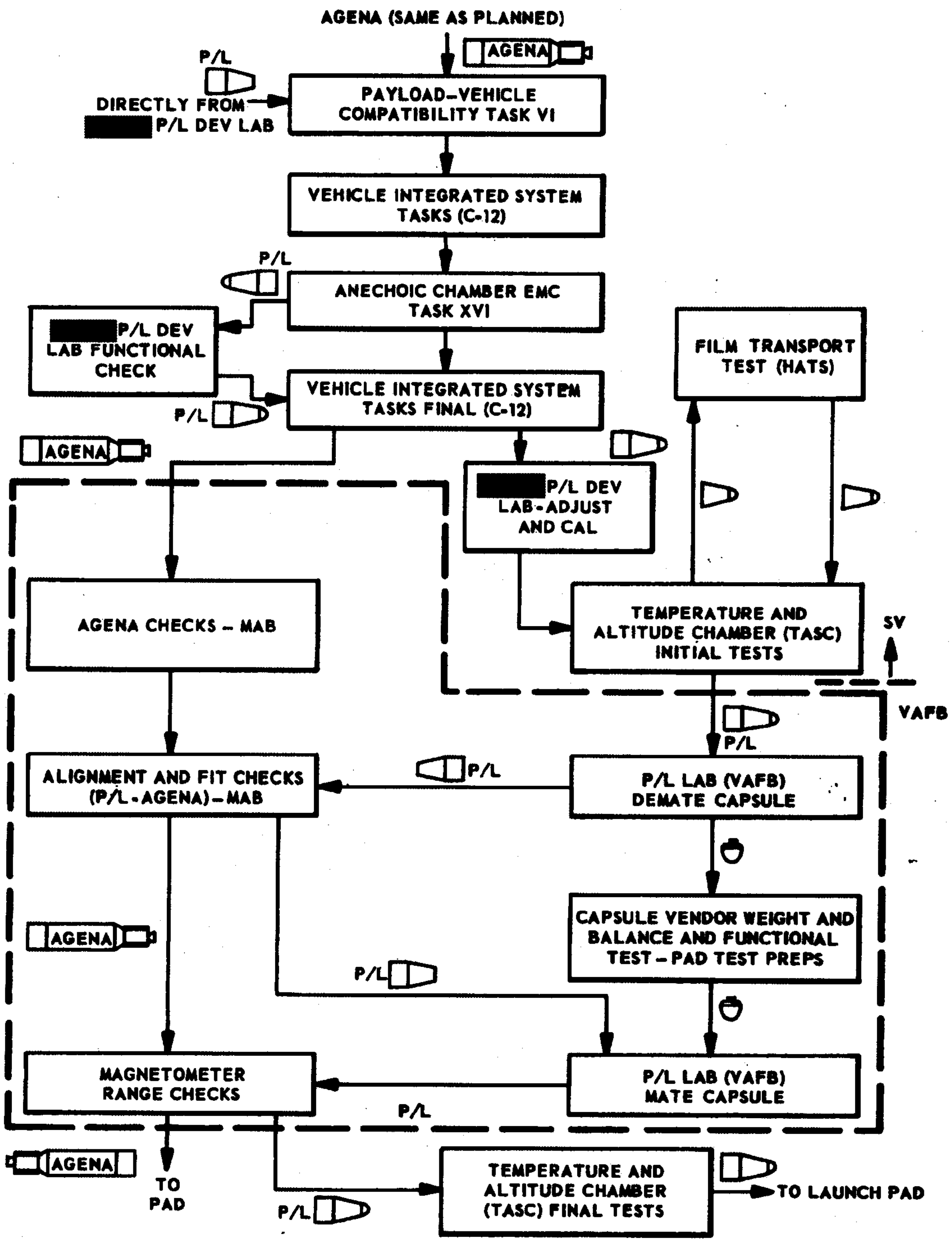

SUMMARY FIGURE C

2.3.2 Payload Vehicle Testing

Summary

The payload tests defined in the Planned Test Sequence (Para. 2.3.3 of this Section) were completed and the primary objectives met. The scope of testing was enlarged to include a special test of the film transport system in a vacuum environment (HATS). Testing order was altered to permit downstream testing to continue, where practical, during periods when a complete set of flight components were not available.

Malfunctions of payload components in the temperature and altitude chamber (TASC) during the Qualification payload tests and Vehicle 2355 payload tests caused the TASC tests to be altered, repeated and the start and completion to be delayed. (Refer to Para. 2.3.3 of this Section). The final TASC run was a complete and continuous test which verified system compliance to all of the initial objectives.

Payload compliance to specifications was demonstrated in the following configurations:

a) Payload Vehicle System (Non-environmental)
   - o Power supply simulating flight batteries.
   - o Test console simulating Agena commands and radar targets.
   - o Vehicle telemeter simulator monitoring telemeter signals.
   - o Transmitter terminated in a dummy load.

b) Payload Vehicle System (Environmental)
   - o Basic equipment used same as Item a) above with the payload in a simulated orbit pressure and tempera-

ture environment.

c) Agena - Payload Integrated Systems Tests (Non-environmental)

- o Payload electrically, but not mechanically mated to the Agena.
- o Power supply simulating flight batteries.
- o Commands from the Agena (hard line from test complex).
- o Telemeter and "hardline" data used to evaluate system performance.
- o Transmitter terminated in a dummy load.

d) Agena - Payload System (Anechoic)

- o Payload electrically and mechanically mated to the Agena.
- o Payload radar antenna installed and transmitting.
- o Power supplied by flight type batteries.
- o Commands from the Agena (air link from test complex).
- o Telemeter (air link) data used to evaluate system performance.
- o Payload data by air link to ground receiver and recorder.
- o Emergency control and monitoring maintained with a minimum number of electrically isolated hardlines.

e) Agena - Payload System (Launch Pad Horizontal)

- o Payload electrically but not mechanically mated to the Agena.
- o Power supply simulating flight batteries.
- o Commands from the Agena (air link from tracking station).
- o Telemeter (air link to ground station) and hardline data

used to evaluate the performance. (Telemetry and payload video data).

- o Recovery capsule energized and evaluated.
- o Transmitter terminated in a dummy load.

f) Booster - Agena - Payload System (Launch Pad Vertical)

- o Payload-Agena-Booster Adapter-Booster mated.
- o Flight batteries installed.
- o Commands from the Agena (air link from tracking station)
- o Telemeter (air link to ground station) used to evaluate system performance.
- o Simulated targets evaluated with the wide band data link only.
- o Transmitter terminated in a dummy load.

At the conclusion of payload testing the following items were out of limits as specified by the Test Procedures:

a) Transmitter power was 0.7 db low.

b) The sensitivity time control (STC) video waveform was 2.2:1 maximum to minimum and should have been a maximum of 2.0:1.

c) Delay from "ON GATE" to the start of STC was 35 microseconds and should have been 31 microseconds maximum.

d) The accelerometer in the Transmitter-Modulator unit was inoperative.

During the TASC tests unexplained transients were observed on the -2KV and +4.5KV power supply monitors. Instrumentation indicated, and analysis verified that the transients on the two power supplies were not related. The 2KV problems was localized to the RF-IF Unit. This unit was removed after the TASC test was completed and operated through a special test at Goodyear. The spiking was determined to be occurring in an output filter capacitor in the -2KV supply and was not of a potential failure nature. The -2KV problem and the four (4) out-of-limits items listed in this section were all acceptable to Goodyear to Lockheed and to the Air Force as flight worthy conditions. The +4.5KV transients appeared in the first four (4) of the thirteen simulated orbits in the TASC test. They did not appear in the last nine simulated orbits in TASC or in any of the subsequent testing. Refer to Par 2.1.2 and Par. 3.1 of this report for a more detailed discussion.

2.3.2.1 [redacted] Payload Development Lab, Lockheed

a) General

The payload system was assembled and checked out in the [redacted] payload development lab at Lockheed-Sunnyvale. Components of the payload system were obtained from Lockheed-Goodyear and the Recovery System Vendor. Goodyear supplied five (5) flight radar components with mounting hardware and the AGE required to check each component individually and interconnected as a system. A system for recording the wide band data link (WBDL) video was also supplied by Goodyear, termed a ground based recorder. Lockheed provided the payload airframe, flight antenna and waveguide, power conversion equipment, pyro system, compensation magnets and equipment necessary to interconnect, monitor and control the payload system. Lockheed also supplied the AGE required to handle the capsule and payload, a battery simulator, a vehicle telemeter simulator, and payload test aids.

The Recovery System Vendor supplied the recoverable nose section including all of the flight equipment contained within the capsule.

b) Acceptance Tests of Goodyear Components

Goodyear personnel performed acceptance tests on the radar flight components. These components were, 1) Transmitter Modulator (Box #3), 2) RF-IF Unit (Box #4), Reference Computer (Box #5), the Control Unit (Box #6) and the Recorder (Box #7). Each Box had its own Maintenance Tester which was used initially to perform the Acceptance Tests, then retained in the P/L Dev. Lab to troubleshoot and revalidate boxes whenever problems were isolated during subsequent testing. The Recorder Maintenance Tester, in conjunction with a Flight Recorder, was used as a recording system for the WBDL video during integrated system tests. At the conclusion of the Acceptance Tests, by Goodyear, the radar flight components were turned over to Lockheed for installation in the payload airframe and system tests.

c) Payload Assembly

The payload airframe (conical and cylindrical equipment racks) was received from Lockheed manufacturing with the wire harness and the conventional power equipment installed. This conventional power equipment consisted of, 1) power switch junction box, 2) 400 cps three-phase 115 VAC inverter, 3) 2000 cps single-phase 115 VAC inverter, 4) 28 vdc regulated power supply and ampere hour meter. The high voltage (4.5KV) power supply designed and developed for this payload arrived separately and was installed at the P/L Dev. Lab. In addition to the Goodyear radar flight boxes and the high voltage power supply the following major items were installed to complete the payload system, except for the Recovery Capsule:

- o Intermediate film guide roller
- o Waveguide monitor heaters
- o Pressure monitor system

- o Compensation magnets
- o Capsule disconnect hardware
- o Pressure Diaphragm and vent boxes

d) Payload System Test

Configuration - Three basic pieces of AGE were used to power, control and monitor the payload during payload system test. (1) A 200 ampere 28 VDC adjustable power supply simulated the flight battery power; (2) The Payload System Test Set simulated the payload commands from the Agena, provided monitor points and equipment to read out preselected payload parameters, and contained the radar transponder. The transponder was used to generate simulated targets used to evaluate the performance of the system; (3) The last basic console was the Vehicle Telemeter Simulator. This unit was used to monitor the payload telemeter points, provide $\pm$ 28 VDC regulated telemeter excitation and make a continuous recording of the payload power conversion equipment currents and voltages.

The Recovery Capsule was mated to the payload conical equipment rack during payload system test and the film takeup unit energized. The subsystems of the Recovery Capsule not related to the film takeup were not energized and the related commands and monitor points were intercepted or simulated by the capsule simulator which was located in the conical equipment rack.

The transmitter was terminated in a dummy load on the antenna feed waveguide located external to the cylindrical rack skin, during all system tests in the [redacted] payload development lab.

Test - The payload system test in the [redacted] Development Lab was the first time that the payload was operated in the payload airframe utilizing flight wire harness, power conversion equipment and a Recovery Capsule. This test was to be conducted without disassembly of the components of the payload system. If the removal of a box was required to make an adjustment, the testing reverted back to the Payload System Adjustment and Calibration Procedure, which was conducted by Goodyear.

The following is an outline of the payload system tests.

- o Continuity of wire harness per latest released drawings.
- o Hookup
  - Payload to AGE
  - Conical rack to Recovery Capsule
  - Power bus to return resistance check
  - Waveguide heaters functional
- o Power Application
  - Apply power in discrete steps with continuous voltage and current monitoring with galvanometer strip recorders
- o Ampere Hour Meter Test

- Verify at least one step of each of the telemeter outputs

o Film Tracking and Transport

- Verify film tracking from the recorder supply spool to the Recovery Capsule takeup spool

o Telemetry Compatibility Test

- Verify all telemeter signals present and within acceptable limits

o Verification of payload Commands

- Verify each simulated Agena command results in the required payload response

o System Timing Checks

- Basic Reference Computer, RF-IF and Transmitter-Modulator timing relationships and pulse shapes.
- WBDL Sync Pulse Check - pulse shape and timing of the synchronization pulse on the leading edge of the wide band data link video.
- PRF Jitter Checks - measure of the short time stability of the pulse repetition rate.
- Recorder Timing - intensity gate and CRT sweep retrace timing.

o Receiver Tests

- Bandwidth
- Attenuator - measure range of gain adjustments

- Threshold Sensitivity at minimum, maximum and center gain positions
- Dynamic range of the AGC
- Systems Noise level and Sensitivity Time Control Waveform

o Transmitter Tests

- RF power output
- RF spectrum width
- RF pulse width

o Radar Resolution

- Film transport speed
- Azimuth and range resolution

2.3.2.2 Test Complex SCOC-12 (Preliminary Test)

The payload was electrically mated to the Agena using interface extension cables, to permit housing the payload for security measures. A dummy antenna (artificial load) was connected at the payload antenna feed-line interface point on the payload cylindrical section skin, to prevent high power radiation in the complex. Operating power for the Agena and payload was furnished from an external source connected to the internal battery terminals. Range and Azimuth target test signals (artificial targets) were injected through a coax cable from a test transponder. The payload data track (video) information was transmitted through the wide band data link to a receiver in the SCOC and recorded in a ground base recorder (similar to the Payload Box 7).

Subsystems were tested progressively to prepare for a system level test. A complete system test was conducted to demonstrate compliance with specified test requirements, and to verify vehicle/payload subsystem functional compatibility. This system level test was treated as a preliminary verification of the prescribed system performance to insure readiness for a set of simulated orbits in an Anechoic Chamber (radio frequency quiet room). At the conclusion of satisfactory tests, the Agena and payload were moved into the Anechoic Chamber

Payload Preliminary Data Evaluation. Telemetry records and payload data track (film record) were examined and no payload malfunction or payload functional data discrepancies noted that would affect Anechoic Chamber testing (simulated orbits).

2.3.2.3 Anechoic Chamber (Annexed to SCOC-12)

The Agena, Recovery Capsule, Payload, and Payload Antenna were electrically and mechanically mated in the actual configuration for flight. Type 1-A batteries were processed and installed for satellite operating power (these batteries are electrically similar to flight batteries, Type 1-D). Extension cables (approximated 110 feet) were used for umbilicals, test plugs and radio frequency communications between the satellite and SCOC-12. These long cables provided SCOC-12 facilities for satellite check-out prior to T-0 functions, similar to launch pad operations. All launch functions such as operating power, RF links and telemetry were verified as ready for simulated launch. The primary guidance programmer (SS/D) was run to automatic shut-down during removal of the umbilicals and test plugs. A special umbilical cable was installed to control emergency shut-down, guidance attitude control, and the orbital programmer (SS/H) START/STOP. The satellite was then raised to the center of the Anechoic Chamber (30 feet wide, 30 feet high, and 60 feet long) suspended on non-conducting cables. Air-link communications were established between the satellite and SCOC-12 for command control and telemetry by using the Agena mounted antennas and auxiliary antennas. Field strength measuring antennas were installed inside the Anechoic Chamber and cable connected to receivers outside of the chamber. The payload data track (video) information was transmitted through the wide band data link to a receiver in the SCOC and recorded in a ground base recorder (similar to the payload recorder), to simulate on-orbit operation.

Two (2) engineering orbits were run to demonstrate subsystems compatibility and to check all control and monitor functions, with the payload operating (in conjunction with all of the Agena radio frequency equipment) for a full five (5) minute period in each pass. Six (6) standard (same sequence) orbits were run to measure the radiated electromagnetic spectrum signature over the range of eighty-eight (88) to ten-thousand (10,000) megacycles; three (3) orbits for wide band (payload data) transmitter Number One and three (3) orbits for wide band transmitter Number Two. There were no conducted noise measurements or susceptibility tests conducted. Fourteen (14) standard orbits were planned but the satellite was shut down at the end of the eighth (8th) because all required data were gathered and recorded. The payload and payload antenna were demated and the Agena moved back into SCOC-12 for the final system test for DD-250 (Customer acceptance).

NOTE: Vehicle 2356 Anechoic Chamber tests were completed prior to shipping the 2355 payload to VAFB for flight. These tests consisted of seventy-nine (79) simulated orbits in the same electrical and mechanical configuration as 2355, with flight batteries (Type 1-D) installed and run to power depletion. The orbital sequences were those planned for flight and used in the 2355 flight program.

Payload Telemetry Test Data Evaluation. There were no payload malfunctions or payload functional telemetry data discrepancies noted. These data were gathered through the satellite-borne telemetry as in actual orbit. Analysis of the recorded radio frequency spectrum signature radiated from the satellite (including the payload) indicated no potential radio frequency problems on the launch pad or in flight, e.g., malfunctions or degradation of data due to satellite subsystem interactions generated by radio frequency sources.

2.3.2.4 Test Complex SCOC-12 (Final System Tests)

The Agena and payload were restored to the same configuration as the preliminary system tests. Subsystems were rechecked to verify satisfactory operation. A complete satellite electrical-electronics system test was conducted for final acceptance (DD-250) with essentially the same sequence used in the preliminary test (preparation for the Anechoic Chamber tests).

Payload Telemetry Test Data Evaluation. There were no payload functional telemetry data discrepancies noted. Excessive distortion of the payload 400 CPS 3-Phase did affect the Box 7 data track (film recorder) by defocusing the cathode ray tube beam and caused a short sweep, but it did not affect the information transmitted through the wide band data link. The problem was resolved by the installation of the correct power factor correction capacitors.

Non-Flight Components. Payload Box 2 (4.5 KV supply) and Box 3 (transmitter) installed during the system tests were not flight environment (altitude) qualified. These items did not affect interfaces or payload ground test performance, and were replaced with flight qualified units after the final system tests and prior to payload system altitude test.

2.3.2.5 Temperature and Altitude Simular Chamber, (TASC)

The objective of this test was to demonstrate satisfactory payload operation during simulated orbits in a simulated space temperature and pressure environment. The payload system was placed in the chamber (TASC) and the monitoring and control lines brought out through pressure fittings. The test equipment used exclusive of environmental instrumentation was the same as that used in the [redacted] Payload Development Laboratory (Par. 2.3.2.1) plus sixteen (16) channels of Sanborn Strip Recorders. The TASC facility provided temperature recording for thermocouplers and calorimeters used to monitor the payload system. The commutated telemeter signals from the Vehicle Telemeter Simulator were routed to the Data Reduction and Processing Equipment (DRAPE) area, and recorded on magnetic tape. Failures during test, primarily in high voltage components caused this test to cover a total time span of approximately ninety (90) days. Refer to Par. 2.3.3-Test Schedules, Planned vs Actual. During this period the test procedure was revised; however, the scope of the test did not change significently; for this reason the outline of the final procedure is shown here and the chronology of the tests is defined in Par. 2.3.3, Test Schedules.

a) Payload Hookup

- Suspend the payload in the chamber
- Payload to AGE
- Power bus to ground resistance check

- Transmitter terminated in a dummy load located in the environmental chamber

b) Pre-environmental Confidence Check

- Apply power with continuous recorder monitoring.
- Verify all telemeter points present and are being recorded by DRAPE.
- Verify receipt of commands to the payload.
- Measure transmitter power pulse width and basic timing
- Measure receiver noise level and sensitivity time control (STC) wave-form.
- Insert a transponder signal and timing signals into the payload for resolution and speed checks.
- Remove the payload system from the chamber; remove the film and reinstall the payload in the chamber.
- Evaluate the film for range resolution and speed.

c) Simulated Pre-launch and Ascent Checks

- Simulate an orbital pass at ambient pressure with full instrumentation for reference data.
- Heat the waveguide.
- Pump down the chamber to 10^{-5}mm Hg.
- Start thermal simulation.

d) Simulated Orbital Passes (Typically as follows)

- Warm-up on by the System Tester

- Pre-operate - after 300 seconds.
- Operate On - after 30 seconds additional.
- The entire payload commanding capability was now exercised, through one or more orbits including:

  All altenuation Positions (Gain Steps)

  All PRF Steps

  Clutterlock Short and T.C. #1, T.C. #2

  Built-in-Test
- All payload power measurements were taken - including transmitted power.
- Range targets were simulated.
- System timing measurements were made.
- Time Delay Override was tested.
- Operate OFF - maximum of 630 seconds after warmup on.

e) Evaluation - Following each of the orbital simulations, the data (except film) was evaluated during the delay period between orbits. The film data was processed to a controlled gamma following removal of the payload from the chamber, and was evaluated on a light table and in an optical correlator, to determine quality and resolution.

f) Problems - The total series on the payload in the altitude chamber was principally characterized by repetitive failures of high voltage components. This test period included the span from 9/3/64 to 12/2/64. The failed payload components included primarily the high voltage components in the transmitter. Altitude testing had previously been in progress on the Qualification System (Payload System #1) since earlier in 1964 (April - May) and had resulted in numerous failures. As a result of these failures on the Qualification System, Goodyear had instituted corrective action on high voltage breakdown control which had been incorporated into the payload for 2355. The details of the failures-type and corrective action-are available on the Goodyear Report AKP-II-596, Volume I.

Summary of TASC Testing.

The payload vehicle to Agena interface was thoroughly validated during the C-12 tests and the Anechoic Chamber tests, as described above. The TASC testing was continued through a time period which permitted incorporation of all final engineering changes into the radar payload by Goodyear, and through extensive altitude testing these changes were validated. The wisdom of the continued testing at simulated altitudes was reaffirmed during the mission-on orbit.

2.3.2.6 VAFB Simulated Flight

The payload was electrically mated to the Agena using interface extension cables, to permit housing the payload in the payload transporter van for security measures. A dummy antenna (artificial load) was connected at the payload antenna feed-line interface point on the payload cylindrical section skin, to prevent high power radiation in the van and for security measures. Range target test signals (artificial targets) were injected through a coax cable from a test transponder. Operating power for the Agena and payload was furnished from an external source connected to the internal battery terminals. Payload data track (video) was transmitted to VTS-1 (Vandenberg Tracking Station, also known as COOKE), and VAFB Bldg. [redacted] through the wide band data air-link for recording in ground base recorders (similar to payload Box 7). Agena and payload telemetry data were transmitted through an air-link to VTS-1 and VAFB Bldg. [redacted]. Real time commands for the Agena and payload were transmitted through an air-link to the launch pad from the VTS-1 PRELORT Radar (a distance of approximately 7 statute miles). During preparations for the simulated flight, a test was conducted to insure compatibility of the AGE/Agena/Payload interface/VTS-1. Phase One (1) of the simulated flight consisted of the back-up functions programmed to occur in case of primary function failures. The prime source of recovery command initiation was the VHF ZEKE secure link. The capsule recovery sequence was exercised, i.e., arm, transfer and descent sequence. The simulated flight test (Phase Two) was conducted in the sequence of terminal count-down with umbilicals and test plugs, removal of umbilicals and test plugs, ascent, orbit sequences with payload operating, initiation of recovery sequence (capsule arm-transfer pyrotechnic firing signal). All payload real time and stored time commands were exercised. This demonstrated compatibility of the integrated satellite system comprised of the booster, Agena, payload and VTS-1 in a simulated launch and flight sequence. After successful conclusion, the payload and capsule were returned to the payload area in VAFB Bldg. [redacted] for flight servicing.

Payload Performance Evaluation. There were no radar payload malfunctions or payload functional telemetry data discrepancies noted that affected performance or data gathering. During the simulated flight, a noise was heard in payload Box 7 which was determined to be a defective bearing in the film supply spool; this was replaced in the payload area (Bldg. [redacted]).

Capsule Performance Evaluation. The capsule recovery sequence was not exercised in Phase Two of the simulated flight due to the test configuration of the interconnects. The guidance programmer (SS/D) actuated transfer signal, which was correctly programmed on for two (2) seconds in flight, was test-harness wired through the capsule battery circuits (in place of squib activated batteries) to the recovery programmer. This programmer requires 28 VDC for more than 2600 seconds to complete the recovery sequence. However, the guidance programmer (SS/D) removed the 28 VDC in 1.96 seconds which stopped the recovery sequence. Satisfactory performance was demonstrated during the back-up tests. The normal configuration (flight configuration) would incorporate flight batteries which are squib activated. The application of 28 VDC for 1.96 seconds to this circuit would activate the batteries and the batteries would then supply power to the recovery programmer. The test configuration, which did not include batteries, therefore only started the programmer and kept power on for 1.96 seconds. Telemetry monitors (two) verified that power was applied across the interface. The programmer operation was subsequently verified completely.

2.3.2.7 Special Project Laboratory - Lockheed, VAFB (Bldg. [redacted]

General - The primary use of this area was for flight preparation of the payload system. These preparations required work in the following general areas:

a) Incorporation of all outstanding unaccomplished work which preceded flight preparations.

b) Demating and remating of Recovery Capsule for flight preparation.

c) Installation of flight, final hardware such as access door screws, mating bolts and compensation magnets.

d) Pyro circuit checkout and squib installation.

e) Final preparation of thermal surfaces.

f) Installation of flight film and batteries.

g) Payload functional system test.

After the launch pad system test, Phase II, Simulated Flight was completed, the payload system was returned to the laboratory. The RF-IF Unit A400-3 was removed and sent to the Goodyear facility at Phoenix to investigate transients on the -2 KV power supply.

A special check of the Recorder A700-3 was made and the source of a noise discovered during launch pad system test, Phase II, simulated flight was isolated. A maladjustment of a bearing on the support shaft for the recorder film supply reel was the cause. The shaft and the bearing were replaced.

RF-IF A400-3 was returned from Goodyear and reinstalled in the payload system. Because the RF-IF had been removed, a special validation test (Special Test Procedure 2355-7) was performed. At the completion of STP 2355-7 the laboratory portion of the Flight Readiness Test Procedure (V2000303) was completed and the payload system moved to the launch pad.

Special Test Procedure (STP-2355-7) - The objective of this test was to re-validate the payload system after the RF-IF unit was reinstalled.

The configuration for this test was similar to the [redacted] P/L Development Laboratory tests. Breakout boxes and a power monitor console with a galvanometer recorder were used in place of the Vehicle T/M Simulator. With this exception the other basic consoles were the same as used in the [redacted] P/L Development Laboratory.

The following is an outline of the checks that were made:

a) Hookup
  - o Payload to AGE
  - o Power bus to return resistance check

b) Power Application
  - o Apply power with continuous voltage and current monitoring with galvanometer strip recorders.

c) Telemeter Points
  - o Measured the value of a few critical T/M points.

d) System Timing Checks
  - o Transmitter timing

e) Receiver Tests
  - o Video level and limiting

- o Attenuator - measure range of gain adjustments
- o Threshold sensitivity
- o Dynamic range of the AGC

f) Transmitter Tests

- o RF Pulse Width
- o RF Power output - measured at the cylindrical section skin with an accurate waveguide configuration.

Payload Flight Readiness (V2000303) - The main objectives of this test were to: checkout and load the pyro system; verify film tracking speed and target resolution; load flight film and expose the head end with reference targets and make a reference measurement of the transmitter RF output power.

The configuration for this test was identical to the STP 2355-7 test except for some of the test equipment used to measure the transmitter output power. This test utilized the same configuration for measuring transmitter output that was required during the subsequent checks (R-3 Day) at the launch pad.

The final pyro preps which are called out in V2000303 were made at the launch pad with the complete Booster-Agena-Payload flight system mated in the vertical position and the radar antenna installed. The remaining operations of this procedure were performed in the Special Project Laboratory and are outlined below:

a) * Hookup

- o Recovery Capsule to Conical Section

b) * Power Application

c) Pyro Circuits Checkout

d) * Film Tracking

- o Observe film through access door for proper tracking after final mate of the Recovery Capsule

e) * Payload System Performance

- o Transponder generated test targets and timing signals fed to the receiver and the resultant data film analyzed for range resolution, speed and light leaks.

f) Transmitter Power Output

- o Measure with a set of equipment to be used later at the launch pad for the final power measurement.

g) Final Film Preps

- o Load flight film
- o Transponder generated test targets fed to the receiver and used to expose approximately 21 feet at the head end of the flight film.

h) Pyro Installation at Launch Pad

NOTE: * V2000303 and STP 2355-7 concurrently

Payload Performance Evaluation - Three (3) out of limits values were recorded during the Special Project Laboratory tests. These were:

a) Transmitter power was 0.7 db low

b) Sensitivity Time Control (STC) video waveform was 2.2:1 maximum to minimum and should have been a maximum of 2.0:1

c) Delay from the "ON GATE" to the start of STC was 35 microseconds and should have been 31 microseconds maximum.

2.3.2.8 VAFB R-3 Day Tests

Final mating in a vertical position and in a launch configuration was completed, except for the payload antenna and associated fairing. A dummy antenna (artificial load) was connected at the payload antenna feed-line interface on the payload cylindrical skin section, to prevent high power radiation in the area and for security measures. Operating power was furnished from the installed flight batteries (Type 1-D). Range target test signals (artificial targets) were injected through a coax cable from a test transponder. Payload data track (video) information was transmitted through the wide band data link to VTS-1 and VAFB Bldg [redacted] (payload area). Agena and payload telemetry data were transmitted to VTS-1 and VAFB Bldg. [redacted] (LMSC Telemetry Ground Station). Real-time commands for the Agena and payload were transmitted from the VTS-1 PRELORT Radar site. Stored-time commands were exercised by wire-line controls through the Vehicle/AGE interface (instead of running the orbital programmer). A payload command sequence was run to validate interferences that had been broken after simulated flight. Transmitted power was measured and verified to be the same as measured in the payload laboratory, Bldg. [redacted] i.e., 0.7 db (15 percent) low. The payload was commanded to the condition planned for launch, e.g., PRF Step 11, Time Constant Number One (1) and receiver gain to AGC (Step 1). The capsule status telemetry verified correct continuity loop, water seal and separation switch position. During the course of the R-3 day checks, every interface circuit and every interface function were verified in the flight configuration - and were not disturbed in any way after that time. R-3 Day Payload Evaluation - There were no payload malfunctions or payload functional telemetry data discrepancies noted. Capsule telemetry was satisfactory.

~~SECRET~~ SPECIAL HANDLING

2.3.2.9 VAFB Launch Count-Down

During the final count-down for launch, stored-time commands were exercised by wire-line controls to put the payload into a PRE-OPERATE Mode, and real-time commands transmitted from the VTS-1 PRELORT Radar to insure launch status, i.e., PRF Step 11, Time Constant One and receiver gain to AGC (Step 1). The payload OPERATE command was not transmitted because the payload antenna fairing was installed. Test Mode and Film Drive Motor were commanded on and payload test information transmitted through the wide band to VTS-1 and VAFB Bldg. [redacted] (payload area). Agena and payload telemetry was transmitted to VTS-1 and VAFB Bldg. [redacted].

Payload Performance and Telemetry Data Evaluation. All payload GO/NO-GO telemetry and launch status were verified to be as specified. The completion of the count-down, the R-3 day checks and the horizontal simulated flight completely revalidated the total flight configuration with a single exception - the radar did not transmit through the flight antenna while at VAFB. Every other payload function was exercised in the final flight configuration. Since the total satellite including the antenna was operated in an orbital mode in the Anechoic Chamber and since RF power measurements were made of transmitter power input at the antenna fitting during the R-3 day checks, the full system was validated for flight.

2.3.2.10 Recovery Subsystem Testing

The Recovery Subsystem, which was furnished as GFE, (Government Furnished Equipment) was first received in the Payload Development Laboratory, reference Par. 2.3.2.1 above. The interface between the recovery capsule was carefully defined early in the program insofar as electrical and mechanical requirements were concerned, for power, telemetry, commands and mechanical alignment. The Recovery Subsystem is described here as a separate subsystem.

A Recovery Subsystem, as defined by Engineering Drawing List Number 222-750, Serial Number 588, was flown as part of the payload assembly on Vehicle 2355. To describe the unit and discuss assembly, installation, subsystem testing, system testing, launch preparation, and flight, this portion of the report is divided into two general sections.

Section I describes the configuration and operation of each of the sub-elements of the recovery system. Section II describes the program test philosophy and the test sequences. A description of the modification to the basic configuration, made during the test and preparation span, is included in Section II.

Section I - System Configuration Description.

Figure 2.3.2.10.1 is an "ON-BOARD" profile, included to aid in describing the relative physical location of parts and to complement the following description of the recovery system functional elements. The recovery system is comprised of six separate and independent functional elements.

1 ABLATIVE SHIELD
2 WATER BALLAST SYSTEM
3 SINK VALVE ASSEMBLY
4 BALLAST WEIGHT
5 RECOVERY BATTERY
6 RECOVERY PROGRAMMER
7 TELEMETER SET
8 COLLECTOR ASSEMBLY
9 WATER SEAL
10 AFT COVER
11 FLASHING LITE
12 PARACHUTE
13 THERMAL COVER
14 STUB ANTENNA
15 SPIN/DESPIN GAS SUPPLY
16 SPIN/DESPIN VALVES
17 THRUST CONE
18 RETRO-ROCKET
19 CAPSULE
20 THRUST CONE PYROS
21 THERMAL COVER/FOREBODY PYROS
22 SEPARATION PYROS
23 DISCONNECT PYROS

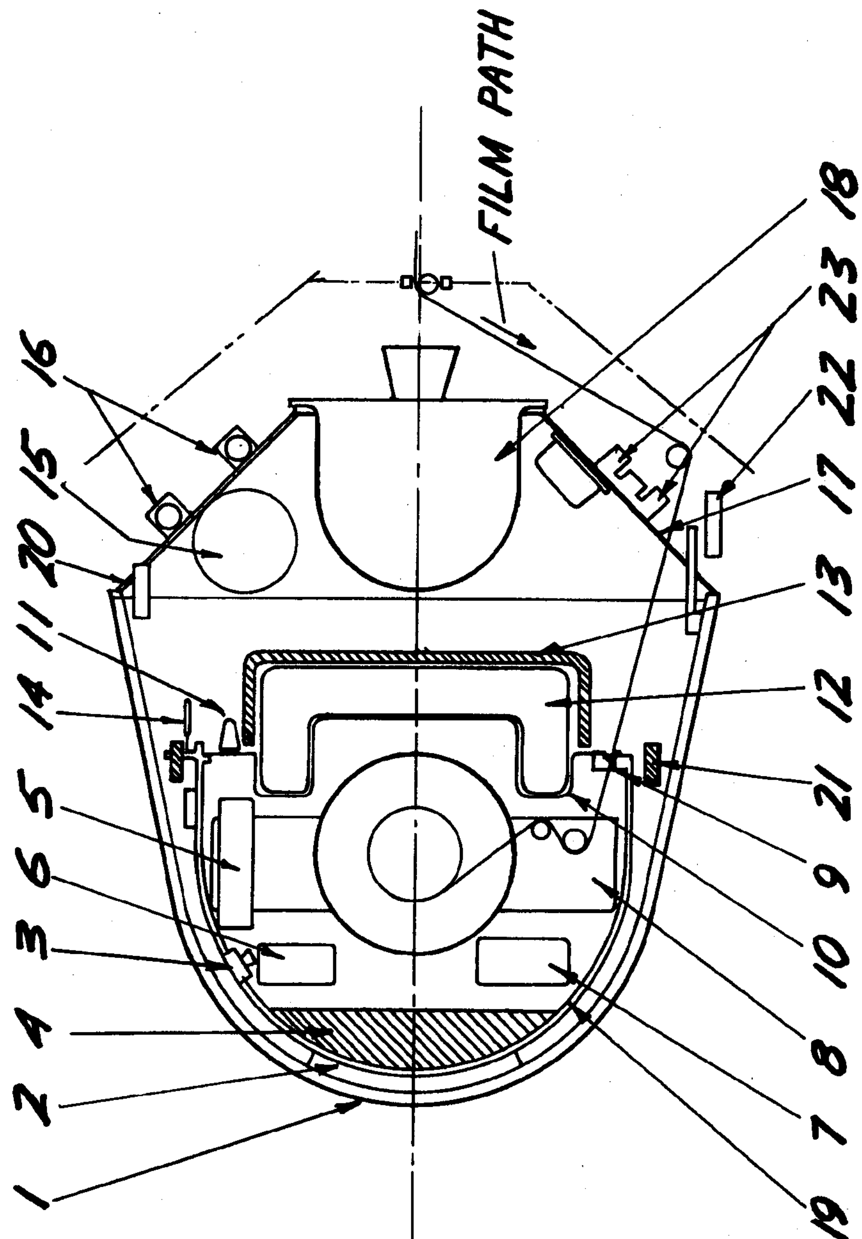

Figure 2.3.2.10.1 - Recovery System Assembly

The film transport system provides a precision aligned take-up cassette assembly, that includes intermediate rollers to control film alignment, a torque motor which provides a positive tension on the film coming from the recorder, and telemeter signal sources required to indicate the amount of film transported, and to grossly indicate the velocity of film being transported.

The takeup motor operates on 28.3 VDC regulated voltage from the payload DC/DC Type X voltage regulator. The feed-back control circuitry is shown in Figure 5 with a parallel transistor voltage control network. The bias of Q401 and Q402 is controlled by a potentiometer which is positioned by the puck arm. The puck arm senses hub diameter and changes bias voltage with increasing hub diameter. The transistors conduct more heavily, thus increasing motor torque. The correction of torque produced by this network was nearly linear through the range of potentiometer control.

The pressure system includes valves to assure the release of internal ambient pressure during ascent, to allow the equalization of pressure during descent, to provide a light sealed interior after the capsule is separated from the payload, and the floatation vent valve allows the release of internal pressure from the capsule, if the capsule is not caught, and is in the sea for the pre-set 76 hours and the sink valve (salt water actuated) has allowed sea water to enter. The floatation vent release valve opens when the cpasule internal pressure exceeds the capsule external pressure by more than 0.1 psig. (This valve is open during ascent). This valve relieves any pressure built up internally due to the entry of sea water, and ultimately enough water enters so that bouyancy is overcome and the capsule sinks. The ascent/descent valves operate at 2 psig differential, with a designed flow rate of twice the amount required by the planned trajectory (vertical velocities) incurred in the flight of 2355.

The telemeter system provides the indicated film transport information signals, temperature sensor information from the cassette assembly, the forebody, and the batteries. After separation, a self contained telemeter system, independent of the Agena telemeter system, provides three channels of telemetry information which indicate the sequence of events and operation of the pyrotechnic system. The telemetry transmitter is an FM/FM Type, with a 100 kc bandwidth, operating on a frequency of 228.2 mc (crystal controlled), with a power of 1.8 watts. It modulates three IRIG channels. Channels 7 and 9 monitor breakwire and despin events, plus thrust cone battery voltage. When the thrust cone is ejected, a relay switches to the series of events related to the parachute ejection system. Channel 11 telemeters a $\pm$ 5 g accelerometer to measure retro thrust during orbit ejection. A display of the three telemetry channels 7, 9 and 11 is shown in Figure 2.3.2.10.2, and the corresponding sequence of operations is given in Table I. The tracking beacon is a self-contained aerial recovering homing aid, used to determine the capsule position during the recovery aircraft positioning. The recovery (tracking) beacon is a crystal controlled VHF beacon, operating 235 mcs with a minimum power output (peak) of 7.5 watts. It produces a pulsed output from a PRF of 1000 to 700 in a saw-tooth pattern with a pulse deviation of 30 micro-

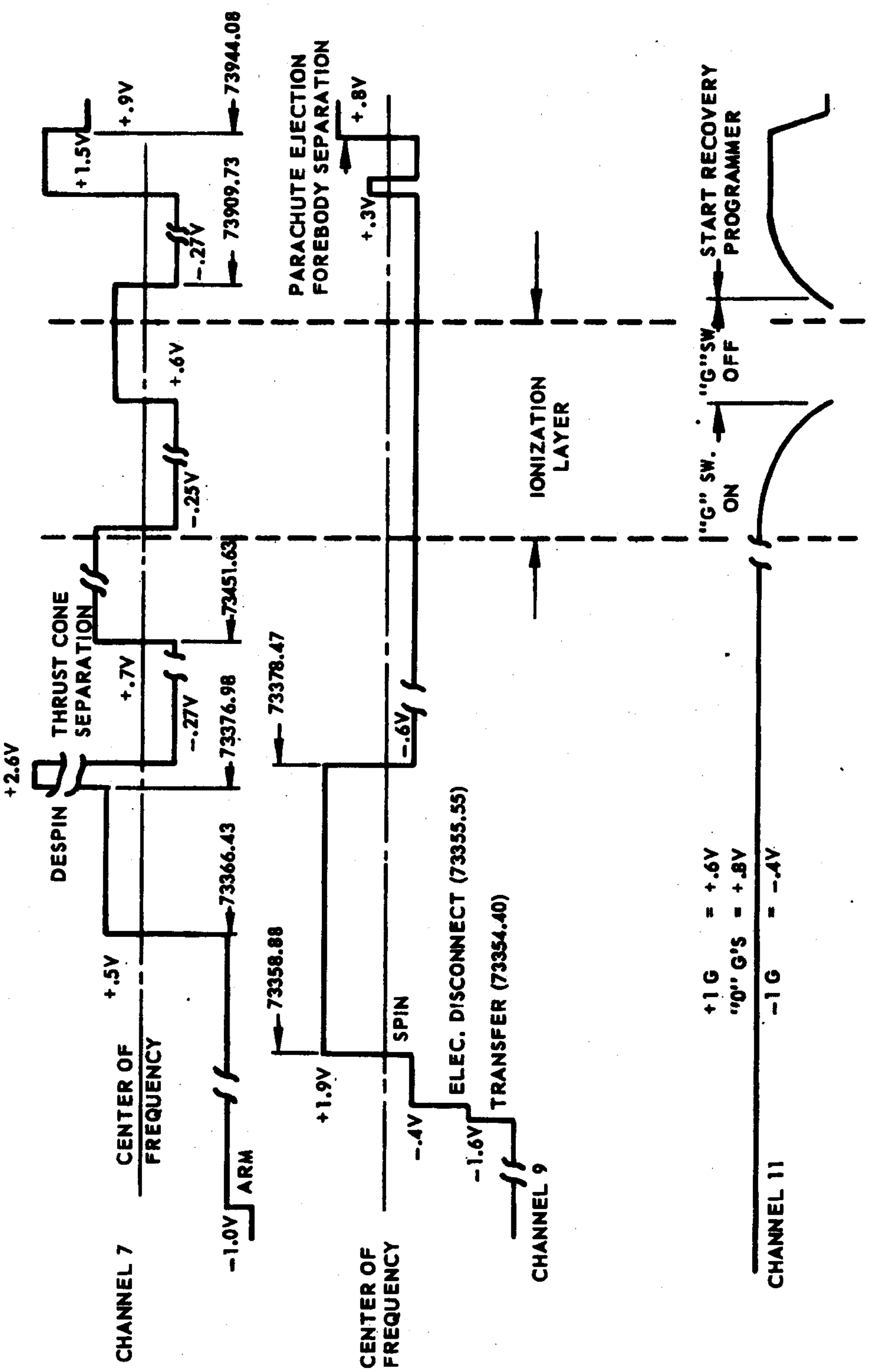

Figure 2.3.2.10.2 Recovery T/M - Sequence of Events

seconds over a one second period. A flashing light also aids acquisition at night with a flash repetition rate of 60-90 per minute, visible at least 8 nautical miles from 10,000 feet against a night background.

The propulsion system is comprised of a retro rocket providing the thrust to initiate a recovery system trajectory independent of, and counteracting the orbital velocity of the orbital vehicle. The TE-236A retro rocket (P/N 863C772 P3) is a solid propellant rocket containing a nominal 40.2 pound charge which burns for 10 seconds and provides a nominal retro-velocity of 1250 feet per second. The Isp is 260 sec. The nozzle vacuum expansion ratio is 18.3:1. Rocket total weight is 62.9 pounds. The cold gas spin system initiates a rotation of the recovery vehicle about its longitudinal axis, to approximately 70 rpm, to assure gyroscopic stability of the recovery vehicle during re-entry. The cold gas despin slows the capsule rotation rate to a residual of approximately 10 rpm prior to parachute operation. The cold gas pressure spheres are 73 cubic inches and will hold approximately .60 - .70 pounds of Nitrogen/Freon 14 mixture each. This will spin a capsule with a mass amount of inertia of 6 slug feet^2 in excess of 60 rpm. The despin gas load is calculated to allow a residual spin rate of 10 rpm. Figure 2.3.2.10.3 is a pictorial diagram of the recovery profile to depict the general sequence of events, as described above and in Table I.

The parachute system is composed of a 5.4 ft. diameter drogue chute and a 28.9 ft. diameter main chute. Actuation of the parachute system involves squibs, lanyards and cable cutters. The drogue chute is deployed by the

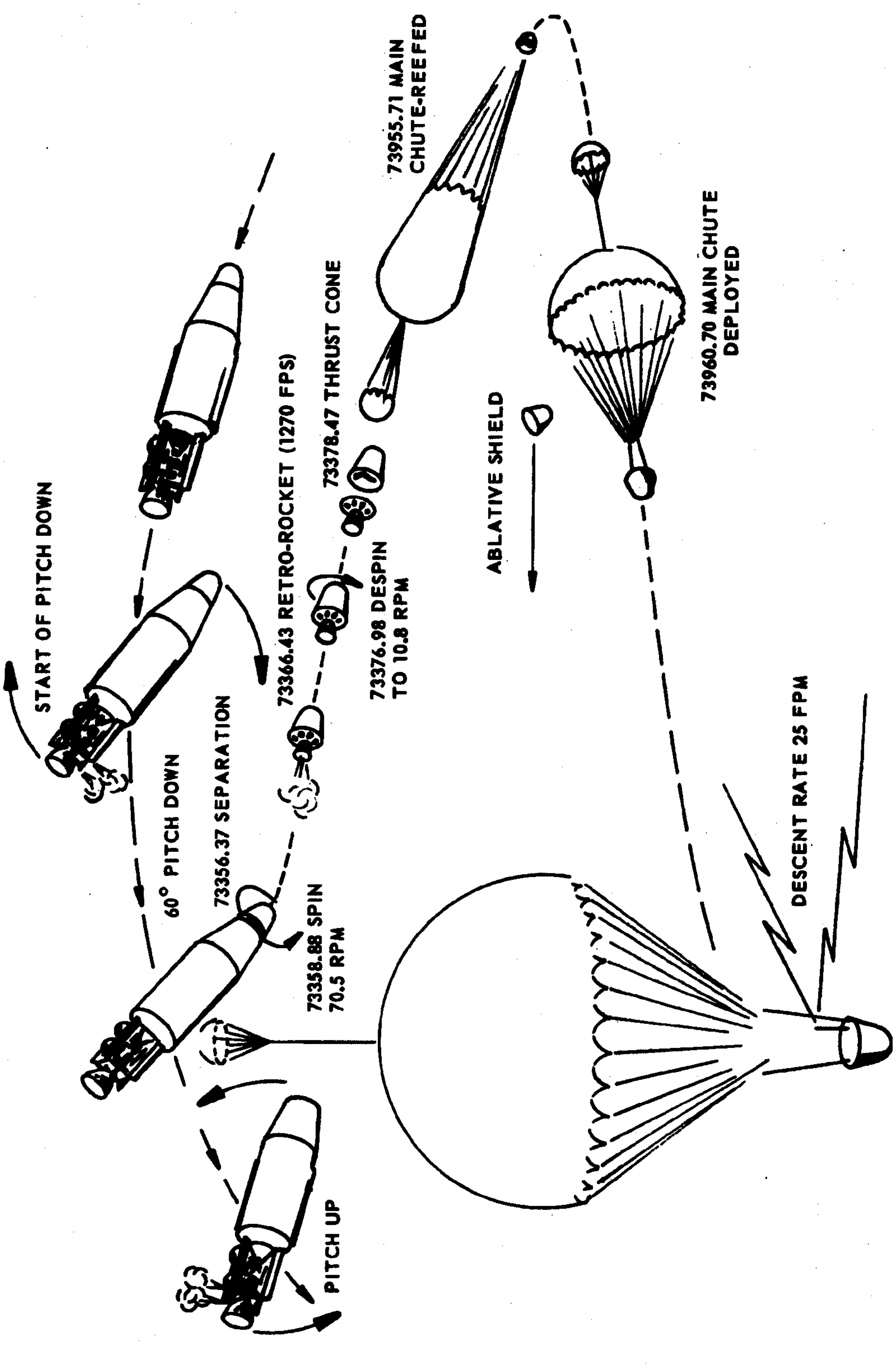

Figure 2.3.2.10.3 Recovery Event Time Profile

thermal cover which is released by detonating explosive bolts. The drogue chute initiates the main chute bag cutter squibs by lanyard release. Four seconds after initiation the bag cutters release the main chute in a reefed condition. The dynamic force on the reefed main chute initiates squibs which, after six seconds, actuate cutters of the reefing line at the perifery of the main chute. The main chute slows the descent rate of the capsule to the atmospheric descent rate of 25 feet per minute, at 20,000 feet of altitude. (See note below)

In addition to normal circuit redundancy, designed into the recovery system, there are two independent capabilities in the system which provide backup. The first is the Hayden Timer (relay system) which initiates backup recovery pyro events as given in Table I. The second backup capability is the water floatation ballast system. This system positions a hemi-spherical weight below the capsule nose, at the end of a flexible arm, which assists in maintaining the capsule in an aft-cover UP position. The ballast system primary control is a double mechanical latch device, which is armed by lanyard pull as the ablative shield is separated from the recovery system, and completely released at water impact. If for any reason water recovery is required, correct and stable capsule orientation in the water provides maximum benefit from the flashing lite and beacon during search and surveillance for water pick-up.

Note: The sequence depicted in Figure 2.3.2.10.3 is descriptive of the typical recovery sequence of events; however, for additional realism, the times are the actual times for 2355, as also given in Part III, Para. 3.7.3.

TABLE I

EVENT	FUNCTION
ARM #1 (Only)	Start Hayden Timer
	Initiates Telemeter
ARM #1 or #2	Close K-1 (Beacon ON) Primary to K-2
	Close K-2 - Secondary to K-1
	Close Thermal Relay
	Powers Dimple Motors - CLOSE Water Seal (Film Cutter)
	Power to Recovery Programmer
TRANSFER	Applies Thrust Cone Battery
	Close K-3 (Beacon ON Back-up)
	Powers Electrical Disconnect Squibs
	Arms Recovery Programmer
DISCONNECT	Electrical Disconnect Complete
	Start Thrust Cone Programmer Events
Spin	Ignition of Spin System Gas Valve, Spin-up to 65 RPM ± 10 RPM
Retro	Ignition of retro-rocket provides counter orbit velocity to 1250 fps (Normal)

TABLE I (Continued)

EVENT	FUNCTION
De-spin	Ignition of De-spin System Gas Valves, Counters Spin System to provide 10 RPM residual spin rate
Thrust Cone OFF	Conditions Recovery System for activity below the ionization layer at "G" Switch opening. Sets up TM System for Channels 7, 9 and 11.
"G" Switch Closure (Actuates at 3 G's) Deceleration	Initiates Flashing Lite. Provides a Beacon Backup.
"G" Switch OPEN (Actuates between 6 & 3 G's) Deceleration Complete.	Recovery Programmer starts after 34 seconds, K-7, K-8, K-9 and K-10 actuate. Initiates Parachute deployment.
EJECTION SQUIBS	Removes Thermal Cover which starts Drogue Chute out. Forebody (Ablative Shell) is released, which arms the Water Ballast System. Drogue Chute pulls Reefing Lanyard which releases Main Canopy in reefed condition. Time delay Reefing Cutter deploys Main Chute.

TABLE I (Continued)

EVENT	FUNCTION
TRACKING BEACON	228 mc with audio modulation is used to provide directional finding signal.
TELEMETER (CHANNELS 7, 9, 11)	Excitation voltage from -0.27 VDC to 4.9 VDC. At 0.0 VDC, shall deviate, center frequency - 45 percent. At 2.5 VDC, shall deviate to center frequency. At 5.0 VDC, shall deviate to center frequency + 45 percent. The RMS outputs of Channels 7, 9, 11 shall be within 10 percent of each other. Channel 7 = 2300 cps c.f. Channel 9 = 3900 cps c.f. Channel 11 = 7350 cps c.f.
HAYDEN TIMER	Initiated at ARM, starts to time out. At +180 seconds, provides Thrust Cone back-up command. At +2100 seconds, provides Chute Ejection squib backup command. Assures Thermal Cover OFF, and Ablative Shield OFF to assure no random re-entry.

TABLE I (Continued)

EVENT	FUNCTION
WATER BALLAST SYSTEM	Mechanical Sea-Anchor System, assures aft cover-up position in heavy seas. Assures flashing lite visibility, maximum beacon ground plane, provides best Capsule position for preventing water seepage. Initiated to cocked position by Forebody separation, released to active position at water impact.
PRESSURE SYSTEM	Assures release of internal ambient pressure during ascent. Allows increasing pressure to enter during re-entry, while maintaining light-tight condition with water seal closed. Includes one valve to work in conjunction with sink valve system, to allow submersion after pre-determined floatation life. Sink valve allows sea water to enter, relief valve relieves internal pressure build-up and allows displacement to submerge Capsule.

Section II - Test Performance and Modification

Figure 2.3.2.10.4 is included to describe the test and handling sequence of the Recovery System, indicate the progressive testing philosophy, and to graphically display the test philosophy. The test philosophy applied to the Recovery Subsystem was in consonance with the test philosophy applicable throughout the handling of the Program hardware; namely that of rigorous preparation and checkout on an individual subsystem basis, progressing to the system level. Following each subsystem or system level test, any malfunctions or data discrepancies were revalidated, and if there were no discrepant conditions, the system integrity which had been established by the test was maintained by a process of hardware configuration control which precluded random checks, handling and special tests. The system was validated for flight in the full configuration, less certain pyros and batteries, with the mandatory requirement being a flight configuration demonstration of all circuits and all functions. The control philosophy compelled design integration review and design compatibility by review of control documents, specifications, test procedures and test results at the GFE supplier. An overall test sequence and document review was completed prior to the receipt of first recovery system as Government Furnished Equipment to the Program. The compatibility of the recovery system and the payload contractor subsystem was confined to verifying mechanical alignment, film tracking, and film tension. All of these requirements were satisfied in the payload vehicle test laboratory. The compatibility of the recovery system and the Agena Vehicle is confined to power and command signals carried in LMSC harnesses. These functions were validated in the payload

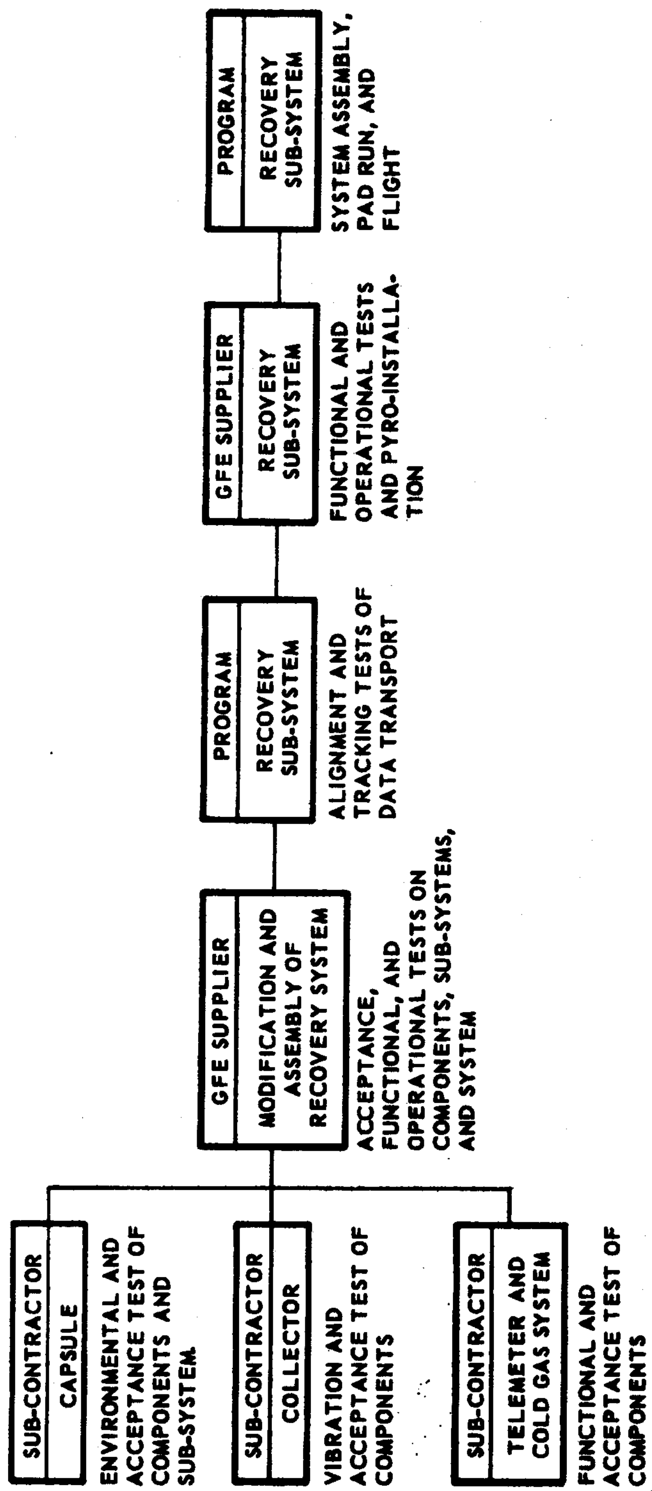

Figure 2.3.2.10.4 Responsibility Flow Diagram

vehicle test laboratory using program peculiar test aids, at the recovery system to payload vehicle interface. The checkout of recovery system functions, peculiar to recovery, were performed only by the vendor, prior to reaching the launch base. The established test plan minimized redundant testing, assured configuration control at each test milestone and assured that the test configuration was that of the flight system. A very close liaison was maintained during subsystem and system testing with the GFE supplier, to assure consistency of test philosophy. During the test span, two modifications were made to the configuration of the recovery subsystem. A review of available recovery trajectory data indicated that the weight of the recovery system should be increased from the original 87-90 pounds, to approximately 120 pounds, suspended weight on the parachute. Parachute qualification test data was minimal in regards to capsule weights below 110 pounds, due to the fact that the previous qualification test objectives had been to substantiate descent rates, loading and shock resulting from the various stages of deployment and air catch activities. There were no stringent weight restrictions imposed on the payload vehicle at this time, so a change was made to add weight inside the capsule. Thirty pounds of lead ballast was pour-formed to the capsule forward internal spherical shape, adhesive bonded in place and restrained by brackets to an integral structural member of the capsule. Tension and shear testing was imposed on representative samples of the adhesion joint. Based on requirements dictated by the launch environment, which imposes G's along the longitudinal axis, testing verified a joint strength 10 times that required. The safety factor did not include the strength provided by the brackets and was based on minimum adhesion factors, so was very conservative. The added ballast raised the weight of capsule as previously described to a suspended weight of 120 pounds, allowed the use of existing trajectory planning information, obviated the requirements for parachute testing, and made existing qualification data applicable. The addition of the ballast did not require moving any other components, or configuring any bracketry. The installation is permanent. A second modification of the recovery system was made to the takeup cassette torque motor power control circuits. During a thermal-altitude payload system test, telemeter information indicated that the system was not transporting film consistently at the required 5.00 ± .03 inches per second. The capsule assembly was checked thoroughly, and the cassette assembly was tested extensively for thermal effect, extended stall time, and continuous duty. There were no indicated malfunction excepting a slow film movement on an intermittent basis. After a payload contractor review of the recorder transport system for speed stability and the influence of an increase in takeup cassette tension, and after vendor testing, the change shown in Figure 2.3.2.10.5 was incorporated. Prior to this change, takeup tension was measured in a static or stalled motor condition. Tension at a four inch dia. takeup was 2.5 pounds and at an eleven inch dia. takeup spool was 1.7 pounds. These values are within the original specification limits. Since the tension had been measured in a stall condition, the running torque was lessened due to the back EMF generated during motor operation, which decreased the voltage drop across the motor and therefore decreased the motor current. Subsequent to the circuit change, tension was measured with the film moving at

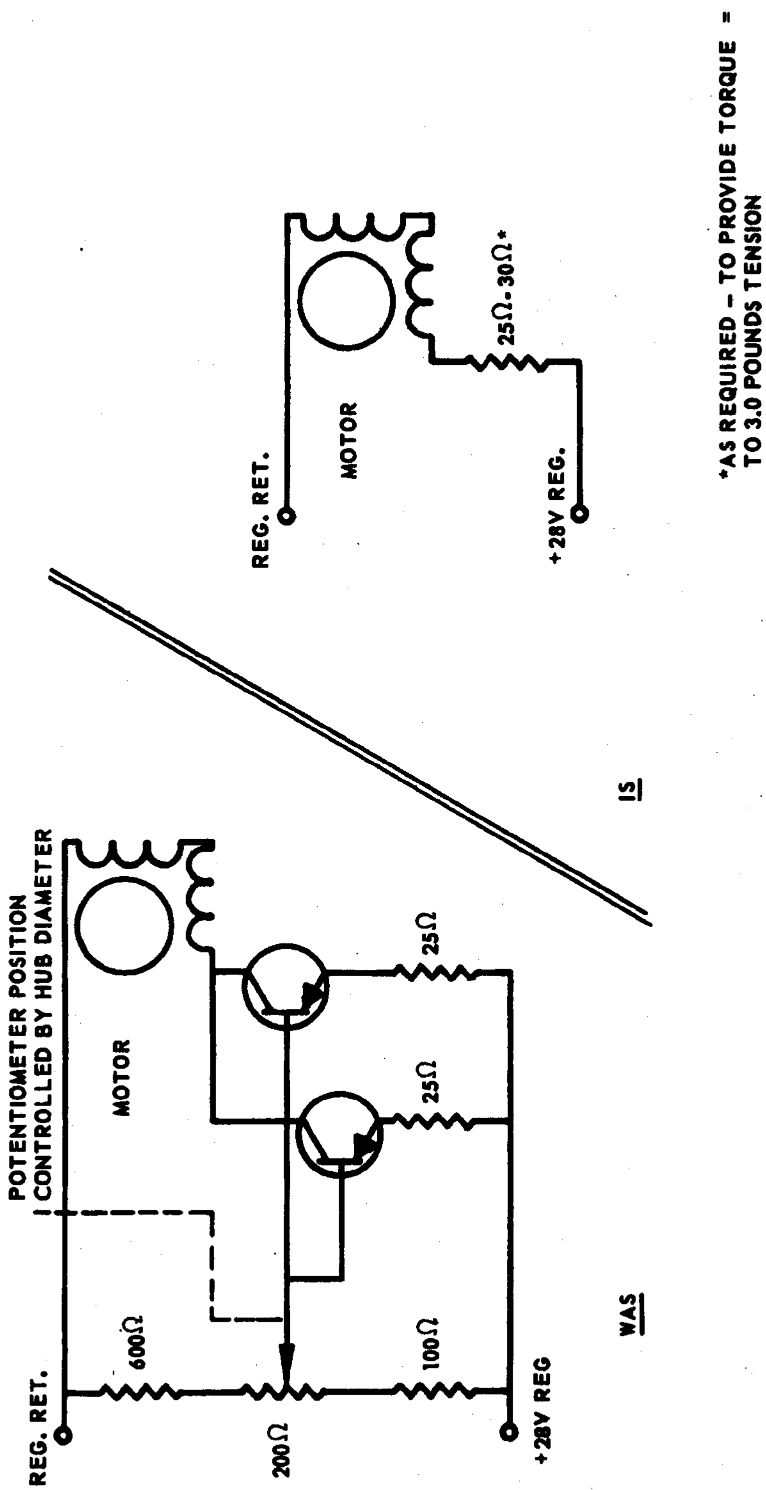

Figure 2.3.2.10.5 Torque Motor Circuit Modification

approximately 5 inches per second, and also with the takeup in a static or stalled condition. The tension with the film moving with an 8.0 inch diameter takeup spool was 3.0 pounds, and at an 11.0 inch dia. takeup was 2.5 pounds. The increased tension was verified at the vendor and in the payload test labs. Thorough testing of the payload system with the increased takeup tension verified that the film transport speed of 5.0 ± .03 inches per second was stable. Further testing at altitude and at ambient yielded acceptable film speed variations when evaluated on the University of Michigan correlator.

During the entire test span in the Sunnyvale area, the only component that was replaced in the recovery system was the recovery telemeter set. During tests at the GFE supplier facility, prior to the final payload system test at altitude, the unit indicated some drift in center frequency and was replaced. During subsequent tests at the supplier and during pad testing at VAFB, the replacement unit was verified to be stable in frequency. Payload and vehicle testing, prior to shipment to VAFB verified only film speed, transport system stability and takeup ON-OFF control within the recovery subsystem. Thrust cone programmed events, recovery programmed events, pyrotechnic events, beacon characteristics, and telemeter system performance were verified as indicated above, at the GFE supplier. and during validation testing on the pad at VAFB. There were no test failures during VAFB testing. The pad simulated flight data anomaly associated with the recovery programmer was the only test discrepancy. The test configuration did not include thrust cone batteries, and in lieu of these batteries which are squib actuated, power was to be supplied from the vehicle sequence (SS/D) timer. The normal flight duration of the sequence timer switch closure is 1 to 2 seconds, to activate the squib activated batteries, which then supply power. The timer switch closure time is normally set, for test reasons only, at approximately 30 seconds, sufficient for the duration of thrust cone programmer events. Power was removed in this test after approximately 2 seconds by the sequence timer, preventing the issuance of thrust cone programmer events. All functions were subsequently properly verified.

2.3.3 Test Schedules

The progress of testing this radar payload, with the associated failures caused serious schedule disruptions. This fact, which was properly recognized at all management levels as unavoidable on this system, with the development problems involved, resulted in continual schedule revisions. The causes of the failures were eventually corrected and the payload was demonstrated successfully through a simulated mission at altitude, prior to shipment to the launch base.

The schedules are summarized, and presented as accomplished, for record purposes.

VEHICLE 2355 SCHEDULE SUMMARY

Vehicle 2355 (AFT of STA 228)

DATE	REFERENCE	CART	DD-250	MAB	PAD
6-20-63	DT22	2-17-64	4-28-64	5-11-64	5-28-64
9-27-63	I/O 23-22	4-21-64	7-6-64	7-18-64	8-5-64
11-1-63	DT23	4-21-64	7-6-64	7-18-64	8-5-64
2-7-64	DT24	4-21-64	7-6-64	7-18-64	8-5-64
2-24-64	I/O 1-24	4-21-64	7-6-64	7-18-64	8-5-64
5-25-64	I/O 19-24	*4-27-64	7-22-64	8-11-64	8-28-64
6-22-64	DT25		7-22-64	8-11-64	8-28-64
6-29-64	I/O 1-25		7-27-64	8-11-64	9-11-64
8-14-64	I/O 9-25		*8-28-64	10-13-64	10-30-64
10-28-64	DT26 PRELIM			11-18-64	12-14-64
11-10-64	DT26 PRELIM			*12-2-64	*12-21-64

* Final Schedule

Vehicle 2355 Payload (FWD of STA 228)

DATE	REFERENCE	DD-250
11-1-63	M/S DT 23	7-6-64
9-26-64	AC04001	10-14-64
10-24-64	AC04059	11-9-64
10-26-64	AC04060	11-9-64
10-30-64	AC04117	11-9-64

DT = Lockheed Official Schedule-Date Table

2.3.3.1 Schedules

Original Schedule - Planned

o Receive A/C Payload boxes and AGE at Lockheed		2-15-64
o Receive payload equipment racks at [redacted] Dev. Lab.		2-17-64
o Acceptance tests of the Goodyear boxes on maintenance testers.	2-15	2-19-64
o Installation of P/L equipment in the P/L equipment racks	2-20	2-24-64
o Payload system test using Goodyear system tester and LMSC vehicle simulator	2-25	4-3-64
o Temperature and altitude tests of P/L system in TASC	4-9	4-23-64
o Receive Agena D at systems test complex C-12		4-21-64
o Preliminary integrated Agena/P/L System tests thru simulated flight, C-12	4-24	5-12-64
o Simulated flight in the anechoic chamber - Agena/P/L EMI test	5-13	6-11-64
o Final integrated Agena/P/L systems tests thru simulated flight, C-12	6-12	6-30-64
o Engineering buy off		7-1-64
o Vehicle and payload DD-250's		7-6-64
o Ship vehicle, payload and P/L AGE to VAFB		7-7-64
o Vehicle/Payload alignment and fit checks - MAB	7-8	7-9-64
o Payload preps for pad tests in P/L lab	7-10	7-20-64
o Agena checks - MAB	7-10	7-20-64
o Magnetometer Range Checks Agena/Payload		7-21-64
o Launch pad Agena subsystem tests	7-22	7-23-64
o Launch pad AGE/vehicle/P/L compatibilities	7-24	7-26-64

o Launch pad systems test phase I (backup commands)		7-27-64
o Launch pad systems test phase II (simulated flight)		7-28-64
o Vehicle/Payload and Nose section mate - pad	7-29	8-1-64
o Mate Solid Motors		8-4-64
o Countdown and Launch		8-5-64

2.3.3.2 Final Schedule - Actual

o Receive A/C Payload Boxes & AGE at LMSC	2-24-64 - 3-21-64
o Receive Payload equipment racks at [redacted] Dev. Lab.	2-24-64
o Acceptance tests of the Goodyear Boxes on Maintenance Testers	2-24-64 - 3-21-64
o Installation of P/L equipment in the P/L equipment racks	2-24-64 - 3-23-64
o Payload System Test using Goodyear System Tester and LMSC Vehicle Simulator	4-16-64 - 5-7-64
o Receive Agena D at Systems Test Complex C-12 (CART)	4-27-64
o Preliminary integrated Agena/P/L Systems Tests thru Simulated Flight C-12	5-7-64 - 5-25-64
o Simulated flight in the Anechoic Chamber Agena-P/L EMI Test	5-25-64 - 6-10-64
o Final integrated Agena-P/L System Tests thru Simulated Flight C-12	7-6-64 - 7-9-64
o Agena DD-250	8-28-64
o Agena Ship to VAFB	9-1-64
o Temperature and Altitude Tests of P/L System in TASC	9-3-64 - 12-2-64
o Altitude Test of Goodyear Flight Recorder & Recovery Capsule (HATS)	10-28-64 - 10-30-64
o Vehicle/Payload Alignment and Fit Checks - MAB	11-10-64 - 11-18-64
o Agena Checks - MAB	9-1-64 - 9-24-64
o Magnetometer Range Checks Agena/Payload	11-19-64 - 11-20-64
o Payload DD-250	12-2-64
o Ship Payload to VAFB	12-2-64
o Launch Pad Agena Subsystem Tests	11-30-64 - 12-3-64

o Launch Pad AGE Vehicle/P/L/ Compatibilities	12/4/64
o Launch Pad Systems Test Phase I (Backup Commands)	12/5/64 - 12/7/64
o Launch Pad Systems Test Phase II (Simulated Flight)	12/7/64 - 12/8/64
o Payload Lab Flight Preps of Payload	12/12/64- 12/14/64
o Vehicle/Payload and Nose Section Mate - Pad	12/14/64- 12/15/64
o Vehicle Systems R Day Checks	12/15/64
o Mate Solid Motors	12/18 & 12/19/64
o Countdown & Launch	12/21/64

2.4 Data Handling - Processing and Flow

2.4.1 General The data retreival flow from the recovered capsule film and from the GBOE (Ground Based Operating Equipment) in the tracking stations is shown in block diagram form in Figure 2.4.1.1. The film containing the stored video data, both recovered and from the stations, is correlated at the [redacted] after processing at SPPL. The data handling and processing is discussed further in this section, as relates to the correlation process, the correlator used and the format of the data film upon which the video data is recorded. A brief discussion of the properties of a sine wave diffraction grating were given in Para. 2.2.2. The correlation process is discussed functionally in this section. The correlation functional description, the Precision Optical Processor information and the data format details for this section were provided by the [redacted]

2.4.2 Correlation - Functional Description

The radar system under discussion is one which employs data-processing to yield an azimuth resolution capability which is two to three orders of magnitude finer than that provided by the physical width of the radiated beam itself. The processor chosen for the 2355 mission is a coherent optical device commonly referred to as a "correlator" or "optical processor"; the processor accepts as an input a developed transparency upon which video data has been properly stored, and generates as an output a second transparency containing the fine-

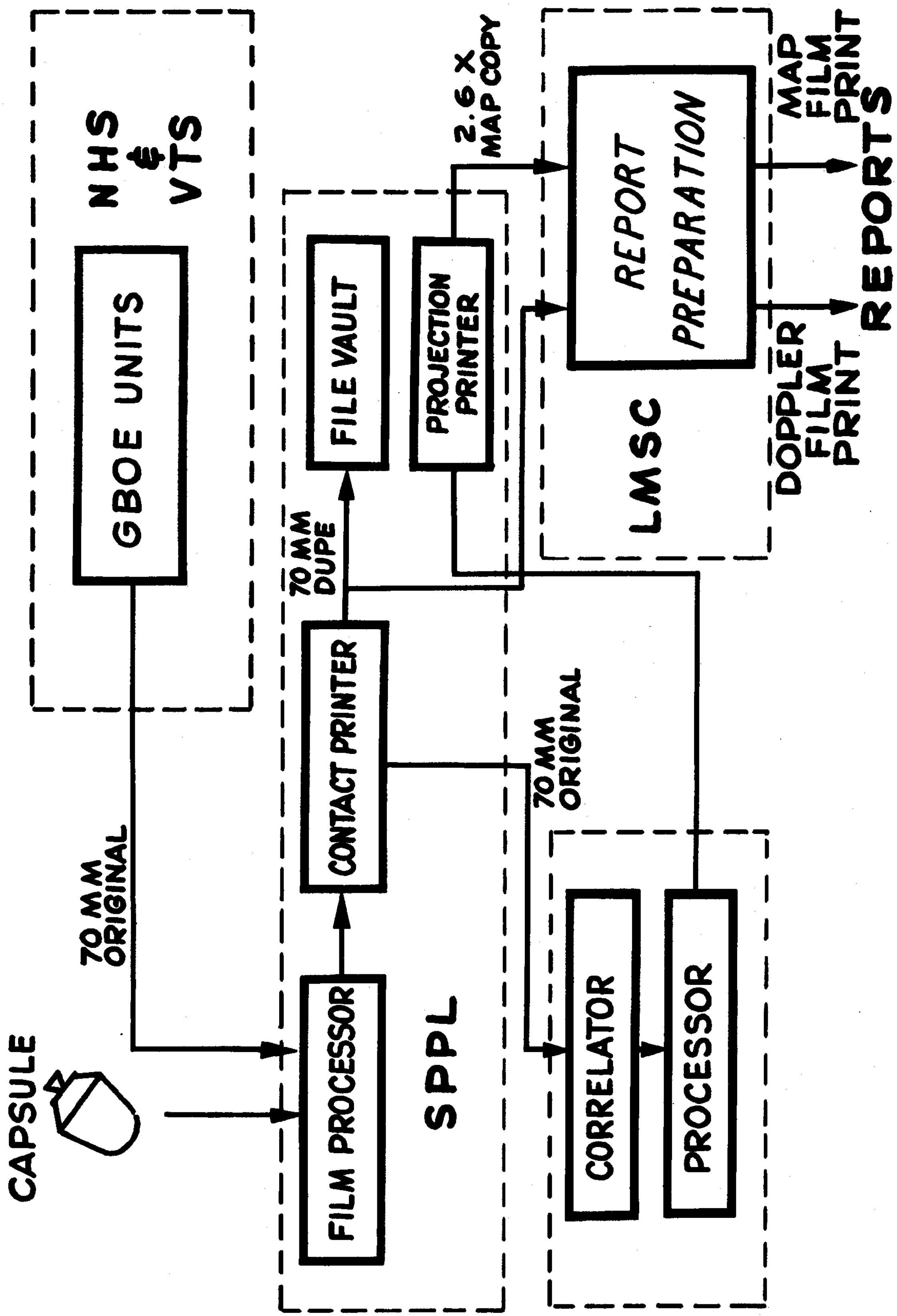

Figure 2.4.1.1 - Data Flow-Block Diagram

resolution radar imagery. This is depicted in Figure 2.4.2.1. The data transparency is that generated by one of the three recorders, either that within the radar payload, or one of the recorders at NHS or VTS which accept the video output of the Wide Band Data Link. The format of this data transparency is described below in Para. 2.4.4. Figure 2.4.2.2 is an enlarged print of such a data transparency, and has "range" data stored using the cross-track dimension while "azimuth" data is stored using the along-film dimension. The video data manifests itself in the form of a density variation whose parameters are precisely controlled as a function of target position and radar crossection. The "history" of a single point-target reflecting object is easily seen at the location indicated by the arrow; the information embodied in this target history is utilized in the generation of the fine-resolution imagery.

The theory of optical processing and its application to coherent radar data has been discussed extensively in the unclassified and classified literature (Refs. 1-5). Some of the pertinent properties of the processor will be summarized in Para. 2.4.3 below, while the scale factors of the output product are given in Para. 2.4.4.

2.4.3 [redacted] Precision Optical Processor (POP)

In order for all program objectives to be met, a data processor was required which was beyond the state-of-the-art at the time of program initiation, but which appeared feasible if implemented using coherent optical techniques and a sufficient degree of precision. The technical

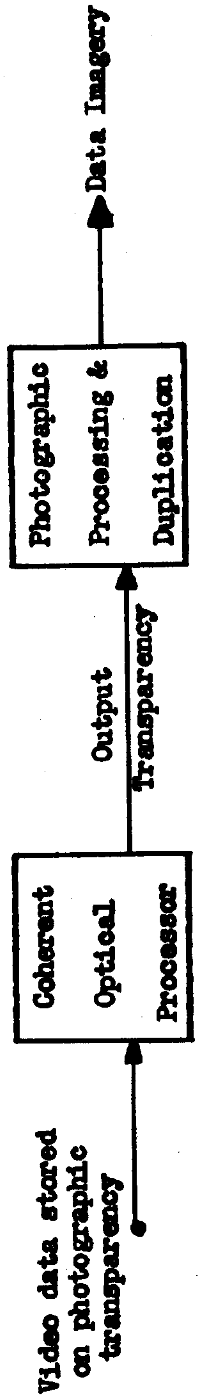

Figure 2.4.2.1 - Correlator Function

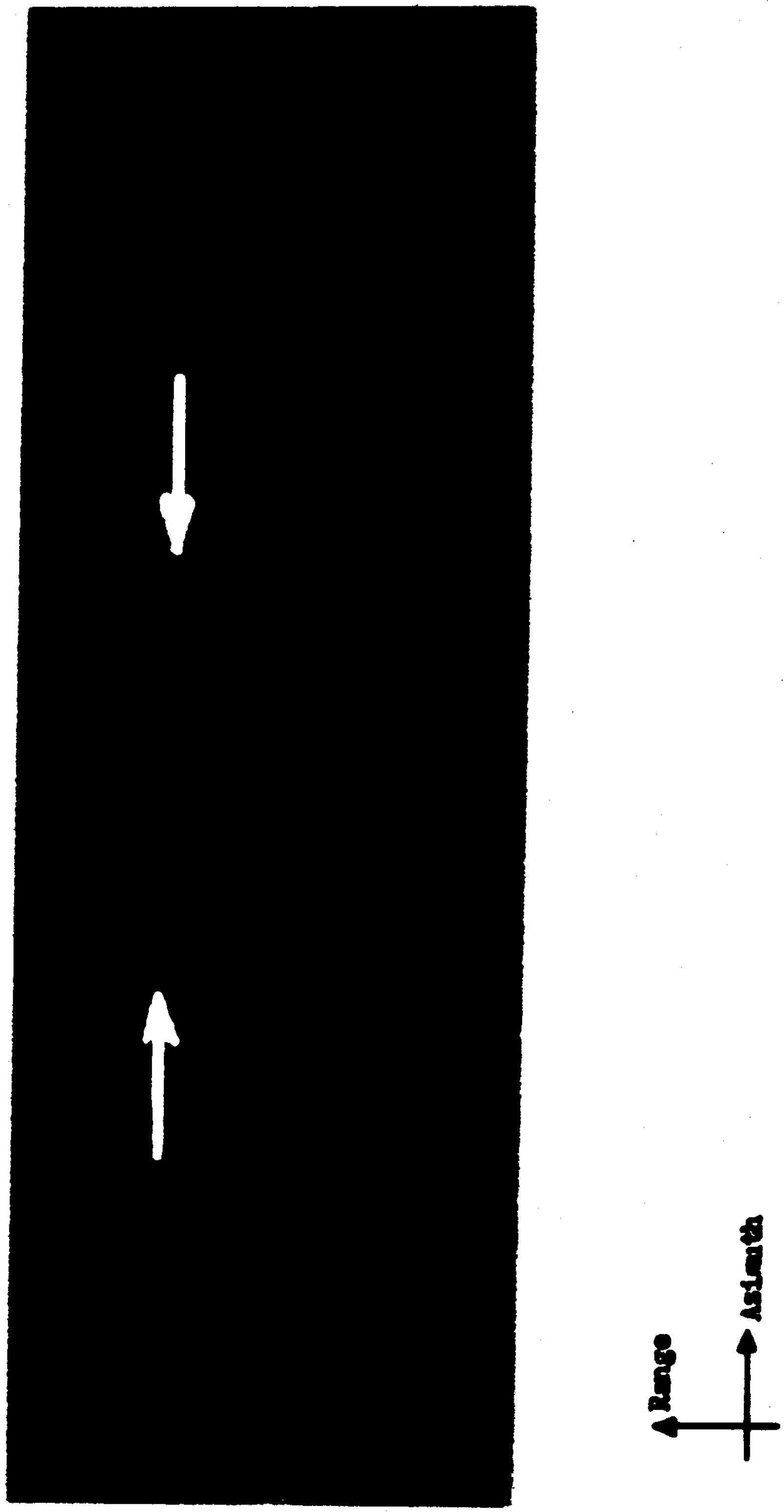

Figure 2.4.2.2 - Enlarged Print of Data Transparency

features of the required processor were as follows:

a) An optical system incorporating cylindrical as well as spherical elements, which would be very nearly diffraction-limited over 60 mm apertures in the dimension in which the cylinders had optical focusing properties, and which would introduce only negligible degradation on data stored at 50 lines per mm in the transverse dimension;

b) A source of light sufficiently monochromatic and spatially coherent to permit azimuth compression ratios of at least 1000:1 to be realized;

c) A film drive system whose accuracy and stability was sufficient to guarantee that degradation of the video data by the processor would be negligible;

d) A reasonable processing speed, preferably one comparable with the data collection rate of a satellite-borne radar system;

e) Inherent properties which minimise the insertion of additive optical noise into the output imagery; and

f) A degree of flexibility sufficient to permit optimum processing of coherent video data collected under a wide variety of possible orbital flight paths and non-nominal operating conditions.

It was found that a processor satisfying the above requirements could be instrumented; furthermore, it was expedient to surpass the minimum requirements for the 2355 flight in certain respects, thus providing a processor which could be used for later flights of more advanced radars capable of finer azimuth and range resolution.

The resulting processor is depicted by the block diagram of Figure 2.4.3.1. A photograph of the assembled processor is shown in Figure 2.4.3.2. The laser light source includes a Spectra Physics Model 116 helium-neon laser which provides a suitably coherent and monochromatic C.W. optical output at a wavelength of 6328 A°, with an average power output of 30 milliwatts. The properly collimated illumination emergent from the collimation system is incident upon the data transparency which is immersed in a liquid, contained between optical flats, whose refractive index approximates that of the data-film base material. The data film is uniformly transported in the "azimuth" direction past the viewing aperture. The anamorphic telescope serves to form a fine-resolution optical image of the radar reflectivity of the terrain being mapped; the dimensions of this image are controlled by the focal lengths and locations of the elements of the telescopes. The optics are selected and adjusted to provide an image which moves without distortion in the azimuth direction; this image is "tracked" by a recording camera and generates a fine-resolution transparency. The "aspect ratio" of the output map (i.e., the ratio of azimuth scale factor to range scale factor) is such that two targets separated by the distance Δ in

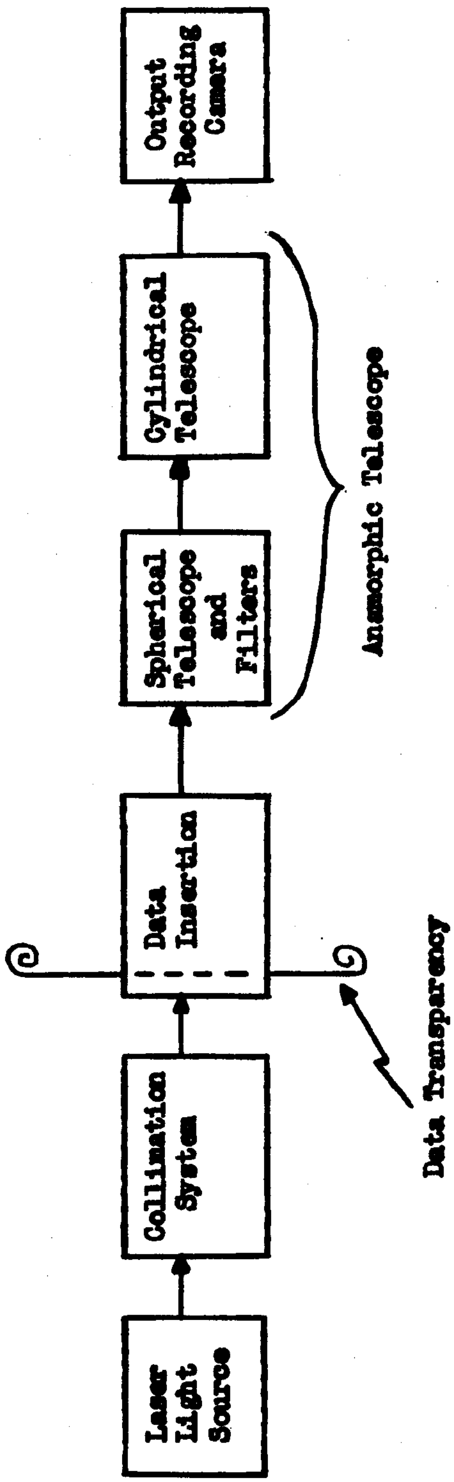

Figure 2.4.3.1 - Block Diagram, Precision-Optical Processor

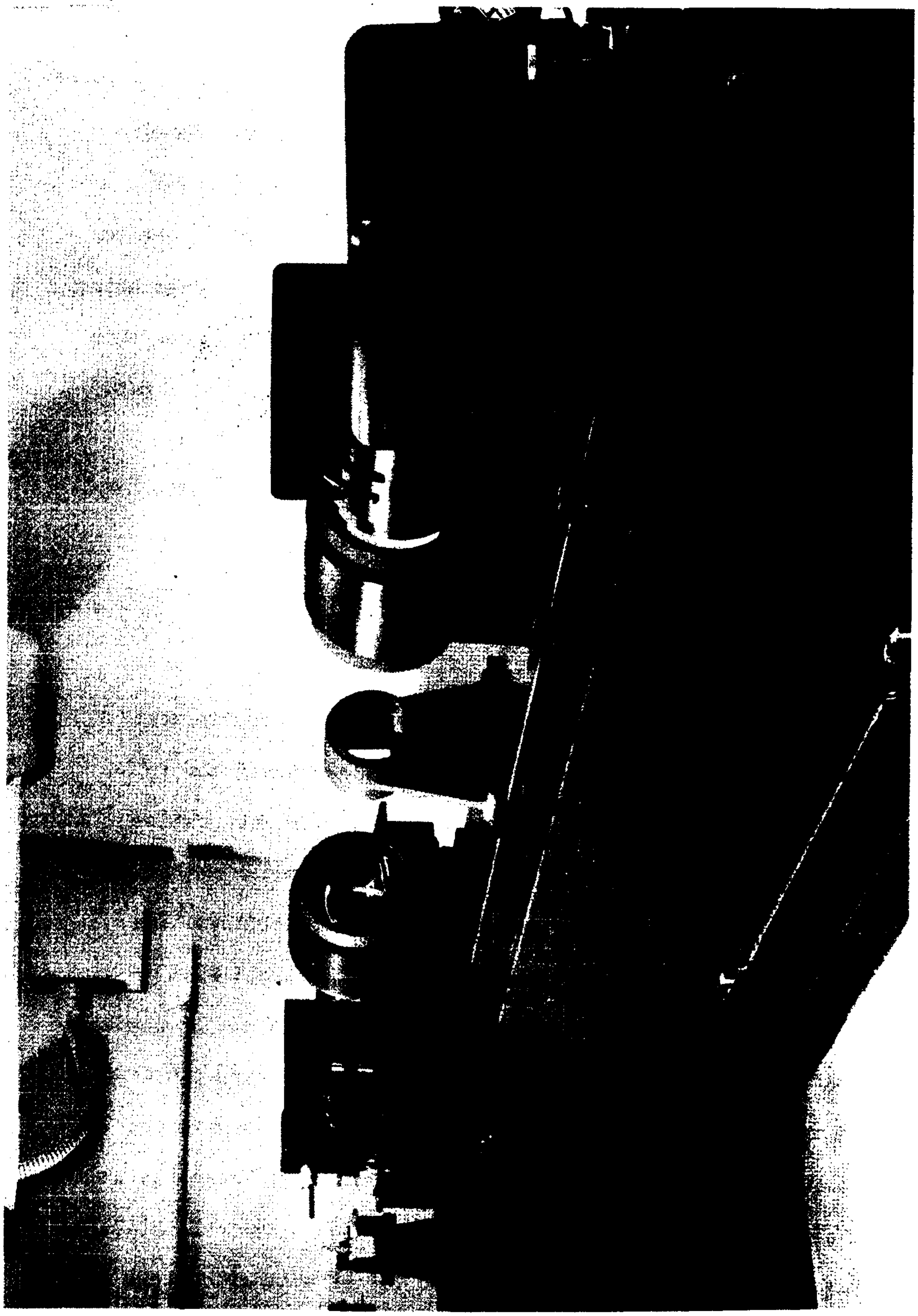

Figure 2.4.3.2 - [redacted] Precision Optical Processor

slant range as well as in azimuth will also appear to be equally separated in the range azimuth coordinates on the output transparency. Because the system operates at the relatively steep depression angle of 55°, targets separated by a distance Δ in slant range are in fact a greater distance apart on the earth's surface, the separation in this case being 1.6 Δ in ground range. The imagery shown later in this report has this property; a 1:1 aspect ratio of slant range to azimuth separation has been preserved. This choice of aspect ratio is arbitrary, and an approximate restitution to a 1:1 ground range-azimuth aspect ratio can be made by "shrinking" the azimuth scale of the output imagery appropriately. This can be accomplished by readjustment of the telescopes.

The processor described above meets all the technical requirements imposed upon it. The cylindrical and spherical elements of the telescopes have sufficient quality to permit azimuth compression ratios of the order of 5000:1 to be realized, with range-dimension recording densities of 100 line/mm, assuming compatible video recording. The laser light source provides sufficient coherence to permit such operation. The film drive units incorporate optical tachometer-feedback and are referenced to stable oscillators in order to provide jitter-free motion over a wide range of film speeds. The high power output of the laser together with the tracking capability permits processing at a speed equivalent to the speed of data collection for a typical satellite. The tracking feature also serves to minimize the effects of optical noise, which arises unavoidably in systems which employ highly coherent illumination. Flexibility to accomodate varying orbital speed during a mission without use of an incorrect aspect ratio is available through adjustment of the telescopes. Further flexibility can be obtained at the expense of the tracking feature through use of "spatial-plane" processing modes; these were not employed and will not be discussed further in this report.

2.4.4 Data Format

2.4.4.1 Data Transparency The video data recorded in the satellite and in the ground based recorders was recorded on 70 millimeter Eastman Kodak film, S. O. 119. The recorder CRT sweep covered a width of approximately 27.5 millimeters. The format of the data film is shown in Figure 2.4.4.1. This film, after processing at SPPL is the input data to the optical correlator, reference Figure 2.4.2.1 above.

2.4.4.2 Format of the Output Radar Imagery The output transparency upon which the fine-resolution radar imagery is recorded is a 70 mm wide film, of which a strip 27 mm in width is used for image recording. The scale factors and orientations are shown in Figure 2.4.4.2. The original output transparencies are recorded such that optical density increases monotonically with target reflectivity in localized areas; because of the AGC feature of the radar, widely separated targets of the same radar crossection do not necessarily yield target indications of equal density. The original transparencies are magnified by a factor of 2.60:1 and recorded in either of two forms:

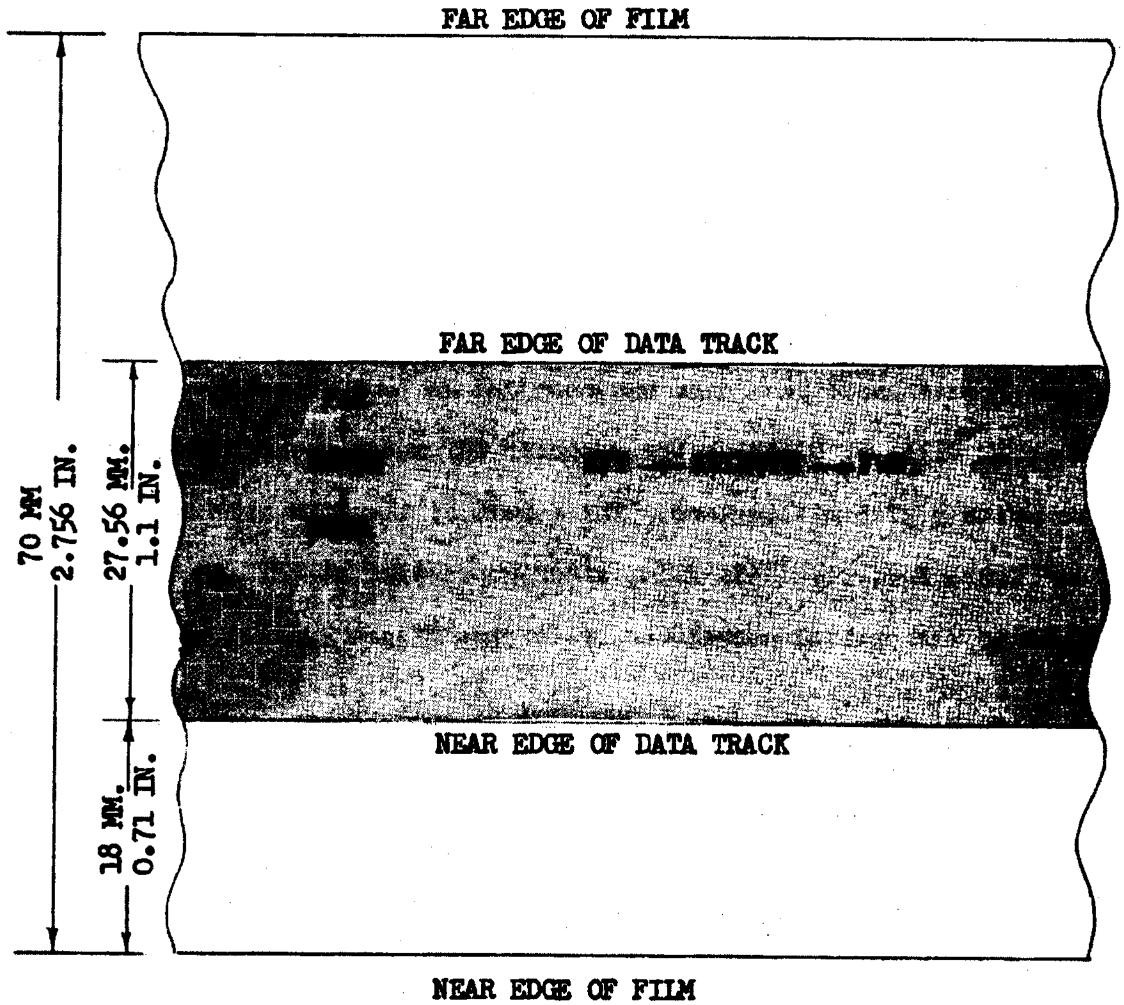

Figure 2.4.4.1 - Data format viewed from emulsion side of film

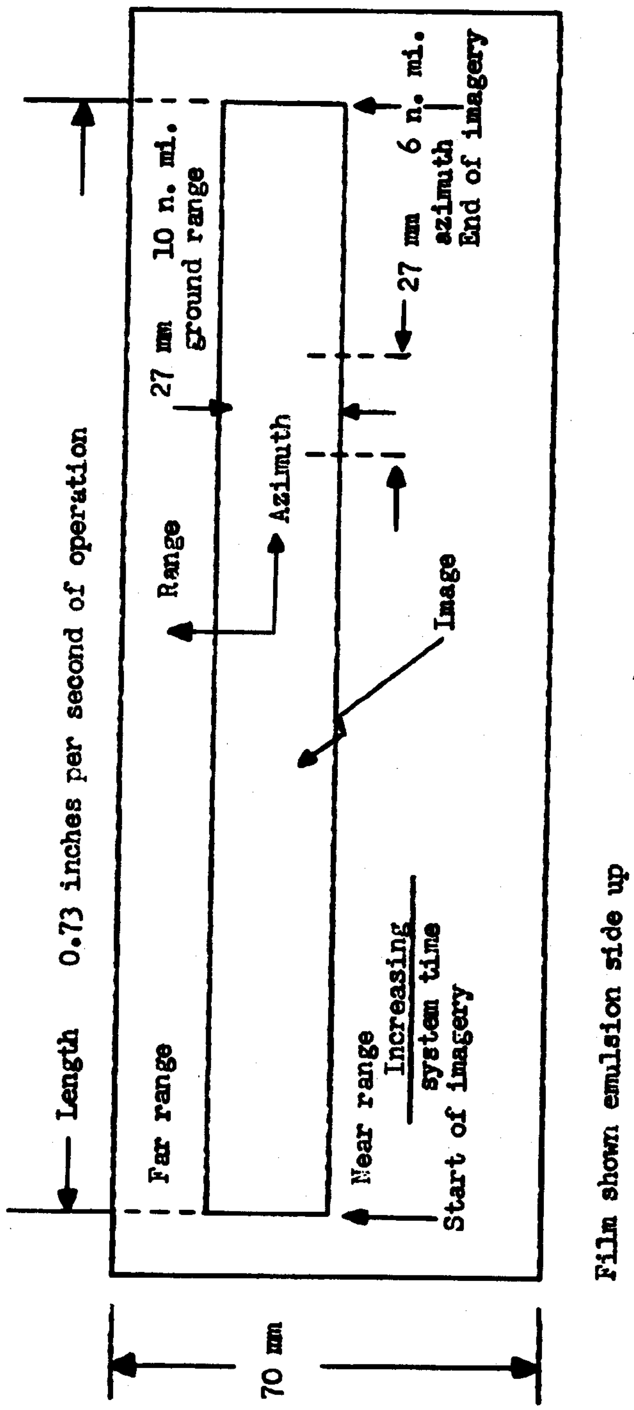

Figure 2.4.4.2 - Format of Output Transparency

a) A positive transparency in which bright targets appear as spots of high optical transmissivity, or

b) A positive paper print in which bright targets appear as white spots.

Both products have the following scale factors.*

1.00 n. mi. in azimuth	0.184 inches along the film length.
1.00 n. mi. in slant range, or 1.69 n. mi. in ground range	0.111 inches in the cross-film dimension.

Neither of these products is of adequate quality to fully preserve the system resolution and dynamic range; the degradations are more severe on the paper prints than is the case for the positive transparencies.

The paper prints, which are used as illustrative material later in this report, have a resolution capability of perhaps 6 lines per mm; at the scale factors corresponding to the 2.6:1 enlargements, this poor resolution completely dominates the quality of the imagery. The resulting ground-range resolution is of the order of 150 feet while the resulting azimuth resolution is of the order of 90 to 100 feet. The degradations in the positive transparencies (not presented in this report) are not as severe. In either case, imagery to the scale of the 2.6:1 enlargements is useful primarily for orientation and descriptive purposes only, and

* The azimuth scale factors differ by roughly 0.5 per cent for Northbound and Southbound passes. The ground-range scale factors vary slightly as a result of depression angle variation across the beam and terrain tilt, and as a function of true depression angle.

not for detailed study of the target complexes. Detailed examinations require the use of enlargements of greater magnification, the use of the original output transparencies, or in special instances the observation of the optical output of the processor prior to recording.

References

1. [redacted]

2. [redacted]

3. [redacted]

4. [redacted]

5. [redacted]